THÈSE

UNIVERSITÉ DE PAU ET DES PAYS DE L'ADOUR

École doctorale des Sciences Exactes et leurs Applications

UNIVERSIDAD DEL PAÍS VASCO UPV/EHU

Escuela de Master y Doctorado

Soutenue le 16 Décembre 2016

par **Laura ETCHENAUSIA**

pour obtenir le grade de docteur
de l'Université de Pau et des Pays de l'Adour
et de l'Universidad del País Vasco UPV/EHU
Spécialité : Chimie et Physico-chimie des Polymères

Synthesis and characterization of thermoresponsive poly(*N*-vinylcaprolactam)-based particles by emulsion polymerization by using a reactive macromolecular stabilizer

MEMBRES DU JURY

RAPPORTEURS

- Sagrario PASCUAL — Maître de conférences/HDR, Université du Maine
- Christine BRESSY — Maître de conférences/HDR, Université de Toulon

EXAMINATEURS

- Julien NICOLAS — Directeur de recherche CNRS, Université Paris Sud 11
- Pablo TABOADA — Professeur, Universidade de Santiago de Compostela

DIRECTEURS DE THÈSE

- Maud SAVE — Directrice de recherche CNRS, Université de Pau et des Pays de l'Adour
- Jacqueline FORCADA — Professeur, Universidad del País Vasco UPV/EHU

UNIVERSITÉ DE PAU ET DES PAYS DE L'ADOUR

eman ta zabal zazu

Universidad del País Vasco — Euskal Herriko Unibertsitatea

A ma famille,

Remerciements

L'ensemble des travaux présentés dans ce mémoire a été réalisé au sein de l'Equipe de Physique et Chimie des Polymères (EPCP) de l'institut IPREM (Unité mixte de recherche UMR 5254 CNRS, Université de Pau et des Pays de l'Adour) et également au sein du groupe Bionanoparticles group de l'institut POLYMAT, Université du Pays Basque. J'adresse mes remerciements aux responsables de ces laboratoires pour m'avoir donné l'opportunité de réaliser mes travaux de recherche pas l'accès à tous les équipements scientifiques nécessaires.

Je remercie l'Université de Pau et des Pays de l'Adour ainsi que l'Université du Pays Basque pour le financement de cette thèse en cotutelle.

Je tiens à adresser mes remerciements au Docteur Sagrario Pascual et au Docteur Christine Bressy, pour m'avoir fait l'honneur de juger mes travaux de thèse en tant que rapporteurs. Je remercie également le Professeur Pablo Taboada d'avoir accepté de faire partie de mon jury et le Professeur Julien Nicolas d'avoir accepté la présidence de mon jury de thèse.

Mes plus vifs remerciements s'adressent au Docteur Maud Save. Merci d'avoir cru en moi depuis le début, de m'avoir toujours poussée à me dépasser, d'avoir toujours été là pour me guider et d'avoir toujours été présente quand j'en avais besoin. J'ai énormément appris sur le plan scientifique et humain pendant ces trois années et demie à vos côtés et je n'aurai sincèrement pu espérer avoir une meilleure directrice de thèse. Je vous dois beaucoup aujourd'hui.

Me gustaría también agradecer a mi otra directora de tesis, el Profesor Jacqueline Forcada, por siempre haberme recibido tan bien en San Sebastian. Eskerrik asko Jacqueline por su ayuda, todo lo que aprendí durante esos tres años pasados a su lado y por todos los buenos momentos que compartimos.

También me gustaría dar las gracias al Profesor Pablo Taboada por haberme dado la oportunidad de pasar un mes en su grupo de investigación en Santiago de Compostela. Gracias por toda su ayuda durante este mes y durante la escritura de mi manuscrito. Agradezco a Eva Villar-Alvarez por todo su apoyo durante mi estancia y su simpatía.

Je tiens également à remercier tous les membres permanents de l'EPCP pour leur aide, disponibilité et gentillesse. Je remercie plus particulièrement le Docteur Elise Deniau et le Docteur Abdel Khoukh pour leur contribution à ce travail de thèse.

Une thèse n'est pas simplement un bel accomplissement personnel mais aussi une aventure riche en émotions et en rencontres. A ce titre, je souhaiterais remercier sincèrement TOUTES les personnes que j'ai côtoyées pendant ces trois ans, pour tous les moments que nous avons partagés et qui ont fait de cette thèse un souvenir si exceptionnel. La liste étant longue, il serait compliqué pour moi de tous vous citer mais sachez que j'ai vraiment passé de superbes années à vos côtés. Un merci particulier à Laetitia, Aurélie (alias Cobi), Céline, Arthur, Eunkyung, Hussein, Hongyao, Wissem, Laurent, Charlotte, Armelle, Maude, Samuel pour leur gentillesse et leur aide durant ces trois années. Spéciale dédicace à mes anciens collègues du N214 Juju et Momo pour tous les bons moments passés et pour m'avoir appris que la vengeance n'est souvent pas la meilleure des solutions (bizut un jour, bizut toujours) ;). Merci à Jesùs d'avoir égayé ma période de rédaction avec ses « chistes » et de m'avoir aidé la dernière semaine pour les cadeaux de thèse de Xavier. Gracias a todas las personas que encontré en San Sebastián por haberme recibido tan bien cada vez que fue allí, fue un placer conoceros. Gracias a Aintzane, Marta, Ane, David, Iban, Iñigo, entre otros. Garbiñe te quería agradecer por todo tu suporte durante esos tres años. Gracias por haberme animado y escuchado cuando más lo necesitaba, gracias por toda tu ayuda y tu amistad.

Cette thèse n'aurait pas été la même sans mon « bestou », alias Xavier. Merci pour tout ce que tu m'as apporté, pour ton soutien, pour tous les services que tu m'as rendus et pour avoir toujours su trouvé les mots pour me réconforter. Bien plus qu'un colloc j'ai trouvé en toi un ami, un confident et je te remercie sincèrement. Bien que nos chemins se séparent ici, je sais que notre amitié perdurera.

Merci à mes frères Jean-Baptiste et Théo et à Mattea de m'avoir épaulée et encouragée tout au long de ces années. Enfin je remercie mes parents de leur soutien sans faille et d'avoir toujours su me conseiller dans mes choix tout en me laissant libre de prendre des décisions. Merci d'avoir fait de moi la personne que je suis aujourd'hui.

List of abbreviation

A-4F: asymmetric flow field-flow fractionation
Abs: absorbance
ACPA: 4,4’-azobis(4-cyano)pentanoic acid
ADIBA (or VA-044): 2,2'-azobis[2-(2-imidazolin-2-yl)propane] dihydrochloride
AETAC: [2-(acryloyloxy)ethyl]trimethylammonium chloride
AIBN: azobis(isobutyronitrile)
ATRP : atom transfer radical polymerization
BSA: bovine serum albumin
C: concentration
CCK-8: cell counting kit-8
$CDCl_3$: deuterated chloroform
Co-MRP: cobalt-mediated radical polymerization
CRP: controlled radical polymerization
CTA: chain transfer agent
CTAB: cetyltrimethylammonium bromide
C_{tr}: transfer constant
D.L: drug loading
Đ: dispersity
DDI: double deionized water
DDS: drug delivery systems
D_h: hydrodynamic diameter
DLS: dynamic light scattering
DMEM: Dulbecco’s modified eagle’s medium
DMSO-d_6: deuterated dimethyl sulfoxide
d*n*/d*c*: refractive index increment
DOSY: diffusion-ordered spectroscopy
DOXO: doxorubicin hydrochloride
DSC: differential scanning calorimetry
D_v: volume-average diameter
E.E: entrapment efficiency
e.g.: *exempli gratia*
EBP: ethyl-2-bromopropionate
EGDMA: ethylene glycol dimethacrylate
EtOH: ethanol
f_A: molar fraction of A
F_A: molar fraction of the A monomer incorporated into the copolymer
FBS: fetal bovine serum
FD: functionalization degree
FDA: food and drug administration

FTIR: Fourier transformed Infrared spectroscopy
i.e.: *id est*
I: average scattered intensity
k_B: Boltzmann constant
k_d: dissociation rate constant
k_p: propagation rate constant
KT: Kelen-Tüdös
k_{tr}: transfer rate constant
l: length
LAM: less activated monomer
LCST: lower critical solution temperature
M: molar mass
m: weight
MADIX: macromolecular design via interchange of xanthate
MALDI-TOF MS: Matrix assisted laser desorption ionization-time of flight mass spectrometry
MALLS: multi angle light scattering detector
MeOH: methanol
M_n: number-average molar mass
M_w: weight-average molar mass
n_A: number of moles of A
NLLS: nonlinear least-squares
NMP: nitroxide mediated polymerization
NMR: nuclear magnetic resonance spectroscopy
N_p: number of particles
OMRP: organometallic-mediated radical polymerization
P(AETAC): poly[2-(acryloyloxy)ethyl]trimethylammonium chloride
PBS: phosphate buffered saline
PCS: photon correlation spectroscopy
PEG: poly(ethylene glycol)
PISA: polymerization induced self-assembly
PVA: poly(vinyl alcohol)
PVAc: poly(vinyl acetate)
PVCL: poly(*N*-vinylcaprolactam)
R6G: rhodamine 6G
RAFT: reversible addition/fragmentation chain transfer
RDRP: reversible-deactivation radical polymerization
R_g: gyration radius
RI: refractometer
RITP: reversible iodine transfer polymerization
R_θ: Rayleigh ratio
SDBS: sodium dodecylbenzenesulfonate

SDS: sodium dodecyl sulfate
SEC: size exclusion chromatography
SLS: static light scattering
T: temperature
t: time
T_{cp}: cloud point temperature
TEM: transmission electron microscopy
T_g: glass transition temperature
THF: tetrahydrofuran
TRIZMA: tris(hydroxymethyl)aminomethane hydrochloride buffer
V: volume
VA: vinyl alcohol
VAc: vinyl acetate
VCL: *N*-vinylcaprolactam
VOC's: volatile organic compounds
VP: *N*-vinylpyrrolidone
VPTT: volume phase transition temperature
w_A: weight fraction of A
x_A: individual conversion of monomer A
X_m: overall molar conversion
X_w: overall weight conversion
ε: molar extinction coefficient
η: viscosity
λ: wavelength
ρ: density
τ: solids content
Φ: swelling-ratio

Contents

PART II

Introduction

I. Context and state of the art

Over the past decade, effort has been dedicated to the development of nanoscale materials whose specific properties make them suitable for the design of new functional materials for a wide range of applications. New opportunities have been realized in all branches of technology ranging from optical systems, electronic, chemical and automotive industries to environmental engineering and medicine.[1] In the latest field, attention has been focused on the elaboration of novel nanoparticles for diverse uses such as diagnostic imaging, biosensors, nucleic acid or drug delivery, implantable devices, drug delivery, and so on.[1-3]

Stimuli-responsive polymers are a class of advanced polymers exhibiting properties tuned by an external stimuli such as temperature, light, pH, specific molecules or enzymes, among others.[4, 5] These polymers have received considerable attention within the last decade, due to their wide range of applications, especially in the biomedical field where they can be envisaged as potential drug delivery systems or biosensors.[6, 7] Among these stimuli-responsive polymers, thermoresponsive polymers undergo a conformation phase transition in response to a change of temperature. The behavior of any polymer in a solvent is related to the balance between solvent-solvent, solvent-polymer and polymer-polymer interactions. For thermoresponsive polymers presenting a lower critical solution temperature (LCST) in water, the polymer-water interactions (mainly by hydrogen bonding) are predominant below the LCST and therefore the polymer chains are soluble in water. At higher temperatures, the hydrogen bonding between polymer and water are disrupted, in favor to polymer-polymer hydrophobic interactions and so the polymer collapses in a separate phase.[8] The most extensively studied thermoresponsive polymer is the poly(*N*-isopropylacrylamide) (PNIPAAm) which has a LCST of 32°C, around physiological temperature. However, it is not biocompatible,[9] which limits its potential applications, especially in the biomedical field. Therefore, thermoresponsive and biocompatible polymers such as poly((oligo ethylene glycol) (meth)acrylates) (P((OEG)(M)A)[10, 11] or poly(*N*-vinylcaprolactam) (PVCL),[9, 12] which also present a LCST near to physiological temperature, have raised an increasing interest over the last years. Poly(*N*-vinylcaprolactam) is a 7-membered ring type polymer (**Scheme 1**) which is biocompatible, water-soluble, non-ionic and exhibits a LCST in water ranging between 30 and 40°C.[9, 12-14]

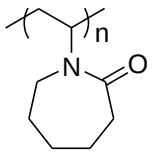

Scheme 1. Chemical structure of poly(*N*-vinylcaprolactam).

The polar amide group of PVCL creates favorable associations with surrounding water molecules by hydrogen bonding below the LCST and hydrophobic interactions (seven-membered ring) predominate above the LCST.[15, 16] Contrary to PNIPAAm polymer, which presents a Type II thermoresponsive phase behavior in water (*i.e.* its critical temperature is relatively insensitive to changes in varying molar mass, polymer concentration, and/or pH), PVCL shows a "classical" Flory-Huggins thermoresponsive phase behavior in water (Type I). This means that the phase transition of PVCL in water is dependent on its molar mass and polymer concentration.[9] It has been observed that the value of the cloud point temperature decreases upon increasing both the polymer chain-length and concentration.[15, 17, 18] As for other thermoresponsive polymers, the temperature in which the change of PVCL chain solvation state occurs can also be tuned by means of the introduction of co-monomers in the polymer chains.[19-22]

Nano- or microgels are crosslinked polymer particles, able to swell in a good solvent and prevented from dissolution by crosslinking. According to IUPAC's definitions, microgels are crosslinked particles with diameters ranging from 0.1 to 100 µm whereas nanogels present diameters between 1 and 100 nm.[23] In this manuscript, the term microgel will be preferred to the term nanogel due to the size of the synthesized thermoresponsive particles (*i.e.* hydrodynamic diameters > 100 nm). During the last decades, a special interest has been focused on the development of microgels based on thermoresponsive polymers.[24-27] These microgel particles present a volume phase transition temperature (VPTT) in water, *i.e.*, they undergo a volumetric transition from a swollen to a collapsed state by increasing the temperature (**Figure 1**). Thermoresponsive microgels are very promising materials due to their unique properties, making them interesting for cosmetics,[28, 29] photonic crystals,[30] stabilizers of pickering emulsions[31] or CO_2-absorbents.[32] In the biomedical field, they have been envisaged for

applications such as in biosensors, cell culture substrates, drug delivery systems, among others.[33-35]

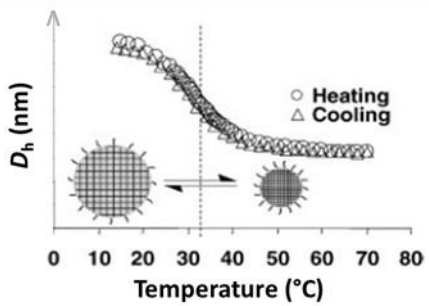

Figure 1. Evolution of the average hydrodynamic diameter (D_h) of a thermosensitive microgel as a function of the temperature.

For the synthesis of microgels by radical polymerization of vinylic monomers, various processes of polymerization in dispersed media can be distinguished depending on the initial experimental conditions related to the nature of the continuous phase, the presence of initial monomer droplets or of a soluble monomer, the solubility of initiator and the presence of surfactant.[36, 37] Indeed, thermoresponsive microgels have been synthesized by emulsion polymerization, precipitation polymerization and inverse miniemulsion polymerization. The main characteristics of such processes are reported in **Table 1**.

Table 1. Features of the different processes of polymerization in dispersed media used for the synthesis of thermoresponsive microgels.

Process	Continuous phase	Initiator	Dispersed phase	Size	Surfactant	Ref
Emulsion	H_2O	Soluble in the continuous phase	Monomer droplets and polymer colloids	50 nm – 1 µm	Either yes or no	9
Aqueous dispersion / precipitation	H_2O	Soluble in the continuous phase	Polymer colloids	100 nm – 1 µm	Yes, for dispersion only	38
Inverse miniemulsion	Organic solvent	Water soluble	Monomer droplets and polymer colloids	300 – 500 nm	Yes	39

At the initial state of the batch emulsion polymerization process, the water-insoluble monomer is dispersed in water as monomer droplets by stirring. The aqueous phase contains a water-soluble initiator (either redox or thermal initiator) and surfactants which adsorb on the surface of the monomer droplets stabilizing them by means of electrostatic stabilization, steric stabilization or electro-steric stabilization depending on the nature of the surfactant (ionic/non-ionic, molecular/macromolecular). The amount of surfactant is generally higher than that

needed to stabilize monomer droplet surface and so, if its concentration in water is above its critical micellar concentration (cmc), the surfactant self-assembles into micelles swollen by the monomer (**Scheme 2.A**). The polymerization of the water-soluble fraction of monomer is initiated in the aqueous phase, forming oligoradical species. As they grow, these oligoradicals become hydrophobic enough so they can either enter into the micelles swollen by the monomer (heterogeneous or micellar nucleation) or precipitate in the aqueous phase (homogeneous nucleation). The process called nucleation corresponds to the formation of the primary polymeric particles (nuclei). In the case of seeded emulsion polymerization, this nucleation is separately performed during the synthesis of the latex particles used as seed. The polymerization reaction is then allowed to continue inside the particles by diffusion of the monomer from the monomer droplets through the aqueous phase (**Scheme 2.B**). A semi-continuous process can be implemented to process in starved-feed condition and limit the presence of monomer droplets. At the end of the polymerization, a dispersion of colloidal polymeric particles in water (latex) is obtained (**Scheme 2.C**).

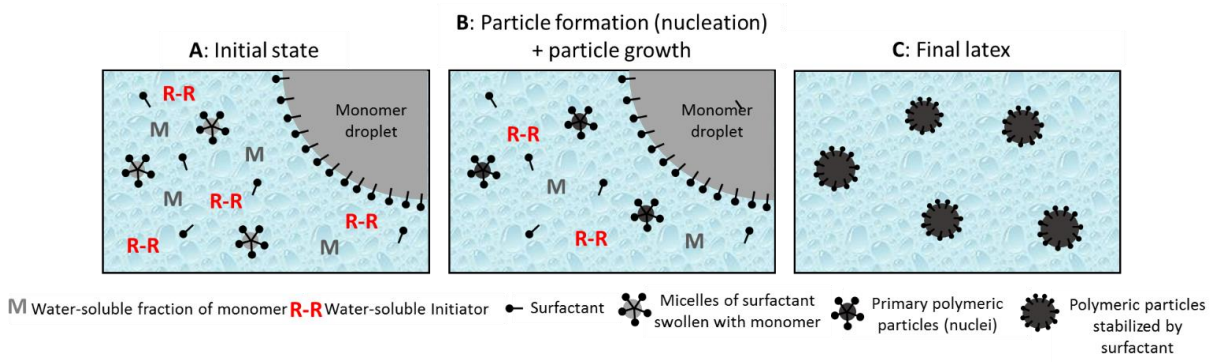

Scheme 2. Representation of the emulsion polymerization process.

Another type of heterogeneous polymerization process in aqueous media employed for the preparation of thermoresponsive microgels is the precipitation polymerization process (**Scheme 3**). In this case, the monomer is water-soluble and the polymer precipitates in the water continuous phase as the reaction temperature is far above the phase transition temperature of the polymer in water. The water-soluble initiator initiates the polymerization in the aqueous phase, producing oligoradicals, which become hydrophobic when reaching a certain chain-length and thus precipitate in the aqueous phase to form the particle precursors (or nuclei). The size of these nuclei will increase, either by adsorption of other oligoradicals, or by monomer polymerization, or by aggregation of various nuclei, until reaching a certain size for which stable polymeric particles dispersed in water are formed. The stability of these particles is

ensured by the ionic fragments of the initiator that remain at the particle surfaces. When a stabilizer is used to ensure the system stability, the term aqueous dispersion polymerization is used instead of precipitation polymerization.[38, 40]

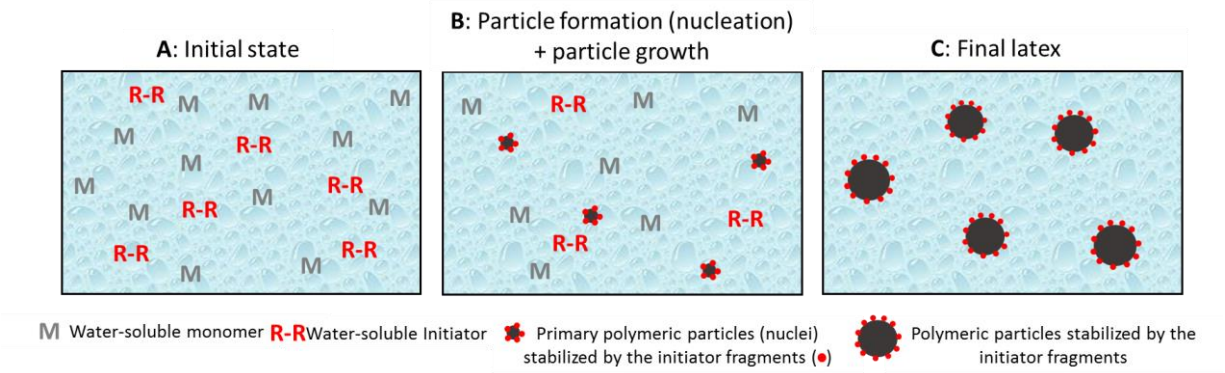

Scheme 3. Representation of the precipitation polymerization process.

Inverse miniemulsion was also a convenient strategy to synthesize microgels by copolymerizing a hydrophilic monomer and crosslinker in aqueous monomer droplets dispersed in an organic phase and stabilized by a non-ionic surfactant.[39, 41]

Note that, apart from the easy implementation of both emulsion and precipitation polymerization processes, from an engineering viewpoint, a water-based continuous phase favors heat transfer of the exothermic polymerization reaction and facilitates polymer recovery from the reactor at the end of the synthesis. Moreover, they are environmentally safe processes meeting one of the green chemistry principles concerning the decrease of volatile organic compounds (VOC's) as solvents are not required.

While PNIPAAm or poly(oligo(ethylene glycol) (meth)acrylate)-based microgels are generally synthesized by precipitation/dispersion polymerization,[28, 29, 38, 42] PVCL-based microgels synthesis follows either a precipitation or an emulsion polymerization process depending on the initial VCL concentration ($[VCL]_{limit,\ water}$ = 41 $g.L^{-1}$).[9, 38] It should be mentioned that, whatever the employed process (emulsion or precipitation/aqueous dispersion polymerization), thermoresponsive microgels are generally synthesized at relatively low initial solids content in order to prevent a macroscopic gelation (< 5wt-%).[43]

The combination of controlled radical polymerization and polymerization in aqueous dispersed media addressed this limitation of solids content.[44, 45] Controlled Radical Polymerization (CRP) (also recently named reversible-deactivation radical polymerization

(RDRP)[46]) techniques, are based on the establishment of a dynamic equilibrium between propagating radicals and dormant species (**Scheme 4**). This phenomenon allows to reduce undesirable side reactions between radicalar growing chains that generally occur in a free radical polymerization process (irreversible termination and transfer reactions).

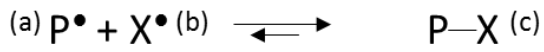

Scheme 4. Reversible deactivation equilibrium taking place during a controlled radical polymerization: (a) active chain, (b) control agent, (c) dormant chain.

The main CRP techniques can be distinguished by the control agents involved in the equilibrium and the type of radical trapping reaction. For example, in Atom Transfer Radical Polymerization (ATRP),[47, 48] alkyl halogens and transition metal species are used in a reversible redox equilibrium while in Nitroxide Mediated Polymerization (NMP),[49, 50] the control is ensured by nitroxides in thermal equilibrium with alkoxyamines. Both NMP and ATRP are based on reversible termination reactions. On the contrary, the Reversible Addition/Fragmentation chain Transfer (RAFT) polymerization[51-53] is based on reversible transfer reactions involving thiocarbonylthio compounds as control agents. When xanthate species (dithiocarbonates) are involved, the term MAcromolecular Design via Interchange of Xanthate (MADIX) was initially used,[54, 55] and it is now used in combination with RAFT.

In this thesis, we will focus on RAFT/MADIX polymerization technique. RAFT is a versatile technique that proved to be efficient for a wide range of monomers with various functional groups and to enable polymerization in homogeneous and heterogeneous media.[56] The RAFT polymerization process starts with a classical initiation step where an initiator dissociates into radicals to initiate the polymerization.[56, 57] The propagating radical $P_n^{\bullet}$ is then able to add on the double bond of a thiocarbonylthio compound (which is the control agent, 1 in **Scheme 5**), to form an intermediate radical (2 in **Scheme 5**) that will fragment into a dormant polymer (3 in **Scheme 5**) and a novel radical $R^{\bullet}$. This radical also initiates the polymerization to provide propagating radical $P_m^{\bullet}$ that will reversibly add onto the double bond of the dormant polymeric thiocarbonylthio compound (3 in **Scheme 5**), followed by fragmentation. Rapid equilibrium between the active propagating radicals ($P_n^{\bullet}$ and $P_m^{\bullet}$) and the dormant polymeric thiocarbonylthio compound (3 in **Scheme 5**) allows for controlling the polymerization. Radical-radical termination occurs as in conventional free radical polymerization but the level is minimized.

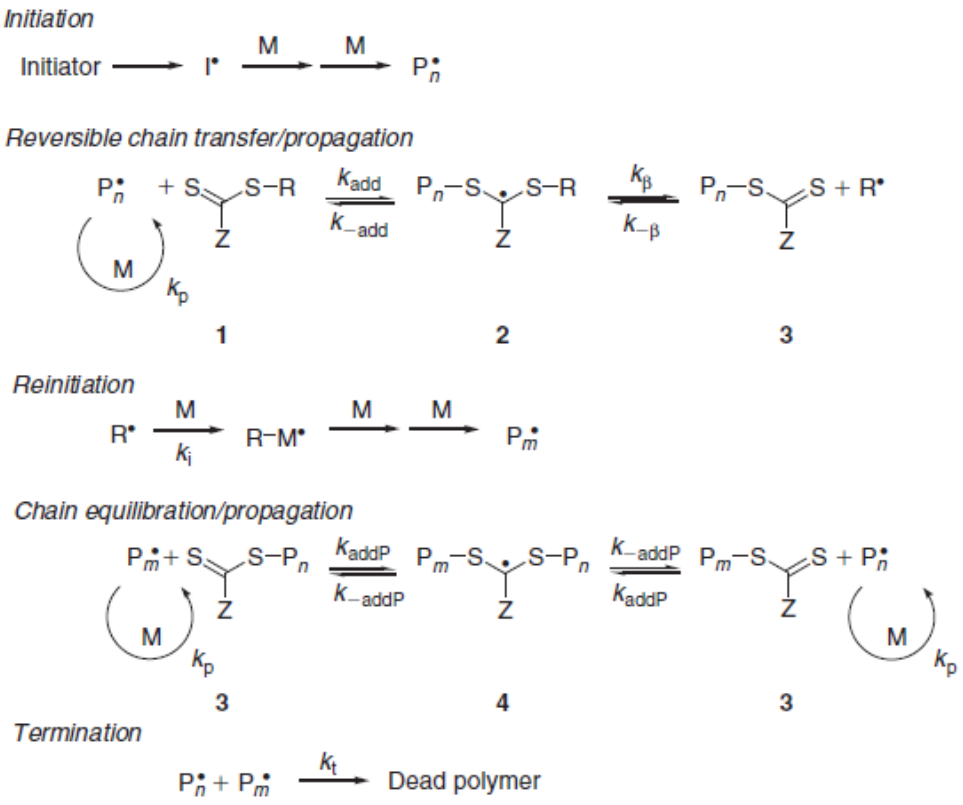

Scheme 5. Mechanism of RAFT polymerization technique (from reference 58).

The RAFT agents are classified as a function of their activation group (Z) (**Scheme 6**). This group is of high importance, as it will govern the rate of addition-fragmentation and thus the rate of the main equilibrium between active and dormant species in the RAFT process. Depending on the nature of the Z group, dithioesters can be distinguished from dithiocarbonates (xanthates), dithiocarbamates or trithiocarbonates (**Scheme 6**). The free radical leaving group (R) must be a good homolytic leaving group with respect to the nature of the $P_n^•$ macromolecular radical.

R: Free-radical leaving group

CH_2-Ph

$CH(CH_3)$-Ph

$C(CH_3)_2$-Ph

$C(CH_3)_2$-CN

$C(CH_3)_2$-COOEt

$C(CH_3)_3$

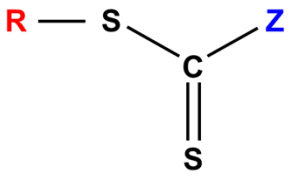

Z : Activation group

Dithioesters : Ph, CH_3, CH_2-Ph

Dithiocarbonates (=Xanthates) : O-Ph, O-Et

Dithiocarbamates : NEt_2, pyrrole, pyrrolidone

Trithiocarbonates : S-R

Scheme 6. RAFT agents classification.[52, 53]

Depending on the monomer being polymerized by the RAFT process, the choice of the RAFT agent and especially its Z group is of crucial importance (**Scheme 7**), as it will govern the efficiency of the global process. For less activated monomers (LAM) like vinyl acetate (VAc) and VCL, because of the high reactivity of the propagating radical $P_n^{\bullet}$, the addition onto the thiocarbonylthio compound is favored. Therefore, the Z group need to destabilize the intermediate radical (2 and 4 in **Scheme 5**) in order to promote its rapid fragmentation. Electron-donor type Z groups are appropriate, electing xanthate (Z = *O*-alkyl) or dithiocarbamate (Z = *N*,*N*-dialkyl) agents suitable for controlling the polymerization of LAM (**Scheme 7**). On the contrary, for styrenic or (meth)acrylate monomers, the propagating radical $P_n^{\bullet}$ being stabilized, the addition is unfavorable and should be promoted by using Z group able to stabilize the intermediate radical (2 and 4 in **Scheme 5**). As a result, trithiocarbonate or dithioester type RAFT agents, which possess electron-withdrawing groups, are generally used (**Scheme 7**). As previously mentioned, the free radical leaving group (R) must be a good homolytic leaving group with respect to the attacking radical $P_n^{\bullet}$ and thus it also needs to be carefully chosen depending on the monomer being polymerized (**Scheme 7**).

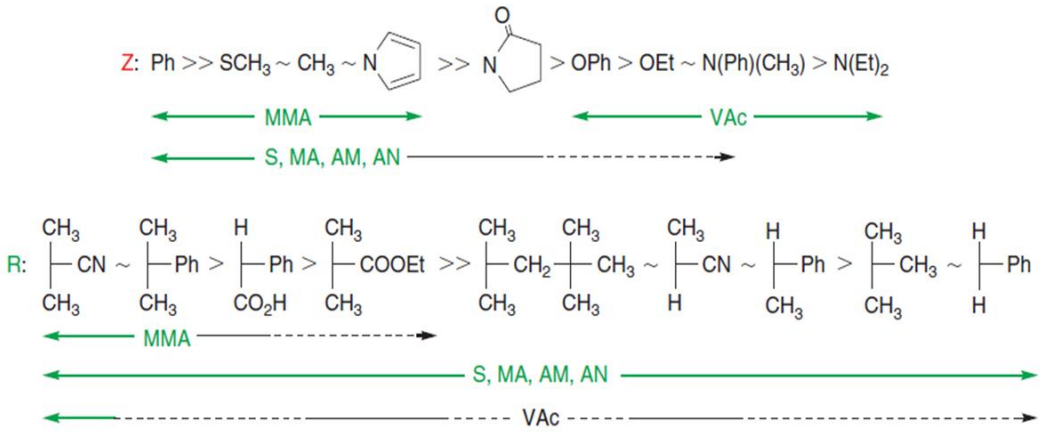

Scheme 7. Choice of the suitable RAFT agent as a function of the monomer being polymerized (from reference 58).

In a controlled polymerization process, all the chains are ideally initiated at the same time (fast initiation) and grow simultaneously. Therefore, it is possible to control the macromolecular chain length with narrow molar mass distribution (low dispersity, $Đ = M_w/M_n$) and to reach a high degree of chain-end functionality. Among the different architectures accessible with CRP techniques, block copolymers are of high interest, especially when they are composed of immiscible blocks. Indeed, they are able to self-assemble in a selective solvent for one of the blocks, which confers them many applications. Hydrophilic/hydrophobic block copolymers which are amphiphilic, are probably the most studied systems.

For polymerization process carried out in aqueous media, where the use of a stabilizer is generally required to maintain the system stability, the *in-situ* formation of stabilizing amphiphilic copolymers simultaneously to the particle growing has been considered. This strategy relies on the use of a reactive macromolecular stabilizer, *i.e.*, a hydrophilic polymer with a living chain-end, that will act as both a macromolecular stabilizer and a control agent for the polymerization in aqueous dispersed media. In a first approach (**Scheme 8**), the chain extension of the reactive stabilizer led to the *in-situ* formation of stabilizing amphiphilic diblock copolymers concomitantly to the particle growth by non-controlled free radical polymerization.[59-62] It allows to synthesize stable polymer particles with functional macromolecular shell, avoiding the use of molecular surfactants (surfactant-free process) and thus to develop more environmentally friendly polymerization processes.

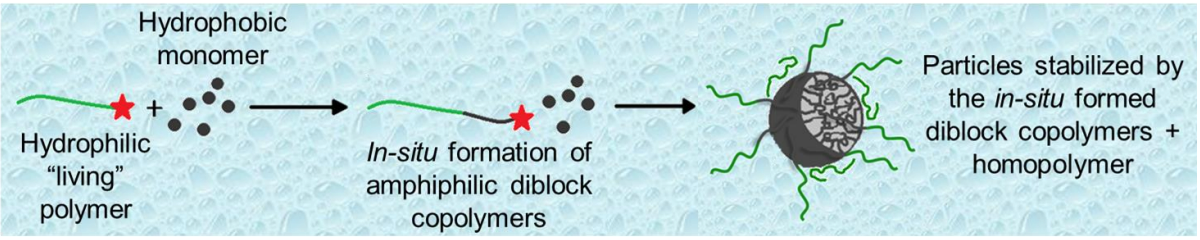

Scheme 8. Schematic representation of the *in-situ* formation of stabilizing amphiphilic copolymer simultaneously to particle growth by emulsion polymerization.

In a second approach (**Scheme 9**), a high degree of control of the second growing block is targeted to promote the *in-situ* formation of pure amphiphilic block copolymer self-assembled particles synthetized by emulsion polymerization.[63]

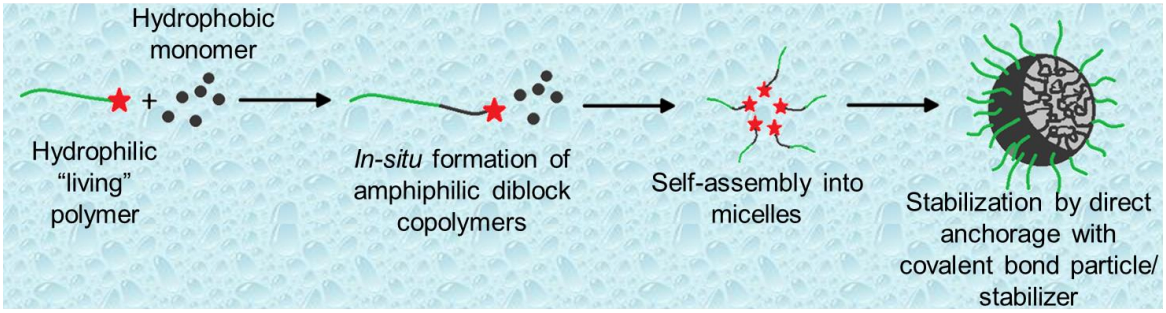

Scheme 9. Schematic representation of the Polymerization Induced Self-Assemby (PISA) methodology.

This concept was first introduced by Hawkett *et al.*[64] in order to control the polymerization of *n*-butyl acrylate by RAFT polymerization using poly(acrylic acid) oligomer functionalized by a trithiocarbonate chain end. The group of Charleux showed in 2005 that this methodology was also efficient to implement nitroxide-mediated polymerization in emulsion.[65] This concept was further named *"polymerization-induced self-assembly"* (PISA) and represents an emerging field to synthesize block copolymer self-assembled particles either by emulsion polymerization,[63] or by aqueous dispersion polymerization[66] or by non-aqueous dispersion polymerization.[67] By tuning the volume fraction of the hydrophilic and hydrophobic blocks, stable hairy latex particles with multiple morphologies can be produced at high solids content by surfactant-free emulsion polymerization (**Figure 2**).

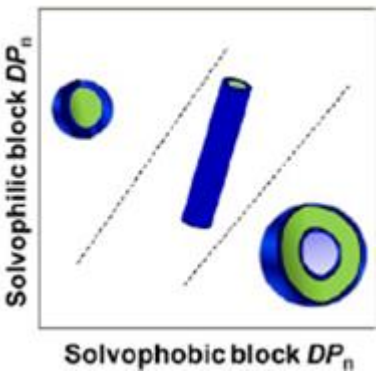

Figure 2. Particles morphologies obtained by polymerization-induced self-assembly (PISA) depending on the volume fraction of the hydrophilic and hydrophobic blocks (from reference 63).

Over the last decade, PISA method has also been successfully applied to the synthesis of thermoresponsive microgels, allowing to produce stable microgel dispersions up to 20 wt-% of initial solids content, in the absence of molecular surfactant. For example, Delaittre *et al.*,[44, 68] synthesized poly(*N*,*N*-diethylacrylamide)-based thermosensitive microgels from an hydrophilic poly(sodium acrylate) based macroalkoxyamine using nitroxide mediated polymerization technique. When *N*,*N'*-methylenebisacrylamide (MBA) was used as crosslinker, chemically crosslinked microgels with covalent bonds between the polymer chains forming the network were synthesized while the copolymerization of *N*,*N*-diethylacrylamide (DEAAm) with styrene as hydrophobic co-monomer produced physically crosslinked microgels by means of hydrophobic interactions between the polymer chains of the inner network (**Scheme 10**).

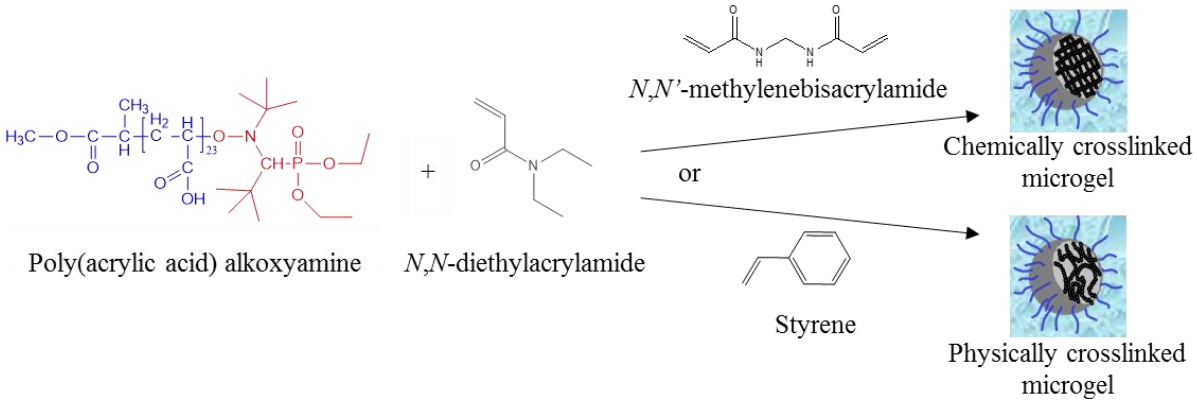

Scheme 10. PISA method applied to the synthesis of chemically[44] and physically[68] crosslinked thermoresponsive microgels.

Concomitantly to this first example of the use of a macromolecular control agent for the synthesis of thermoresponsive microgels,[44] An *et al.*[45] reported the synthesis of PNIPAAm thermoresponsive microgels via an hydrophilic poly(dimethylacrylamide) (P(DMAAm))

macromolecular RAFT agent. Since these first studies, different thermoresponsive microgels were synthesized by using reactive macromolecular stabilizers, mainly macromolecular RAFT agents. These studies are gathered in **Table 2**. From **Table 2**, it appears that the use of a reactive hydrophilic polymer as stabilizer and control agent for the synthesis of thermoresponsive microgels allows to increase the solids content of the final microgel dispersion up to 30 wt-%. The continuous phase was either water or an hydroalcoholic continuous phase. Various polymers have been used as macro-CTA to reach thermoresponsive microgels with functional macromolecular shell. When the macromolecular control agent is soluble in organic solvent, the successful chain-extension of this precursor block is evidenced by means of performing experiments in the absence of crosslinker, allowing further characterization of the macromolecular features of the formed block copolymers by size exclusion chromatography.

To date, the synthesis of PVCL-based thermoresponsive particles by heterogeneous polymerization by using a reactive polymeric stabilizer has never been reported.

Table 2. Summary of studies devoted to the use of a reactive hydrophilic polymer as stabilizer and control agent for the synthesis of thermoresponsive microgels.

CRP technique / Control agent	Reactive macromolecular stabilizer	Polymer of the core	Crosslinker	Continuous phase	Solids content (wt-%)	D_h (nm)	Ref
RAFT / TTC-CNC3 or CDB	P(PEGMA) or PEO_{100}-TTC	P(MEO_2MA) or P(MEO_2MA-*co*-PEGMA)	P(EGDMA)	Water	1.5	$D_{swollen}$ = 50 – 80 $D_{collapsed}$ = 40 - 60	69
RAFT / TTC-C12 or TTC-C3	P(DMAAm)	P(NIPAAm)	MBA	Water	3	$D_{swollen}$ = 70 – 200 $D_{collapsed}$ = 40 - 100	45
RAFT / TTC-C12	PEO_{40} and PEO-*b*- P(DMAAm)	P(DEAAm)	MBA	Water	3 to 16	$D_{swollen}$ = 70 – 140 $D_{collapsed}$ = 50 - 120	70
RAFT TTC-C12	PEO_{10}	P(DMAEMA)	MBA	Water	4 to 5	$D_{swollen}$ = 150 – 400 (AIBN) $D_{swollen}$ = 10 (ACVA) $D_{collapsed}$ = non specified	71
RAFT / BE-TTC	P(DMAAm)	P(MEOA-*co*-PEGA)	P(EGDA)	Water	10 to 30	$D_{swollen}$ = 40 – 100 $D_{collapsed}$ = 30 - 80	72
NMP / Alkoxyamine MONAMS	P(ANa)	P(DEAAm-*co*-S)	-	Water	20	$D_{swollen}$ = 120 $D_{collapsed}$ = 95	68
NMP / Alkoxyamine MONAMS	P(ANa)	P(DEAAm)	MBA	Water	20	$D_{swollen}$ = 90 – 190 $D_{collapsed}$ = 50 - 120	44
RAFT / CDB	P(MEO_2MA-*co*-PEGMA)	P(MEO_2MA)	DEGDMA	Water/propanol (1:4 v:v)	2	$D_{swollen}$ = 90 - 300 $D_{collapsed}$ = 40 - 250	73
RAFT / CDB	P(GAPMAAm) or P(LAEMAAm)	P(MEO_2MA-*co*-GAPMAAm) or P(MEO_2MA-*co*-LAEMAAm)	DMAEP	Water/propanol (4:1 v:v)	4	$D_{swollen}$ = 85 - 315 $D_{collapsed}$ = 35 - 45	74
RAFT / CDB	P(MPC)	P(MEO_2MA-*co*-AEMAAm)	DMAEP	Water/propanol (4:1 v:v)	5	$D_{swollen}$ = 80 – 150 $D_{collapsed}$ = 50 - 110	75
RAFT / CDB	P(GAEMAAm) or P(GAPMAAm)	P(MEO_2MA-*co*-AEMAAm) or P(NIPAAm-*co*-AEMAAm)	DMAEP	Water/1,4-dioxane (3:2 v:v)	6	$D_{swollen}$ = 120 - 190 $D_{collapsed}$ = 60 - 80	76, 77
RAFT / ETC	PMEO_2A-*b*-PDMAAm or PNIPAAm-*b*-PDMAAm	PNIPAAm or P(MEO_2A)	MBA	Water/ethanol (65:35, v:v) Or Water	10	$D_{swollen}$ = 100 - 150 $D_{collapsed}$ = non specified	78

RAFT / ETC	P(DMAAm) or P(DMAAm-*b*-*n*BA)	PNIPAAm Or P(NIPAAm-*b*-*n*BA) or P(NIPAAm-*b*-FA) or P(NIPAAm-*b*-HEAAm) or P(NIPAAm-*b*-DAAAm) or	MBA or HDDA	Water/ethanol (3:1 v:v)	10	$D_{swollen}$ = 60 - 90 $D_{collapsed}$ = 45 - 55	79
RAFT / CDB	P(LAEMAAm) or P(LAEMAAm-*co*-AEMAAm) or P(LAEMAAm-*co*-MAA)	P(MEO_2MA) or P(MEO_2MA-*co*-LAEMAAm) or P(MEO_2MA-*co*-AEMAAm)	MBA	Water/propanol (4:1 v:v)	-	$D_{swollen}$ = 85 - 180 $D_{collapsed}$ = 60 - 95	80

Control agent: TTC-C12: *S*-1-dodecyl-*S'*-2-(2,2'-dimethylacetic acid) trithiocarbonate; TTC-C3: *S*-3-(propionic acid)-*S'*-2-(2,2'-dimethylacetic acid) trithiocarbonate; TTC-CNC3: 4-cyano-4-(ethylsulfanylthiocarbonyl)sulfanylpentanoic acid; CDB: 4-cyanopentanoic acid dithiobenzoate; BE-TTC: Benzyl ethyl trithiocarbonate; ETC: 2-ethylsulfanylthiocarbonylsulfanyl-propionic acid methyl ester.

Crosslinker: MBA: *N*,*N'*-methylenebisacrylamide; P(EGDMA): poly((ethylene glycol) dimethacrylate); P(EGDA): poly(ethylene glycol) diacrylate; DEGDMA: di(ethylene glycol) dimethacrylate; DMAEP: 2,2-dimethacroyloxy-1-ethoxypropane; HDDA: 1,6-hexanediol diacrylate.

Reactive macromolecular stabilizer/Polymer of the core: P(ANa): poly(sodium acrylate); P(DEAAm): poly(*N*,*N*-diethylacrylamide); P(DMAAm): poly(*N*,*N*-dimethylacrylamide); P(NIPAAm): poly(*N*-isopropylacrylamide); PEO: poly(ethylene oxide); P(DMAEMA): poly(*N*,*N'*-dimethylaminoethyl methacrylate); P(PEGMA): poly(poly(ethylene glycol) methyl ether methacrylate); P(MEO_2MA): poly(di(ethylene gycol) methyl ether methacrylate); P(MEOA): poly(2-methoxyethyl acrylate); P(PEGA): poly(poly(ethylene glycol) methyl ether acrylate); P(MPC): poly(2-methacryloyloxyethyl phosphorylcholine); P(S): poly(styrene); P(AEMAAm): poly(2-aminoethyl methacrylamide hydrochloride); P(GAEMAAm): poly(2-glucoamidoethyl methacrylamide); P(GAPMAAm): poly(2-glucoamidopropyl methacrylamide); P(LAEMAAm): poly(2-lactobionamidoethyl methacrylamide);P(*n*BA): poly(*n*-butyl acrylate); P(FA): poly(fluorescein O-acrylate); P(HEAAm): poly(N-(2-hydroxyethyl)acrylamide); P(DAAAm): poly(diacetone acrylamide); P(MAA): poly(methacrylic acid); P(MEO_2A): poly(di(ethyleneglycol) ethyl ether acrylate).

II. Objectives

The main objective of this PhD thesis was to synthesize and characterize PVCL-based thermoresponsive particles by surfactant-free batch emulsion polymerization, using a reactive macromolecular stabilizer.

One of the crucial points of this work consisted in using a hydrophilic reactive macromolecular stabilizer with a suitable end-group able to implement a fast-reversible reaction with the growing radical chains of the core-forming polymer. VCL is a non-conjugated monomer, which can only be polymerized via radical polymerization. Like for vinyl ester based monomers, the controlled radical polymerization (CRP) of vinyl amides has long been recognized as a challenge due to the difficulty in controlling the equilibrium between the non-stabilized radicals and the dormant species.[12, 81] In the recent years, various controlled radical polymerization techniques have been successfully applied to the control of VCL polymerization. These techniques include organometallic-mediated radical polymerization (OMRP),[19, 82, 83] ATRP,[84-86] and RAFT/MADIX polymerization.[17, 20-22, 87-106] It should be mentioned that all these studies concerning the control of VCL polymerization have been conducted in bulk or solution. So far, the control of VCL polymerization in aqueous dispersed media has not been investigated yet.

In this thesis, RAFT polymerization was elected as the CRP technique of choice for designing reactive macromolecular stabilizers suitable for VCL polymerization. It has been shown that the control of VCL polymerization by RAFT was mainly mediated by xanthates,[17, 20-22, 88-93, 97, 99-104, 106] and more scarcely by either dithiocarbamates,[87, 97, 101] or trithiocarbonate chain transfer agents (CTA).[87, 94-96]

In the present work, a xanthate was chosen for the design of the macromolecular chain transfer agent as reactive stabilizer. For that purpose, two strategies can be envisaged: 1) the chain-end functionalization of a preformed hydrophilic polymer with a xanthate agent or 2) the use of a xanthate agent to control the polymerization of a hydrophilic monomer. Both approaches were considered in this thesis, the first one in Chapter 2 of Part I and the second strategy was developed in Chapters 1 and 2 of Part II.

As summarized in **Table 3**, we investigated the synthesis of two types of PVCL-based thermoresponsive colloidal particles by surfactant-free emulsion polymerization carried out in the presence of a reactive macromolecular stabilizer.

Table 3. Summary of the developed strategies for the synthesis of PVCL-based thermoresponsive particles in aqueous dispersed media by using a reactive macromolecular stabilizer.

PART I - Physically crosslinked PVCL-based thermoresponsive particles	*PART II - Chemically crosslinked PVCL-based thermoresponsive microgels*
- Macromolecular reactive stabilizer synthesized by chain-end functionalization of a preformed polymer with a xanthate agent - *In-situ* synthesis of amphiphilic diblock copolymers simultaneously to particle growth (PISA) - Copolymerization of VCL with a hydrophobic co-monomer to prepare thermoresponsive particles via hydrophobic interactions	- Macromolecular reactive stabilizer synthesized by RAFT/MADIX polymerization of a cationic monomer - Involvement of the reactive chain-end of the cationic polymer in the stabilization efficiency of microgels - Copolymerization with a difunctional co-monomer to synthesize crosslinked thermoresponsive particles

For the synthesis of physically crosslinked thermoresponsive PVCL-based particles (Part I, **Scheme 11**), a poly(ethylene glycol)-xanthate was used as macromolecular chain transfer agent. Poly(ethylene glycol) is a biocompatible hydrophilic polymer widely used as stabilizer of particles, colloids, micelles. Vinyl acetate was chosen as the hydrophobic co-monomer, which polymerization can be successfully controlled by RAFT/MADIX technique using xanthate agents.[107-111]

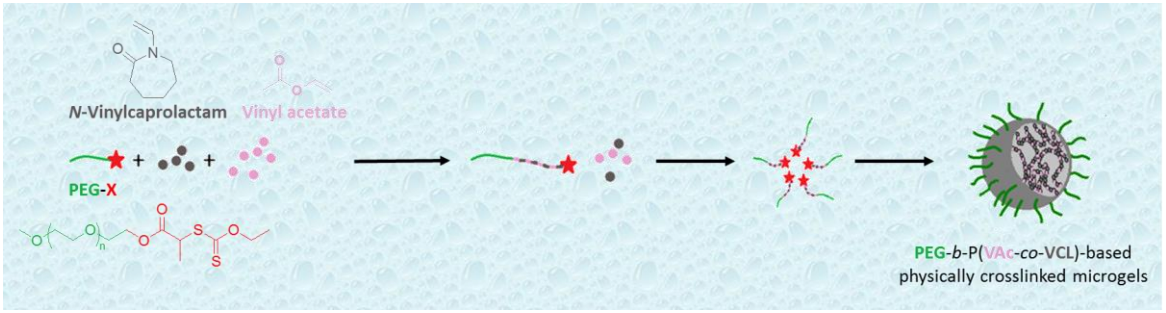

Scheme 11. Schematic representation of the synthesis by an emulsion polymerization process of the physically crosslinked PVCL-based particles by PISA.

For the synthesis of chemically crosslinked PVCL-based thermoresponsive particles (Part II, **Scheme 12**), a cationic poly([2-(acryloyloxy)ethyl]trimethylammonium chloride) was selected as macromolecular reactive stabilizer. Cationic polymers are attractive polymers due to their unique properties: they possess an antibacterial activity, they can interact with negatively charged molecules of interest (such as biomolecules, catalyst…), they can be deposited onto anionic surface (cellulose, mica, magnetic particles…), they can be used as flocculants, among others applications.[112] Thanks to their ability to electrostatically interact with relevant biological polyanions (SiRNA, DNA, proteins…), anionic tissues, anionic drugs and anionic inorganic particles, cationic polymers are very promising materials for biomedical applications and especially for the design of cargo carriers. In addition, they are known to facilitate cellular uptake via interaction with the negatively-charged cell membrane.[112]

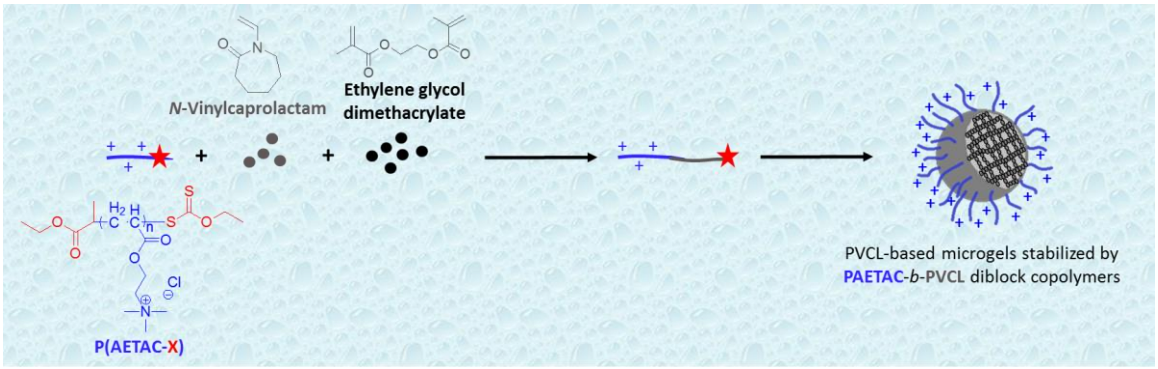

Scheme 12. Schematic representation of the synthesis of chemically crosslinked PVCL-based particles by using a reactive cationic macromolecular stabilizer by an emulsion or a precipitation polymerization process.

III. Contents

The present manuscript is divided into two main parts according to the two types of PVCL-based thermoresponsive particles presented in **Table 3**.

The first part (Part I) is devoted to the synthesis of PVCL-based block copolymer self-assembled thermoresponsive particles by emulsion polymerization, using a xanthate-terminated poly(ethylene glycol) (PEG-X) as macromolecular chain-transfer agent. Vinyl acetate (VAc) is used as hydrophobic co-monomer with the aim of synthesizing physically crosslinked thermoresponsive particles by means of hydrophobic interactions between VAc units.

The first chapter of this Part I describes a preliminary study to investigate the control of the RAFT/MADIX copolymerization of VAc and VCL in bulk. The reactivity ratios for VAc and VCL copolymerization are carefully determined by different methods. The effect of the P(VAc-*co*-VCL) copolymer composition on glass transition temperature, phase transition temperature and thermoresponsive self-assembly of the copolymers in water is also investigated.

The second chapter presents the synthesis of PVCL-based thermoresponsive particles by emulsion polymerization. The stabilization and growth of the P(VAc-*co*-VCL) block is controlled by a PEG macromolecular chain transfer agent. The functionalization of the chain-end of a commercially available PEG with a xanthate moiety is described. Insight into the control of RAFT/MADIX emulsion copolymerization of VAc and VCL as well as the features of the synthesized thermoresponsive colloidal particles, in relationship with the initial VAc monomer feed ratio is provided. The hydrolysis of thermoresponsive PEG-*b*-P(VAc-*co*-VCL) copolymers is attempted to produce poly(vinyl alcohol) (PVA)-based thermoresponsive copolymers upon methanolysis of PVAc under mild conditions.

The second part (Part II) is focused on the synthesis and characterization of cationic PVCL-based thermoresponsive microgels that are evaluated as potential drug nanocarriers.

The first chapter depicts the synthesis of the cationic poly[2-(acryloyloxy)ethyl]trimethylammonium chloride (P(AETAC)) polymers by RAFT/MADIX polymerization mediated by a xanthate molecular chain-transfer agent. The characterization of these polymers using different analytical techniques is described.

The second chapter presents the synthesis and characterization of the cationic thermoresponsive PVCL-based microgels by heterogeneous polymerization processes from the

P(AETAC-X) reactive cationic macromolecular chain-transfer agents. The influence of different synthesis variables (*i.e*, the concentrations of monomer, stabilizer, crosslinker and initiator) on the colloidal features of the microgel particles is thoroughly investigated. The inner morphology of the microgels is assessed by high-resolution ^{1}H transverse relaxation NMR measurements. Furthermore, the comparison of the stabilization efficiency of the reactive cationic stabilizers with the one of non-reactive P(AETAC) homologue is provided.

In the third chapter, the potential of the cationic thermoresponsive poly(*N*-vinylcaprolactam)-based microgels for drug delivery systems is assessed. For that purpose, the stability of the cationic PVCL-based microgels during incubation at 37°C in different biological mimicking media is monitored. The *in-vitro* cytotoxicity of bare and doxorubicin-loaded PVCL-based microgels using HeLa (cervical cancer cells) and RAW 264.7 (macrophage cells) cell lines is investigated. In addition, the microgel cellular uptake pathways are studied by confocal fluorescence microscopy using different inhibitors. Finally, the uptake and release of doxorubicin are evaluated.

IV. References

1. Riehemann, K.; Schneider, S. W.; Luger, T. A.; Godin, B.; Ferrari, M.; Fuchs, H. *Angewandte Chemie* **2009,** 48, (5), 872-97.
2. Naahidi, S.; Jafari, M.; Edalat, F.; Raymond, K.; Khademhosseini, A.; Chen, P. *Journal of controlled release : official journal of the Controlled Release Society* **2013,** 166, (2), 182-94.
3. Samanta, A.; Medintz, I. L. *Nanoscale* **2016,** 8, (17), 9037-95.
4. Gil, E.; Hudson, S. *Progress in Polymer Science* **2004,** 29, (12), 1173-1222.
5. Stuart, M. A.; Huck, W. T.; Genzer, J.; Muller, M.; Ober, C.; Stamm, M.; Sukhorukov, G. B.; Szleifer, I.; Tsukruk, V. V.; Urban, M.; Winnik, F.; Zauscher, S.; Luzinov, I.; Minko, S. *Nature materials* **2010,** 9, (2), 101-13.
6. De Las Heras Alarcon, C.; Pennadam, S.; Alexander, C. *Chemical Society reviews* **2005,** 34, (3), 276-85.
7. Hoffman, A. S. *Advanced drug delivery reviews* **2013,** 65, (1), 10-6.
8. Nayak, S.; Lyon, L. A. *Angewandte Chemie* **2005,** 44, (47), 7686-708.
9. Ramos, J.; Imaz, A.; Forcada, J. *Polym. Chem.* **2012,** 3, (4), 852-856.
10. Lutz, J. F.; Akdemir, O.; Hoth, A. *Journal of the American Chemical Society* **2006,** 128, (40), 13046-7.
11. Vancoillie, G.; Frank, D.; Hoogenboom, R. *Progress in Polymer Science* **2014,** 39, (6), 1074-1095.
12. Cortez-Lemus, N. A.; Licea-Claverie, A. *Progress in Polymer Science* **2016,** 53, 1-51.
13. Vihola, H.; Laukkanen, A.; Valtola, L.; Tenhu, H.; Hirvonen, J. *Biomaterials* **2005,** 26, (16), 3055-64.
14. Liu, J.; Debuigne, A.; Detrembleur, C.; Jerome, C. *Advanced healthcare materials* **2014,** 3, (12), 1941-68.

15. Tager, A. A.; Safronov, A. P.; Sharina, S. V.; Galaev, I. Y. *Colloid & Polymer Science* **1993,** 271, (9), 868-872.
16. Kirsh, Y. E.; Yanul, N. A.; Kalninsh, K. K. *European Polymer Journal* **1999,** 35, (2), 305-316.
17. Beija, M.; Marty, J. D.; Destarac, M. *Chemical communications* **2011,** 47, (10), 2826-8.
18. Yang, Y.; Tang, G.; Hu, M.; Shao, L.; Li, J.; Bi, Y. *Polymer* **2015,** 68, 213-220.
19. Kermagoret, A.; Fustin, C.-A.; Bourguignon, M.; Detrembleur, C.; Jérôme, C.; Debuigne, A. *Polymer Chemistry* **2013,** 4, (8), 2575.
20. Zhao, X.; Coutelier, O.; Nguyen, H. H.; Delmas, C.; Destarac, M.; Marty, J.-D. *Polym. Chem.* **2015,** 6, (29), 5233-5243.
21. Peng, H.; Kather, M.; Rübsam, K.; Jakob, F.; Schwaneberg, U.; Pich, A. *Macromolecules* **2015,** 48, (13), 4256-4268.
22. Peng, H.; Xu, W.; Pich, A. *Polym. Chem.* **2016,** 7, (31), 5011-5022.
23. Slomkowski, S.; Alemán, J. V.; Gilbert, R. G.; Hess, M.; Horie, K.; Jones, R. G.; Kubisa, P.; Meisel, I.; Mormann, W.; Penczek, S.; Stepto, R. F. T. *Pure and Applied Chemistry* **2011,** 83, (12).
24. Saunders, B. R.; Laajam, N.; Daly, E.; Teow, S.; Hu, X.; Stepto, R. *Advances in colloid and interface science* **2009,** 147-148, 251-62.
25. Roy, D.; Brooks, W. L.; Sumerlin, B. S. *Chemical Society reviews* **2013,** 42, (17), 7214-43.
26. Hertle, Y.; Hellweg, T. *Journal of Materials Chemistry B* **2013,** 1, (43), 5874.
27. Forcada, J., Responsive Polymeric Nanoparticles. In *Controlled Release Systems: Advances in Nanobottles and Active Nanoparticles*, Herk, A. M. V.; Forcada, J.; Pastorin, G., Eds. Pan Stanford: 2015; pp 21-36.
28. Boularas, M.; Gombart, E.; Tranchant, J.-F.; Billon, L.; Save, M. *Macromolecular Rapid Communications* **2015,** 36, (1), 79-83.
29. Boularas, M.; Deniau-Lejeune, E.; Alard, V.; Tranchant, J.-F.; Billon, L.; Save, M. *Polym. Chem.* **2016,** 7, (2), 350-363.
30. Zhang, Q. M.; Xu, W.; Serpe, M. J. *Angewandte Chemie International Edition* **2014,** 53, (19), 4827-4831.
31. Destribats, M.; Eyharts, M.; Lapeyre, V.; Sellier, E.; Varga, I.; Ravaine, V.; Schmitt, V. *Langmuir* **2014,** 30, (7), 1768-1777.
32. Yue, M.; Hoshino, Y.; Ohshiro, Y.; Imamura, K.; Miura, Y. *Angewandte Chemie International Edition* **2014,** 53, (10), 2777-2777.
33. Kawaguchi, H. *Polymer International* **2014,** 63, (6), 925-932.
34. Lyon, L. A.; Meng, Z.; Singh, N.; Sorrell, C. D.; St John, A. *Chemical Society reviews* **2009,** 38, (4), 865-74.
35. Smeets, N. M. B.; Hoare, T. *Journal of Polymer Science Part A: Polymer Chemistry* **2013,** 51, (14), 3027-3043.
36. Daniel, J. C.; Pichot, C., *Les latex synthétiques, Elaboration, propriétés, applications*. TEC and DOC edition Lavoisier: 2006.
37. Barandiaran, M. J.; Cal, J. C. d. l.; Asua, J. M., Emulsion Polymerization. In *Polymer Reaction Engineering*, Blackwell Publishing Ltd: 2008; pp 233-272.
38. Pich, A.; Richtering, W. *Advances in Polymer Science* **2010,** 234, 1-37.
39. Medeiros, S. F.; Santos, A. M.; Fessi, H.; Elaissari, A. *Journal of Polymer Science Part A: Polymer Chemistry* **2010,** 48, (18), 3932-3941.
40. Kawaguchi, S.; Ito, K. *Advances in Polymer Science* **2005,** 175, 299-328.
41. Klinger, D.; Aschenbrenner, E. M.; Weiss, C. K.; Landfester, K. *Polym. Chem.* **2012,** 3, (1), 204-216.
42. Pelton, R. *Advances in colloid and interface science* **2000,** 85, (1), 1-33.
43. Pelton, R. *Macromolecular Symposia* **2004,** 207, (1), 57-66.

44. Delaittre, G.; Save, M.; Charleux, B. *Macromolecular Rapid Communications* **2007,** 28, (15), 1528-1533.
45. An, Z.; Shi, Q.; Tang, W.; Tsung, C. K.; Hawker, C. J.; Stucky, G. D. *Journal of the American Chemical Society* **2007,** 129, (46), 14493-9.
46. Jenkins, A. D.; Jones, R. G.; Moad, G. *Pure and Applied Chemistry* **2009,** 82, (2).
47. Wang, J.-S.; Matyjaszewski, K. *Journal of the American Chemical Society* **1995,** 117, (20), 5614-5615.
48. Matyjaszewski, K. *Macromolecules* **2012,** 45, (10), 4015-4039.
49. Georges, M. K.; Veregin, R. P. N.; Kazmaier, P. M.; Hamer, G. K. *Macromolecules* **1993,** 26, (11), 2987-2988.
50. Nicolas, J.; Guillaneuf, Y.; Lefay, C.; Bertin, D.; Gigmes, D.; Charleux, B. *Progress in Polymer Science* **2013,** 38, (1), 63-235.
51. Chiefari, J.; Chong, Y. K.; Ercole, F.; Krstina, J.; Jeffery, J.; Le, T. P. T.; Mayadunne, R. T. A.; Meijs, G. F.; Moad, C. L.; Moad, G.; Rizzardo, E.; Thang, S. H. *Macromolecules* **1998,** 31, (16), 5559-5562.
52. Chong, Y. K.; Krstina, J.; Le, T. P. T.; Moad, G.; Postma, A.; Rizzardo, E.; Thang, S. H. *Macromolecules* **2003,** 36, (7), 2256-2272.
53. Chiefari, J.; Mayadunne, R. T. A.; Moad, C. L.; Moad, G.; Rizzardo, E.; Postma, A.; Thang, S. H. *Macromolecules* **2003,** 36, (7), 2273-2283.
54. Charmot, D.; Corpart, P.; Adam, H.; Zard, S. Z.; Biadatti, T.; Bouhadir, G. *Macromolecular Symposia* **2000,** 150, 23-32.
55. Destarac, M.; Bzducha, W.; Taton, D.; Gauthier-Gillaizeau, I.; Zard, S. Z. *Macromolecular Rapid Communications* **2002,** 23, (17), 1049-1054.
56. Moad, G.; Rizzardo, E.; Thang, S. H. *Australian Journal of Chemistry* **2012,** 65, (8), 985.
57. Moad, G.; Rizzardo, E.; Thang, S. H. *Australian Journal of Chemistry* **2005,** 58, (6), 379.
58. Moad, G.; Rizzardo, E.; Thang, S. H. *Australian Journal of Chemistry* **2006,** 59, (10), 669.
59. dos Santos, A. M.; Pohn, J.; Lansalot, M.; D'Agosto, F. *Macromolecular Rapid Communications* **2007,** 28, (12), 1325-1332.
60. Bernard, J.; Save, M.; Arathoon, B.; Charleux, B. *Journal of Polymer Science Part A: Polymer Chemistry* **2008,** 46, (8), 2845-2857.
61. Manguian, M.; Save, M.; Charleux, B. *Macromolecular Rapid Communications* **2006,** 27, (6), 399-404.
62. Bathfield, M.; D'Agosto, F.; Spitz, R.; Charreyre, M.-T.; Pichot, C.; Delair, T. *Macromolecular Rapid Communications* **2007,** 28, (15), 1540-1545.
63. Charleux, B.; Delaittre, G.; Rieger, J.; D'Agosto, F. *Macromolecules* **2012,** 45, (17), 6753-6765.
64. Ferguson, C. J.; Hughes, R. J.; Pham, B. T. T.; Hawkett, B. S.; Gilbert, R. G.; Serelis, A. K.; Such, C. H. *Macromolecules* **2002,** 35, (25), 9243-9245.
65. Delaittre, G.; Nicolas, J.; Lefay, C.; Save, M.; Charleux, B. *Chemical communications* **2005**, (5), 614-6.
66. Warren, N. J.; Armes, S. P. *Journal of the American Chemical Society* **2014,** 136, (29), 10174-85.
67. Derry, M. J.; Fielding, L. A.; Armes, S. P. *Progress in Polymer Science* **2016,** 52, 1-18.
68. Delaittre, G.; Save, M.; Gaborieau, M.; Castignolles, P.; Rieger, J.; Charleux, B. *Polymer Chemistry* **2012,** 3, (6), 1526.
69. Shen, W.; Chang, Y.; Liu, G.; Wang, H.; Cao, A.; An, Z. *Macromolecules* **2011,** 44, (8), 2524-2530.
70. Rieger, J.; Grazon, C.; Charleux, B.; Alaimo, D.; Jérôme, C. *Journal of Polymer Science Part A: Polymer Chemistry* **2009,** 47, (9), 2373-2390.

71. Yan, L.; Tao, W. *Polymer* **2010,** 51, (10), 2161-2167.
72. Liu, G.; Qiu, Q.; An, Z. *Polym. Chem.* **2012,** 3, (2), 504-513.
73. Kotsuchibashi, Y.; Narain, R. *Polymer Chemistry* **2014,** 5, (8), 3061.
74. Ahmed, M.; Narain, R. *Molecular pharmaceutics* **2012,** 9, (11), 3160-70.
75. Bhuchar, N.; Sunasee, R.; Ishihara, K.; Thundat, T.; Narain, R. *Bioconjugate chemistry* **2012,** 23, (1), 75-83.
76. Sunasee, R.; Wattanaarsakit, P.; Ahmed, M.; Lollmahomed, F. B.; Narain, R. *Bioconjugate chemistry* **2012,** 23, (9), 1925-33.
77. Ahmed, M.; Wattanaarsakit, P.; Narain, R. *Polymer Chemistry* **2013,** 4, (13), 3829.
78. Li, Y.; Ye, Z.; Shen, L.; Xu, Y.; Zhu, A.; Wu, P.; An, Z. *Macromolecules* **2016,** 49, (8), 3038-3048.
79. Xu, Y.; Li, Y.; Cao, X.; Chen, Q.; An, Z. *Polym. Chem.* **2014,** 5, (21), 6244-6255.
80. Quan, S.; Wang, Y.; Zhou, A.; Kumar, P.; Narain, R. *Biomacromolecules* **2015,** 16, (7), 1978-86.
81. Harrisson, S.; Liu, X.; Ollagnier, J.-N.; Coutelier, O.; Marty, J.-D.; Destarac, M. *Polymers* **2014,** 6, (5), 1437-1488.
82. Thomassin, J.-M.; Mathieu, K.; Kermagoret, A.; Fustin, C.-A.; Jérôme, C.; Debuigne, A. *Polym. Chem.* **2015,** 6, (10), 1856-1864.
83. Hurtgen, M.; Liu, J.; Debuigne, A.; Jerome, C.; Detrembleur, C. *Journal of Polymer Science Part A: Polymer Chemistry* **2012,** 50, (2), 400-408.
84. Jiang, X.; Li, Y.; Lu, G.; Huang, X. *Polym. Chem.* **2013,** 4, (5), 1402-1411.
85. Singh, P.; Srivastava, A.; Kumar, R. *Journal of Polymer Science Part A: Polymer Chemistry* **2012,** 50, (8), 1503-1514.
86. Tang, G.; Hu, M.; Ma, Y.; You, D.; Bi, Y. *RSC Adv.* **2016,** 6, (49), 42786-42793.
87. Shao, L.; Hu, M.; Chen, L.; Xu, L.; Bi, Y. *Reactive and Functional Polymers* **2012,** 72, (6), 407-413.
88. Gois, J. R.; Costa, J. R.; Popov, A. V.; Serra, A. C.; Coelho, J. F. *RSC advances* **2016,** 6, (21), 16996-17007.
89. Liu, J.; Detrembleur, C.; De Pauw-Gillet, M.-C.; Mornet, S.; Duguet, E.; Jérôme, C. *Polym. Chem.* **2014,** 5, (3), 799-813.
90. Cai, T.; Li, M.; Zhang, B.; Neoh, K.-G.; Kang, E.-T. *J. Mater. Chem. B* **2014,** 2, (7), 814-825.
91. Liang, X.; Kozlovskaya, V.; Cox, C. P.; Wang, Y.; Saeed, M.; Kharlampieva, E. *Journal of Polymer Science Part A: Polymer Chemistry* **2014,** 52, (19), 2725-2737.
92. Liu, F.; Kozlovskaya, V.; Medipelli, S.; Xue, B.; Ahmad, F.; Saeed, M.; Cropek, D.; Kharlampieva, E. *Chemistry of Materials* **2015,** 27, (23), 7945-7956.
93. Barabanova, A. I.; Blagodatskikh, I. V.; Vyshivannaya, O. V.; Klimova, T. P.; Grinberg, N. V.; Burova, T. V.; Muranov, A. V.; Lozinskii, V. I.; Grinberg, V. Y.; Peregudov, A. S.; Khokhlov, A. R. *Doklady Chemistry* **2015,** 465, (1), 253-256.
94. Singh, P.; Srivastava, A.; Kumar, R. *Polymer* **2015,** 57, 51-61.
95. Ponce-Vargas, S. M.; Cortez-Lemus, N. A.; Licea-Claveríe, A. *Macromolecular Symposia* **2013,** 325-326, (1), 56-70.
96. Cortez-Lemus, N. A.; Licea-Claverie, A. *Journal of Polymer Science Part A: Polymer Chemistry* **2016,** 54, (14), 2156-2165.
97. Bi, Y.; Yan, C.; Shao, L.; Wang, Y.; Ma, Y.; Tang, G. *Journal of Polymer Science Part A: Polymer Chemistry* **2013,** 51, (15), 3240-3250.
98. Tebaldi, M. L.; Leal, D. A.; Montoro, S. R.; Petzhold, C. *Materials Research* **2014,** 17, 191-196.

99. Karesoja, M.; Karjalainen, E.; Hietala, S.; Tenhu, H. *The journal of physical chemistry. B* **2014,** 118, (36), 10776-84.
100. Tian, W.; Lv, X.; Huang, L.; Ali, N.; Kong, J. *Macromolecular Chemistry and Physics* **2012,** 213, (23), 2450-2463.
101. Wan, D.; Zhou, Q.; Pu, H.; Yang, G. *Journal of Polymer Science Part A: Polymer Chemistry* **2008,** 46, (11), 3756-3765.
102. Hou, L.; Wu, P. *Soft Matter* **2014,** 10, (20), 3578-86.
103. Yu, Y. C.; Kang, H. U.; Youk, J. H. *Colloid and Polymer Science* **2012,** 290, (12), 1107-1113.
104. Yu, Y. C.; Li, G.; Kim, J.; Youk, J. H. *Polymer* **2013,** 54, (22), 6119-6124.
105. Aguirre, G.; Ramos, J.; Heuts, J. P. A.; Forcada, J. *Polymer Chemistry* **2014,** 5, (15), 4569.
106. Peng, H.; Rübsam, K.; Huang, X.; Jakob, F.; Karperien, M.; Schwaneberg, U.; Pich, A. *Macromolecules* **2016,** 49, (19), 7141-7154.
107. Stenzel, M. H.; Cummins, L.; Roberts, G. E.; Davis, T. P.; Vana, P.; Barner-Kowollik, C. *Macromolecular Chemistry and Physics* **2003,** 204, (9), 1160-1168.
108. Favier, A.; Barner-Kowollik, C.; Davis, T. P.; Stenzel, M. H. *Macromolecular Chemistry and Physics* **2004,** 205, (7), 925-936.
109. Bernard, J.; Favier, A.; Zhang, L.; Nilasaroya, A.; Davis, T. P.; Barner-Kowollik, C.; Stenzel, M. H. *Macromolecules* **2005,** 38, (13), 5475-5484.
110. Theis, A.; Davis, T. P.; Stenzel, M. H.; Barner-Kowollik, C. *Polymer* **2006,** 47, (4), 999-1010.
111. Bernard, J.; Favier, A.; Davis, T. P.; Barner-Kowollik, C.; Stenzel, M. H. *Polymer* **2006,** 47, (4), 1073-1080.
112. Ramos, J.; Forcada, J.; Hidalgo-Alvarez, R. *Chemical reviews* **2014,** 114, (1), 367-428.

- PART I -

Physically crosslinked PVCL-based thermoresponsive particles

Introduction of Part I

Thermoresponsive polymers are polymers that undergo a conformation phase transition in response to a change of temperature.[1-4] Among the several well-known thermoresponsive polymers, poly(*N*-vinylcaprolactam) (PVCL) has raised an increasing interest over the last years as reported in recent reviews.[5-7] This biocompatible polymer, with lower critical solution temperature (LCST) in water ranging between 30 – 40 °C,[5, 8] is attractive for different applications such as delivery systems,[6, 9, 10] particle stabilization[11] or emulsion stabilization.[12] An effective means of tuning the temperature in which the change of PVCL-chain solvation state occurs is to control both the polymer chain length,[13-16] and the introduction of co-monomers in the polymer chain.[15-18] It is thus of interest to control the molar mass and the co-monomer distribution along the chain when synthesizing thermoresponsive statistical copolymers. Among the different co-monomers that can be used to tune the phase transition temperature of PVCL chains in water, vinyl acetate (VAc) is an attractive co-monomer due to the wide range of applications of poly(vinyl acetate). Poly(vinyl acetate) (PVAc) is used in a vast number of applications, the most common being binder for adhesive formulation, for the paper industry and for latex paints.[19, 20] Moreover, PVAc is approved by Food and Drug Administration (FDA) and it is a precursor of poly(vinyl alcohol) (PVA) which is a biocompatible and biodegradable hydrophilic polymer that is used in many technical (textile, papermaking) or food applications.[20] PVA is for instance used as efficient thickener, protective colloids, component of water-soluble film useful for packaging.[20] Nowadays, the raw materials for vinyl acetate monomer are produced from fossil resources. In the context of sustainable development, it can be mentioned that bioethanol produced from renewable resource could substitute the feedstock for these raw materials (**Figure 1**). Therefore, if the "vinyl acetate circle" can be closed by the important steps of hydrolysis and complete biodegradation of vinyl ester-based polymers to carbon dioxide, the whole production of PVAc could be switched to a renewable, sustainable and CO_2-neutral production process based on bioethanol (**Figure 1**).[20]

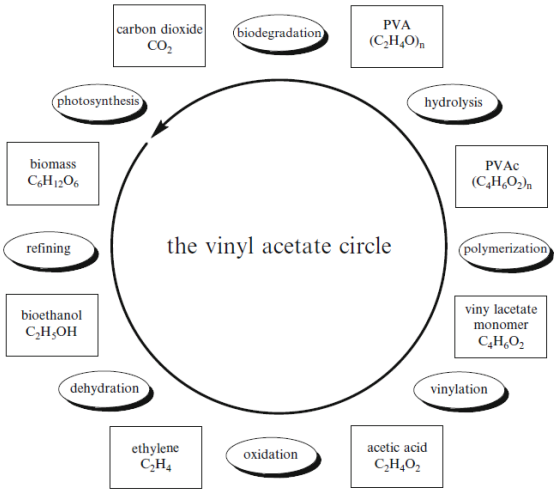

Figure 1. Vision of the "VAc circle" wholly based on ethanol as a raw material source (from reference 20).

The first chapter of this Part I will present a study of the macromolecular features and the microstructure of P(VAc-*co*-VCL) amphiphilic copolymers synthesized by controlled radical polymerization in homogeneous media. Their self-assembly behavior in water will be considered.

It is also of interest to implement the synthesis of the P(VAc-*co*-VCL) from homogeneous media (bulk) to polymerization in aqueous dispersed media. Emulsion polymerization is one of the most widely used process to industrially produce polymers as colloids dispersed in a continuous water phase. This polymerization process presents many advantages compared to polymerizations performed in bulk or in organic solution. Indeed, the use of water as continuous phase facilitates heat transfer of the exothermic polymerization, decreases the viscosity of the final product which facilitates polymer recovery from the reactor at the end of the polymerization and is more environmentally safe by limiting the amount of volatile organic compounds. In this context, the synthesis of the thermoresponsive P(VAc-*co*-PVCL) statistical copolymers by emulsion polymerization is attractive. This will be the purpose of the work reported in the second chapter of this Part I. Via the use of a poly(ethylene glycol) (PEG) macromolecular chain-transfer agent, we will study the synthesis of PEGylated particles of P(VAc-*co*-PVCL) copolymers directly in the aqueous phase by emulsion polymerization. The thermoresponsive behavior of the particles formed by hydrophobic intermolecular interactions will be explored in detail.

References

1. Liu, R.; Fraylich, M.; Saunders, B. R. *Colloid and Polymer Science* **2009,** 287, (6), 627-643.
2. Aseyev, V.; Tenhu, H.; Winnik, F. M. *Advances in Polymer Science* **2010,** 242, 29-89.
3. Roy, D.; Brooks, W. L.; Sumerlin, B. S. *Chemical Society reviews* **2013,** 42, (17), 7214-43.
4. Vancoillie, G.; Frank, D.; Hoogenboom, R. *Progress in Polymer Science* **2014,** 39, (6), 1074-1095.
5. Ramos, J.; Imaz, A.; Forcada, J. *Polymer Chemistry* **2012,** 3, (4), 852-856.
6. Liu, J.; Debuigne, A.; Detrembleur, C.; Jerome, C. *Advanced healthcare materials* **2014,** 3, (12), 1941-68.
7. Cortez-Lemus, N. A.; Licea-Claverie, A. *Progress in Polymer Science* **2016,** 53, 1-51.
8. Vihola, H.; Laukkanen, A.; Valtola, L.; Tenhu, H.; Hirvonen, J. *Biomaterials* **2005,** 26, (16), 3055-64.
9. Rejinold, N. S.; Muthunarayanan, M.; Divyarani, V. V.; Sreerekha, P. R.; Chennazhi, K. P.; Nair, S. V.; Tamura, H.; Jayakumar, R. *Journal of colloid and interface science* **2011,** 360, (1), 39-51.
10. Singh, P.; Srivastava, A.; Kumar, R. *Polymer* **2015,** 57, 51-61.
11. Liu, J.; Detrembleur, C.; De Pauw-Gillet, M.-C.; Mornet, S.; Duguet, E.; Jérôme, C. *Polymer Chemistry* **2014,** 5, (3), 799-813.
12. Verbrugghe, S.; Bernaerts, K.; Du Prez, F. E. *Macromolecular Chemistry and Physics* **2003,** 204, (9), 1217-1225.
13. Tager, A. A.; Safronov, A. P.; Sharina, S. V.; Galaev, I. Y. *Colloid & Polymer Science* **1993,** 271, (9), 868-872.
14. Beija, M.; Marty, J. D.; Destarac, M. *Chemical communications* **2011,** 47, (10), 2826-8.
15. Peng, H.; Kather, M.; Rübsam, K.; Jakob, F.; Schwaneberg, U.; Pich, A. *Macromolecules* **2015,** 48, (13), 4256-4268.
16. Peng, H.; Xu, W.; Pich, A. *Polym. Chem.* **2016,** 7, (31), 5011-5022.
17. Zhao, X.; Coutelier, O.; Nguyen, H. H.; Delmas, C.; Destarac, M.; Marty, J.-D. *Polymer Chemistry* **2015,** 6, (29), 5233-5243.
18. Kermagoret, A.; Fustin, C.-A.; Bourguignon, M.; Detrembleur, C.; Jérôme, C.; Debuigne, A. *Polymer Chemistry* **2013,** 4, (8), 2575.
19. Harrisson, S.; Liu, X.; Ollagnier, J.-N.; Coutelier, O.; Marty, J.-D.; Destarac, M. *Polymers* **2014,** 6, (5), 1437-1488.
20. Amann, M.; Minge, O., Biodegradability of Poly(vinyl acetate) and Related Polymers. In *Synthetic Biodegradable Polymers*, Rieger, B.; Künkel, A.; Coates, G. W.; Reichardt, R.; Dinjus, E.; Zevaco, T. A., Eds. Springer Berlin Heidelberg: 2012; Vol. 245, pp 137-172.

PART I - CHAPTER 1. RAFT/MADIX bulk copolymerization of vinyl acetate and *N*-vinylcaprolactam: kinetics, control, copolymer composition and thermoresponsive self-assembly

I. Introduction

During the last decades, controlled radical polymerization (CRP), also recently named reversible- deactivation radical polymerization (RDRP),[1] has been extensively investigated to precisely control molar mass, dispersity, architecture and microstructure of a wide range of (co)polymers.[2] The most developed CRP techniques are nitroxide mediated polymerization (NMP),[3, 4] atom transfer radical polymerization (ATRP),[5, 6] copper(0)-mediated radical polymerization,[7-10] reversible addition-fragmentation chain transfer (RAFT)[11-13] including macromolecular design via the interchange of xanthates (MADIX),[14, 15] reversible iodine transfer polymerization (RITP)[16] and organometallic-mediated radical polymerization (OMRP).[17, 18] Some RDRP techniques have been successfully transposed from homogeneous system in bulk or solution to heterogeneous systems such as emulsion polymerization,[19-22] dispersion polymerization[23-25] and surface-initiated polymerization from solid substrates.[26-29]

Despite the interest of the so-called less activated monomers (LAM) such as vinyl acetate (VAc), *N*-vinylcaprolactam (VCL) or *N*-vinylpyrrolidone (VP), the controlled radical polymerization of these non-conjugated monomer has been implemented only since the recent years, in RAFT/MADIX polymerization,[30-37] OMRP,[38-43] RITP[44] and ATRP.[45-47] RAFT/MADIX polymerization afforded the possibility to synthesize various PVCL-based copolymers such as block copolymers (P(VAc-*b*-VCL),[32] P(VCL-*b*-VP)[48]) or statistical copolymers (P(VP-*stat*-VCL)[49, 50]). Cobalt-mediated polymerization also produced well-defined P(VAc-*b*-VCL),[40] P(VCL-*b*-(VCL-*stat*-VP)),[42] P(VAc-*b*-VCL-*b*-VAc), P(VCL-*b*-(VCL-*stat*-VP)-*b*-VCL) di- and triblock copolymers[40] and P(VCL-*stat*-VAc),[39] P(VCL-*stat*-VP)[42] statistical copolymers. Among controlling the molar mass and dispersity via RDRP, copolymerization kinetics and associated effect on copolymer composition assist in the design of statistical copolymers with suitable performances. Indeed, both copolymer composition and monomer distribution of statistical polymer sequences can affect properties such as phase transition temperature,[39, 49, 51] block-statistical copolymer self-assembly,[52, 53] cyclization[54] and rheological properties of copolymers self-assembled either in water[55, 56] or in bulk.[57, 58] It requires the most accurate values of the reactivity ratios. However, the discrepancy between the values of reactivity ratios reported in the literature for VAc and VCL copolymerization (r_{VAc} = 0.63 and r_{VCL} = 0.31 (bulk),[59, 60] r_{VAc} = 0.36 and r_{VCL} = 1.06 (bulk),[39, 61] r_{VAc} = 0.35 and r_{VCL} = 2.5 (media not reported),[62, 63] r_{VAc} = 0.3 and r_{VCL} = 2.2 (ethanol),[59] r_{VAc} = 0.3 and r_{VCL} = 1.3 (butanol)[59]) provides uncertainty in the monomer sequence along the chain. This might limit the development of more complex materials based on VAc and VCL copolymers. It is thus of

interest in the present work to explore how effective is RAFT/MADIX polymerization at controlling the copolymerization of VAc and VCL monomers for various initial monomer feed compositions. Special attention is dedicated to the copolymer compositions. Nonlinear least-squares methods and linearization methods are examined to accurately determine the reactivity ratios of VAc and VCL. The influence of the P(VAc-*co*-VCL) copolymer composition on glass transition temperature, phase transition temperature, and copolymer self-assembly is investigated.

II. Experimental part

1. Materials

Vinyl acetate (VAc, Sigma Aldrich, 99 %$^{+}$) was mixed with inhibitor removers (Sigma Aldrich, 0.1 g of inhibitor remover for 50 mL of VAc) for 30 minutes prior to being filtered and used for polymerization. *N*-vinylcaprolactam (VCL, Sigma Aldrich, 98 %) was distilled under reduced pressure (P = 0.05 mmHg) in the presence of hydroquinone (Sigma Aldrich, 99 %$^{+}$). Azobis(isobutyronitrile) (AIBN, Sigma Aldrich, 98 %), 1,3,5-trioxane (Sigma Aldrich, ≥ 99 %), diethyl ether (Sigma Aldrich, ≥ 99.8 %), ethyl-2-bromopropionate (EBP; Sigma Aldrich, 99 %) and potassium ethyl xanthogenate (Sigma Aldrich, 96 %) were used as received. Acetone (VWR, technical grade, 98 %) was dried over molecular sieves (Sigma Aldrich, 4 Å, 4-8 mesh beads) for 24 hours.

2. Synthesis of the *O*-ethyl-*S*-(1-ethoxycarbonyl)ethyldithiocarbonate molecular chain-transfer agent

The *O*-ethyl-*S*-(1-ethoxycarbonyl)ethyldithiocarbonate molecular transfer agent was synthesized according to a previously described procedure.[64] Prior to the reaction, acetone was dried over molecular sieves overnight. Ethyl-2-bromopropionate (3.0 g, 16 mmol) and dried acetone (19.7 g, 20 mL) were introduced in a 50 mL round-bottom flask maintained in an ice-bath. Then potassium ethyl xanthogenate (4.0 g, 25 mmol, 1.5 × n_{EBP}) was added by shots of 0.5 g during 30 minutes under stirring. The mixture was stirred for 24 h at 0° C. The solution was filtered three times in order to eliminate the potassium bromide salts formed during the synthesis. After removing acetone by rotary evaporation, the crude product was purified by flash column chromatography (Teledyne Isco Combiflash Rf 75 flash chromatography) on silica column (RediSep normal-phase silica flash columns, 40 g column size for 2 g of product to purify) using a mobile phase of dichloromethane. Fractions containing the pure product were

pooled and the solvent was removed by rotary evaporation. After being dried for overnight under vacuum, the final product was obtained as a yellow oil (yield: 60 %).

3. General procedure for the synthesis of P(VAc-*co*-VCL) statistical copolymer in bulk

Polymerizations were performed with a total of 5 g of monomers, varying the initial molar fraction of VAc and VCL from $f_{VAc,0}$ = 0 to 1. The initial concentration of xanthate agent was ranging from 1.6 to 2.4 mol.L^{-1} and the ratio between monomer concentration and xanthate agent concentration ranged between 420 and 460 (**Table 1**).

In a typical experiment (Expt 7 in **Table 2**), xanthate agent (36.5 mg, 1.10 × 10^{-4} mol), AIBN (5.4 mg, 3.30 × 10^{-5} mol), VCL (2.00 g, 1.44 × 10^{-2} mol), 1,3,5-trioxane (0.887 g, 9.86 × 10^{-3} mol) and VAc (3.04 g, 3.53 × 10^{-2} mol) were introduced into a 10 mL round-bottom flask and stirred magnetically. The mixture was degassed by nitrogen bubbling during 3 minutes in an ice bath. The flask was weighed before and after degassing to ensure the absence of VAc evaporation during this step. A sample was withdrawn under nitrogen at time t = 0. The round-bottom flask was placed into an oil bath previously heated to 65°C. Samples were withdrawn every hour until the reaction was stopped (6 hours) by cooling down in an ice-water bath and by the introduction of oxygen in the mixture. Individual conversions of monomers were calculated from nuclear magnetic resonance spectra using 1,3,5-trioxane as internal standard (Equation 1).

$$x_{\text{mono.}} = \mathbf{1} - \frac{\left(I_{1\text{H}_{\text{mono.}}} / I_{1\text{H}_{\text{triox.}}}\right)_t}{\left(I_{1\text{H}_{\text{mono.}}} / I_{1\text{H}_{\text{triox.}}}\right)_0} \qquad \text{Equation 1}$$

$I_{1H,triox}$ corresponds to the integral of one proton of 1,3,5-trioxane (5.1 ppm, 6 H) used as internal standard and $I_{1H,mono}$ corresponds to either the integral of the proton of VCL monomer at 3.6 ppm ($I_{1H,VCL}$, 2 H) or VAc monomer at 7.1-7.4 ppm ($I_{1H,VAc} = I_{7.1\text{-}7.4\ ppm} - I_{1H,VCL}/2$) (see **Figure 1**).

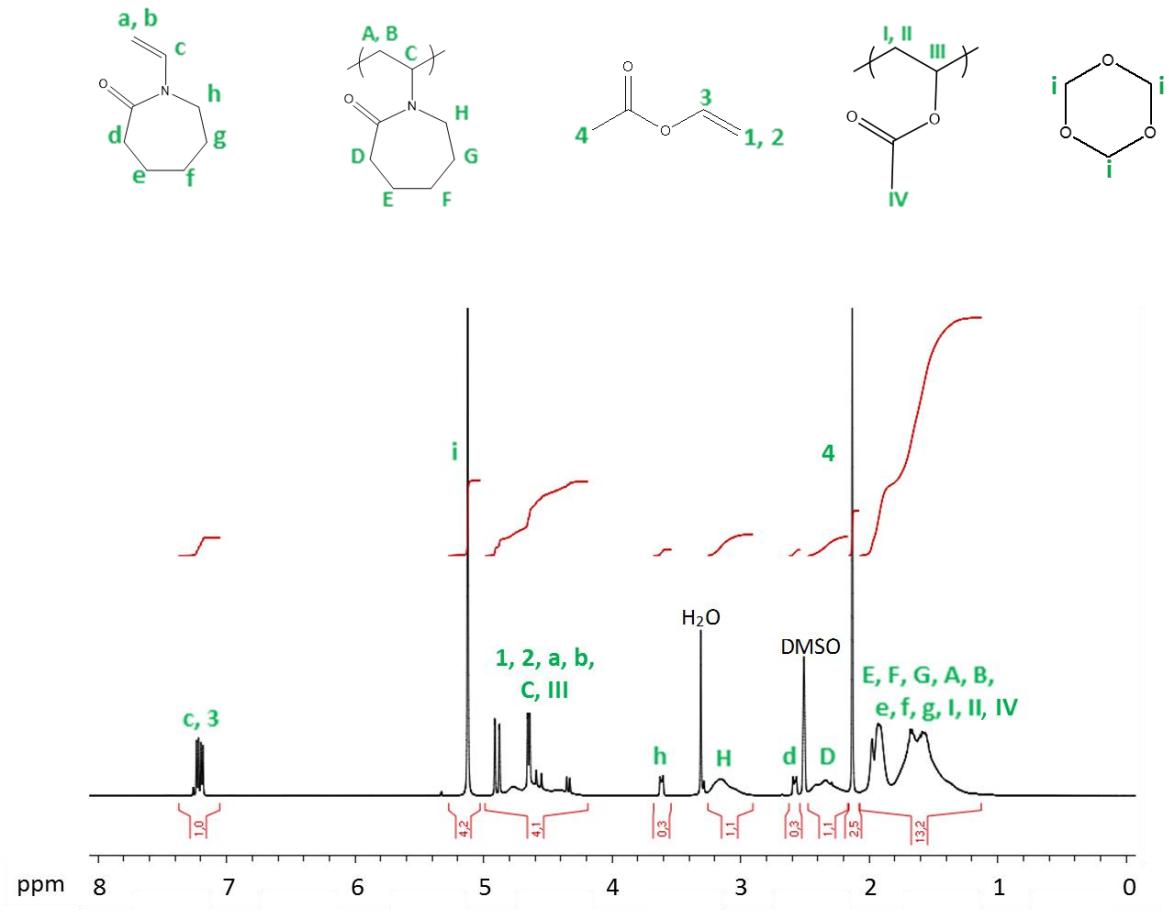

Figure 1. ^{1}H NMR spectrum in DMSO-d_6 of the crude solution ($t_{polym.}$ = 4 h) of VAc/VCL copolymerization for polymerization carried out with $f_{VAc,0}$ = 0.71.

The final overall molar and weight conversions (respectively named X_m and X_w) were calculated from the monomer individual conversions (x_{VAc}, x_{VCL}, Equation 1) according to Equation 2 and Equation 3 (n_0 and m_0 are respectively the initial number of moles and the initial mass of each monomer).

$$X_m = \frac{x_{VAc} \times n_{0,VAc} + x_{VCL} \times n_{0,VCL}}{n_{0,VAc} + n_{0,VCL}} \quad \text{Equation 2}$$

$$X_w = \frac{x_{VAc} \times m_{0,VAc} + x_{VCL} \times m_{0,VCL}}{m_{0,VAc} + m_{0,VCL}} \quad \text{Equation 3}$$

The molar fraction of the VAc monomer incorporated into the copolymer (F_{VAc}) was calculated from the monomer individual conversion (x_{VAc}, x_{VCL}, Equation 1) and the initial number of moles of monomers ($n_{0,VAc}$ and $n_{0,VCL}$), according to Equation 4.

$$F_{VAc} = \frac{x_{VAc} \times n_{0,VAc}}{x_{VAc} \times n_{0,VAc} + x_{VCL} \times n_{0,VCL}} \quad \text{Equation 4}$$

The weight fraction of VAc in the copolymer (w_{VAc}) was obtained from Equation 5, considering the molar fraction of the monomers in the copolymer (F_{mono}, Equation 4) and the molar masses of each monomer (M_{VCL} = 139 g.mol^{-1} and M_{VAc} = 86 g.mol^{-1}).

$$w_{VAc} = \frac{F_{VAc} \times M_{VAc}}{F_{VAc} \times M_{VAc} + F_{VCL} \times M_{VCL}}$$ Equation 5

4. Characterization methods

Nuclear Magnetic Resonance (NMR) spectroscopy. NMR spectra were recorded using a Bruker 400 MHz spectrometer at 25 °C. ^{1}H measurements were performed at frequencies of 400 MHz and ^{13}C measurements at 100 MHz. Deuterated dimethyl sulfoxide DMSO-d_6 and deuterated chloroform $CDCl_3$ were used as solvents for respectively the crude and precipitated polymers. $CDCl_3$ was used as solvent for the characterization of the xanthate agent.

Dynamic Light Scattering (DLS). The measurements of the hydrodynamic diameter D_h, as a function of the temperature for the P(VAc-*co*-VCL) copolymers dispersed at 5 g.L^{-1} in deionized water, were carried out on a Nano-ZS, Model ZEN3600 (Malvern, UK) zetasizer at an angle of 173°. A He-Ne 4.0mW power laser was used, operating at a wavelength of 633 nm. For evaluation of the data, the DTS (Nano) program was used. The hydrodynamic diameters were calculated from the diffusion coefficient using the Stokes-Einstein equation $D_h = \frac{k_B T}{3\pi\eta D}$ where T is absolute temperature, η the viscosity of the solvent, k_B the Boltzmann constant and D the diffusion coefficient. The hydrodynamic diameters of the P(VAc-*co*-VCL) copolymers were also measured accurately using an ALV setup (Langen, Germany). The value of D_h below the cloud point was calculated from the diffusion coefficient using the Stokes-Einstein equation and was extrapolated to zero concentration and zero-q values.

Static Light Scattering (SLS). Light scattering measurements were performed on an ALV setup (Langen, Germany), consisting of a 22 mW He−Ne laser, operating at a wavelength of λ = 632.8 nm, an ALV CGS/8F goniometer, an ALV High QE APD detector, and an ALV 5000/EPP multibit, multiautocorrelator. All the measurements were carried out at temperature below the cloud point, for scattering angles, θ, ranging from 30° to 150°. For P(VAc-*co*-VCL) copolymers with F_{VAc} inferior to 0.3, the measurements were performed at polymer concentrations ranging between 1 g.L^{-1} and 20 g.L^{-1} while for the P(VAc-*co*-VCL) copolymer with F_{VAc} of 0.53, the temperature of measurement was set at 10°C at polymer concentrations range of 1 - 4 g.L^{-1}. The weight-average molar mass of the scatterers (M_w) was determined using the Zimm equation

(Equation 6). The average scattered intensity of the sample (I_{sample}) is measured in relation to the average scattered intensity of the solvent ($I_{solvent}$) and a standard ($I_{standard}$). The Rayleigh ratio (R_θ) of the sample, which corresponds to the normalized contribution of the sample to the scattering intensity, is then determined based on the known Rayleigh ratio of the standard ($R_{\theta,standard}$, here we used toluene with $R_{\theta,Toluene}$ = 2.79 x 10^{-5} cm^{-1}), see Equation 7. The ratio $K.c/R_\theta$ can then be determined using equations 6 to 9, taking into account the wavelength of the laser (λ), the refractive index of the standard ($n_{standard}$), the refractive index increment (dn/dc) of the sample and Avogadro's number (N_A).

$$\frac{K.c}{R_\theta} = \frac{q^2 R_g^2}{3M_w} + \frac{1}{M_w} + 2A_2c \quad \text{Equation 6}$$

$$R_\theta = \frac{I_{sample} - I_{solvent}}{I_{standard}} R_{\theta,standard} \quad \text{Equation 7}$$

$$\boldsymbol{K} = \frac{4\pi^2 n_{standard}^2 (dn/dc)^2}{N_A \lambda^4} \quad \text{Equation 8}$$

$$q = \frac{4\pi n_{solvent}}{\lambda} sin\frac{\theta}{2} \quad \text{Equation 9}$$

For all of the samples, the resulting distribution of relaxation times obtained via DLS was bimodal. To account for the presence of the larger aggregates in the SLS experiments, the relative scattered intensity contributions from fast and slow modes of relaxation were determined from the DLS data, which allowed for the calculation of the Rayleigh ratio for the fast mode only ($R_{\theta,fast}$, Equation 10).[65-67]

$$R_{\theta,fast} = A_{fast}(\theta) \frac{I_{sample}(\theta) - I_{solvent}(\theta)}{I_{standard}(\theta)} R_{\theta,standard} \quad \text{Equation 10}$$

A_{fast} (θ) is the scattered intensity contribution from the fast mode of relaxation at a given scattering angle determined by DLS, I_{sample}, $I_{solvent}$, and $I_{standard}$ are the scattered intensities at angle θ, by the sample, solvent, and reference liquid, respectively, and $R_{\theta,standard}$ is the Rayleigh ratio for the toluene used as the standard. The $K.c/R_{\theta,fast}$ values were averaged across the different q-values and plotted versus concentration to determine the absolute weight-average molar mass ($M_{w,\,aggregate}$) (**Figure 2**). The aggregation number was calculated as follows: $N_{agg} = M_{w,aggregate}/M_{w,polymer}$, with $M_{w,polymer}$ corresponding to M_w of the copolymer measured by SEC in THF from MALLS detector.

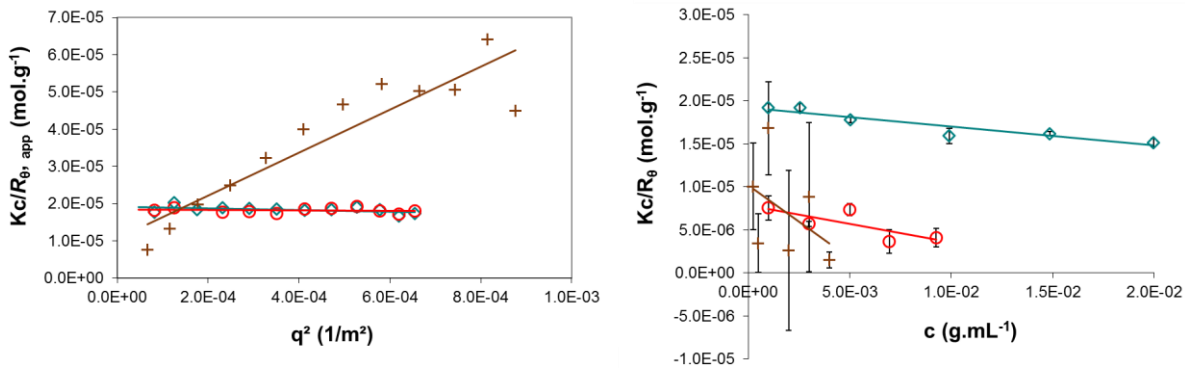

Figure 2. (a) Angular dependence of $K.c/R_\theta = f(q^2)$ measured at 3 g.L^{-1} and **(b)** concentration dependence of $K.c/R_\theta$ for copolymers with ◇ F_{VAc} = 0.19, ○ F_{VAc} = 0.28 and + F_{VAc}= 0.53.

The specific refractive index increment values (d*n*/d*c*) of the aqueous solutions of copolymers were determined at 20°C with a T-rEX (Wyatt) differential refractometer, operating at a wavelength of λ = 632 nm, at concentrations ranging from 0.2 to 1 g.L^{-1}. The following values were measured: d*n*/d*c* = 0.177 ± 0.001 mL.g^{-1} (F_{VAc} = 0.28), d*n*/d*c* = 0.171 ± 0.005 mL.g^{-1} (F_{VAc} = 0.19) and d*n*/d*c* = 0.163 ± 0.008 mL.g^{-1} (PVCL). According to these values, the d*n*/d*c* of the copolymer with F_{VAc} = 0.53 was extrapolated at 0.186 mL.g^{-1} (**Figure 3**).

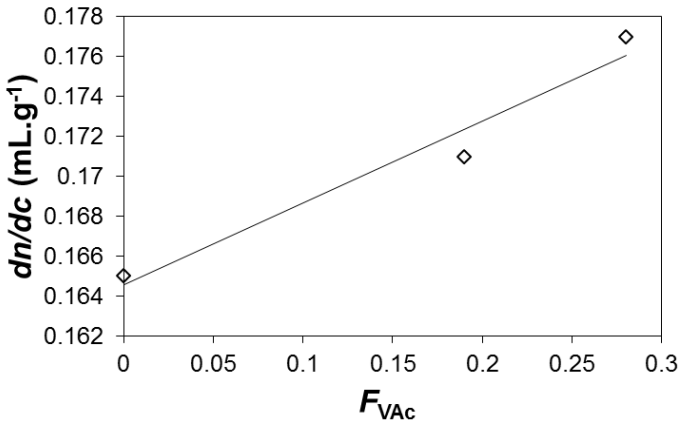

Figure 3. Refractive index increment *(*d*n*/d*c)* of P(VAc-*co*-VCL) copolymers in water versus F_{VAc}.

Size Exclusion Chromatography (SEC). The SEC system operates in THF, at 30°C (flow rate: 1mL.min^{-1}). The SEC apparatus is equipped with a Viscotek VE 1122 automatic injector, a set of Shodex columns (KF 801, KF 8025, KF 804 et KF 806 from Waters) working in series, a Wyatt Heleos II Multi Angle Laser Light Scaterring detector (MALLS, 18 angles, λ_0 = 664.4 nm), a refractive index (RI) detector Viscotek VE 3580 and a Viscotek VE 3210 UV-visible detector. Toluene was used as flow marker. All (co)polymer samples were prepared at 5 g.L^{-1}

concentrations. The number-average molar mass (M_n) and molar mass distribution ($Đ$) were obtained from MALLS data using the M_i value of each slice of the chromatogram (see Equation 6 at zero concentration). The experimental M_n were compared to the theoretical number-average molar masses of the copolymers calculated from Equation 11.

$$M_{n,theo.} = M_{xanthate} + X_w \frac{(m_{0,VAc} + m_{0,VCL}) / V_{Total}}{([xanthate]_0 + 0.6[AIBN]_0(1-e^{-k_d * t}))} \quad \text{Equation 11}$$

Here $M_{xanthate}$ corresponds to the molar mass of the molecular xanthate agent ($M_{xanthate}$ = 222 g.mol^{-1}), X_w is the final overall weight conversion (see Equation 3), k_d is the AIBN dissociation constant into dimethylformamide at 60°C (k_d = 6.45 × 10^{-5} s^{-1}), [62] t corresponds to the polymerization time, and $[xanthate]_0$ and $[AIBN]_0$ are respectively the initial concentrations of the chain-transfer agent and the initiator. $m_{0,VAc}$ and $m_{0,VCL}$ are the initial weight of monomers (in g) and V_{Total} (L) is the initial volume of the reaction mixture.

The refractive index increments (dn/dc) of the P(VAc-*co*-VCL) copolymers synthesized by bulk copolymerization were determined using Equation 12.

$$(dn/dc)_{copo.} = w_{VAc} \times \left(\frac{dn}{dc}\right)_{PVAc} + w_{VCL} \times \left(\frac{dn}{dc}\right)_{PVCL} \quad \text{Equation 12}$$

The values of dn/dc of PVCL and PVAc homopolymers were respectively taken from references 33 and 62: $(dn/dc)_{PVCL}$ = 0.109 mL.g^{-1} and $(dn/dc)_{PVAc}$ = 0.0582 mL.g^{-1}. In order to confirm the dn/dc calculation from Equation 12, the dn/dc value was also measured experimentally by SEC via the plot of the RI area of the chromatogram versus the copolymer concentration (see **Figure 4)**. The experimental dn/dc value of P(VAc$_{0.63}$-*co*-VCL$_{0.37}$) copolymer (expt 7 in **Table 2**) ($dn/dc_{exp.}$ = 0.084 mL.g^{-1}) was in good agreement with the dn/dc calculated using Equation 12 ($dn/dc_{calc.}$ = 0.082 mL.g^{-1}). Therefore, for the series of P(VAc-*co*-VCL) copolymers, dn/dc values were calculated from Equation 12.

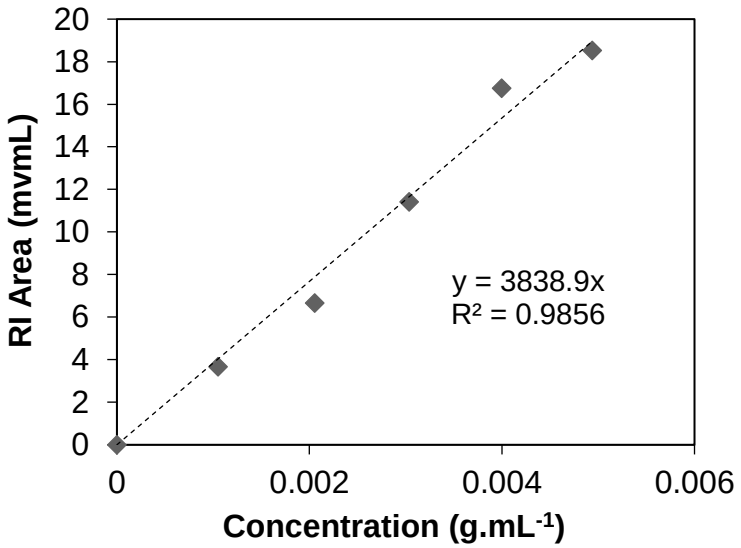

Figure 4. Plots of SEC chromatogram area recorded from refractometer (RI. area) (in THF) as a function of the concentration, for the copolymer with F_{VAc} = 0.63 (expt 7 in Table 2). Symbols: experimental data, dotted line: experimental data linear fit.

$$Slope = \frac{\Delta RI.Area}{\Delta Conc.S} = \frac{RI_{\mathrm{Cal}}}{n_{0,\mathrm{THF}}} \times \frac{\mathrm{d}n}{\mathrm{d}c} \times V_{\mathrm{inj}}$$ Equation 13

With RI_{Cal} = Constant of refractometer instrument, RI_{Cal} = 637 813; $n_{0,\,\mathrm{THF}}$ = THF refractive index, $n_{0,\,\mathrm{THF}}$ = 1.402 ; V_{inj} : injected volume, V_{inj} = 0.1 mL

Differential Scanning Calorimetry (DSC). DSC measurements were carried out using the Q100 apparatus from TA instruments. Analysis were conducted at a heating rate of 10°C/min, under nitrogen gas flow, from 0°C to 200°C. The measurements method included a first heating step from 0 to 200°C at 10°C/min, a cooling step from 200 to 0°C at 10°C/min and a second heating step from 0 to 200°C at 10°C/min. Glass transition temperatures (T_g) of the (co)polymers were measured during the second heating step. (Co)polymers were dried under vacuum for 24 h prior analysis.

Turbidimetry analysis. Turbidimetry measurements of the (co)polymer solutions (0.3 wt-% in water) were performed with a Shimadzu UV-2450PC spectrophotometer, from 13 °C to 33°C (heating/cooling rate: 0.5°C.min^{-1}). Transmittance at 500 nm was plotted versus the temperature. The minimum of the first-order derivative fit of transmittance versus temperature was considered as the temperature of cloud point (T_{cp}) (see **Figure 18**).

III. Results and discussion

1. Synthesis of the *O*-ethyl-*S*-(1-ethoxycarbonyl)ethyldithiocarbonate molecular transfer agent

The *O*-ethyl-*S*-(1-ethoxycarbonyl)ethyldithiocarbonate transfer agent was synthesized according to the procedure described in **Scheme 1**.

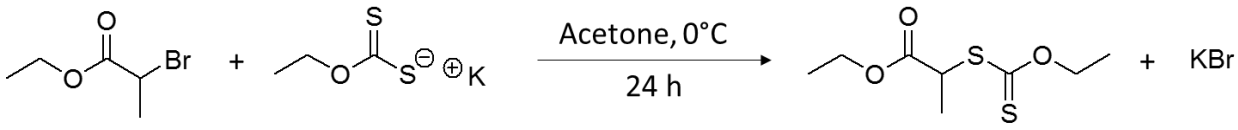

Scheme 1. Synthesis of *O*-ethyl-*S*-(1-ethoxycarbonyl)ethyldithiocarbonate transfer agent (xanthate).

The characteristic signals of the *O*-ethyl-*S*-(1-ethoxycarbonyl)ethyldithiocarbonate are observed in the proton NMR spectrum of the purified product (**Figure 5**).

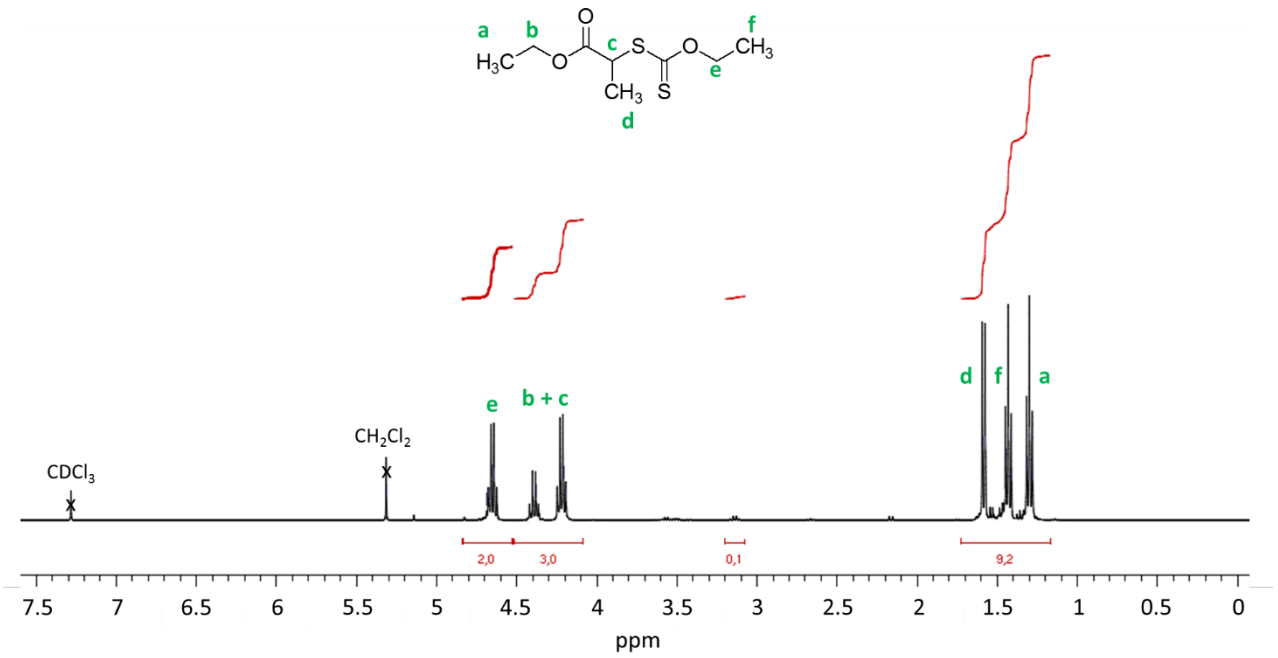

Figure 5. ^{1}H NMR spectrum in $CDCl_3$ of the *O*-ethyl-*S*-(1-ethoxycarbonyl)ethyldithiocarbonate transfer agent.

The C*H*$_3$-CHC(O)Br methyl protons of the initial ethyl-2-bromopropionate exhibit a characteristic signal at 1.9 ppm. This signal of the C*H*$_3$-CH-C(O)OR is shifted towards lower chemical shift (1.6 ppm) in the ^{1}H NMR spectrum of the xanthate. The expected integrals are observed in the ^{1}H NMR spectrum. Indeed, the integral value of protons of ethyl-2-propionate group (*b* + *c* protons) perfectly match the integral of *e* protons from ethyl xanthate moiety, which reveals the absence of an excess of one initial reactant. Some impurities are observed as

multiplet at 3.5 ppm, quadruplet at 3.1 ppm, doublet at 2.2 ppm and triplet at 1.3 ppm. These impurities are not ascribed to residual initial reactants as the chemical shifts are different from ethyl-2-bromopropionate. In order to calculate the purity degree of the *O*-ethyl-*S*-(1-ethoxycarbonyl)ethyldithiocarbonate, it was assumed that the main impurity, whose proton signals can be observed at 3.1 (quadruplet) and 1.3 ppm (triplet), corresponded to ethanol (CH_3 signal at 1.3 ppm and CH_2 signal at 3.1 ppm in NMR tables).[68] Therefore, the purity degree of the xanthate was calculated using Equation 14. The purity degree of the *O*-ethyl-*S*-(1-ethoxycarbonyl)ethyldithiocarbonate transfer agent which spectrum is depicted in **Figure 5** was equal to 95 %.

$$\text{purity degree (\%)} = \frac{n_{\text{xanthate}}}{n_{\text{xanthate}} + n_{\text{EtOH}}} \times 100 \quad \text{Equation 14}$$

With $n_{\text{xanthate}} = I_{\text{c+b}} / 3$ and $n_{\text{EtOH}} = I_{\text{CH2, 3.1 ppm}} / 2$

2. Evaluation of control of RAFT/MADIX copolymerization of VAc and VCL in bulk

Firstly, the level of control of RAFT/MADIX (co)polymerization of vinyl acetate and *N*-vinylcaprolactam mediated by the *O*-ethyl-*S*-(1-ethoxycarbonyl)ethyldithiocarbonate transfer agent was investigated (**Scheme 2**). The polymerizations were carried out in bulk at 65 °C with varying initial monomer feed ratios ($f_{\text{VAc,0}}$) as reported in **Table 1**.

Both VAc and VCL monomers being liquid at 65°C, the polymerization was performed in bulk in order to limit the use of toxic and/or flammable polar solvents such as 1,4-dioxane, chloroform, *N*,*N*-dimethylformamide or anisole, which were previously used as solvents for RAFT (co)polymerization of VCL with other less activated monomers.[32, 33, 49, 69, 70]

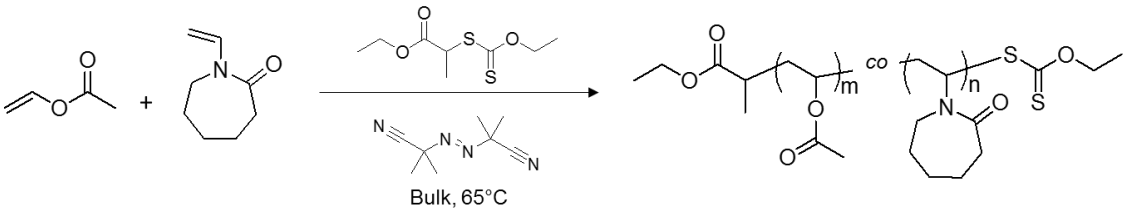

Scheme 2. Synthesis of P(VAc-*co*-VCL) copolymers by RAFT/MADIX polymerization mediated by *O*-ethyl-*S*-(1-ethoxycarbonyl)ethyldithiocarbonate (= xanthate chain transfer agent, CTA) in bulk.

Table 1. Experimental conditions for the (co)polymerizations of VAc and VCL carried out in bulk at 65°C using $[Xanthate]_0/[AIBN]_0 = 3$.

Expt	$f_{VAc,0}$	$[Xanthate]_0$ $mol.L^{-1}$	$\frac{[VAc]_0 + [VCL]_0}{[Xanthate]_0}$
1	0	1.6×10^{-2}	459
2	0.15	1.7×10^{-2}	447
3	0.20	1.8×10^{-2}	449
4	0.30	1.9×10^{-2}	427
5	0.52	2.0×10^{-2}	438
6	0.62	2.2×10^{-2}	422
7	0.71	2.1×10^{-2}	452
8	0.87	2.3×10^{-2}	454
9	1	2.4×10^{-2}	449

The semilogarithmic kinetic plots of the overall molar monomer conversion versus time are linear in the initial range of conversions but some plots curve upwards for higher conversions indicating a steady increase in propagating radical concentration (**Figure 6**). An inhibition period of 60 to 180 minutes was observed in the kinetic plots. Such inhibition period was previously observed in xanthate-mediated vinyl acetate polymerization and was ascribed to the vulnerability of the reactive vinyl acetate propagating radical towards oxygen and by-products generated during the CTA synthesis.[30, 31] The induction period may also be due to initial selective formation of monoadduct but the length of the inhibition period did not show a specific trend with the initial VAc molar feed ratio. A similar range of molar conversion in monomers (40 – 60 %) was reached within 6 hours of RAFT polymerization carried out at 65°C for the entire range of the initial VAc feed compositions ($0 < f_{VAc} < 1$, **Table 2**). Note that a significant increase in the time required to reach 30 % monomer conversion for Co-MRP copolymerization of VAc and VCL was previously reported for $f_{VAc,0} > 0.4$ (48 to 115 h).[39]

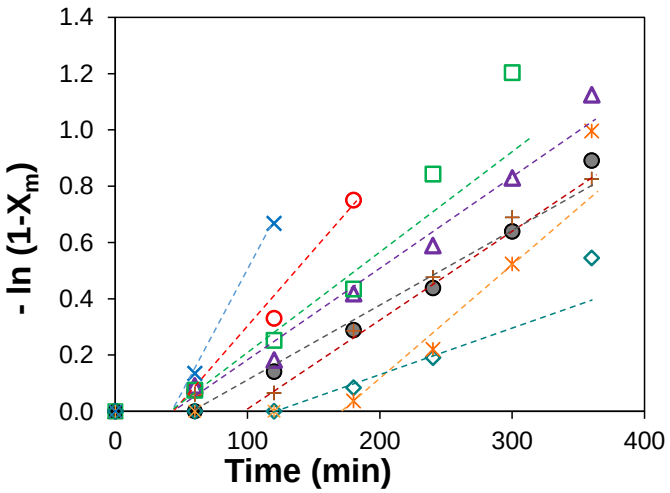

Figure 6. Semilogarithmic plots of overall molar monomer conversion (X_m) versus time: × $f_{VAc,0}$ = 0, ◇ $f_{VAc,0}$ = 0.15, ○ $f_{VAc,0}$ = 0.30, + $f_{VAc,0}$ = 0.52, □ $f_{VAc,0}$ = 0.62, △ $f_{VAc,0}$ = 0.71, ● $f_{VAc,0}$ = 0.87 and ✳ $f_{VAc,0}$ = 1 (expt 1, 2, 4 - 9 in **Table 2**).

Table 2. Final compositions and macromolecular features of the P(VAc-*co*-VCL) copolymers synthesized by RAFT/MADIX copolymerization in bulk at 65°C.

Expt	$f_{VAc,0}$[a]	X_m[b]	X_w[c]	F_{VAc}[d]	d*n*/d*c*$_{polymer}$[e]	$M_{n,theo}$[f]	$M_{n,MALLS}$[g]	$Đ_{MALLS}$[g]	$M_{n,theo}/M_{n,MALLS}$
		%	%		*mL.g*$^{-1}$	*g.mol*$^{-1}$	*g.mol*$^{-1}$		
1	0	56	56	0	0.109	30 519	45 330	1.12	0.67
2	0.15	41	41	0.19	0.103	20 510	48 190	1.19	0.43
4	0.30	51	52	0.28	0.099	25 237	51 530	1.25	0.49
5	0.52	56	57	0.49	0.090	23 669	32 840	1.11	0.72
6	0.62	63	66	0.53	0.088	25 504	35 370	1.10	0.72
7	0.71	56	59	0.63	0.083	23 029	28 650	1.08	0.80
8	0.87	59	60	0.83	0.071	21 695	25 660	1.08	0.85
9	1	63	63	1	0.058	21 085	23 380	1.04	0.90

[a] $f_{VAc,0}$ is the VAc molar fraction in the initial mixture; [b] X_m is the overall monomer molar conversion at 6 h, Equation 2; [c] X_w is the overall monomer weight conversion at 6 h, Equation 3; [d] F_{VAc} is the molar fraction of the monomer into the copolymer, Equation 4; [e] Refractive index increment of the copolymer in THF determined from Equation 12; [f] Theoretical number-average molar mass from Equation 11; [g] Values obtained from the SEC analysis with a MALLS detector.

The experimental molar masses of the series of P(VAc-*co*-VCL) copolymers increase linearly with the overall monomer weight conversion (see **Figure 7**) in accordance with Equation 11. The low dispersity (*Đ*) values of the final (co)polymers which range between 1.25 and 1.04 are consistent with a controlled character of the RAFT/MADIX (co)polymerization mediated by *O*-ethyl-*S*-(1-ethoxycarbonyl)ethyldithiocarbonate chain transfer agent (**Table 2**). Moreover,

the decrease of dispersity (**Figure 7**) and the shift of SEC chromatograms toward low elution volumes throughout the copolymerization reactions (**Figure 8**), both support the controlled character of the RAFT/MADIX copolymerizations at each monomer feed ratio.

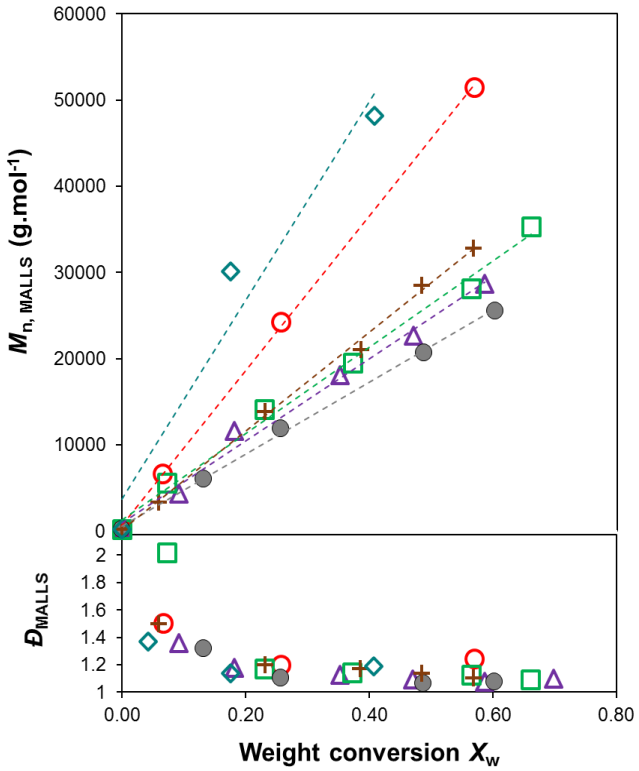

Figure 7. Evolution of $M_{n,MALLS}$ and dispersity versus the overall weight conversion (X_w) for: ◇ $f_{VAc,0}$ = 0.15, ○ $f_{VAc,0}$ = 0.30, + $f_{VAc,0}$ = 0.52, □ $f_{VAc,0}$ = 0.62, △ $f_{VAc,0}$ = 0.71, ● $f_{VAc,0}$ = 0.87 (expt 2 and 4 – 8 in **Table 2**).

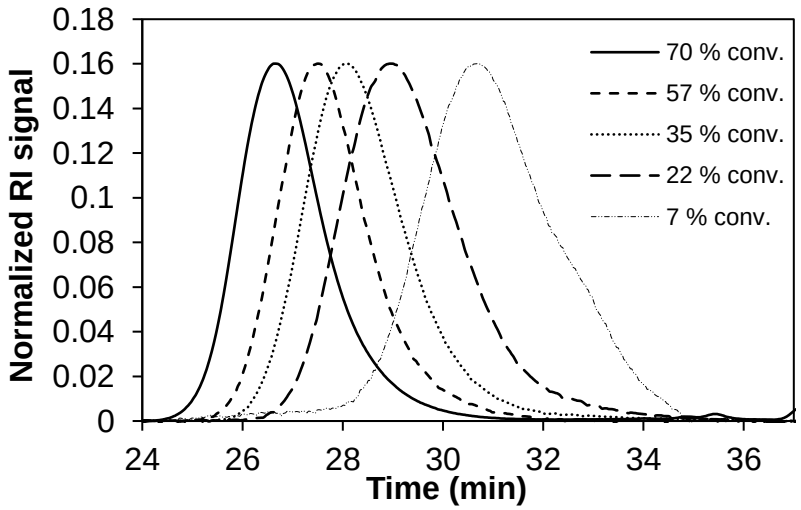

Figure 8. Evolution of the size exclusion chromatograms with monomer conversion for xanthate mediated VAc/VCL copolymerization with $f_{VAc,0}$ = 0.62 (expt 6 in **Table 2**).

The experimental M_n are greater than the theoretical ones, which implies that the RAFT agent is not fully consumed during the course of the polymerization. The xanthate CTA exhibits the characteristic absorption band of a dithiocarbonate group at λ = 355 nm (**Figure 9.a**). Thus, the presence of an additional peak at low elution volume (35.5 mL) observed in the UV-visible SEC traces of the final copolymers (recorded at λ = 355 nm) confirms the incomplete consumption of the xanthate chain transfer agent (CTA) (**Figure 9.b**). The efficiency of the xanthate CTA, calculated on the basis of the ratio between theoretical and experimental M_n rises with the increase of the initial VAc molar fraction (**Table 2**). Such enhancement of CTA efficiency is supported by the analysis of the UV-visible traces of the SEC chromatograms of the final copolymers which depict a decrease in the relative height of the residual CTA peak for higher initial VAc molar fractions (**Figure 9.b**). In summary, both the increase of xanthate efficiency and the decrease of dispersity values (**Table 2**) by increasing $f_{VAc,0}$ from 0 to 1 converge to show that the chain transfer constant to xanthate agent ($C_{tr} = k_{tr}/k_p$) is higher for RAFT/MADIX polymerization of VAc than of VCL. A value of C_{tr} of 25 was reported for *O*-ethyl-*S*-(1-ethoxycarbonyl)ethyldithiocarbonate mediated VAc polymerization,[71] but no value of C_{tr} has been reported for the RAFT/MADIX polymerization of VCL mediated by this xanthate agent. While an increase of dispersity values for higher levels of VAc was reported for the synthesis of P(VAc-*co*-VCL) copolymers by Co-MRP,[39] the present work shows a better control of RAFT VCL/VAc copolymerization by increasing the initial VAc feed ratio.

(a)

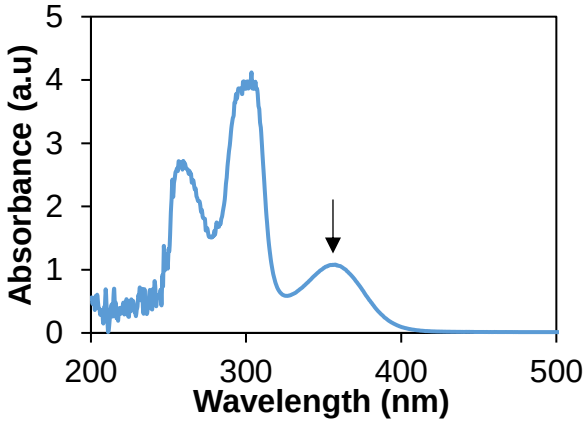

(b)

$f_{VAc,0}$	X_m %	$M_{n,theo}/M_{n,MALS}$	UV height Xanthate, 35.5 mL
0.15	41	0.43	0.16
0.52	56	0.72	0.14
0.62	63	0.72	0.10
0.71	56	0.80	0.08
0.87	59	0.85	0.03

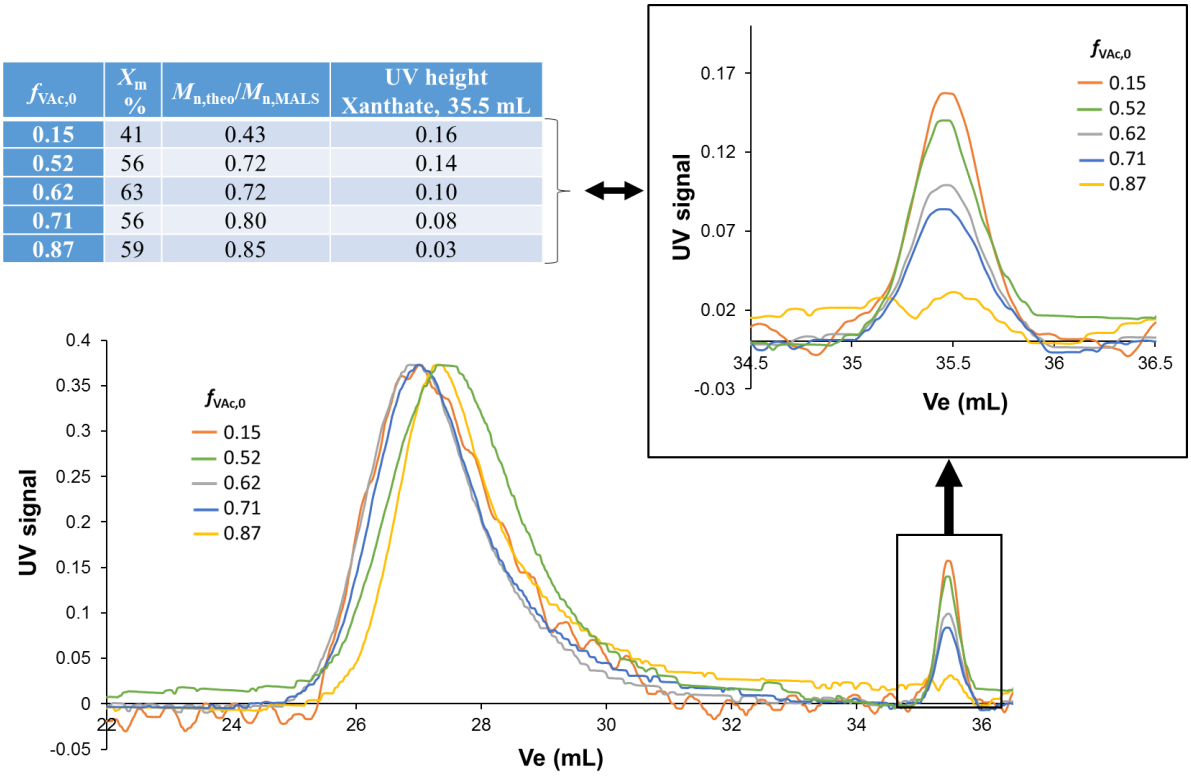

Figure 9. (a) UV-visible spectrum in THF of the *O*-ethyl-*S*-(1-ethoxycarbonyl)ethyldithiocarbonate transfer agent at a concentration of 1.9×10^{-2} mol.L^{-1} ($L_{cuvette}$ = 1 cm); **(b)** UV-visible traces of the SEC chromatograms of the final crude P(VAc-*co*-VCL) copolymers synthesized from various initial VAc feed ratios.

The perfect overlay of the UV-visible (λ = 355 nm) and RI traces of the SEC chromatograms observed for the series of P(VAc-*co*-VCL) copolymers depicts the presence of the dithiocarbonate chain-end and so the living character on the entire molar mass distribution (**Figure 10**).

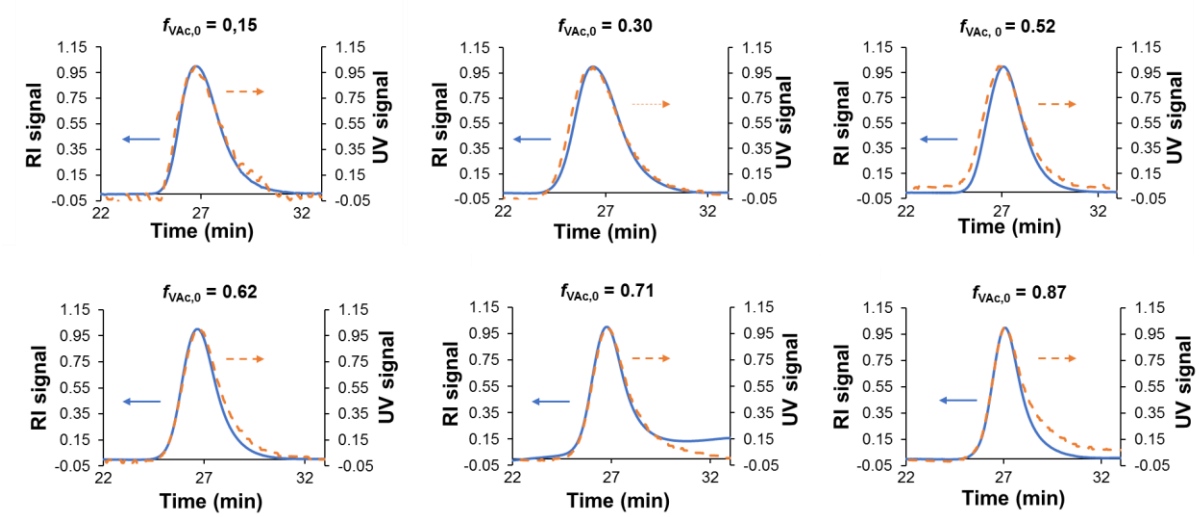

Figure 10. Overlays of the UV-visible (λ = 355 nm) and refractometer (RI) traces of the SEC chromatograms in THF for the series of P(VAc-*co*-VCL) copolymers synthesized from different VAc initial molar fractions ($f_{VAc,0}$).

3. Determination of reactivity ratios and analysis of P(VAc-*co*-VCL) microstructure

Reactivity ratios are most often calculated using a linearization of the Mayo-Lewis equation[72] (either the differential or integrated form). The Kelen-Tüdös (KT) method is one of the most common methods.[73-76] The copolymer composition (F_A) is calculated over a wide range of monomer feed ratios (f_A) for the polymerization stopped at low conversion. The reactivity ratios are estimated through linear regression of the experimental data fitted by the relationship of Equation 15.

$$\eta = [r_A + \left(\frac{r_B}{\alpha}\right)]\times\xi - \frac{r_B}{\alpha} \quad \text{Equation 15}$$

where $\eta = \frac{G}{(\alpha+F)}$, $\xi = \frac{F}{(\alpha+F)}$ with $\alpha = (F_{min} \times F_{max})^{1/2}$,

$$G = \frac{f_A}{f_B} - \left(\frac{f_A/f_B}{F_A/F_B}\right) \text{ and } F = \frac{\left(f_A/f_B\right)^2}{\left(F_A/F_B\right)}$$

The authors later modified the method in order to limit large systemic error in calculation due to the low conversion assumption. The extended Kelen-Tüdös method takes into account the individual monomer conversions.[77] In this method, *F* and *G* are replaced by

$$G = \frac{\left(F_A/F_B\right)-1}{z} \text{ and } F = \frac{\left(F_A/F_B\right)}{z^2} \text{ where } z = \frac{\ln(1-x_A)}{\ln(1-x_B)}$$ with x_A and x_B the individual molar conversions of each monomer. The definitions of η and ξ are similar in Kelen-Tüdös or

extended Kelen-Tüdös methods and Equation 15 is used to calculate the reactivity ratios in both cases. As reported in **Table 3**, similar values of reactivity ratios were calculated from either the Kelen-Tüdös method or the extended Kelen-Tüdös method for RAFT/MADIX copolymerization of VAc and VCL performed in bulk at 65°C (**Table 2**) (r_{VAc} = 0.43 and r_{VCL} = 0.20, **Table 3**).

Nonlinear least-squares (NLLS) methods can also be used to determine the reactivity ratios.[74-76, 78-81] These methods consist in minimizing the sum of squares (SS) as described in Equation 16.

$$SS\ (r_{VAc}, r_{VCL}) = \sum_{i=1}^{n} w_i \times (z_{i,exp.} - z_{i,theo.})^2 \quad \text{Equation 16}$$

Where w_i are the weighting factors (here a constant absolute error was considered, *i.e.*, $w_i = 1$), $z_{i,exp.}$ are the experimental values of the variable z for the experiment i and $z_{i,theo}$ are the theoretical values of the variable z for the experiment i. The best estimate for the reactivity ratios is set for the minimum value of SS. The first nonlinear least-squares method uses the copolymer composition measured at low conversion (F_{VAc}) as the experimental variable (z). The sum of the squares of the residuals was minimized to set the values of reactivity ratios fitting the experimental copolymer composition, F_{VAc} calculated from the individual monomer conversions (Equation 4) with the theoretical copolymer composition calculated from the Mayo-Lewis equation[72] ($F_{VAc,\ theo}$, Equation 17).

$$F_{A,\ theo.} = \frac{r_A f_A^2 + f_A f_B}{r_A f_A^2 + 2 f_A f_B + r_B f_B^2} \quad \text{Equation 17}$$

The theoretical data of the $F_{VAc} = f(f_{VAc,0})$ plots fit the experimental data for values of reactivity ratios of r_{VAc} = 0.37 and r_{VCL} = 0.16 (**Figure 11**). This *S* profile is in good agreement with the evolution of the individual monomer conversions versus time displayed in **Figure 8**. Indeed, for initial VAc fractions below the azeotropic composition ($f_{VAc,0,azeotropic} = \frac{(1 - r_{VCL})}{(2 - r_{VCL} - r_{VAc})} = 0.57$), VAc is more rapidly consumed than VCL while the opposite trend is observed for $f_{VAc,0}$ higher than $f_{VAc,0,\ azeotropic}$ (**Figure 11**).

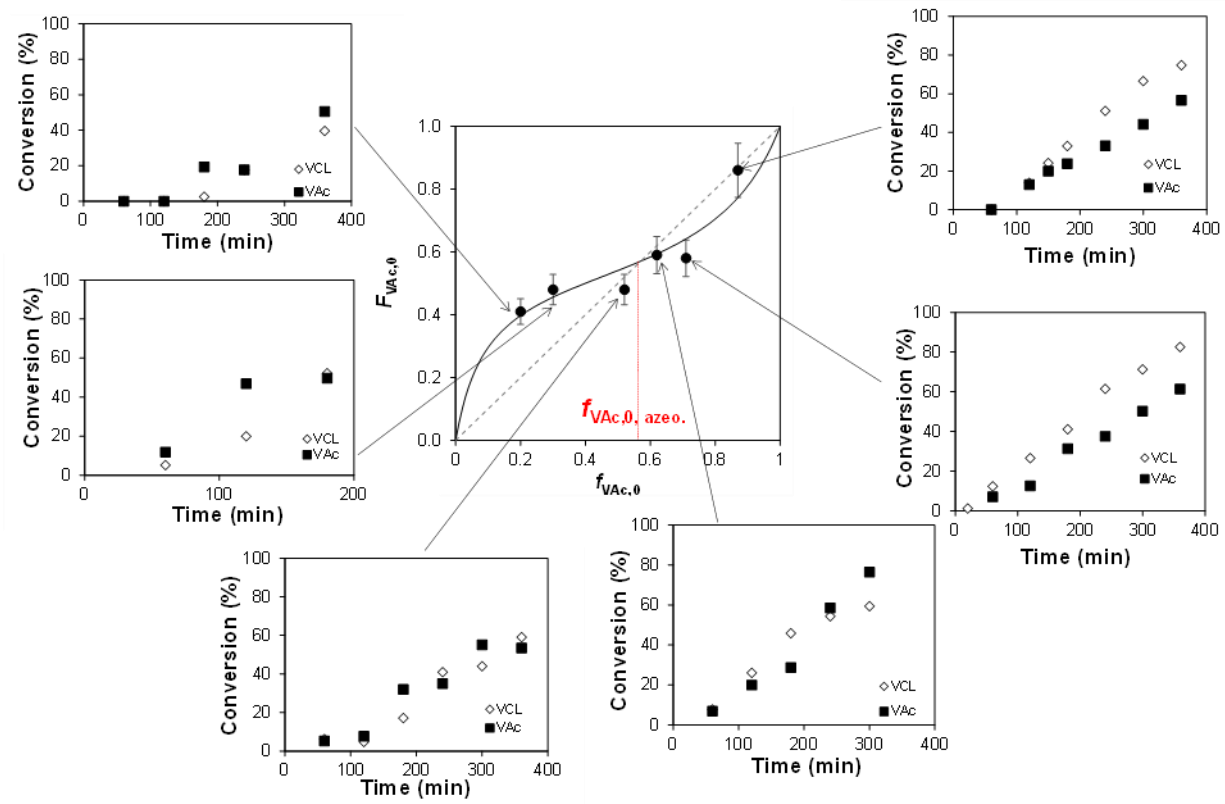

Figure 11. Experimental values of $F_{VAc,0}$ (●) versus $f_{VAc,0}$ and evolution of monomer individual conversions with time for different monomer initial molar feed ratios. The black curve corresponds to the nonlinear fit of Lewis-Mayo equation with r_{VAc} = 0.37 and r_{VCL} = 0.16. The dotted line is the azeotropic curve. The error bar was set on the basis of the error bar from NMR technique used to determine $F_{VAc,0}$.

The second nonlinear least-squares method is based on the integrated form of the copolymerization equation.[82, 83] Equation 18 accurately describes the drift of the monomer feed ratio (f_{VAc}) over the course of copolymerization in relationship with the values of reactivity ratios. This composition drift model provides an enhanced number of analyzed experimental data and therefore the curve fitting method decreases the uncertainty of reactivity ratio measurements.

$$X_m = 1 - \left(\frac{f_A}{f_{A,0}}\right)^{\alpha} \times \left(\frac{f_B}{f_{B,0}}\right)^{\beta} \times \left(\frac{f_{A,0} - \delta}{f_A - \delta}\right)^{\gamma} \quad \text{Equation 18}$$

Where X_m is the overall molar monomer conversion, $\alpha = \frac{r_B}{1 - r_B}$, $\beta = \frac{r_A}{1 - r_A}$, $\gamma = \frac{1 - r_A \times r_B}{(1 - r_A) \times (1 - r_B)}$ and $\delta = \frac{1 - r_B}{2 - r_A - r_B}$. The composition of the monomer feed was calculated from Equation 19.

$$f_A = \frac{f_{A,0} \times (1 - x_A)}{f_{A,0} \times (1 - x_A) + (1 - f_{A,0}) \times (1 - x_B)} \quad \text{Equation 19}$$

The experimental values of f_{VAc} and X_m were fitted to the integrated form of the copolymer composition equation (Equation 18) using the visualization of the sum of squares space method.[78, 84] The reactivity ratios were calculated as r_{VAc} = 0.33 and r_{VCL} = 0.29. The point estimates and 95% joint confidence interval are displayed in **Figure 12**. The interval for r_{VAc} (0.24 - 0.45) is slightly narrower than for r_{VCL} (0.15 - 0.49).

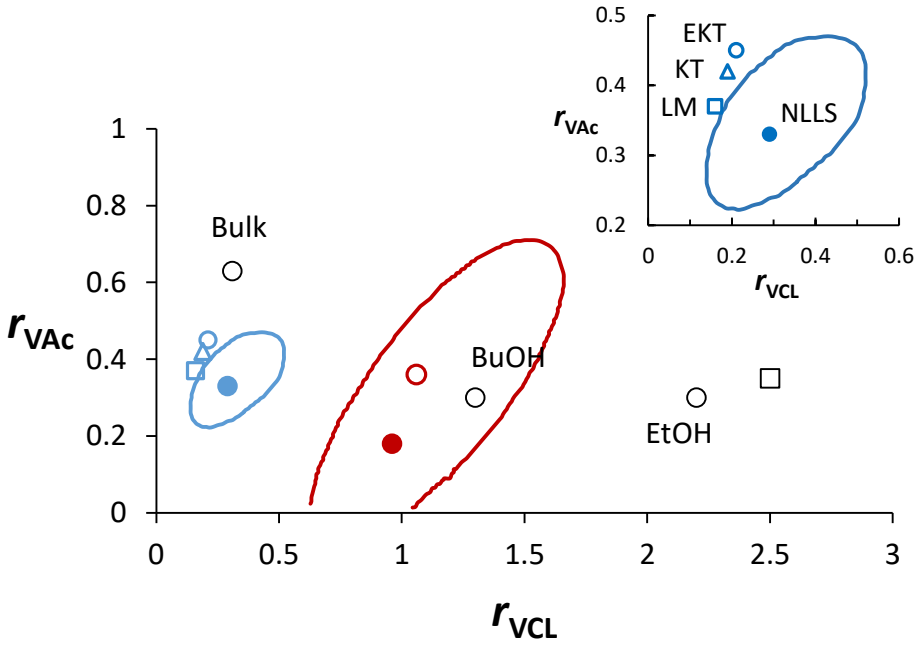

Figure 12. Reactivity ratios (points) and 95 % joint confidence regions (lines) for copolymerizations of VAc and VCL. Blue: data of the present work. Red: data from reference 39 (open circle: reported reactivity ratios; closed circle and line: best estimate and 95 % joint confidence region from NLLS fitting of Skeist equation of their experimental data). Black: circles data from reference 59 in various solvents and square from references 62, 63 (solvent not specified). Inset: reactivity ratios calculated from this work using various methods: KT: Kelen-Tüdös at low conversion; EKT: Extended Kelen-Tüdös; LM: fitting Lewis-Mayo at low conversion; NLLS: NLLS fitting to Skeist equation (with 95 % joint confidence region).

The theoretical values of X_m were calculated with the integrated form of the copolymerization equation (Equation 18) using the values of reactivity ratios determined using NLLS method. The theoretical plots of f_{VAc} versus X_m perfectly fit the experimental data during the course of polymerization for the whole series of VAc/VCL copolymerizations (**Figure 13**). The composition drift is rather limited for initial VAc molar fractions above 0.5, but it is slightly more pronounced for lower initial fractions of VAc ($f_{VAc,0} < 0.4$). Regarding plots of **Figure 13**, the formation of statistical copolymers with homogeneously distributed VAc and VCL units is expected as the overall monomer conversion was limited to 70 % for the series of copolymers (**Table 2**).

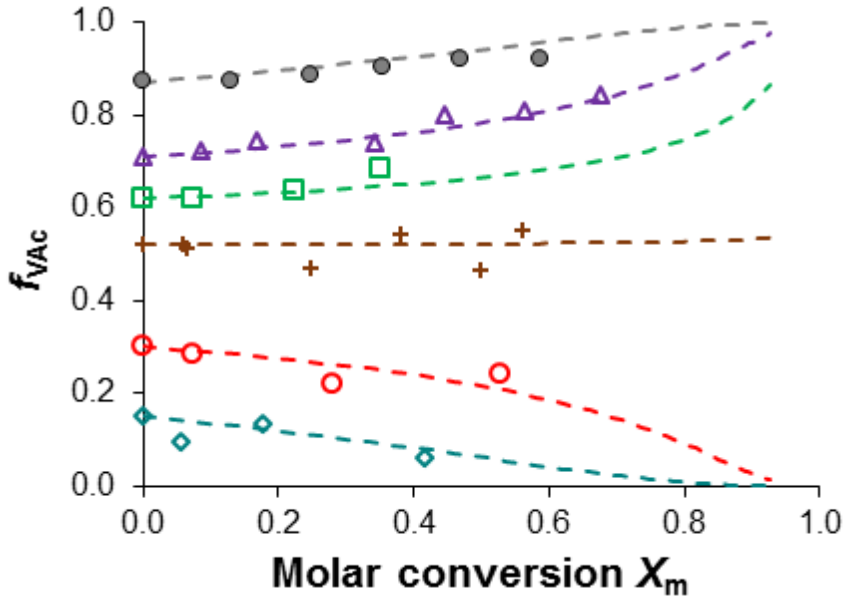

Figure 13. Variation of the VAc composition in the monomer feed (f_{VAc}) versus the molar conversion. Symbols: plots of experimental data of f_{VAc} (Equation 19) versus X_m, ◇ $f_{VAc,0}$ = 0.15, ○ $f_{VAc,0}$ = 0.30, + $f_{VAc,0}$ = 0.52, □ $f_{VAc,0}$ = 0.62, △ $f_{VAc,0}$ = 0.71 and ● $f_{VAc,0}$ = 0.87. The dotted lines correspond to the calculated values of X_m (Equation 18) for given theoretical values of f_{VAc}.

Table 3 summarizes the values of reactivity ratios of VAc and VCL calculated in the present work with linearization techniques or nonlinear least-squares methods. As depicted in **Figure 12**, the three sets of reactivity ratios calculated from KT, e-KT and Lewis-Mayo NLLS method (Equation 17) were at the close outer limit of the 95 % joint confidence interval (**Figure 12**). The two first methods take into account the copolymer composition at low conversion. As previously reported by Klumpermann *et al.*,[85] the RAFT agent can influence the monomer selectivity at the early stages of polymerization. Also, previous studies revealed an impact of the RDRP equilibrium implemented by reversible termination on the copolymer composition for very low monomer conversion.[86, 87] Not only did the reactivity ratios reported in the literature exhibit discrepancy between their values, their values were out of the range of the present 95 % joint confidence interval. One reason for very different reactivity ratios between this work and the study of Kermagoret *et al.*[39] might be accounted to the difference between RAFT polymerization and Co-MRP.

Table 3. VAc and VCL reactivity ratio values calculated from the different methods.

Method	r_{VAc}	r_{VCL}
Kelen-Tüdös (KT)	0.42	0.19
Extended Kelen-Tüdös (e-KT)	0.45	0.21
NLLS method based on Lewis-Mayo equation (Equation 17)	0.37	0.16
NLLS method based on the integrated form of the copolymerization equation (Equation 18)	0.33	0.29

P(VAc-*co*-VCL) copolymers with different monomer compositions (expt 6 and 8 in **Table 2**) were analyzed by ^{13}C NMR and the spectra were compared to PVCL and PVAc spectra. The integrality of the spectra is shown in **Figure 14** and two zones of interest are displayed in **Figure 15**. It can be noticed that the characteristic signal of each polymeric unit is influenced by the presence of the neighbor co-monomer distributed homogeneously along the chains. For instance, the methine signal (CH_{II}, 65 – 70 ppm, **Figure 15.b**) of PVAc broadens by increasing the fraction of VCL.

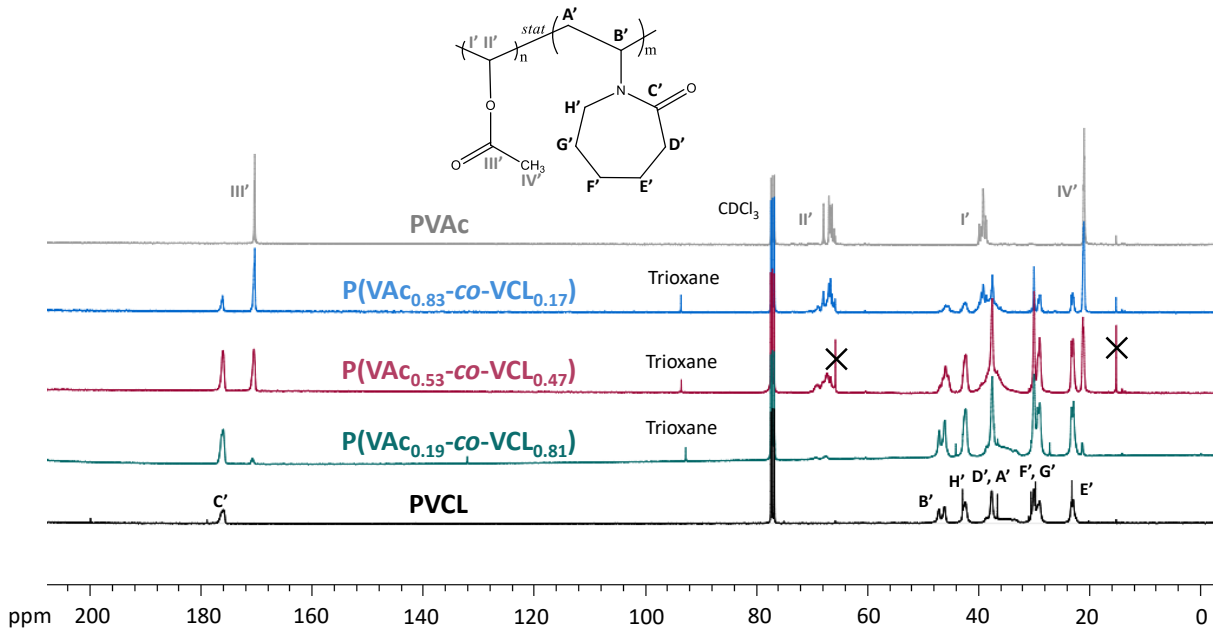

Figure 14. ^{13}C NMR spectra of precipitated PVAc, P($VAc_{0.19}$-*co*-$VCL_{0.81}$), P($VAc_{0.53}$-*co*-$VCL_{0.47}$), P($VAc_{0.83}$-*co*-$VCL_{0.17}$) and PVCL (co)polymers in $CDCl_3$.
Residual trioxane (internal standard used for VAc/VCL copolymerizations) and diethyl ether (marked by cross, solvent of precipitation) are observed.

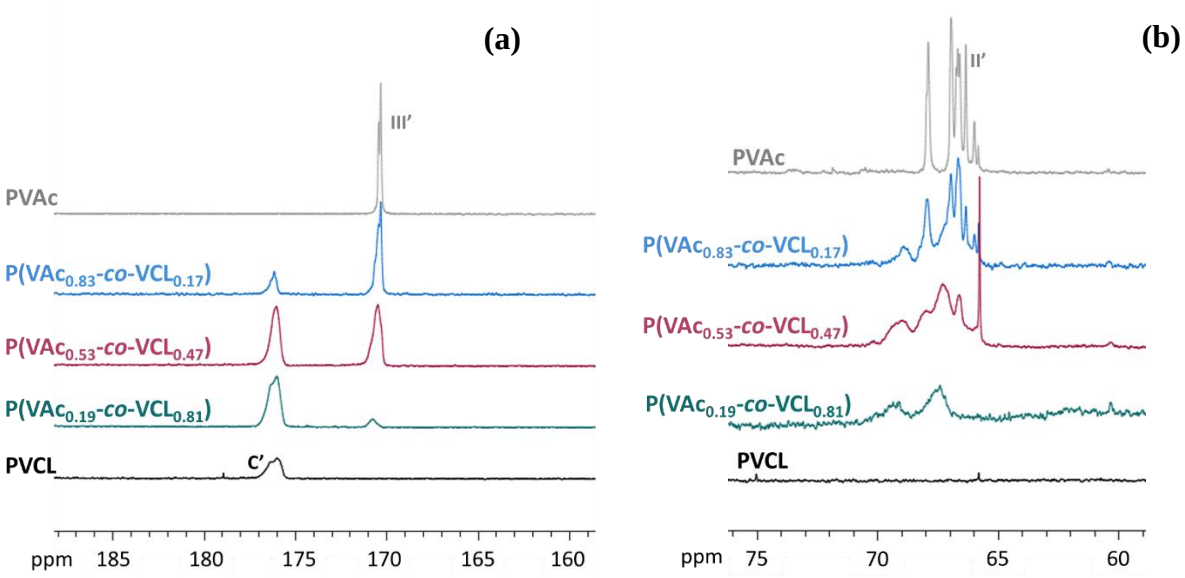

Figure 15. ^{13}C NMR spectra of PVAc, P(VAc$_{0.19}$-*co*-VCL$_{0.81}$) (expt 2 in **Table 2**), P(VAc$_{0.53}$-*co*-VCL$_{0.47}$) (expt 6 in **Table 2**), P(VAc$_{0.83}$-*co*-VCL$_{0.17}$) (expt 8 in **Table 2**) and PVCL (co)polymers in $CDCl_3$: **(a)** zoom on the PVAc and PVCL carbonyl signal range; **(b)** zoom on the PVAc methine signal range.

The copolymer compositions can be calculated on the basis of the integrals of the well-resolved carbonyl signals at 170 – 180 ppm of each polymer unit of the P(VAc-*co*-VCL) copolymer (**Table 4**). Such ^{13}C NMR compositions match the compositions calculated either from the individual monomer conversions (Equation 4) or from the integrals of the proton NMR spectra of the copolymers (**Table 4** and **Figure 16**).

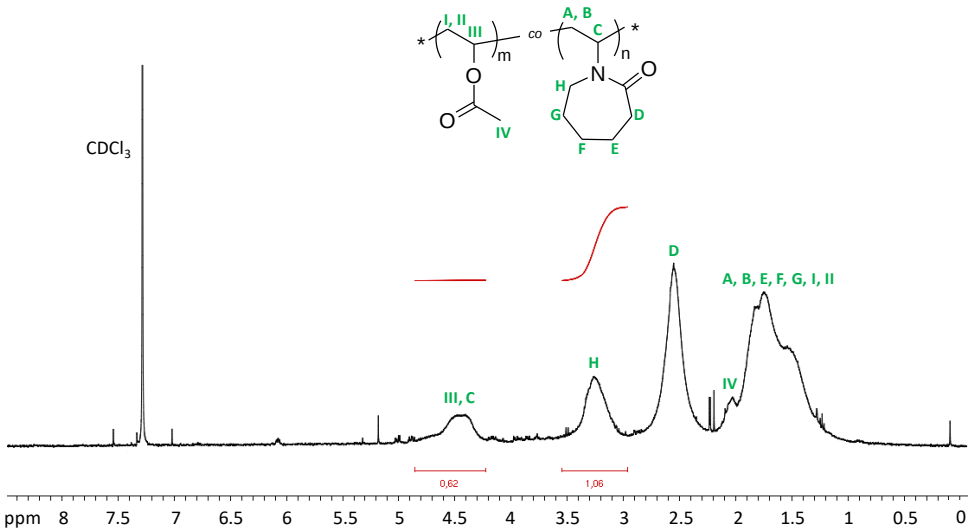

Figure 16. ^{1}H NMR spectrum of the precipitated P(VAc$_{0.19}$-*co*-VCL$_{0.81}$) copolymer in $CDCl_3$.

Table 4. Comparison of the molar fractions of VAc in the copolymers calculated by different methods.

Expt	F_{VAc}[a]	F_{VAc}[b]	F_{VAc}[c]
2	0.11	0.19	0.15
6	0.47	0.53	0.63
8	0.78	0.83	0.72

[a] Molar fraction of VAc in the P(VAc-*co*-VCL) copolymers, determined from ^{13}C NMR signal integrals: $F_{VAc} = \frac{I_{C=O,PVAc}}{I_{C=O,PVAc} + I_{C=O,PVCL}}$ (see **Figure 14**); [b] Molar fraction of VAc in the P(VAc-*co*-VCL) copolymers determined from the individual conversions (Equation 4); [c] Molar fraction of VAc in the P(VAc-*co*-VCL) copolymers determined from ^{1}H NMR signal integrals of the precipitated copolymers (see **Figure 16**): $F_{VAc} = \frac{I_{III,C} - \left(\frac{I_H}{2}\right)}{I_{III,C}}$.

The P(VAc-*co*-VCL) final (co)polymers exhibit a unique glass transition temperature (T_g) characterized by differential scanning calorimetry (**Table 5**).

Table 5. Theoretical and experimental glass transition temperatures of the synthesized (co)polymers.

Expt	F_{VAc}[a]	w_{VAc}[b]	$T_{g,\,theo}$[c] °C	$T_{g,\,exp}$[d] °C
1	0	0	168[d]	168
2	0.19	0.13	147	157
4	0.28	0.19	136	130
5	0.49	0.37	110	115
6	0.53	0.41	105	86
7	0.65	0.53	90	64
8	0.83	0.75	65	49
9	1	1	41[d]	41

[a] F_{VAc} is the molar fraction of VAc in the copolymer, Equation 4; [b] w_{VAc} is the weight fraction of VAc in the copolymer, Equation 5; [c] Calculated from Equation 20 using T_g of PVAc and PVCL measured by DSC (in Kelvin for Equation 20); [d] T_g of (co)polymer measured by DSC.

The good agreement between the experimental T_gs of copolymers and the theoretical ones calculated from Fox-Flory equation (Equation 20) (see **Figure 17** and **Table 5**) confirms the homogeneous distribution of VAc and VCL monomer in the P(VAc-*co*-VCL) chains.

$$\frac{1}{T_{g,\text{theo P(VAc}-co-\text{VCL)}}} = \frac{w_{VAc}}{T_{g,PVAc}} + \frac{w_{VCL}}{T_{g,PVCL}} \quad \text{Equation 20}$$

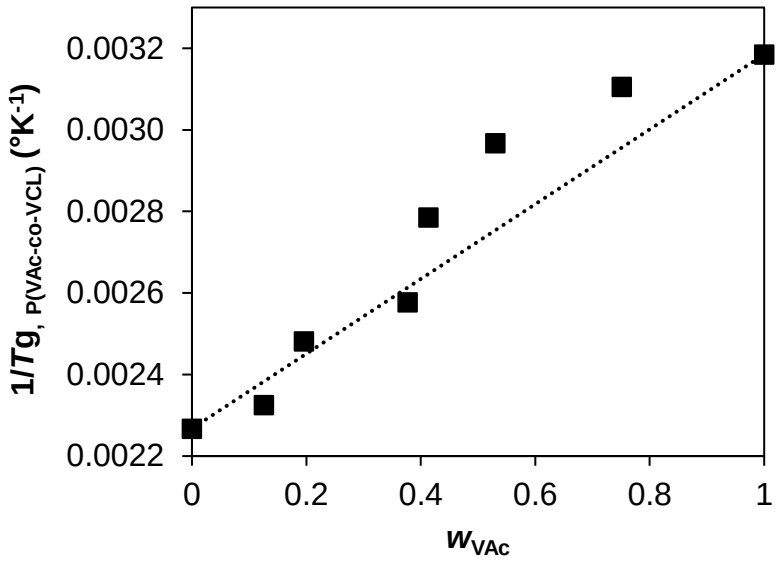

Figure 17. Experimental glass transition temperature of the P(VAc-*co*-VCL) copolymers as a function of the weight fraction of VAc in the copolymer (Equation 5); Dotted line: theoretical glass transition temperature of the copolymers calculated from Equation 20.

4. Thermoresponsive self-assembly of P(VAc-*co*-VCL) copolymers in water.

As mentioned in the PhD introduction, the incorporation of a co-monomer unit is an additional parameter to modify the temperature of cloud point (T_{cp}). As depicted in **Figure 18**, a dependence of the phase transition temperature with the P(VAc-*co*-VCL) copolymer composition is observed by turbidimetry analysis. For low VAc content (F_{VAc} = 0 - 0.28), the polymers in water exhibit a sharp and reversible thermal transition between a clear solution and a cloudy solution above a certain temperature (T_{cp}). This transition is broadened for a higher content of hydrophobic VAc (F_{VAc} = 0.53) but reversibility is still observed. The hysteresis never exceeds 2 °C (**Figure 18**).

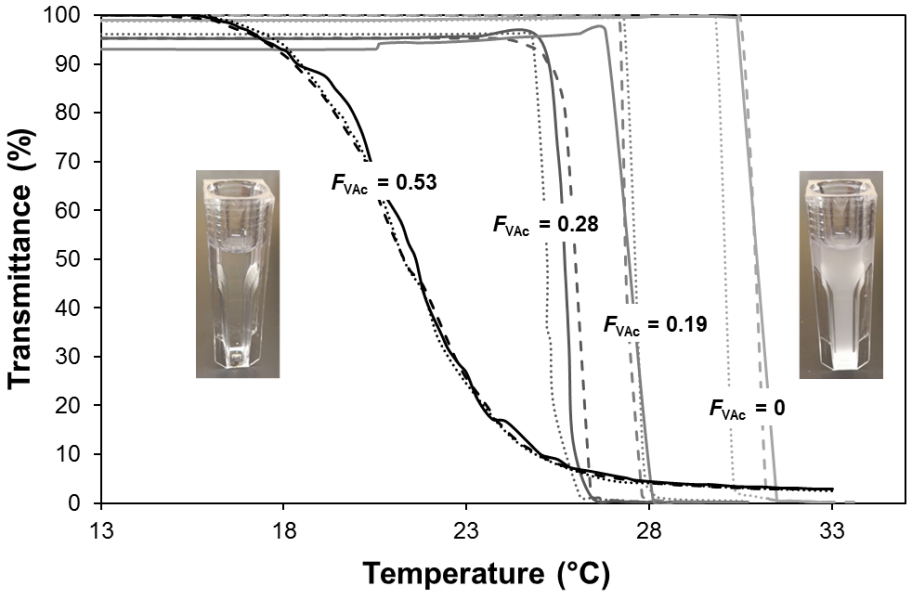

Figure 18. Transmittance at λ = 500 nm versus temperature for aqueous solutions (3 g.L^{-1}) of: P(VAc$_{0.53}$-*co*-VCL$_{0.47}$) copolymer (expt 6 in **Table 2** P(VAc$_{0.28}$-*co*-VCL$_{0.72}$) copolymer (expt 4 in **Table 2**), P(VAc$_{0.19}$-*co*-VCL$_{0.81}$) copolymer (expt 2 in **Table 2**) and PVCL homopolymer (expt 1 in **Table 2**); Full line (—): First heating, Dashed line (- - -): Cooling, Dotted line (···): Second heating; Photos of the solutions below (left) and above (right) the cloud point.

The phase transition temperatures were also measured by means of dynamic light scattering (DLS). **Figure 19** shows the evolution of the hydrodynamic diameter (D_h) as a function of temperature. The increase of D_h from 7 nm to 1.2 µm for P(VAc$_{0.19}$-*co*-VCL$_{0.81}$) reveals the formation of very large aggregates above the transition temperature. The cloud point temperatures obtained by DLS were consistent with the ones measured by UV-visible spectroscopy (**Table 6**). The increasing incorporation of hydrophobic VAc units into PVCL thermoresponsive chains leads to a decrease of the copolymer cloud point temperature (**Figure 20**). As the hydrophobic composition of the copolymers is increased, the hydrogen bonding effect between the copolymer chains and water is lowered while hydrophobic interactions are enhanced, thus lowering the required energy to collapse (*i.e.*, lower T_{cp}).[70, 88]

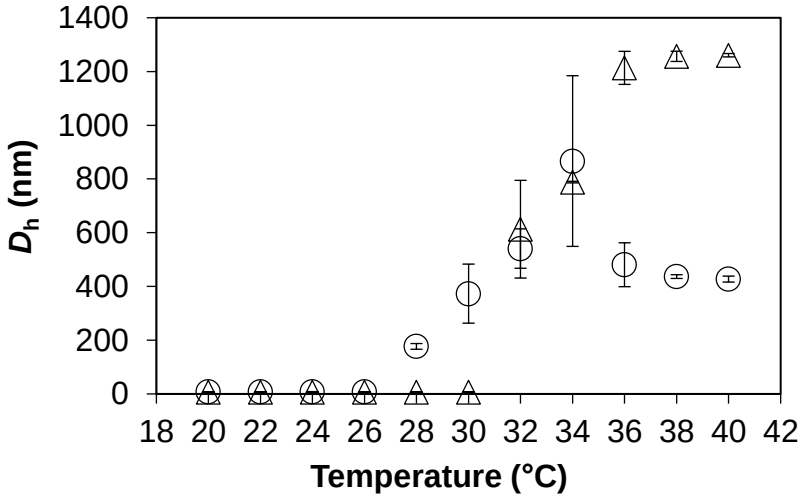

Figure 19. Evolution of hydrodynamic diameters of: △ P($VAc_{0.19}$-*co*-$VCL_{0.81}$) and ○ P($VAc_{0.28}$-*co*-$VCL_{0.72}$) copolymers in water by increasing temperature. Analysis in deionized water at 5 $g.L^{-1}$.

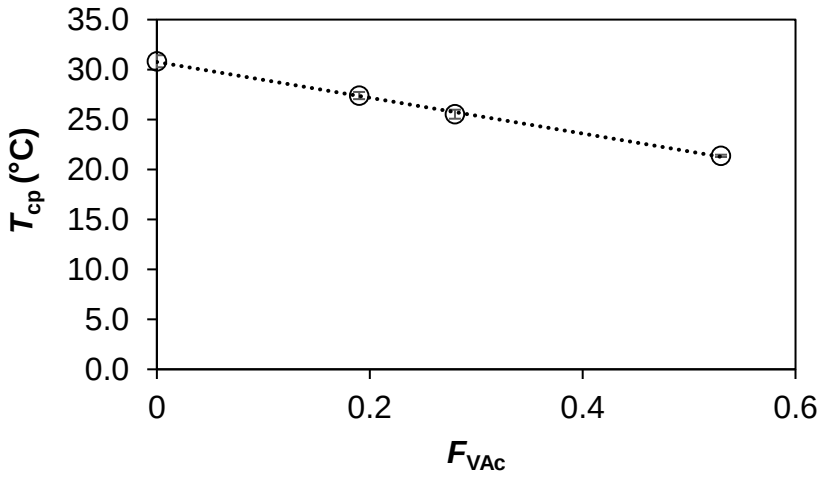

Figure 20. Cloud point temperatures (T_{cp}) of P($VAc_{0.19}$-*co*-$VCL_{0.81}$) (expt 2 in **Table 2**, $M_{n,MALLS}$ = 48 190 $g.mol^{-1}$), P($VAc_{0.28}$-*co*-$VCL_{0.72}$) (expt 4 in **Table 2**, $M_{n,MALLS}$ = 51 530 $g.mol^{-1}$) and P($VAc_{0.53}$-*co*-$VCL_{0.47}$) (expt 6 in **Table 2**, $M_{n,MALLS}$ = 35 370 $g.mol^{-1}$) copolymers and PVCL (expt 1 in **Table 2**, $M_{n,MALLS}$ = 45 330 $g.mol^{-1}$) at 3 $g.L^{-1}$ in water measured by UV-Visible spectroscopy versus the molar fraction of VAc in the copolymer (F_{VAc}).

The characteristics of the P(VAc-*co*-VCL) copolymers dispersed in water were studied by means of dynamic and static light scattering at a temperature below the cloud point temperature (**Table 6**).

Table 6. Characteristics of P(VAc-*co*-VCL) copolymers dispersed in water.

Expt	F_{VAc}	$T_{cp,\ UV\text{-}vis}$[a] °C	$T_{cp,\ DLS}$[b] °C	T[c] °C	$M_{w,\ SLS}$[d] g.mol^{-1}	$N_{agg.}$[d]	$D_{h,DLS}$[d] nm
6	0.53	21.4 ± 0.1	-	10	97 600	3	22.5
4	0.28	25.5 ± 0.5	29.1	25	42 200	1	5.6
2	0.19	27.4 ± 0.4	32.7	25	52 100	1	6.9

[a] Cloud point temperature measured by UV-visible spectroscopy of solutions of copolymers at 3 g.L^{-1} in water, the given value is the average of the cloud point temperature values obtained for the first heating, cooling, and second heating; [b] Cloud point temperature measured by dynamic light scattering of solution of copolymers at 5 g.L^{-1} in water; [c] Temperature of the static light scattering measurements; [d] Data measured on ALV setup (see experimental part, SLS and DLS) at the temperature of measurement reported in this **Table 6**, which corresponds to a temperature below the cloud point.

At all concentrations, the DLS analyses of P(VAc-*co*-VCL) copolymers dispersed in water revealed a main population of small aggregates (fast mode of relaxation) with hydrodynamic diameter (D_h) of 5 to 22.5 nm, depending on the VAc content, and a minor population of larger aggregates of D_h ~ 200 nm (slow mode of relaxation). It would be tempting to assign the slow mode of relaxation to aggregates in equilibrium with the unimers. However, the weight concentration of these large aggregates is negligible given that the scattered light intensity of these aggregates varies only between 30 and 50 %. Indeed, the scattered light intensity being proportional to both M_w and the square of the scatter dimension (R_g^2), the contribution of large aggregates predominates even at very low fraction.[65] Similar populations of large aggregates were reported for poly(ethylene oxide) (PEO) end-capped with dodecyl groups and were identified as spurious aggregates.[65] For P(VAc-*co*-VCL) amphiphilic copolymers with low VAc content (F_{VAc} < 0.3), the fast mode of relaxation corresponds to a value of the apparent D_h below 7 nm. This suggests that the polymers are present as free polymer chains, which is confirmed by an aggregation number of unity measured by SLS (**Table 6**). Note that the light scattered by the minor larger aggregates was accounted in order to accurately determine the absolute weight-average molar mass (M_w) and aggregation number of the fast mode of relaxation (see experimental section). For higher content of VAc (F_{VAc} = 0.53), self-assembly of the P(VAc-*co*-VCL) copolymer into aggregates of three polymer chains (N_{agg} = 3, see **Table 6**) was achieved. The hydrodynamic diameter of the aggregates, measured from the fast mode of relaxation in DLS, was indeed larger (D_h ~ 20 nm). The steeper angular dependence of the light scattered by the P($VAc_{0.53}$-*co*-$VCL_{0.47}$) in comparison with the copolymers with lower VAc content depicts the presence of aggregates for the more hydrophobic copolymer (**Figure 2** in experimental part). These results show that a level of *ca* 50 mol-% of VAc is required to

induce non-covalent intermolecular hydrophobic interactions at temperature below the cloud point, leading to supramolecular assembly.

IV. Conclusions

In summary, the copolymerization of *N*-vinylcaprolactam with the hydrophobic vinyl acetate is successfully controlled by RAFT/MADIX polymerization mediated by the *O*-ethyl-*S*-(1-ethoxycarbonyl)ethyldithiocarbonate chain transfer agent to provide a series of well-defined thermoresponsive poly(*N*-vinylcaprolactam-*co*-vinyl acetate) copolymers with tunable phase transition temperatures and glass transition temperatures. Regardless the initial monomer feed ratio, the synthesis of statistical copolymers fulfills the features of a controlled polymerization with a linear increase of the molar masses and low dispersity values ($Đ$ < 1.3). It should be mentioned that the polymerization control is enhanced by increasing the initial VAc feed ratio. We applied both conventional linearization methods and nonlinear least-squares methods to estimate reliable values of reactivity ratios for VAc and VCL radical polymerization in regards to the disparate values previously reported in the literature. The nonlinear least-squares (NLLS) method based on the integrated form of the copolymerization equation (Skeist equation) provides values of reactivity ratios of r_{VAc} = 0.33 and r_{VCL} = 0.29 with the azeotropic composition calculated at $f_{VAc,0}$ = 0.57. It should be mentioned that the reactivity ratio values calculated either from linearization techniques such as Kelen-Tüdös, extended Kelen-Tüdös or from nonlinear least-squares fitting, based on the Mayo−Lewis equation at low conversion, fall on the outside limit of the 95 % joint confidence region (0.24 < r_{VAc} < 0.45; 0.15 < r_{VCL} <0.49). These results are important to provide information on the copolymer microstructure and clearly indicate a limited monomer compositional drift in the synthesized P(VAc-*co*-VCL) copolymers. Given the nearly homogeneous composition in VAc and VCL along the polymer chains, the ^{13}C NMR signal of the PVAc methine group is thus influenced by the monomer fraction and the values of the copolymer glass transition (T_g) are in accordance with the theoretical T_g of statistical copolymers calculated on the basis of the Fox-Flory law. Turbidimetry analyses of the aqueous solutions of the amphiphilic P(VAc-*co*-VCL) copolymers indicated that the copolymer composition fine-tunes the cloud point temperature (T_{cp}) between 20 and 30 °C. A linear decrease of the cloud point temperature of the aqueous copolymer solution was observed with the increase of VAc molar fraction in the copolymer. It worth emphasizing that a sharp and reversible temperature phase transition was observed for VCL-

rich copolymers while a broadening of this transition occurred for the more hydrophobic P(VAc$_{0.53}$-*co*-VCL$_{0.47}$). The P(VAc-*co*-VCL) copolymers with VAc compositions below 30 mol-% forms unimers in water below T_{cp}, as judged by static light scattering measurements (N_{agg} = 1) and dynamic light scattering (D_h ~ 7 nm). Interestingly, increasing the VAc content up to 53 mol-% is sufficient to induce P(VAc$_{0.53}$-*co*-VCL$_{0.47}$) copolymer self-assembly into small aggregates (N_{agg} = 3, D_h ~ 14 nm) via intermolecular hydrophobic interactions at 10 °C ($T < T_{cp}$). The knowledge of the minimum VAc hydrophobic fraction resulting in association of P(VAc-*co*-VCL) chains at room temperature is of interest for the formation of thermoresponsive supramolecular structures such as physically crosslinked colloidal particles that will be described in the Chapter 2 of Part I.

V. References

1. Jenkins, A. D.; Jones, R. G.; Moad, G. *Pure and Applied Chemistry* **2009,** 82, (2).
2. Braunecker, W. A.; Matyjaszewski, K. *Progress in Polymer Science* **2007,** 32, (1), 93-146.
3. Georges, M. K.; Veregin, R. P. N.; Kazmaier, P. M.; Hamer, G. K. *Macromolecules* **1993,** 26, (11), 2987-2988.
4. Nicolas, J.; Guillaneuf, Y.; Lefay, C.; Bertin, D.; Gigmes, D.; Charleux, B. *Progress in Polymer Science* **2013,** 38, (1), 63-235.
5. Wang, J.-S.; Matyjaszewski, K. *Journal of the American Chemical Society* **1995,** 117, (20), 5614-5615.
6. Matyjaszewski, K. *Macromolecules* **2012,** 45, (10), 4015-4039.
7. Percec, V.; Guliashvili, T.; Ladislaw, J. S.; Wistrand, A.; Stjerndahl, A.; Sienkowska, M. J.; Monteiro, M. J.; Sahoo, S. *Journal of the American Chemical Society* **2006,** 128, (43), 14156-14165.
8. Rosen, B. M.; Percec, V. *Chemical Reviews* **2009,** 109, (11), 5069-5119.
9. Konkolewicz, D.; Wang, Y.; Zhong, M. J.; Krys, P.; Isse, A. A.; Gennaro, A.; Matyjaszewski, K. *Macromolecules* **2013,** 46, (22), 8749-8772.
10. Konkolewicz, D.; Wang, Y.; Krys, P.; Zhong, M. J.; Isse, A. A.; Gennaro, A.; Matyjaszewski, K. *Polym. Chem.* **2014,** 5, (15), 4396-4417.
11. Chiefari, J.; Chong, Y. K.; Ercole, F.; Krstina, J.; Jeffery, J.; Le, T. P. T.; Mayadunne, R. T. A.; Meijs, G. F.; Moad, C. L.; Moad, G.; Rizzardo, E.; Thang, S. H. *Macromolecules* **1998,** 31, (16), 5559-5562.
12. Chiefari, J.; Mayadunne, R. T. A.; Moad, C. L.; Moad, G.; Rizzardo, E.; Postma, A.; Thang, S. H. *Macromolecules* **2003,** 36, (7), 2273-2283.
13. Chong, Y. K.; Krstina, J.; Le, T. P. T.; Moad, G.; Postma, A.; Rizzardo, E.; Thang, S. H. *Macromolecules* **2003,** 36, (7), 2256-2272.
14. Charmot, D.; Corpart, P.; Adam, H.; Zard, S. Z.; Biadatti, T.; Bouhadir, G. *Macromolecular Symposia* **2000,** 150, 23-32.
15. Destarac, M.; Bzducha, W.; Taton, D.; Gauthier-Gillaizeau, I.; Zard, S. Z. *Macromolecular Rapid Communications* **2002,** 23, (17), 1049-1054.

16. Boyer, C.; Lacroix-Desmazes, P.; Robin, J.-J.; Boutevin, B. *Macromolecules* **2006,** 39, (12), 4044-4053.
17. Wayland, B. B.; Poszmik, G.; Fryd, M. *Organometallics* **1992,** 11, (11), 3534-3542.
18. Allan, L. E. N.; Perry, M. R.; Shaver, M. P. *Progress in Polymer Science* **2012,** 37, (1), 127-156.
19. Charleux, B.; Nicolas, J. *Polymer* **2007,** 48, (20), 5813-5833.
20. Charleux, B.; Delaittre, G.; Rieger, J.; D'Agosto, F. *Macromolecules* **2012,** 45, (17), 6753-6765.
21. Monteiro, M. J.; Cunningham, M. F. *Macromolecules* **2012,** 45, (12), 4939-4957.
22. Zetterlund, P. B.; Thickett, S. C.; Perrier, S.; Bourgeat-Lami, E.; Lansalot, M. *Chemical Reviews* **2015,** 115, (18), 9745-800.
23. Warren, N. J.; Armes, S. P. *Journal of the American Chemical Society* **2014,** 136, (29), 10174-10185.
24. Derry, M. J.; Fielding, L. A.; Armes, S. P. *Progress in Polymer Science* **2016,** 52, 1-18.
25. Canning, S. L.; Smith, G. N.; Armes, S. P. *Macromolecules* **2016,** 49, (6), 1985-2001.
26. Pasetto, P.; Blas, H.; Audouin, F.; Boissiere, C.; Sanchez, C.; Save, M.; Charleux, B. *Macromolecules* **2009,** 42, (16), 5983-5995.
27. Blas, H.; Save, M.; Boissiere, C.; Sanchez, C.; Charleux, B. *Macromolecules* **2011,** 44, (8), 2577-2588.
28. Chevigny, C.; Dalmas, F.; Di Cola, E.; Gigmes, D.; Bertin, D.; Boue, F.; Jestin, J. *Macromolecules* **2011,** 44, (1), 122-133.
29. Billon, L.; Save, M.; Cunningham, M. F., Chapter 10 Surface-initiated Nitroxide-mediated Polymerization. In *Nitroxide Mediated Polymerization: From Fundamentals to Applications in Materials Science*, The Royal Society of Chemistry: 2016; pp 406-440.
30. Stenzel, M. H.; Cummins, L.; Roberts, G. E.; Davis, T. P.; Vana, P.; Barner-Kowollik, C. *Macromolecular Chemistry and Physics* **2003,** 204, (9), 1160-1168.
31. Favier, A.; Barner-Kowollik, C.; Davis, T. P.; Stenzel, M. H. *Macromolecular Chemistry and Physics* **2004,** 205, (7), 925-936.
32. Wan, D.; Zhou, Q.; Pu, H.; Yang, G. *Journal of Polymer Science Part A: Polymer Chemistry* **2008,** 46, (11), 3756-3765.
33. Beija, M.; Marty, J. D.; Destarac, M. *Chemical communications* **2011,** 47, (10), 2826-8.
34. Shao, L.; Hu, M.; Chen, L.; Xu, L.; Bi, Y. *Reactive and Functional Polymers* **2012,** 72, (6), 407-413.
35. Guinaudeau, A.; Coutelier, O.; Sandeau, A.; Mazières, S.; Nguyen Thi, H. D.; Le Drogo, V.; Wilson, D. J.; Destarac, M. *Macromolecules* **2014,** 47, (1), 41-50.
36. Shanmugam, S.; Xu, J.; Boyer, C. *Macromolecules* **2014,** 47, (15), 4930-4942.
37. Girard, E.; Liu, X.; Marty, J.-D.; Destarac, M. *Polym. Chem.* **2014,** 5, (3), 1013-1022.
38. Debuigne, A.; Caille, J.-R.; Jérôme, R. *Macromolecules* **2005,** 38, (13), 5452-5458.
39. Kermagoret, A.; Fustin, C.-A.; Bourguignon, M.; Detrembleur, C.; Jérôme, C.; Debuigne, A. *Polymer Chemistry* **2013,** 4, (8), 2575.
40. Hurtgen, M.; Liu, J.; Debuigne, A.; Jerome, C.; Detrembleur, C. *Journal of Polymer Science Part A: Polymer Chemistry* **2012,** 50, (2), 400-408.
41. Miao, X.; Zhu, W.; Zhang, Z.; Zhang, W.; Zhu, X.; Zhu, J. *Polym. Chem.* **2014,** 5, (2), 551-557.
42. Kermagoret, A.; Mathieu, K.; Thomassin, J.-M.; Fustin, C.-A.; Duchêne, R.; Jérôme, C.; Detrembleur, C.; Debuigne, A. *Polym. Chem.* **2014,** 5, (22), 6534-6544.
43. Xue, Z.; Poli, R. *Journal of Polymer Science Part A: Polymer Chemistry* **2013,** 51, (16), 3494-3504.

44. Tonnar, J.; Pouget, E.; Lacroix-Desmazes, P.; Boutevin, B. *European Polymer Journal* **2008,** 44, (2), 318-328.
45. Singh, P.; Srivastava, A.; Kumar, R. *Journal of Polymer Science Part A: Polymer Chemistry* **2012,** 50, (8), 1503-1514.
46. Jiang, X.; Li, Y.; Lu, G.; Huang, X. *Polymer Chemistry* **2013,** 4, (5), 1402-1411.
47. Yang, Y.; Tang, G.; Hu, M.; Shao, L.; Li, J.; Bi, Y. *Polymer* **2015,** 68, 213-220.
48. Liang, X.; Kozlovskaya, V.; Cox, C. P.; Wang, Y.; Saeed, M.; Kharlampieva, E. *Journal of Polymer Science Part A: Polymer Chemistry* **2014,** 52, (19), 2725-2737.
49. Zhao, X.; Coutelier, O.; Nguyen, H. H.; Delmas, C.; Destarac, M.; Marty, J.-D. *Polymer Chemistry* **2015,** 6, (29), 5233-5243.
50. Maji, S.; Zhang, Z.; Voorhaar, L.; Pieters, S.; Stubbe, B.; Van Vlierberghe, S.; Dubruel, P.; De Geest, B. G.; Hoogenboom, R. *RSC Adv.* **2015,** 5, (53), 42388-42398.
51. Vancoillie, G.; Frank, D.; Hoogenboom, R. *Progress in Polymer Science* **2014,** 39, (6), 1074-1095.
52. Bendejacq, D. D.; Ponsinet, V. *The journal of physical chemistry. B* **2008,** 112, (27), 7996-8009.
53. Lejeune, E.; Drechsler, M.; Jestin, J.; Müller, A. H. E.; Chassenieux, C.; Colombani, O. *Macromolecules* **2010,** 43, (6), 2667-2671.
54. Moskowitz, J. D.; Wiggins, J. S. *Polymer* **2016,** 84, 311-318.
55. Charbonneau, C. l.; Chassenieux, C.; Colombani, O.; Nicolai, T. *Macromolecules* **2011,** 44, (11), 4487-4495.
56. Borisova, O.; Billon, L.; Zaremski, M.; Grassl, B.; Bakaeva, Z.; Lapp, A.; Stepanek, P.; Borisov, O. *Soft Matter* **2011,** 7, (22), 10824.
57. Cherifi, N.; Issoulie, A.; Khoukh, A.; Benaboura, A.; Save, M.; Derail, C.; Billon, L. *Polymer Chemistry* **2011,** 2, (8), 1769.
58. Mok, M. M.; Pujari, S.; Burghardt, W. R.; Dettmer, C. M.; Nguyen, S. T.; Ellison, C. J.; Torkelson, J. M. *Macromolecules* **2008,** 41, (15), 5818-5829.
59. Kirsh, Y. E.; Kirsh, I. U. Ė., *Water Soluble Poly-N-Vinylamides: Synthesis and Physicochemical Properties*. Wiley: 1998.
60. Cortez-Lemus, N. A.; Licea-Claverie, A. *Progress in Polymer Science* **2016,** 53, 1-51.
61. Pashkin, II; Kirsh, Y. E.; Zubov, V. P.; Anisimova, T. V.; Kuzkina, I. F.; Voloshina, Y. P.; Krylov, A. V. *Vysokomol. Soedin.* **1993,** 35, (5), A481-A484.
62. Brandrup, J.; Immergut, E. H.; Grulke, E. A., *Polymer Hanbook, 4th Edition*. 2003; p 2336.
63. Skorikova, Y. Y.; Karaputadze, T. M.; Ovsepyan, A. M.; Aksenov, A. I.; Kirsh, Y. E. *Vysokomolekulyarnye Soedineniya Seriya B* **1985,** 27, (11), 869-871.
64. Bernard, J.; Favier, A.; Zhang, L.; Nilasaroya, A.; Davis, T. P.; Barner-Kowollik, C.; Stenzel, M. H. *Macromolecules* **2005,** 38, (13), 5475-5484.
65. Chassenieux, C.; Nicolai, T.; Durand, D. *Macromolecules* **1997,** 30, (17), 4952-4958.
66. Lejeune, E.; Chassenieux, C.; Colombani, O., pH Induced Desaggregation Of Highly Hydrophilic Amphiphilic Diblock Copolymers. In *Trends in Colloid and Interface Science Xxiv*, Starov, V.; Prochazka, K., Eds. 2011; Vol. 138, pp 7-16.
67. Patterson, J. P.; Kelley, E. G.; Murphy, R. P.; Moughton, A. O.; Robin, M. P.; Lu, A.; Colombani, O.; Chassenieux, C.; Cheung, D.; Sullivan, M. O.; Epps, T. H., III; O'Reilly, R. K. *Macromolecules* **2013,** 46, (15), 6319-6325.
68. Gottlieb, H. E.; Kotlyar, V.; Nudelman, A. *Journal of Organic Chemistry* **1997,** 62, 7512-7515.
69. Liu, J.; Detrembleur, C.; De Pauw-Gillet, M.-C.; Mornet, S.; Duguet, E.; Jérôme, C. *Polymer Chemistry* **2014,** 5, (3), 799-813.

70. Peng, H.; Kather, M.; Rübsam, K.; Jakob, F.; Schwaneberg, U.; Pich, A. *Macromolecules* **2015,** 48, (13), 4256-4268.
71. Dufils, P. E.; David, G.; Boutevin, B.; Woodward, G.; Otter, G.; Guinaudeau, A.; Mazières, S.; Destarac, M. *Journal of Polymer Science Part A: Polymer Chemistry* **2012,** 50, (10), 1997-2007.
72. Mayo, F. R.; Lewis, F. M. *Macromolecules* **1944,** 66, 1594-1601.
73. Kelen, T.; Tüdos, F. *Macromol. Sci. Chem.* **1975,** A9, 1-27.
74. Hunley, M. T.; Beers, K. L. *Macromolecules* **2013,** 46, (4), 1393-1399.
75. Dréan, M.; Guégan, P.; Detrembleur, C.; Jérôme, C.; Rieger, J.; Debuigne, A. *Macromolecules* **2016,** 49, (13), 4817-4827.
76. Dréan, M.; Guégan, P.; Jérôme, C.; Rieger, J.; Debuigne, A. *Polym. Chem.* **2016,** 7, (1), 69-78.
77. Tüdos, F.; Kelen, T.; Földes-Berezsnich, T.; Turcsanyi, B. *Journal of Macromolecular Science—Chemistry* **1976,** 10, (8), 1513-1540.
78. Van Den Brink, M.; Van Herk, A. M.; German, A. L. *Journal of Polymer Science Part A: Polymer Chemistry* **1999,** 37, (20), 3793-3803.
79. Couvreur, L.; Charleux, B.; Guerret, O.; Magnet, S. *Macromolecular Chemistry and Physics* **2003,** 204, (17), 2055-2063.
80. Lessard, B. t.; Schmidt, S. C.; Marić, M. *Macromolecules* **2008,** 41, (10), 3446-3454.
81. Guerrero-Sanchez, C.; Harrisson, S.; Keddie, D. J. *Macromolecular Symposia* **2013,** 325-326, (1), 38-46.
82. Skeist, I. *Journal of the American Chemical Society* **1946,** 68, (9), 1781-1784.
83. Meyer, V. E.; Lowry, G. G. *Journal of Polymer Science Part A: General Papers* **1965,** 3, (8), 2843-2851.
84. Harrisson, S.; Ercole, F.; Muir, B. W. *Polymer Chemistry* **2010,** 1, (3), 326-332.
85. Klumperman, B.; Chambard, G.; Brinkhuis, R. H. G. **2003,** 854, 180-192.
86. Zapata-González, I.; Hutchinson, R. A.; Matyjaszewski, K.; Saldívar-Guerra, E.; Ortiz-Cisneros, J. *Macromolecular Theory and Simulations* **2014,** 23, (4), 245-265.
87. Konkolewicz, D.; Krys, P.; Matyjaszewski, K. *Accounts of Chemical Research* **2014,** 47, (10), 3028-3036.
88. Peng, H.; Xu, W.; Pich, A. *Polym. Chem.* **2016,** 7, (31), 5011-5022.

*The work presented in this chapter concerning the RAFT/MADIX bulk copolymerization of VAc and VCL mediated by a xanthate molecular chain transfer agent has been published in Macromolecules. Etchenausia, L.; Malho Rodrigues, A.; Harrison, S.; Deniau-Lejeune, E.; Save M. RAFT copolymerization of vinyl acetate and N-vinylcaprolactam: kinetics, control, copolymer compositions and thermoresponsive self-assembly. Macromolecules **2016**, 18, 6799-6809*

Acknowledgements

The Institute of Macromolecular Chemistry, Supramolecular polymer systems Department (Prague, Czech Republic) is sincerely acknowledged for the access to the refractometer facility (for dn/dc measurements) and SLS equipment.

PART I - CHAPTER 2. RAFT/MADIX emulsion copolymerization of vinyl acetate and *N*-vinylcaprolactam: towards physically crosslinked thermoresponsive particles

I. Introduction

In the early 2000s, different research groups have made tremendous efforts to transpose the control of radical polymerization from homogeneous systems (bulk, solution) to heterogeneous systems and especially to the industrially relevant emulsion polymerization process performed in aqueous dispersed media.[1-3] As reported in several reviews, most of the investigations focused on controlling the polymerization in aqueous dispersed media of (meth)acrylic or styrenic monomers,[1-3] while very few studies concerned the controlled radical polymerization of less activated monomers (LAM) such as vinyl acetate (VAc)[4-11] or vinyl chloride (VC).[12] Note that no studies have been reported on CRP of *N*-vinylamides in aqueous dispersed media.

Miniemulsion polymerization was the first promising way to control the RAFT/MADIX polymerization of VAc mediated either by a molecular xanthate chain-transfer agents[4-6] or by a poly(vinyl chloride) macromolecular chain-transfer agent synthesized by implementing RAFT miniemulsion of VC.[12] Cobalt-mediated radical polymerization was also efficient to control the miniemulsion polymerization of VAc.[7] In all these studies, stable PVAc latexes were produced simultaneously to the control over the polymerization characterized by a linear increase of the number-average molar masses with the monomer conversion and average dispersity values ranging between 1.2 and 2.0. Later, the control of VAc polymerization mediated by a molecular chain-transfer agent was implemented in emulsion polymerization.[8, 9] Zhao *et al.* studied the RAFT of VAc in emulsion polymerization using a water-soluble protonated (*N*-*N*-dialkyl dithiocarbamate) (methyl 3-[(morpholin-4-ylcarbonothyol)thio]propanoate) as chain-transfer agent (CTA) (**Scheme 1**).[8] Stable PVAc latexes were synthesized with hydrodynamic diameters below 100 nm but no values of particle size distribution were reported. The synthesized PVAc exhibited number-average molar masses (M_n) ranging between 85 000 – 160 000 g.mol^{-1} with dispersity values $Đ$ increasing from 1.5 to 3.4 by decreasing the initial molar ratio between the molecular CTA and the initiator from 6 to 1.

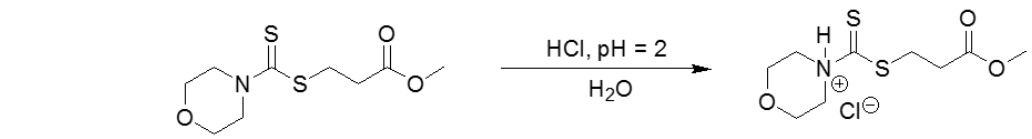

(methyl 3-[(morpholin-4-ylcarbonothioyl)thio]propanoate)

Scheme 1. Water-soluble protonated chain-transfer agent used in reference 8.

Nomura *et al.*[9] interestingly compared RAFT/MADIX polymerization and iodine-transfer radical polymerization to control VAc emulsion polymerization. Ethyl-iodo acetate (EIA, **Scheme 2**) was used as chain transfer agent in iodine-transfer radical emulsion polymerization. For all the experiments, the number-average molar masses of the synthesized PVAc ranged between 5 100 and 16 400 g.mol^{-1} and were close to the theoretical M_n with dispersity values ranging from 2.2 to 4.0. A control experiment performed in the absence of EIA produced PVAc with higher M_n of 88 500 g.mol^{-1} and higher dispersity value ($Đ$ = 5.3), confirming the ability of EIA to control the VAc polymerization in emulsion. The synthesis of stable latexes was achieved except for the experiments performed with the highest [EIA]/[initiator] ratio. For the RAFT/MADIX emulsion polymerizations of VAc, the macromolecular features (M_n and $Đ$) and stability of the final PVAc latexes were studied as a function of the initial molar fractions of monomer, chain transfer agent and initiator. In this study, different xanthates and dithiocarbamates were tested as chain-transfer agents (**Scheme 2**). While satisfactory latex stability was systematically observed with experimental M_n close to the theoretical M_n, the dispersity values of PVAc were lower ($Đ$ = 1.4 to 2.7) with dithiocarbamate compared to xanthate ($Đ$ = 1.4 to 3.7). It was concluded that ethyl-2-(diethylcarbamothioylthio)proponiate was the most efficient CTA to produce stable PVAc latexes with controlled molar masses and dispersity of 1.5. This study highlighted that RAFT/MADIX polymerization ensured a better control of VAc in emulsion polymerization than iodine-transfer radical polymerization. However, the colloidal features of the latex synthesized were sparsely provided all along the study.

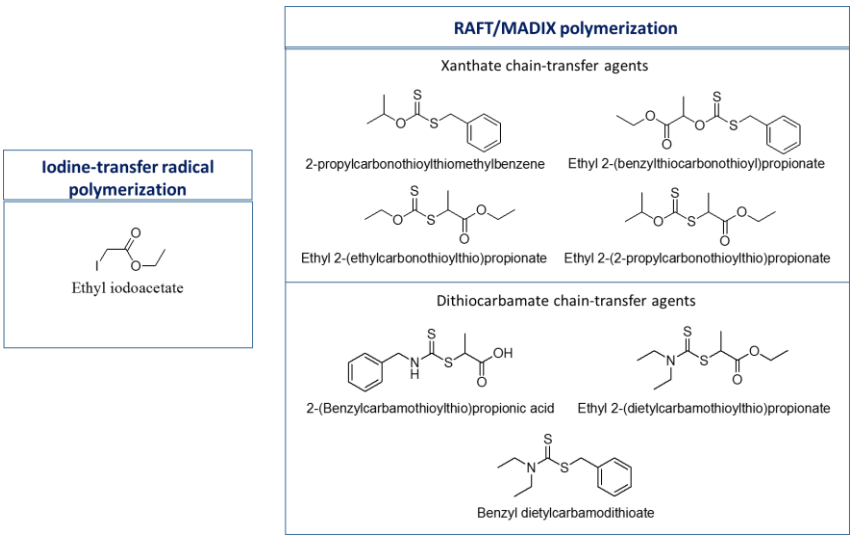

Scheme 2. Chemical structures of the different chain transfer agents (CTA) used in reference 9.

Among the different strategies investigated to implement controlled radical polymerization in aqueous dispersed media, the *in-situ* formation of amphiphilic diblock copolymers simultaneously to the particle growing via emulsion polymerization process, in a concept known as *"polymerization-induced self-assembly"* (PISA), has emerged as the most efficient method.[13, 14] PISA simultaneously addressed several challenges. The use of the reactive hydrophilic polymer producing the initial block copolymer micelles overcame the issue of diffusion of the hydrophobic control agent to the loci of polymerization, hence offering the opportunity to implement controlled radical polymerization in a batch *ab initio* emulsion polymerization process.[15, 16] Moreover, it is a straightforward method to synthesize stable hairy latex particles at high solids content by surfactant-free emulsion polymerization. Finally, it is an alternative route to produce self-assembled block copolymer nano-objects dispersed in polar continuous phase by a one-step method.[13, 14, 17]

Very few studies have been reported on the emulsion polymerization of less activated monomers (LAM) in the presence of a reactive hydrophilic polymer. A first study described the synthesis of a xanthate-functionalized polysaccharide (dextran) to act as efficient reactive stabilizer in emulsion polymerization of VAc.[10] More recently, RAFT/MADIX emulsion polymerization of VAc was performed in the presence of different xanthate-functionalized hydrophilic polymers (poly(ethylene glycol) (PEG), poly(*N*-vinylpyrrolidone) (PNVP) and poly(*N*-acryloymorpholine) (PNAM)).[11] Stable PVAc latexes with diameters ranging from 100 to 350 nm and variable particle size distributions (dispersity from 0.02 to 0.30) were obtained

in all the cases. The linear increase of M_n with the monomer conversion attested of some control of the VAc polymerization with dispersity values ranging between 2.0 and 3.5. Therefore, these xanthate-functionalized polymers efficiently acted as both stabilizers and macromolecular chain transfer agents (macro-RAFT) for VAc emulsion polymerization. However, PNVP and PEG mediated emulsion polymerization exhibited the presence of dead chains of macro-RAFT, ascribed to the presence of degradation products.

Despite the interesting features of the biocompatible thermoresponsive poly(*N*-vinylcaprolactam) (PVCL), controlled radical polymerization of VCL by polymerization in aqueous dispersed media has never been investigated up to now. Herein, we present the first example of emulsion copolymerization of VCL and VAc mediated by a xanthate-functionalized poly(ethylene glycol) (PEG-X) as the reactive macromolecular stabilizer to follow the PISA mechanism. The preliminary study of chapter 1 of Part I of this manuscript demonstrated that xanthate–mediated RAFT/MADIX copolymerization of VAc/VCL was well-controlled in bulk with a close reactivity of both monomers (r_{VAc} = 0.33 and r_{VCL} = 0.29). These P(VAc-*co*-PVCL) amphiphilic copolymers of homogeneous distribution exhibited tunable phase transition temperature and self-assembly behavior depending on the fraction of hydrophobic VAc. Indeed, static light scattering measurements highlighted that P(VAc-*co*-VCL) copolymer with F_{VAc} = 0.53 had the capability to self-assemble in water into trimer aggregates at a temperature below the cloud point temperature, by means of hydrophobic interactions.

The dual objective of the work of the present Chapter 2 is to synthesize the amphiphilic thermoresponsive PEG-*b*-P(VAc-*co*-VCL) block copolymers of controlled molar mass directly in aqueous dispersed media while providing the opportunity to prepare thermoresponsive particles physically crosslinked by hydrophobic interactions (**Scheme 3**). The present work provides insight into the control of RAFT/MADIX emulsion copolymerization of VAc and VCL as well as the features of the synthesized thermoresponsive colloidal particles, in relationship with the initial VAc monomer feed ratio. Moreover, as poly(vinyl alcohol) (PVA) is a biocompatible polymer of interest for a wide field of applications, thermoresponsive P(VA-*co*-VCL) copolymers are prepared by hydrolysis of the P(VAc-*co*-VCL)-based precursor copolymers in methanol.

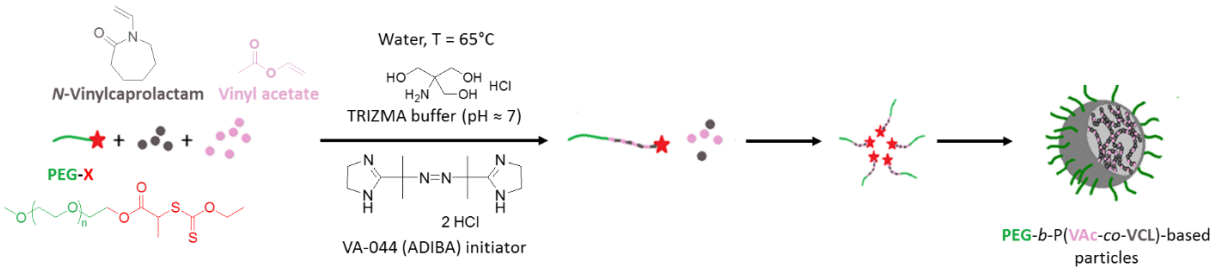

Scheme 3. PEG-*b*-P(VAc-*co*-VCL)-based particles via PISA emulsion polymerization.

II. Experimental part

1. Materials

Vinyl acetate (VAc, Sigma Aldrich, 99 %$^{+}$) was mixed with inhibitor removers (Sigma Aldrich, 0.1 g of inhibitor remover for 50 mL of VAc) for 30 min prior to be filtered and used for polymerization. *N*-vinylcaprolactam (VCL, Sigma Aldrich, 98 %), Poly(ethylene glycol) methyl ether (PEG-OH, M_n = 2 000 g.mol^{-1}, Sigma Aldrich), 2-bromopropionyl bromide (Sigma Aldrich, 97 %), anhydrous dichloromethane (Sigma Aldrich, 99,8 %), triethylamine (Sigma Aldrich, 99 %), potassium ethyl xanthogenate (Sigma Aldrich, 96 %), tris(hydroxymethyl)aminomethane hydrochloride buffer (TRIZMA, Sigma Aldrich, 99 %), potassium hydroxide (Sigma Aldrich, 90 %), methanol (Sigma Aldrich, 99,8 %) and 2,2'-Azobis[2-(2-imidazolin-2-yl)propane] dihydrochloride (ADIBA or VA-044, Wako, 99 %) were used as received. For the emulsion copolymerizations double deionized water was used as continuous medium.

2. Preparation of xanthate-terminated PEG (PEG-X) macro-chain transfer agent by PEG-OH chain-end modification

The xanthate-terminated PEG macro-chain transfer agent was prepared from poly(ethylene glycol) methyl ether (PEG-OH, M_n = 2 000 g.mol^{-1}) using a two-steps procedure (**Scheme 4**).

In the first step, 10 g of PEG-OH were modified using 2-bromopropionyl bromide. For that purpose, PEG-OH was dried *via* cryo-distillation of toluene (25 mL) under reduced pressure. Then, dried PEG-OH (10 g, 5 mmol -OH group), anhydrous dichloromethane (125 mL) and triethylamine (TEA, 2.1 mL, 15 mmol) were introduced in a 250 mL round-bottom flask placed in an ice-bath and mixed at 400 rpm. A solution of 2-bromopropionyl bromide (1.6 mL, 15

mmol) in anhydrous dichloromethane (25 mL) was added drop-wise to the solution over 3 hours. The solution was then stirred for 24 h at room temperature. The solution was filtrated twice to remove the precipitated triethylammonium bromide salts. The polymer solution was concentrated by rotary evaporation and precipitated into cold diethyl ether. The recovered product was dried under vacuum for overnight.

In the second step, PEG-Br and potassium ethyl xanthogenate were dried under vacuum (0.5 mmHg) for 24 h prior to the reaction. PEG-Br (2.01 g, 1 mmol), potassium ethyl xanthogenate (0.56 g, 3.5 mmol) and anhydrous dichloromethane (16 mL) were mixed together in a 50 mL round-bottom flask placed in an ice-bath and stirred at 400 rpm for 24 h at room temperature. The solution was filtrated twice to remove the precipitated salts. The polymer solution was concentrated by rotary evaporation and precipitated into cold diethyl ether prior to be dried under vacuum for overnight. The final xanthate-terminated PEG macro-chain transfer agent (PEG-X) was recovered as a white to slightly yellow powder with a yield of 95 %.

3. General procedure for the RAFT/MADIX emulsion copolymerization of VAc and VCL mediated by a xanthate-terminated PEG macro-chain transfer agent

The reactions were carried out at 10 wt-% of initial solids content, with different initial molar fractions of VAc ($f_{VAc,0}$ = 0.2, expt 1 in **Table 6** and $f_{VAc,0}$ = 0.5, expt 2 in **Table 6**). For both experiments, the $[Monomer]_0/[PEG\text{-}X]_0$ and $[PEG\text{-}X]_0/[ADIBA]_0$ ratios were respectively set at 430 and 3.2 considering 85 % of functionalization of PEG. As example of experiment 2 in **Table 6**, 1,3,5-trioxane (0.40 g, 4.4×10^{-3} mol), TRIZMA buffer (0.15 g, 9.5×10^{-4} mol), PEG-X (LE 242, 0.30 g, 1.0×10^{-4} mol), *N*-vinylcaprolactam (3.10 g, 2.2×10^{-2} mol), vinyl acetate (1.90 g, 2.2×10^{-2} mol) and deionized water (48.00 g) were introduced in a 100 mL round-bottom flask and stirred magnetically at 300 rpm. The mixture was purged with nitrogen for 30 min in an ice-bath. A sample was withdrawn under nitrogen at time t = 0. The round-bottom flask was placed into an oil-bath previously heated to 65°C. The cationic initiator was added under nitrogen flow at 65°C (10.40 mg of ADIBA dissolved in 2 g of deionized water, 3.2×10^{-5} mol of ADIBA). The polymerization reaction was then allowed to continue with stirring for 5h30 at 65°C. At the end of the reaction, a sample was withdrawn and kept at 65°C for DLS analysis. The reaction mixture was subsequently cooled to 25°C and oxygen was introduced in the reaction mixture.

The same protocol was followed for the free radical emulsion copolymerization of VAc and VCL using PEG-OH as stabilizer (expt 3 in **Table 6**).

4. Alkaline hydrolysis of the PEG-*b*-P(VAc-*co*-VCL) copolymers

In a typical experiment, the dialyzed (M_w cut-off: 3500 Da) and freeze-dried PEG-*b*-P(VAc$_{0.17}$-*co*-VCL$_{0.83}$), (expt 1 in **Table 6**, 0.10 g, 6.2 × 10^{-6} mol) was introduced in a 10 mL round-bottom flask and dissolved in 2.9 g of methanol. A solution of 38.1 mg of KOH (6.8 × 10^{-4} mol, [KOH] = 1.4 × 10^{-1} mol.L^{-1}) dissolved in 1.0 g of methanol was then added to the flask. The mixture was stirred at room temperature for 18 h. Subsequently, the solution was dialyzed against distilled water through a Spectra/Pore membrane (M_w cut-off: 3500 Da) for 48 h and the PEG-*b*-P(VA-*co*-VCL) copolymer was recovered by freeze-drying. The same procedure was followed for the alkaline hydrolysis of PEG-*b*-P(VAc$_{0.47}$-*co*-VCL$_{0.53}$) copolymer (expt 2 in **Table 6**).

5. Characterization methods

Nuclear Magnetic Resonance (NMR) spectroscopy. NMR spectra were recorded using a Brüker 400 MHz spectrometer, at 25°C, except for the characterization of PEG-*b*-P(VA-*co*-VCL) copolymers which was performed at 80°C. ^{1}H measurements were performed at frequencies of 400 MHz and ^{13}C measurements at 100 MHz.

For the characterization of PEG-OH, PEG-Br and PEG-X polymers, $CDCl_3$ was used as solvent. For the copolymerization reaction performed in emulsion, different methodologies were tested for the determination of individual VCL conversion by NMR. Analysis were performed either on the crude samples or after water and VAc evaporation. Different solvents were also examined: $CDCl_3$ and deuterated acetone acetone-d_6.

$CDCl_3$ was used as solvent for the ^{13}C NMR analysis of PEG-*b*-P(VAc-*co*-VCL) copolymers. DMSO-d_6 was used as solvent for the DOSY-NMR analysis of dialyzed and freeze-dried PEG-*b*-P(VAc-*co*-VCL) copolymers before and after alkaline hydrolysis.

The final overall molar conversion (X_m) was calculated from nuclear magnetic resonance spectra in acetone-d_6 using 1,3,5-trioxane as internal standard (Equation 1).

$$X_m = 1 - \frac{\left(I(1H_{VAc} + 1H_{VCL}) / I1H_{triox.}\right)_t}{\left(I(1H_{VAc.} + 1H_{VCL}) / I1H_{triox.}\right)_0}$$ Equation 1

$I_{1H,triox}$ corresponds to the integral of one proton of 1,3,5-trioxane (5.1 ppm, 6 H) used as internal standard and $I_{(1H,VAc\ +\ 1H,VCL)}$ corresponds to the integral of the vinylic protons of both VCL monomer and VAc monomer at 7.1-7.4 ppm ($I_{7.1\text{-}7.4\ ppm} = I_{1H,VAc} + I_{1H,VCL}$).

The compositions of the PEG-*b*-P(VAc-*co*-VCL) copolymers (F_{EG}, F_{VAc} and F_{VCL}) were calculated on the basis of the integrals of the protons of each polymer unit of ^{1}H NMR spectra (**Figure 1**) of the dialyzed and freeze-dried copolymers (Equation 2 to Equation 4).

$$F_{VAc} = \frac{n_{VAc}}{n_{VAc} + n_{VCL} + n_{EG}} = \frac{I_{IV}/3}{\frac{I_b}{4} + I_{C,III}}$$ Equation 2

$$F_{VCL} = \frac{n_{VCL}}{n_{VAc} + n_{VCL} + n_{EG}} = \frac{I_{C,III} - I_{IV}/3}{\frac{I_b}{4} + I_{C,III}}$$ Equation 3

$$F_{EG} = \frac{n_{VCL}}{n_{VAc} + n_{VCL} + n_{EG}} = \frac{\frac{I_b}{4}}{\frac{I_b}{4} + I_{C,III}}$$ Equation 4

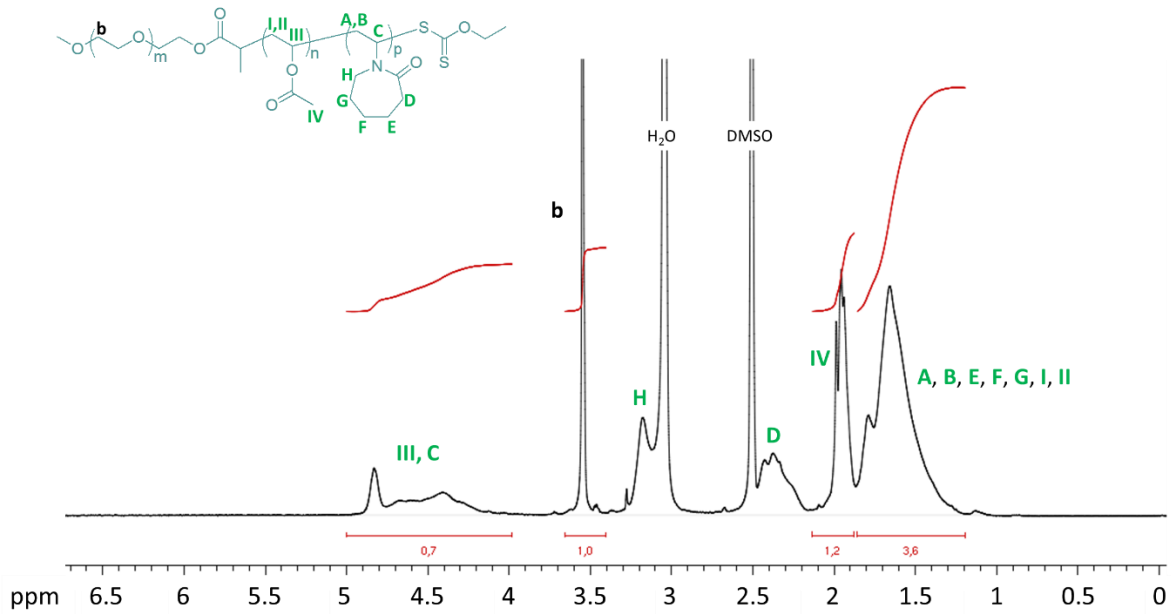

Figure 1. ^{1}H NMR spectrum in DMSO-d_6 of the dialyzed and freeze-dried PEG-*b*-P($VAc_{0.47}$-*co*-$VCL_{0.53}$).

The compositions of the P(VAc-*co*-VCL) blocks (F_{VAc} and F_{VCL}) were calculated on the basis of the integrals of the well-resolved carbonyl signals at 170 – 180 ppm of each polymer unit of

the P(VAc-*co*-VCL) copolymer (Equation 5 and **Figure 2**) and on the basis of the integrals of the protons of each polymer unit of ^{1}H NMR spectra (Equation 6 and **Figure 1**).

$$F_{VAc} = \frac{I_{C=O,PVAc}}{I_{C=O,PVAc} + I_{C=O,PVCL}} \quad \text{Equation 5}$$

$$F_{VAc} = \frac{I_{IV}/3}{I_{III,C}} \quad \text{Equation 6}$$

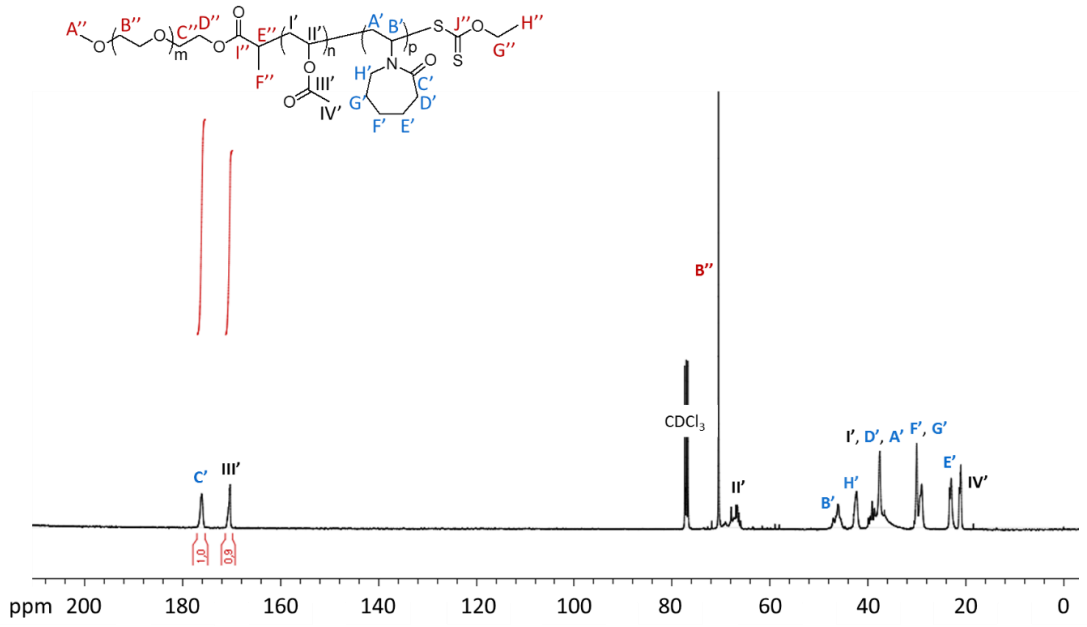

Figure 2. ^{13}C NMR spectra in $CDCl_3$ of the dialyzed and freeze-dried PEG-*b*-P($VAc_{0.47}$-*co*-$VCL_{0.53}$).

The copolymers synthesized by emulsion polymerization were characterized by DOSY NMR spectroscopy in DMSO-d_6. The NMR DOSY experiments were performed using the bipolar longitudinal eddy current delay pulse sequence (BPLED). The spoil gradients were also applied at the diffusion period and the eddy current delay. Typically, a value of 2 ms was used for the gradient duration (δ), 150 ms for the diffusion time (Δ), and the gradient strength (g) was varied from 1.67 G.cm^{-1} to 31.88 G.cm^{-1} in 32 steps. Each parameter was chosen to obtain 95 % signal attenuation for the slowest diffusion species at the last step experiment. The pulse repetition delay (including acquisition time) between each scan was larger than 2s. Data acquisition and analysis were performed using the Bruker Topspin software (version 2.1). The T1/T2 analysis module of Topspin was used to calculate the diffusion coefficients and to create 2-D spectra with NMR chemical shifts along one dimension and the calculated diffusion coefficients along the other.

Size Exclusion Chromatography (SEC). The SEC system operates in THF, at 30°C (flow rate: 1mL.min^{-1}). The SEC apparatus is equipped with a Viscotek VE 5200 automatic injector, a pre-column and two columns (Styragels HR 5E and 4E (7.8 × 300 mm)) working in series, a Wyatt Heleos II Multi Angle Laser Light Scattering detector (MALLS, 18 angles, λ_0 = 664.4 nm), a viscosimeter detector (Wyatt Viscostar II), a refractive index (RI) detector Viscotek VE 3580 and a Viscotek VE 3210 UV-visible detector. Toluene was used as flow marker. All (co)polymer samples were prepared at 3 g.L^{-1} concentrations. The number-average molar mass (M_n) and molar mass distribution ($Đ$) were obtained from MALLS data using the M_i value of each slice of the chromatogram (Zimm-plot equation, see experimental part of the Part I - Chapter 1). The experimental M_n are compared to the theoretical number-average molar masses of the copolymers calculated from Equation 7.

$$Mn_{theo.} = M_{\mathrm{PEG-X}} + X_m \frac{[\mathrm{M}]_0 \times (f_{\mathrm{VAc},0} \times M_{\mathrm{VAc}} + f_{\mathrm{VCL},0} \times M_{\mathrm{VCL}})}{[(f \times [\mathrm{PEG-X}]_0 + [\mathrm{Initiator}]_0\ (1-e^{-k_d \times t})]}$$ Equation 7

Where $M_{\mathrm{PEG\text{-}X}}$ corresponds to the molar mass of the PEG-X macromolecular chain-transfer agent ($M_{\mathrm{n,\ PEG\text{-}X,\ MALLS}}$ = 2 240 g.mol^{-1}), X_m is the final overall molar conversion calculated from NMR spectra (see Equation 1), f is the PEG-X functionality (f = 0.85), k_d is the initiator dissociation constant ($k_{d,\ \mathrm{ADIBA,\ water,\ 70°C}}$[18] = 6.7 × 10^{-4} s^{-1}), t is the polymerization time, $[\mathrm{Xanthate}]_0$, $[\mathrm{Initiator}]_0$ and $[\mathrm{M}]_0$ are the initial concentrations of respectively the chain-transfer agent, the initiator and monomer ($[\mathrm{M}]_0 = [\mathrm{VAc}]_0 + [\mathrm{VCL}]_0$). $f_{\mathrm{VAc},0}$ and $f_{\mathrm{VCL},0}$ are the initial monomer feed ratios. M_{VAc} and M_{VCL} are the molar masses of each monomer (M_{VCL} = 139 g.mol^{-1} and M_{VAc} = 86 g.mol^{-1}).

The refractive index increments (dn/dc) in THF of the PEG-*b*-P(VAc-*co*-VCL) copolymers synthesized by emulsion copolymerization were determined using Equation 8.

$$(\mathrm{d}n/\mathrm{d}c)_{\mathrm{copo}} = w_{\mathrm{PEG}} \times \left(\frac{\mathrm{d}n}{\mathrm{d}c}\right)_{\mathrm{PEG}} + w_{\mathrm{PVAc}} \times \left(\frac{\mathrm{d}n}{\mathrm{d}c}\right)_{\mathrm{PVAc}} + w_{\mathrm{PVCL}} \times \left(\frac{\mathrm{d}n}{\mathrm{d}c}\right)_{\mathrm{PVCL}}$$ Equation 8

The dn/dc value of PEG homopolymer was reported in reference 19 $(\mathrm{d}n/\mathrm{d}c)_{\mathrm{PEG}}$ =0.068 mL.g^{-1}. The values of dn/dc of PVCL and PVAc homopolymers were respectively taken from references 20 and 19: $(\mathrm{d}n/\mathrm{d}c)_{\mathrm{PVCL}}$ = 0.109 mL.g^{-1} and $(\mathrm{d}n/\mathrm{d}c)_{\mathrm{PVAc}}$ = 0.0582 mL.g^{-1}.The weight fractions (w, Equation 9) of each polymeric component were calculated on the basis of the molar fractions determined using Equation 2 to Equation 4 and the molar mass of the monomer unit as reported in Equation 9 for VAc weight fraction for instance.

$$w_{\mathrm{VAc}} = \frac{F_{\mathrm{VAc}} \times M_{\mathrm{VAc}}}{F_{\mathrm{VAc}} \times M_{\mathrm{VAc}} + F_{\mathrm{VCL}} \times M_{\mathrm{VCL}} + F_{\mathrm{EG}} \times M_{\mathrm{EG}}}$$ Equation 9

with F_{mono} the molar fraction of the monomers in the copolymer and M_{mono} the molar masses of each monomer unit.

Turbidimetry analysis. Prior analysis samples were dialyzed against distilled water through a Spectra/Pore membrane (M_w cut-off: 3500 Da) for 48 h and recovered by freeze-drying. Turbidimetry measurements of the (co)polymers solutions (0.3 wt-% in water) were performed with a Shimadzu UV-2450PC spectrophotometer, from 13°C to 33°C (heating rate: 0.5°C/min). Transmittance at 500 nm was plotted versus the temperature. The minimum of the first-order derivative fit of transmittance versus temperature was considered as the temperature of cloud point ($T_{cloud\ point}$).

Dynamic Light Scattering (DLS). The hydrodynamic diameters (D_h) of the latex particles synthesized by emulsion copolymerization of VAc and VCL mediated by xanthate-terminated PEG macromolecular chain-transfer agent were measured at 55°C directly after withdrawing the latex at the end of the polymerization, without cooling step. Before analysis, samples were diluted by a factor 100 in warm distilled water and were characterized with a Vasco DL135 Cordouan Technologies equipment at λ_{laser} = 657 nm.

The evolution of the final average hydrodynamic diameters of aqueous solutions of PEG-*b*-P(VAc-*co*-VCL) copolymers before and after hydrolysis were measured as a function of the temperature, by dynamic light scattering (DLS), using a Zetasizer Nano ZS instrument (Malvern Instruments). A He-Ne 4.0mW power laser was used, operating at a wavelength of 633 nm. For evaluation of the data, the DTS (Nano) program was used. The hydrodynamic diameters were calculated from the diffusion coefficient using the Stokes-Einstein equation $D_h = \frac{k_B T}{3\pi\eta D}$ where T is absolute temperature, η the viscosity of the solvent, k_B the Boltzmann constant and D the diffusion coefficient. For the analysis of PEG-*b*-P(VAc-*co*-VCL), measurements were carried out at a solids content of 0.005 wt-% from 10°C to 55 °C, every to 2°C, except between 30 and 40°C where measurements were recorded each 1°C. Before each scan, the sample was maintained at the set temperature for 10 minutes. The analysis of P(VAc-*co*-VA-*co*-VCL) copolymers dispersed in deionized water were carried out at a concentration of 5 $g.L^{-1}$ from 10°C to 70°C, every 2°C.

UV-visible spectroscopy. PEG-X polymer was characterized by UV-Visible spectroscopy in a mixture of water:isopropanol (67:33 v:v%), with a Shimadzu UV-2450PC spectrophotometer. The molar extinction coefficient of the molecular xanthate agent ($\varepsilon_{xanthate}$) was previously determined in water:isopropanol (67:33 v:v%) from the slopes of absorbance versus concentration at λ = 355 nm, $\varepsilon_{xanthate,\ 355\ nm}$ = 54 L.mol^{-1}.cm^{-1}.

Fourier transform Infra-red (FTIR) spectroscopy. Spectra of the dialyzed and freeze-dried PEG-*b*-P(VAc-*co*-VCL) copolymers before and after hydrolysis were recorded on a FTIR NICOLET Magna-IR560, at 25°C. Attenuated total reflectance (ATR) mode was used.

Gravimetric analysis. For emulsion copolymerizations, we attempted to calculate the individual conversion in VAc by gravimetry on the basis of Equation 10.

$$x_{VAc} = \frac{\tau_{PVAc,exp.}}{\tau_{PVAc,theo.}} \quad \text{Equation 10}$$

with $\tau_{PVAc,exp.} = Dry\ extract - \tau_{salts}$

$$Dry\ extract = \frac{(m_{cup+\ dried\ sample} - m_{empty\ cup})}{(m_{cup+\ withdrawn\ sample} - m_{empty\ cup})} \text{ and } \tau_{salts} = \frac{m_{non-volatile\ compounds}}{m_{latex,0}}$$

and $\tau_{PVAc,theo.} = m_{VAc,0} / m_{latex,0}$

In τ_{salts} equation, the mass of non-volatile compounds includes the masses of VCL monomer, PEG-X macro-chain transfer agent, ADIBA initiator, TRIZMA buffer and 1,3,5-trioxane. For all the performed experiments, it should be pointed out that the conversions of VAc monomer estimated gravimetrically (Equation 10) were systematically negatives, meaning that τ_{salts} was overestimated in the calculation of $\tau_{PVAc,exp}$. Such overestimation was ascribed to the partial evaporation of VCL while it was initially considered as a non-volatile compound (VCL monomer being solid at room temperature). To quantify this VCL partial evaporation, 0.25 g of VCL were mixed with 0.254 g of VAc and 5.08 g of water in an aluminum cup. The cup was placed under a fume-hood for 48 h to reach a complete evaporation of VAc monomer and water. The residual mass was equal to 0.164 g, which indicated 34 % of VCL evaporation. Consequently, the calculation of the individual conversion in VAc is not achievable. We thus attempted to probe the individual conversion in VCL by ^{1}H NMR spectroscopy. Note that due to the VCL partial evaporation, the dried samples could not be analyzed for an accurate calculation of VCL conversion. The crude samples were poured into $CDCl_3$ for proton NMR

analysis but the intense signal of water overlaps with the only isolated signal of VCL monomer. Therefore, it was impossible to accurately determine individual monomer conversion of VCL neither.

III. Results and discussion

1. Preparation of xanthate-terminated PEG (PEG-X) macro-chain transfer agent

The xanthate-terminated PEG macro-chain transfer agent was synthesized in a two steps procedure from commercially available PEG-OH, according to **Scheme 4**. In the first step the hydroxyl end-group of PEG-OH was esterified with 2-bromopropionyl bromide, using triethylamine (TEA) as a base. The second step involved the nucleophilic substitution of potassium ethyl xanthogenate with PEG-Br leading to the xanthate-terminated PEG macro-chain transfer agent named as PEG-X throughout this work.

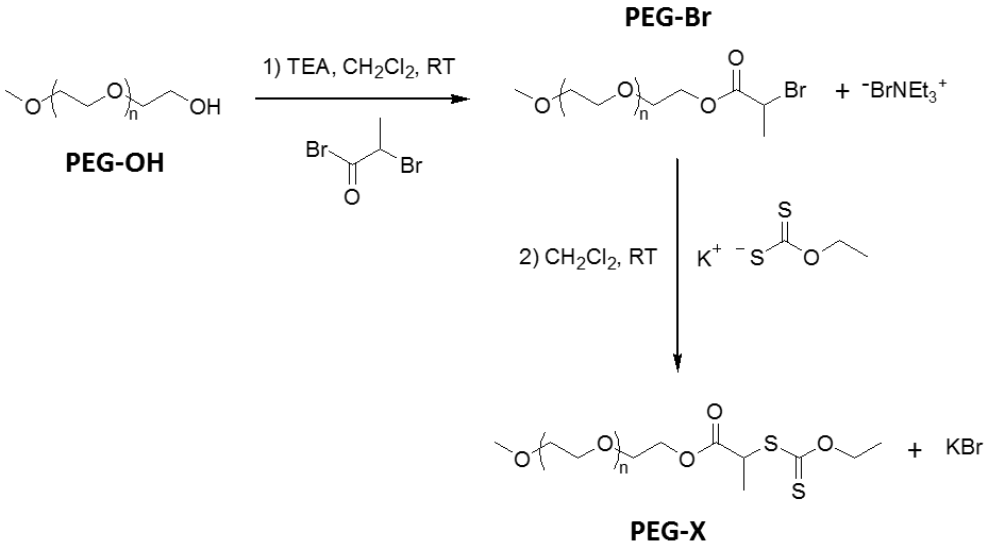

Scheme 4. Preparation of PEG-X macro-chain transfer agent.

The number-average molar mass of PEG-OH given by the supplier is 2 000 g.mol^{-1}, which corresponds to an average degree of polymerization (DP) equals to 44. The DP can also be calculated by proton NMR on the basis of the ratio between the peak integrations of the methylene protons of the PEG backbone (*b* protons at 3.5 ppm, $I_b = 1.17 – I_c = 1.17 - 2 \times I_a/3$

= 1.07, Figure 3 and **Table 2**) and the chain-end methyl protons at 3.3 ppm (*a*, I_a = 0.016, **Figure 3** and **Table 2**) : DP = I_b / (4 × I_a/3) = 47.

In addition, the PEG-OH was analyzed by SEC system running in THF eluent and equipped with a MALLS detector. As reported in **Table 1**, the number-average molar mass of PEG-OH was 2 200 g.mol^{-1} with a dispersity of 1.03.

Table 1. Macromolecular features of the commercially available PEG-OH.

	Supplier	**NMR**	**SEC using MALLS detector**
Mn *g.mol^{-1}*	2 000	2 160	2 200
DP	44	47	48

The efficiency of the PEG chain-end modification was monitored by ^{1}H NMR and ^{13}C NMR for each step (Figure 3 and Figure 4). It should be mentioned that PEG-Br and PEG-X were both precipitated into diethyl ether prior NMR analyses (see experimental part).

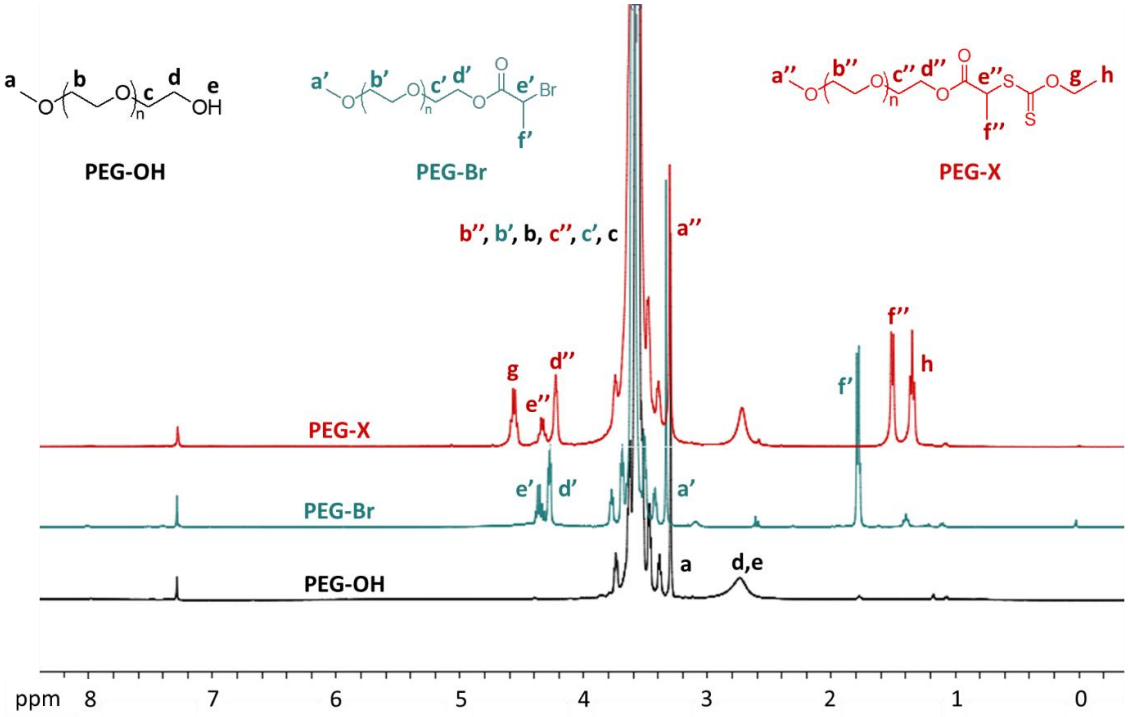

Figure 3. ^{1}H NMR spectra in $CDCl_3$ of the initial PEG-OH and the precipitated derivatized PEG-Br and PEG-X.

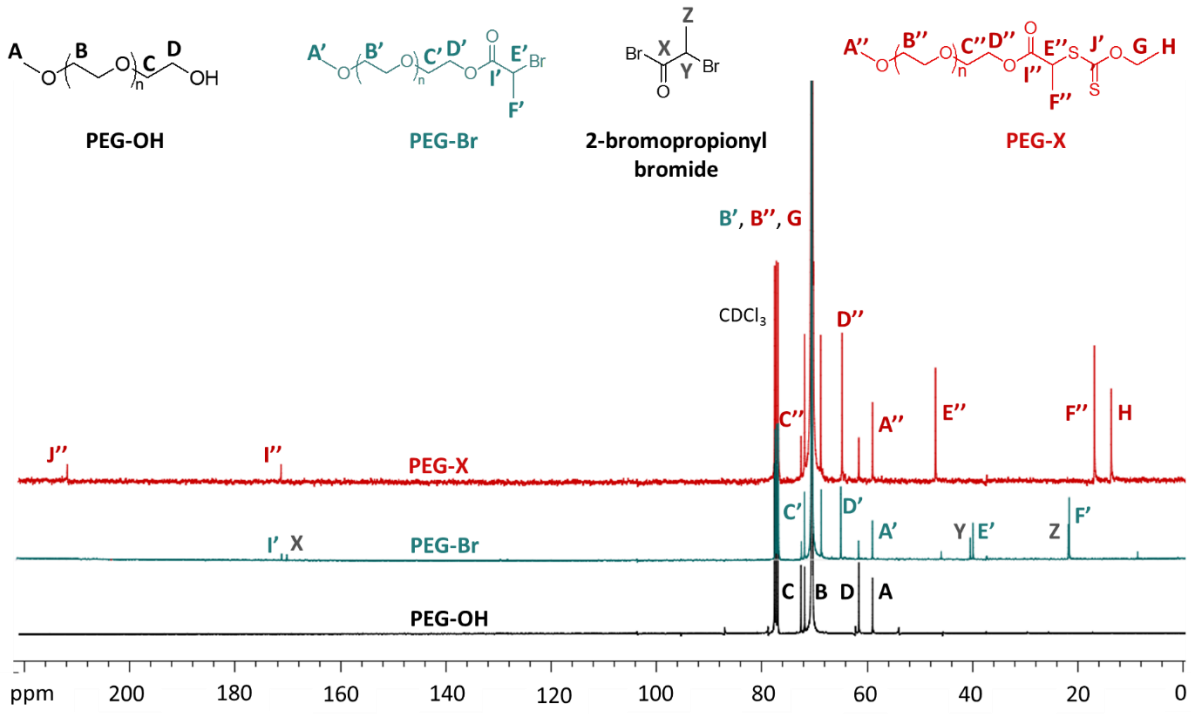

Figure 4. ^{13}C NMR spectra in $CDCl_3$ of the initial PEG-OH and the precipitated PEG-Br and PEG-X.

The proton and carbon NMR analyses of PEG-OH, PEG-Br and PEG-X (**Figure 3** and **Figure 4**) both confirm the successful functionalization of the PEG chain-end. The first incorporation of the 2-bromopropionyl end-group onto PEG-OH is confirmed by the presence of the corresponding methine and methyl groups (respectively *e'* at 4.3 ppm and *f'* at 1.8 ppm in ^{1}H NMR (**Figure 3**) and *E*' at 40 ppm and *F*' at 20 ppm in ^{13}C NMR (**Figure 4**). In the second step, the appearance of new peaks characteristics of the xanthogenate end-group at 1.3 ppm (methyl protons *h* in **Figure 3**) and 4.6 ppm (methylene protons *g* in **Figure 3**), as well as the shift of the methyl protons *f'* from 1.8 ppm in PEG-Br to 1.5 ppm in PEG-X (*f''* in **Figure 3**), confirm the effective preparation of the xanthate-terminated PEG. The ^{13}C NMR (**Figure 4**), confirms this result as a complete shift of the signals corresponding to *E'* and *F'* carbons of the PEG-Br towards *E''* and *F''* signals of PEG-X is observed, in the absence of residual *E'* and *F'*.

The functionalization degree of PEG was calculated from the integrals of the PEG-OH, PEG-Br and PEG-X characteristic protons summarized in **Table 2**.

Table 2. Integral values of the characteristic protons of PEG-OH, PEG-Br and PEG-X

PEG-OH	I_a	I_{b+c}	I_{d+e}					
	0.016	1.017	0.015					
PEG-Br	$I_{a'}$	$I_{b'+c'}$	$I_{d'}$	$I_{e'}$	$I_{f'}$			
	0.016	1.018	0.010	0.006	0.022			
PEG-X	$I_{a''}$	$I_{b''+c''}$	$I_{d''}$	$I_{e''}$	$I_{f''}$	I_g	I_h	$I_{2.8\ ppm} = I_{d+e}$
	0.013	1.024	0.007	0.003	0.011	0.008	0.011	0.010

For the first step (**Scheme 4**), the functionalization degree (*FD*) of PEG-OH by 2-bromopropionyl bromide was calculated considering the ratio between the integrations of the signals of the propionyl bromide end-group (*e'*, *f'*, **Figure 3**) and characteristic signals of the initial PEG-OH (*a'*, *b'* in **Figure 3**). As reported in **Table 4,** the average functionalization degree is above 100 %. The detailed analysis of the ^{13}C NMR spectrum of PEG-Br indeed reveals the presence of residual 2-bromopropionyl bromide as its characteristic carbon signals at 22, 42 and 165 ppm (*X*, *Y* and *Z* carbons, **Figure 4**) can be observed. This excess of molecular compound is not present in the ^{13}C NMR spectrum of PEG-X, so the precipitation of PEG-X provides a suitable purification step.

Table 3. Determination of the functionalization degree (FD) of PEG-OH by 2-bromopropionyl bromide.[a]

Calculation	FD (%)	Average FD (%)
$\frac{I_{f'}/3}{I_{b'}/(4\times47)} = \frac{I_{f'}/3}{I_{a'}/3}$	137	**129 ± 12**
$\frac{I_{e'}}{I_{b'}/(4\times47)} = \frac{I_{e'}}{I_{a'}/3}$	120	

[a] Functionalization degree, FD (%) = $100\times\frac{n_{\text{PEG-Br}}}{n_{\text{PEG-Br}}+n_{\text{PEG-OH}}}$

The signal corresponding to the $\underline{C}H_2OH$ carbon of the chain-end of PEG-OH (δ = 62 ppm, *D* carbon, **Figure 4**), observed in the ^{13}C NMR spectrum of PEG-Br indicates the presence of residual PEG-OH. On the basis of reference 21, the quantitative comparison of integral values of signals in ^{13}C NMR is suited in the case of comparison of similar carbons. Therefore, it is

possible to determine the amount of residual PEG-OH in PEG-Br as the *B'*, *D'* carbons are equivalents (methylene groups). On the basis of the integral values reported in **Table 4,** the molar fraction of residual PEG-OH in PEG-Br is equal to 17 mol-%.

Table 4. Determination of the amount of residual PEG-OH by ^{13}C NMR.

	PEG-Br
$\boldsymbol{I_{PEG\text{-}Br}}$[a]	1.0
$\boldsymbol{I_{PEG\text{-}Br} + I_{PEG\text{-}OH}}$[b]	1.2
Residual PEG-OH[c]	
molar %	17

[a] $I_{PEG\text{-}Br} = I_{D';}$ [b] $I_{PEG\text{-}Br} + I_{PEG\text{-}OH} = I_{B'} / (2 \times 47)$; [c] Residual PEG-OH (molar %) = $(1 - \frac{I_{PEG\text{-}Br}}{I_{PEG\text{-}Br+\ PEG\text{-}OG}}) \times 100$.

For the second step corresponding to the reaction of PEG-Br with potassium ethyl xanthogenate (**Scheme 4**), the yield of propionyl bromide converted into xanthate function was calculated by comparing the integrals of the characteristic protons of the xanthate end group (*g*, *h* in **Figure 3**) with the integrals of the propionyl group (*f*'' protons in **Figure 3**). The values reported in **Table 5** highlight a complete conversion of bromopropionyl bromide group into the propionyl xanthate group (average functionalization degree = 105 %).

Table 5. Determination of the functionalization degree of PEG-Br by potassium ethyl xanthogenate and fraction of xanthate-functionalized PEG in the PEG sample.

Yield of PEG-Br converted to PEG-X [a]			**Fraction of PEG-X** [b]	
Calculation	$\frac{I_h/3}{I_{f''}/3}$	$\frac{I_g/2}{I_{f''}/3}$	$\frac{I_h/3}{I_{a''}/3}$	$\frac{I_g/2}{I_{a''}/3}$
Value (%)	100	109	85	92
Average value (%)	**105 ± 6**		**89 ± 5**	

[a] Functionnalization degree (FD), $= 100 \times \frac{n_{PEG\text{-}X}}{n_{PEG\text{-}X^+}\ n_{PEG\text{-}Br}}$, [a] Fraction of PEG-X $= 100 \times \frac{n_{PEG\text{-}X}}{n_{PEG\text{-}X^+}\ n_{PEG\text{-}OH}}$

It should be noticed that the ratio between the integrals of *h*, *g* protons from ethyl xanthate group of PEG-X and *a''* protons arising from all the PEG chains is below the unity which is the sign of the residual PEG-OH that was observed in the PEG-Br sample. The average fraction of xanthate-functionalized PEG-X in the final PEG sample corresponds to 89 mol-%.

The UV-visible spectrum of PEG-X in a water/isopropanol mixture confirms the successful derivatization of the PEG chain-end since the characteristic absorption band of the xanthate agent at λ = 355 nm could be observed (**Figure 5**).

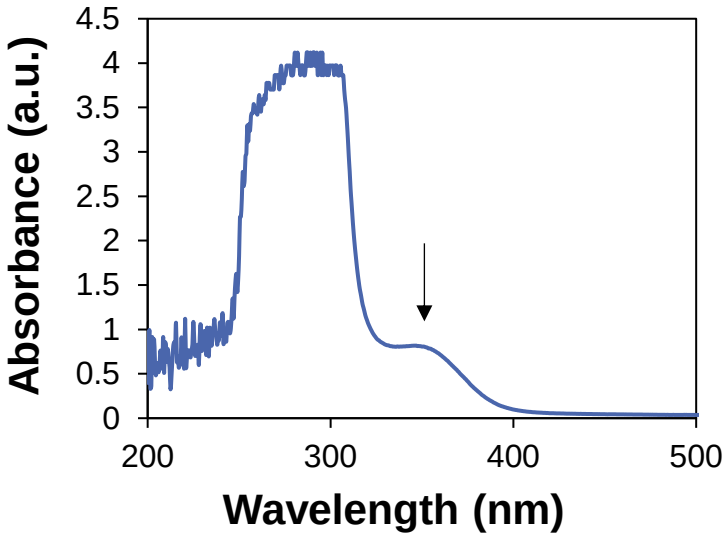

Figure 5. UV-visible spectrum of PEG-X at 1.9 × 10^{-2} mol.L^{-1} (42 g.L^{-1}) in a mixture of water and isopropanol (67:33 v:v %).

On the basis of the absorbance value at 355 nm ($Abs_{355\ nm}$ = 0.781) and on the number-average molar mass of the PEG-X ($M_{n,PEG\text{-}X}$), it is possible to determine the number of moles of xanthate group per PEG chains, *i.e.*, the functionalization degree (Equation 11).

$$\text{Number of xanthate per PEG chain} = \frac{[\text{Xanthate}]_0}{[\text{PEG}]_0} = \frac{\left(\frac{Abs_{355\ nm}}{l \times \varepsilon_{355\ nm}}\right)}{\left(\frac{m_{PEG}}{M_{n,PEG-X}}\right)/V} \qquad \text{Equation 11}$$

Where $[Xanthate]_0$ and $[PEG]_0$ are respectively the molar concentrations (mol.L^{-1}) of xanthate and PEG chains, l is the cuvette length (l = 1 cm), $\varepsilon_{355\ nm}$ is the molar extinction coefficient of the molecular xanthate measured at 355 nm in 67:33 v:v % water/isopropanol mixture ($\varepsilon_{355\ nm}$ = 54 L.mol^{-1}.cm^{-1}, see Part 2 - Chapter 1), m_{PEG} is the mass of PEG (m_{PEG} = 0.083 g), and V is the volume of the PEG solution prepared for UV-analysis (V = 2 × 10^{-3} L).

The average value of 78 % of xanthate functionalization using $M_{n,PEG\text{-}X}$ of PEG-X determined by SEC-MALLS ($M_{n,PEG\text{-}X,\ MALLS}$ = 2 240 g.mol^{-1}) is in the range of the average fraction of 89 mol-% of PEG-X in the PEG sample calculated by ^{1}H NMR.

The perfect overlay of the UV-visible (λ = 355 nm) and RI traces of the SEC chromatograms of PEG-X also corroborates a high level of chain-end functionalization with the presence of the dithiocarbonate chain-end over the entire molar mass distribution (**Figure 6**).

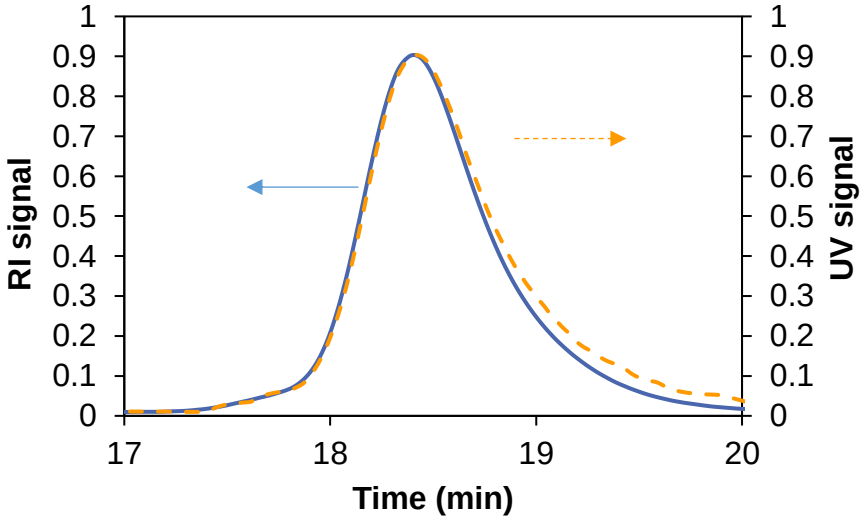

Figure 6. Overlay of the UV-visible (λ = 355 nm) and refractometer (RI) traces of the SEC chromatograms in THF for the PEG-X polymer.

In conclusion of this part, 85 mol-% of the PEG-OH chains were successfully functionalized with the xanthate moiety to produce a macromolecular chain transfer agent that can act as a reactive steric stabilizer in the synthesis of block copolymer particles by emulsion polymerization.

2. RAFT/MADIX emulsion copolymerization of VAc and VCL mediated by a xanthate-terminated PEG macro-chain transfer agent

Delaittre *et al.*[22] previously reported the benefits provided by polymerization induced self-assembly (PISA) in the synthesis of physically crosslinked poly(*N*,*N*-diethylacrylamide-*co*-styrene) thermoresponsive particles prepared by aqueous dispersion polymerization via the reactive nitroxide-capped poly(acrylic acid). In this work, the prepared xanthate-functionalized poly(ethylene glycol) (PEG-X) is involved as reactive stabilizer and control agent in the RAFT/MADIX emulsion copolymerization of VAc and VCL carried out at 65°C, using ADIBA as water-soluble initiator (**Table 6**). On the basis of the results obtained in the first chapter of the manuscript concerning the bulk copolymerization of VAc and VCL, the P(VAc-*co*-VCL)

statistical copolymers are insoluble in water at 65°C. Moreover, both monomers are water insoluble at a concentration of 10 wt-% based on water, hence forming monomer droplets at the initial state. It is thus expected that the mechanism will follow an emulsion polymerization process. The particle growing and stabilization should be guaranteed by the *in-situ* synthesis of the amphiphilic PEG-*b*-P(VAc-*co*-VCL) block copolymers.

Table 6. Experimental conditions for the emulsion copolymerizations of VAc and VCL performed at 65°C with 10 wt-% of initials solids content in water.

Expt	$f_{VAc,0}$[a]	**[ADIBA]$_0$** *mol.L^{-1}$_{H2O}$*	**Stabilizer**	**[Stabilizer]$_0$** *g.L^{-1}$_{H2O}$*	**Stabilizer** *wt-% based on monomers*	$\frac{[PEG\text{-}X]_0}{[ADIBA]_0}$	$\frac{[VAc]_0+[VCL]_0}{[PEG\text{-}X]_0}$
1	0.2	5.4×10^{-4}	PEG-X	4.9	5.4	3.2	430
2	0.5	5.9×10^{-4}	PEG-X	5.4	6.0	3.2	430
3	0.5	5.9×10^{-4}	PEG-OH	5.4	6.0	-	-

[a] $f_{VAc,0}$ is the VAc molar fraction in the initial monomer feed; The initial concentration of [PEG-X] considers the 85 mol-% of functionalization of PEG.

It should be mentioned that stable latex particles were formed during the course of polymerization in the absence of coagulum or phase separation for both syntheses carried out at different initial monomer feed ratios (see **Table 6** and **Table 7**, expt 1 and 2). This suggests that the PEG-X efficiently acts as steric stabilizer during the emulsion copolymerization of VAc and VCL. Note that 80-85 % of monomer conversion is reached by emulsion copolymerization (**Table 7**) while the monomer conversion was limited to 50-60 % in bulk for a similar 6 h of polymerization (see **Table 7** and Chapter 1 of Part I (Table 2)).

Table 7. Results of emulsion copolymerization of VAc and VCL mediated by PEG-X macromolecular chain transfer agent.[a]

Expt	F_{VAc}[b]	F_{VAc}[c]	X_m[d] %	$M_{n,theo}$[e] *g.mol^{-1}*	$M_{n,SEC}$[f] *g.mol^{-1}*	$Đ$[f]	$D_{h,\ 55°C}$[g] *nm*	*Copolymer*[h]
1	0.17	0.17	80	32 520	16 700	1.6	149 (0.98) / 654 (0.02)	PEG_{49}-*b*-$P(VAc_{0.17}$-*co*-$VCL_{0.83})_{111}$
2	0.47	0.52	85	31 490	19 790	2.0	94 (0.99) / 1087 (0.09)	PEG_{49}-*b*-$P(VAc_{0.47}$-*co*-$VCL_{0.53})_{154}$

[a] 10 wt-% of initial solids content and T = 65°C; [b] Molar fraction of VAc in the P(VAc-*co*-VCL) block, determined from ^{13}C NMR signal integrals (Equation 5 and **Figure 2**); [c] Molar fraction of VAc in the P(VAc-*co*-VCL) block, determined from ^{1}H NMR signal integrals (Equation 6 and **Figure 1**); [d] X_m is the overall monomer molar conversion at 5h30 of polymerization determined by ^{1}H NMR, Equation 1; [e] Theoretical number-average molar mass from Equation 7; [f] Values obtained from the SEC analysis with a MALLS detector with $(dn/dc)_{PEG\text{-}b\text{-}P(VAc0.17\text{-}co\text{-}VCL0.83)}$ = 0.099 mL.g^{-1} and $(dn/dc)_{PEG\text{-}b\text{-}P(VAc0.47\text{-}co\text{-}VCL0.53)}$ = 0.088 mL.g^{-1} (Equation 9); [g] Hydrodynamic diameters of PEG-*b*-P(VAc-*co*-VCL) copolymer dispersions (0.5 g.L^{-1}) measured at 55°C at the end of the reaction (without cooling), the values in brackets correspond to the number intensity of each population; [h] PEG_x-*b*-$P(VAc_{0.17}$-*co*-$VCL_{0.83})_y$ with *x* and *y* the degrees of polymerization of the blocks, $y = \frac{(M_{n,MALLS,P(VAc-co-VCL)} - M_{n,MALLS,PEG-X})}{(F_{VAc} \times M_{VAc} + F_{VCL} \times M_{VCL})}$.

For the sake of comparison, emulsion copolymerization of VAc and VCL with an initial molar fraction of VAc equals to 0.5 ($f_{VAc,0}$ = 0.5) was carried out using a non-reactive PEG-OH hydrophilic polymer as the sole stabilizer (expt 3 in **Table 6**). The growing polymer spontaneously precipitated during the emulsion copolymerization of VAc and VCL to produce a large coagulum representing 97 wt-% of the polymer (**Figure 7**).

Figure 7. Pictures of the coagulum (left) and of the dispersion (right) recovered at the end of the emulsion copolymerization of VAc and VCL using non-reactive PEG-OH as stabilizer (expt 3 in **Table 6**).

These results highlight the crucial role played by the reactive xanthate chain-end of the PEG-X polymer during the emulsion polymerization process, ensuring the colloidal stability of the formed particles by means of the *in-situ* formation of self-assembled block copolymers. Indeed, as displayed in **Figure 8**, the shift of the SEC chromatograms towards lower elution volumes suggests that the PEG-X was chain extended by P(VAc-*co*-VCL) block.

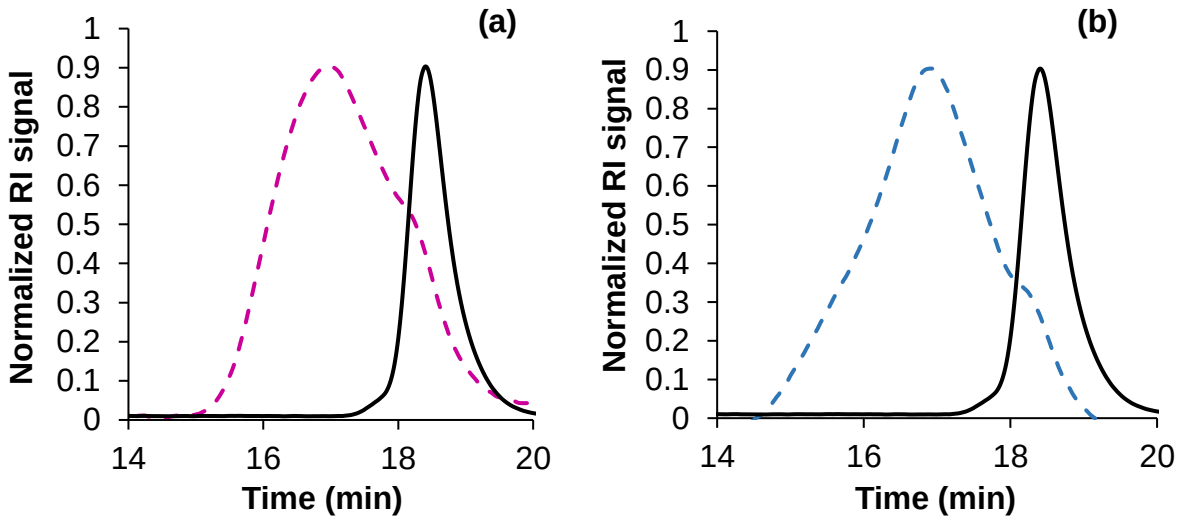

Figure 8. Size exclusion chromatograms in THF: PEG-X (full line) and PEG-*b*-P(VAc-*co*-VCL) copolymers synthesized by RAFT/MADIX emulsion polymerization: **(a)** PEG_{49}-b-$P(VAc_{0.17}$-co-$VCL_{0.83})_{111}$ (expt 1 in **Table 7**) and **(b)** PEG_{49}-*b*-$P(VAc_{0.47}$-*co*-$VCL_{0.53})_{154}$ (expt 2 in **Table 7**).

The chromatograms of the final block copolymers display a shoulder arising from residual PEG, including the 15 mol-% of PEG-OH present in PEG-X. This can also be ascribed to an incomplete consumption of the initial macromolecular PEG-X chain transfer agent as suggested by Binauld *et al.*[11] for RAFT/MADIX emulsion polymerization of VAc mediated by a xanthate-functionalized PEG. The incomplete consumption of the macromolecular RAFT agent is at the origin of higher values of experimental M_n compared to theoretical M_n of the block copolymers (**Table 7**). The low efficiency of xanthate was also observed for bulk VAc/VCL copolymerization mediated by a molecular xanthate agent (Chapter 1 of Part I).

To assess the effective formation of the PEG-*b*-P(VAc-*co*-VCL) block copolymers by emulsion polymerization, the final dialyzed samples were analyzed by DOSY NMR spectroscopy. This technique allows for the identification of different components in the mixture by means of the acquisition of two-dimensional spectra which correlate the diffusion coefficient of each

component with their corresponding chemical shifts.[23] As depicted in **Figure 9**, the signals corresponding to PEG and P(VAc-*co*-VCL) blocks are aligned with one diffusion coefficient , which confirms that both blocks are part of the block copolymer structure. DOSY NMR spectra also highlight the presence of residual PEG homopolymer with higher diffusion coefficient of 86 $\mu m^2.s^{-1}$, meaning that the dialysis of the PEG-*b*-P(VAc-*co*-VCL) with a 3.5 kDa cut-off membrane prior analysis did not allow to remove the residual PEG. The diffusion coefficient of PEG_{49}-*b*-$P(VAc_{0.47}$-*co*-$VCL_{0.53})_{154}$ is slightly lower (D = 36 $\mu m^2.s^{-1}$) than the PEG_{49}-*b*-$P(VAc_{0.17}$-*co*-$VCL_{0.83})_{111}$ (D = 45 $\mu m^2.s^{-1}$) according to the higher M_n of the more hydrophobic copolymer (see **Table 7**).

(a)

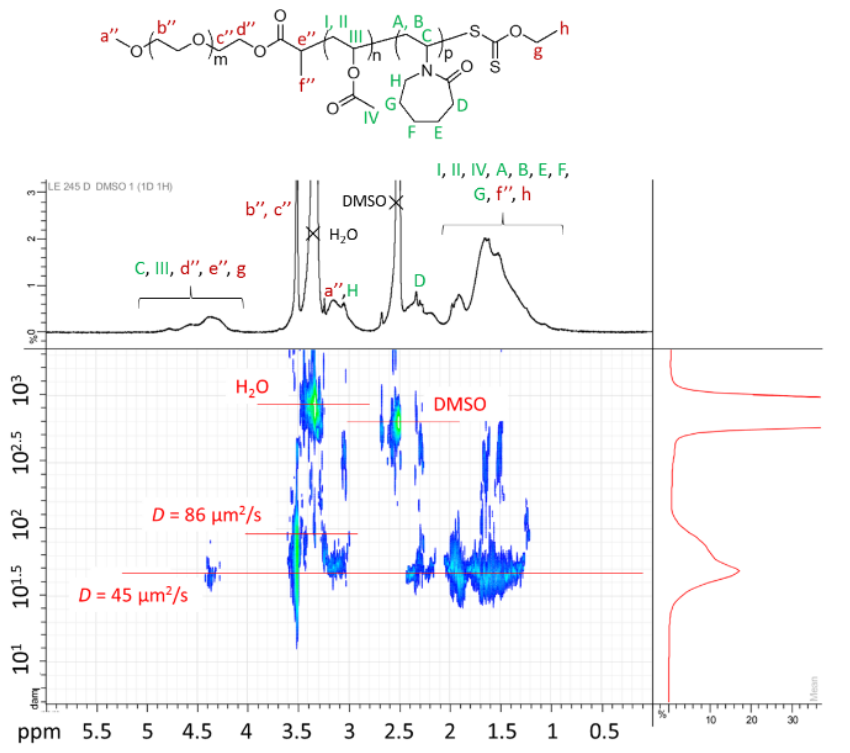

(b)

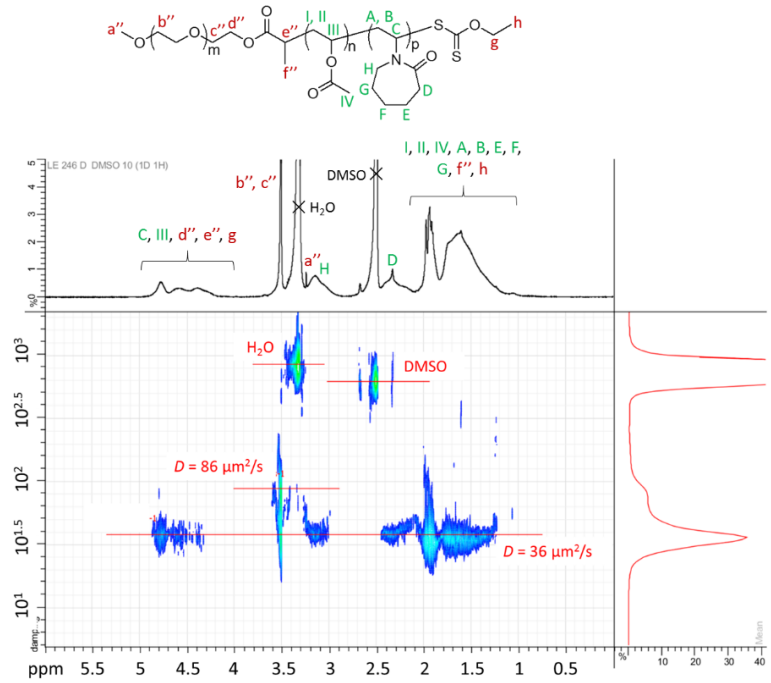

(c)

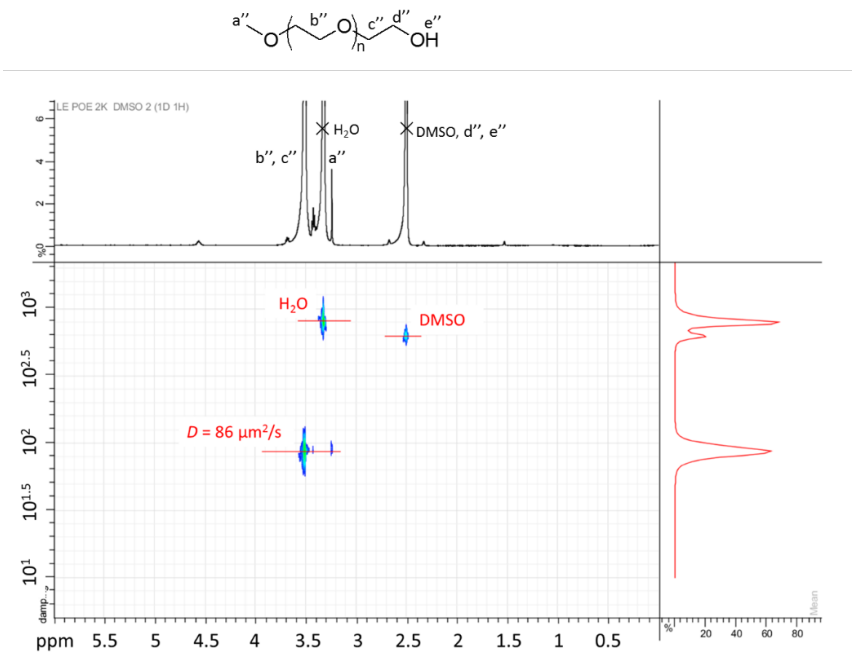

Figure 9. DOSY NMR spectra in DMSO-d_6 of the dialyzed PEG-*b*-P(VAc-*co*-VCL) copolymers synthesized by RAFT/MADIX emulsion polymerization: **(a)** PEG_{49}-*b*-$P(VAc_{0.17}$-*co*-$VCL_{0.83})_{111}$ (expt 1 in **Table 7**) and **(b)** PEG_{49}-*b*-$P(VAc_{0.47}$-*co*-$VCL_{0.53})_{154}$ (expt 2 in **Table 7**); **(c)** Initial PEG-OH homopolymer.

In comparison with the low dispersity values of the statistical P(VAc-*co*-VCL) copolymers synthesized in bulk ($Đ$ < 1.3, see Part I - Chapter 1), the dispersity values of the PEG-*b*-P(VAc-*co*-VCL) copolymers synthesized by emulsion copolymerization are higher ($Đ$ = 1.6 – 2.0) (**Table 7**), also due the presence of residual PEG. It can be mentioned that the dispersity increases by increasing the initial VAc fraction (**Table 7**), which is in opposite trend with the results of bulk VAc/VCL copolymerization (see Part I - Chapter 1). The higher concentration of water solubility limit of VCL in comparison with VAc ($[VCL]_{limit,\ water,\ 25°C}$ = 41 $g.L^{-1}$, $[VAc]_{limit,\ water,\ 20°C}$ = 23 $g.L^{-1}$)[24, 25] might induce an enrichment in VCL for the initial growing oligomer chains produced in the water phase.

The final average composition of the P(VAc-*co*-VCL) block was calculated on the basis of the integrals of the carbonyl peaks of the PVAc and PVCL units (**Table 7**). The determination of the copolymer composition by comparing the integrals of both carbonyls of the ^{13}C NMR spectrum corresponding to each polymer units is of interest because of the good level of resolution. These compositions match those determined from the integrals of ^{1}H NMR spectrum of the PEG-*b*-P(VAc-*co*-VCL) (**Table 7**). The ^{13}C NMR analysis of both PEG_{49}-*b*-$P(VAc_{0.17}$-*co*-$VCL_{0.83})_{111}$ and PEG_{49}-*b*-$P(VAc_{0.47}$-*co*-$VCL_{0.53})_{154}$ copolymers also shows that the characteristic signals of both PVAc and PVCL units are influenced by the presence of the neighbor co-monomer (**Figure 10**). As depicted in Chapter 1, the methine signal ($CH_{II'}$, 65 – 70 ppm) of PVAc and of PVCL ($CH_{B'}$, 45 – 49 ppm) are influenced by the copolymer composition (**Figure 10**).

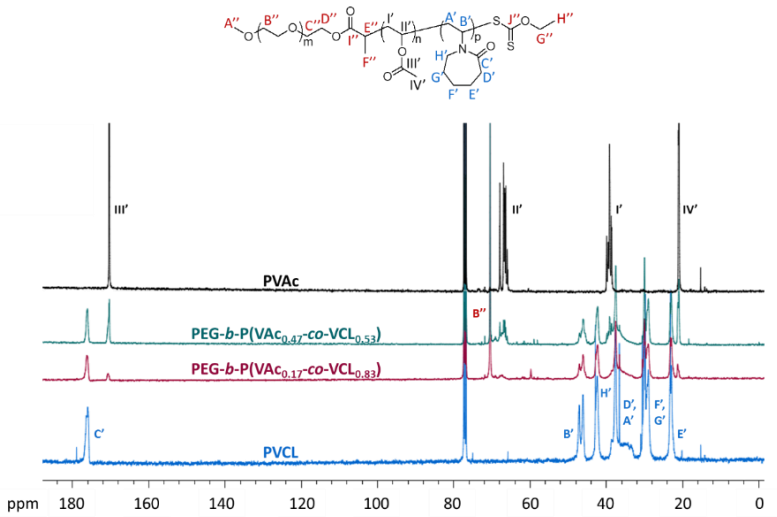

Figure 10. Overlay of the ^{13}C NMR spectra of the precipitated PVAc, PVCL, PEG_{49}-*b*-$P(VAc_{0.17}$-*co*-$VCL_{0.83})_{111}$ and PEG_{49}-$P(VAc_{0.47}$-*co*-$VCL_{0.53})_{154}$ (co)polymers in $CDCl_3$.

The ^{13}C NMR spectra of the PEG-*b*-P(VAc-*co*-VCL) copolymers synthesized by emulsion polymerization were then compared with the ones of their P(VAc-*co*-VCL) with similar composition synthesized in bulk. The signals of both PVAc and PVCL units exhibiting a similar shape between bulk and emulsion copolymers of similar composition ($CH_{II'}$, $CH_{B'}$ in **Figure 11**), the distribution of the co-monomer along the chain probably follows a similar statistic.

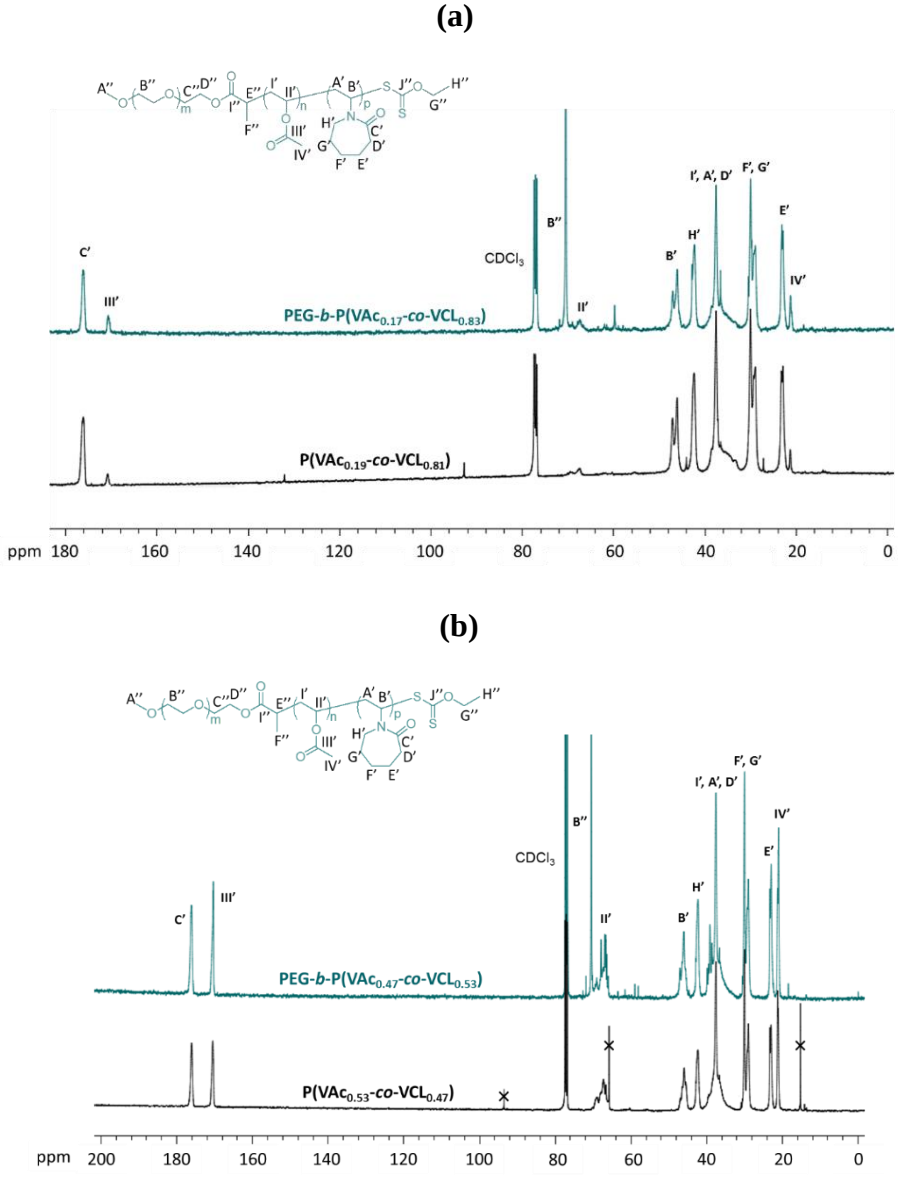

Figure 11. Comparison of ^{13}C NMR spectra in $CDCl_3$ of the VAc/VCL copolymers synthesized either by bulk polymerization (Part I – Chapter 1, precipitated prior to analysis, black spectra) or by emulsion polymerization (green spectra for dialyzed and freeze-dried copolymers). **(a)** PEG_{49}-*b*-$P(VAc_{0.17}$-*co*-$VCL_{0.83})_{111}$ (expt 1 in **Table 6**) and $P(VAc_{0.19}$-*co*-$VCL_{0.81})_{372}$ (see Part I – Chapter 1) copolymers; **(b)** PEG_{49}-*b*-$P(VAc_{0.47}$-*co*-$VCL_{0.53})_{154}$ (expt 2 in **Table 6**) and $P(VAc_{0.53}$-*co*-$VCL_{0.47})_{317}$ (see Part I – Chapter 1) copolymers. Residual trioxane (internal standard used for VAc/VCL copolymerizations) and diethyl ether (marked by cross, solvent of precipitation) are observed in the spectra of the copolymers synthesized in bulk.

The pictures of the dispersion of PEG-*b*-P(VAc-*co*-VCL) particles displayed in **Figure 12** show a macroscopic observation of the latex at different temperatures: 5°C, 20°C and at 50°C.

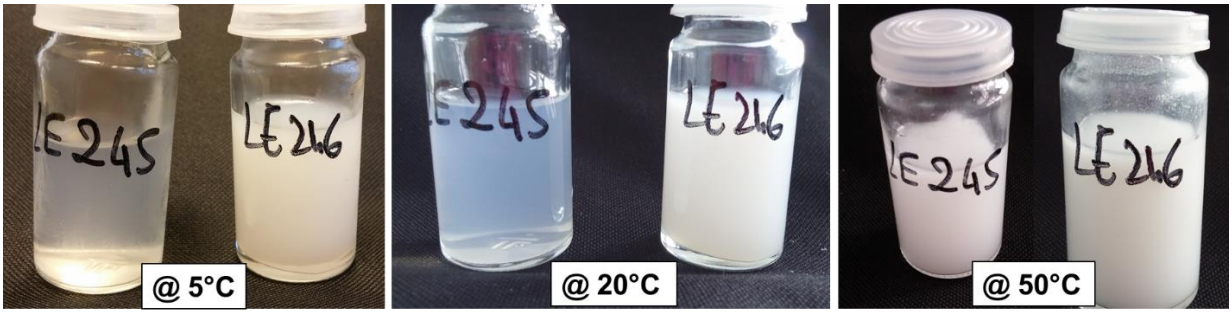

Figure 12. Pictures taken at different temperatures (5°C, 20°C and 50°C) of the final polymer dispersion obtained by PEG-X mediated emulsion copolymerization of VAc and VCL. For each picture, left sample corresponds to: PEG_{49}-*b*-$P(VAc_{0.17}$-*co*-$VCL_{0.83})_{111}$ copolymer (Expt 1 in **Table 7**) and right sample corresponds to PEG_{49}-*b*-$P(VAc_{0.47}$-*co*-$VCL_{0.53})_{154}$ copolymer (Expt 2 in **Table 6**).

The PEG_{49}-*b*-$P(VAc_{0.47}$-*co*-$VCL_{0.53})_{154}$ copolymer synthesized by emulsion polymerization is a white dispersion of diffusing particles in the whole range of temperatures while almost transparent aqueous solutions of PEG_{49}-*b*-$P(VAc_{0.17}$-*co*-$VCL_{0.83})_{111}$ were observed at 5°C (respectively LE 246 and LE 245, **Figure 12**). This suggests that a sufficient level of hydrophobic interactions between the VAc units (47 mol-%) is enable to preserve the integrity of the PEG_{49}-*b*-$P(VAc_{0.47}$-*co*-$VCL_{0.53})_{154}$ particles even at low temperature. The dispersion of PEG_{49}-*b*-$P(VAc_{0.17}$-*co*-$VCL_{0.83})_{111}$ copolymer in water becomes gradually cloudier by increasing the temperature (LE 245, **Figure 12**), which is the sign of a thermoresponsive behavior.

Turbidimetry is a suitable method to monitor the thermoresponsiveness of the PEG-*b*-P(VAc-*co*-VCL) block copolymers synthesized by emulsion copolymerization. The evolution of transmittance versus temperature of the different copolymers is displayed in **Figure 13** and the experimental values of the cloud point temperature are gathered in **Table 8**. The temperature-induced phase transition of the PEG_{49}-*b*-$P(VAc_{0.17}$-*co*-$VCL_{0.83})_{111}$ and PEG_{49}-*b*-$P(VAc_{0.47}$-*co*-$VCL_{0.53})_{154}$ diblock copolymers synthesized by emulsion polymerization are compared with the P(VAc-*co*-VCL) copolymers of similar compositions in VAc/VCL but synthesized in bulk (**Table 8**).

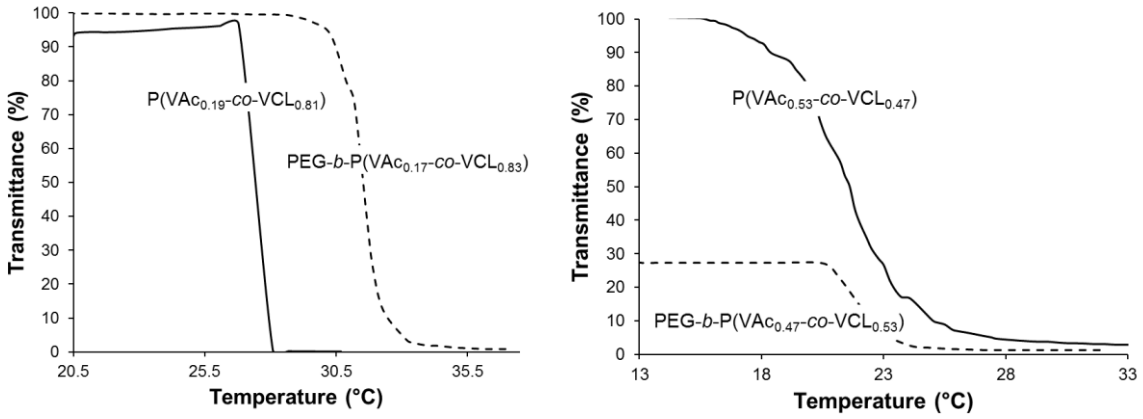

Figure 13. Transmittance at λ=500 nm versus temperature for aqueous solution of PEG-*b*-P(VAc-*co*-VCL) synthesized by RAFT/MADIX emulsion polymerization (dotted lines) and P(VAc-*co*-VCL) copolymers synthesized by RAFT/MADIX in bulk (plain lines): (left) PEG_{49}-*b*-$P(VAc_{0.17}$-*co*-$VCL_{0.83})_{111}$ and $P(VAc_{0.19}$-*co*-$VCL_{0.81})_{372}$ copolymers; (right) PEG_{49}-*b*-$P(VAc_{0.47}$-*co*-$VCL_{0.53})_{154}$ and $P(VAc_{0.53}$-*co*-$VCL_{0.47})_{317}$ copolymers. Polymer concentration of 3 $g.L^{-1}$ (Heating cycle).

Table 8. Comparison of cloud point temperatures of PEG-*b*-P(VAc-*co*-VCL) copolymers synthesized by emulsion polymerization and P(VAc-*co*-VCL) copolymers obtained by bulk polymerization.

Expt	Copolymer	F_{VAc}	$T_{cp,\ UV\text{-}vis}$[a] °C
1	PEG_{49}-*b*-$P(VAc_{0.17}$-*co*-$VCL_{0.83})_{111}$	0.17	32
2	PEG_{49}-*b*-$P(VAc_{0.47}$-*co*-$VCL_{0.53})_{154}$	0.47	22
4	$P(VAc_{0.19}$-*co*-$VCL_{0.81})_{372}$	0.19	27
5	$P(VAc_{0.53}$-*co*-$VCL_{0.47})_{317}$	0.53	22

[a] Measured by UV-visible spectroscopy (λ = 500 nm) of solution of copolymers at 3 $g.L^{-1}$ in water (heating cycle), see **Figure 13** and **Figure 18** in Part I Chapter 1.

The phase transition of PEG_{49}-*b*-$P(VAc_{0.17}$-*co*-$VCL_{0.83})_{111}$ copolymer occurs at higher temperature in comparison to the $P(VAc_{0.19}$-*co*-$VCL_{0.81})_{372}$ copolymer due to the covalent linkage with the PEG hydrophilic block ($T_{cp,UV\text{-}vis,PEG\text{-}b\text{-}P(VAc0.17\text{-}co\text{-}VCL0.83)}$ = 32°C and $T_{cp,UV\text{-}vis,\ P(VAc0.19\text{-}co\text{-}VCL0.81)}$ = 27°C, **Table 8**). The solution of PEG_{49}-*b*-$P(VAc_{0.17}$-*co*-$VCL_{0.83})_{111}$ copolymer allows for 100 % of light transmittance at low temperatures, which is in accordance with the water solubility of the $P(VAc_{0.17}$-*co*-$VCL_{0.83})$ blocks below the cloud point temperature (**Figure 13**). On the other hand, the PEG_{49}-*b*-$P(VAc_{0.47}$-*co*-$VCL_{0.53})_{154}$ copolymer exhibits no shift of the phase transition compared to $P(VAc_{0.53}$-co-$VCL_{0.47})_{317}$ copolymer ($T_{cp,UV\text{-}vis,PEG\text{-}b\text{-}P(VAc0.47\text{-}co\text{-}VCL0.53)}$ = 22°C and $T_{cp,UV\text{-}vis,\ P(VAc0.53\text{-}co\text{-}VCL0.47)}$ = 22°C, **Table 8**). This might traduce

a predominant effect of hydrophobic VAc units on the collapse of polymer chains that are self-assembled into particles at low temperature. Indeed, the 28 % transmittance of the aqueous dispersion of PEG_{49}-*b*-$P(VAc_{0.47}$-*co*-$VCL_{0.53})_{154}$ copolymer observed at low temperature is consistent with the presence of stable diffusing particles even at low temperature (**Figure 12** and **Figure 13**) by means of sufficient hydrophobic interactions between VAc units. For close values of DP of blocks, the more hydrophobic PEG_{49}-*b*-$P(VAc_{0.47}$-*co*-$VCL_{0.53})_{154}$ exhibits a lower temperature of cloud point than the PEG_{49}-*b*-$P(VAc_{0.17}$-*co*-$VCL_{0.83})_{111}$ (**Table 8**).

The hydrodynamic diameters of the particles synthesized by emulsion copolymerization carried out in the presence of the PEG-X stabilizer were measured at 55°C directly at the end of the polymerization process, without cooling the reaction medium (**Table 7**). Two populations of particle diameters were measured for final latex particles but the number-average fraction of the large aggregates above 600 nm remains very low (2-10 %). The average hydrodynamic diameter of the main population of the PEG_{49}-*b*-$P(VAc_{0.47}$-*co*-$VCL_{0.53})_{154}$ particles (D_h = 95 nm) is lower than the one of PEG_{49}-*b*-$P(VAc_{0.17}$-*co*-$VCL_{0.83})_{111}$ particles (D_h = 150 nm), thus indicating a higher number of PEG_{49}-*b*-$P(VAc_{0.47}$-*co*-$VCL_{0.53})_{154}$ particles. The increasing hydrophobicity likely results in the early self-assembly of the PEG-*b*-P(VAc-*co*-VCL) copolymer with higher fraction of hydrophobic VAc counterpart synthesized during the nucleation step, hence producing a higher number of particles. For the experiment performed using PEG-OH as stabilizer, the hydrodynamic diameters of the formed particles were not measured due to the poor stability of the final dispersion composed of precipitated polymer.

We further investigated the thermoresponsive behavior of the PEG-*b*-P(VAc-*co*-VCL) copolymers synthesized by emulsion copolymerization. For that purpose, the aqueous dispersions of amphiphilic copolymers were cooled at room temperature after the polymerization process to be subsequently analyzed by dynamic light scattering. A heating and cooling cycle was applied in the range of 10°C to 55°C, at a polymer concentration of 0.05 $g.L^{-1}$ (**Figure 14**). The temperature-dependence of the hydrodynamic diameters confirms a thermoresponsive phase transition for both types of copolymer particles but with opposite profiles (**Figure 14**).

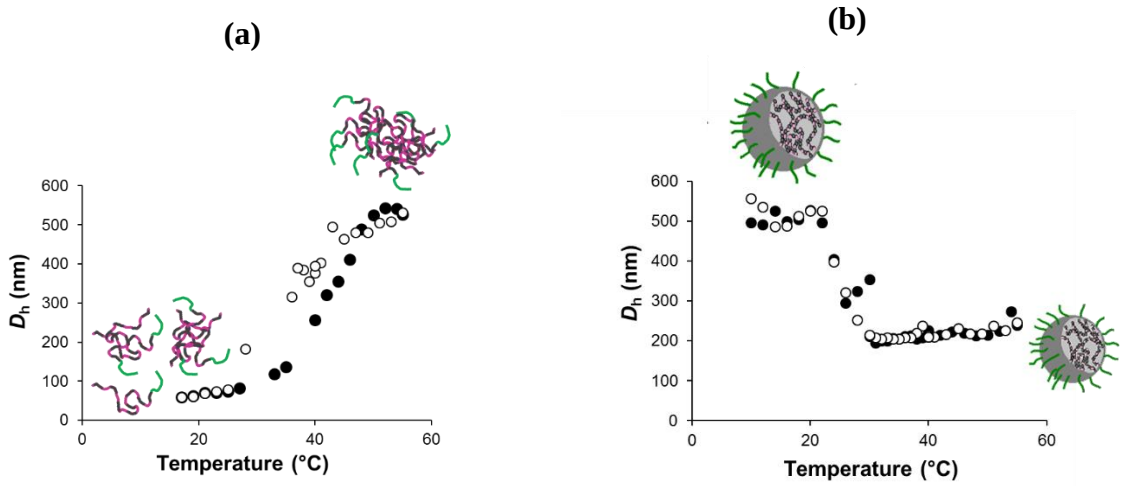

Figure 14. Hydrodynamic diameters as a function of the temperature for the PEG-*b*-P(VAc-*co*-PVCL) dispersions synthesized by emulsion polymerization at 10 wt-% of initial solids content for different initial monomer feed ratio **(a)** F_{VAc} = 0.17 (expt 1 in **Table 6**) and **(b)** F_{VAc} = 0.47 (expt 2 in **Table 6**). (●) 1st heating cycle, (○) cooling cycle of polymer solution at 0.05 g.L^{-1}.

Indeed, for PEG$_{49}$-*b*-P(VAc$_{0.17}$-*co*-VCL$_{0.83}$)$_{111}$ copolymer (expt 1 in **Table 6**), the profile of D_h versus temperature profile (**Figure 14.a**) is close to the one of the (PVAc-*co*-PVCL) statistical copolymers synthesized in bulk (see Part I Chapter 1, Figure 19) in the sense that D_h increases by rising temperature. The very low average count rate measured at low temperature quantifying the diffused light intensity suggests that PEG$_{49}$-*b*-P(VAc$_{0.17}$-*co*-VCL$_{0.83}$)$_{111}$ copolymer chains disassembled into soluble polymers in water at a temperature below 20°C. The presence of objects with diameter of *ca* 600 nm above the phase transition temperature, together with the hysteresis observed between heating and cooling cycles, both support the formation of polydisperse ill-defined aggregates of the PEG$_{49}$-*b*-P(VAc$_{0.17}$-*co*-VCL$_{0.83}$)$_{111}$ copolymer chains by increasing temperature up to 55°C (**Figure 14.a**). Note that the self-assembly induced by dehydration of the hydrophobic PVCL block has been previously investigated for PEG$_{114}$-*b*-PVCL*x* diblock copolymers ($24 < x < 237$).[26] Despite the balanced compositions between the hydrophilic and hydrophobic blocks, the diblock copolymers self-assembled into large aggregates (D_h ~ 300 to 550 nm) instead of well-defined micelles.[26]

Contrary to PEG$_{49}$-*b*-P(VAc$_{0.17}$-*co*-VCL$_{0.83}$)$_{111}$ copolymer, emulsion copolymerization of VAc/VCL performed with 50 mol-% of VAc in the initial feed (expt 2 in **Table 6**) produces stable particles at low temperature by means of sufficient hydrophobic interactions between the VAc units ($D_{h,\ 10\text{-}20°C}$ = 550 nm at T = 10 – 20°C) (**Figure 14.b**). The collapse of the P(VAc$_{0.47}$-

co-VCL$_{0.53}$) blocks within the particles by increasing temperature induces a decrease of the particle diameter down to 250 nm at 55°C. The reversible swelling-to-collapse transition of the PEG$_{49}$-*b*-P(VAc$_{0.47}$-*co*-VCL$_{0.53}$)$_{154}$ particles with almost no hysteresis show the formation of well-defined physically crosslinked thermoresponsive particles of P(VAc$_{0.47}$-*co*-VCL$_{0.53}$) stabilized by the PEG$_{49}$ block (**Figure 14.b**). The volume phase transition temperature (VPTT) of the PEG$_{49}$-*b*-P(VAc$_{0.47}$-*co*-VCL$_{0.53}$)$_{154}$ particles, determined as the minimum of the derivative of the plot of D_h as a function of the temperature, is equal to 26°C at 0.05 g.L^{-1}. This phase transition temperature is lower than the one measured for chemically crosslinked PVCL-based nanogels (~32°C),[27-30] due to the presence of the VAc hydrophobic units. Indeed, as the hydrophobic composition of thermoresponsive copolymers is increased, the hydrogen bonding effect between the copolymer chains and water is lowered while hydrophobic interactions are enhanced, thus lowering the required energy to collapse (i.e., lower T_{cp}).[31, 32] It can be noticed that the D_h of the collapse particles measured after applying a cooling/heating cycle to the PEG$_{49}$-*b*-P(VAc$_{0.47}$-*co*-VCL$_{0.53}$)$_{154}$ particle dispersion ($D_{h,\ 55°C}$ = 250 nm) is higher than the one measured at the end of the polymerization in the absence of any cooling step, *i.e.*, $D_{h,\ 55°C,}$ by number = 94 nm (**Table 7**). This results shows that the particles initially formed by emulsion polymerization were trapped in a kinetically frozen state (out-of-equilibrium).[22] After cooling the latex, some PEG$_{49}$-*b*-P(VAc$_{0.47}$-*co*-VCL$_{0.53}$)$_{154}$ copolymer chains might exchange between the swollen particles formed by hydrophobic interactions, thus producing particles of larger size.

3. Alkaline hydrolysis of the PEG-*b*-P(VAc-*co*-VCL)

Poly(vinyl alcohol) (PVA) is prepared upon alkaline hydrolysis of PVAc under mild conditions (transesterification with methanol) leading to PVA with different degrees of saponification.[33, 34] It has been shown that a degree of saponification of 88 % was optimum to provide a water soluble polymer as the hydrophobic acetyl neighborhood limit the hydrogen bonding between poly(vinyl alcohol) chains.[33] Therefore, the P(VAc-*co*-VCL) copolymers directly synthesized in water by emulsion polymerization are potential precursors of P(VA-*co*-VCL) copolymers. This is a strategy to synthesize by an environmentally friendly process some biocompatible thermoresponsive statistical copolymers with a tunable phase transition (**Scheme 5**).

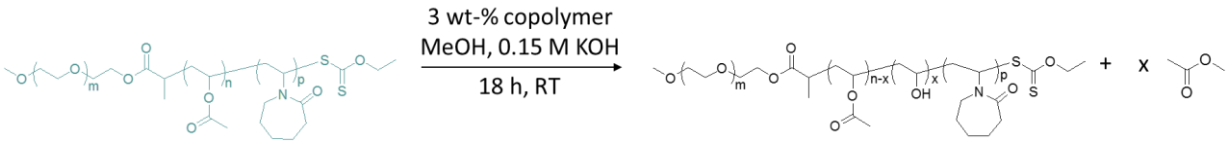

Scheme 5. Alkaline hydrolysis of the PEG-*b*-P(VAc-*co*-VCL) copolymers.

The efficiency of the alkaline hydrolysis of PEG-*b*-P(VAc-*co*-VCL) copolymers was monitored by ^{1}H NMR analysis of the copolymers before and after hydrolysis (**Figure 15**). For both copolymers, the effective hydrolysis was attested by the appearance of the PVA characteristic signals at 3.8 - 4.5 ppm (*N* and *M* protons, **Figure 15**) together with the disappearance of PVAc signals at 4.8 ppm (*III* proton, Figure 15) and 1.8 ppm (*IV* protons, **Figure 15**).

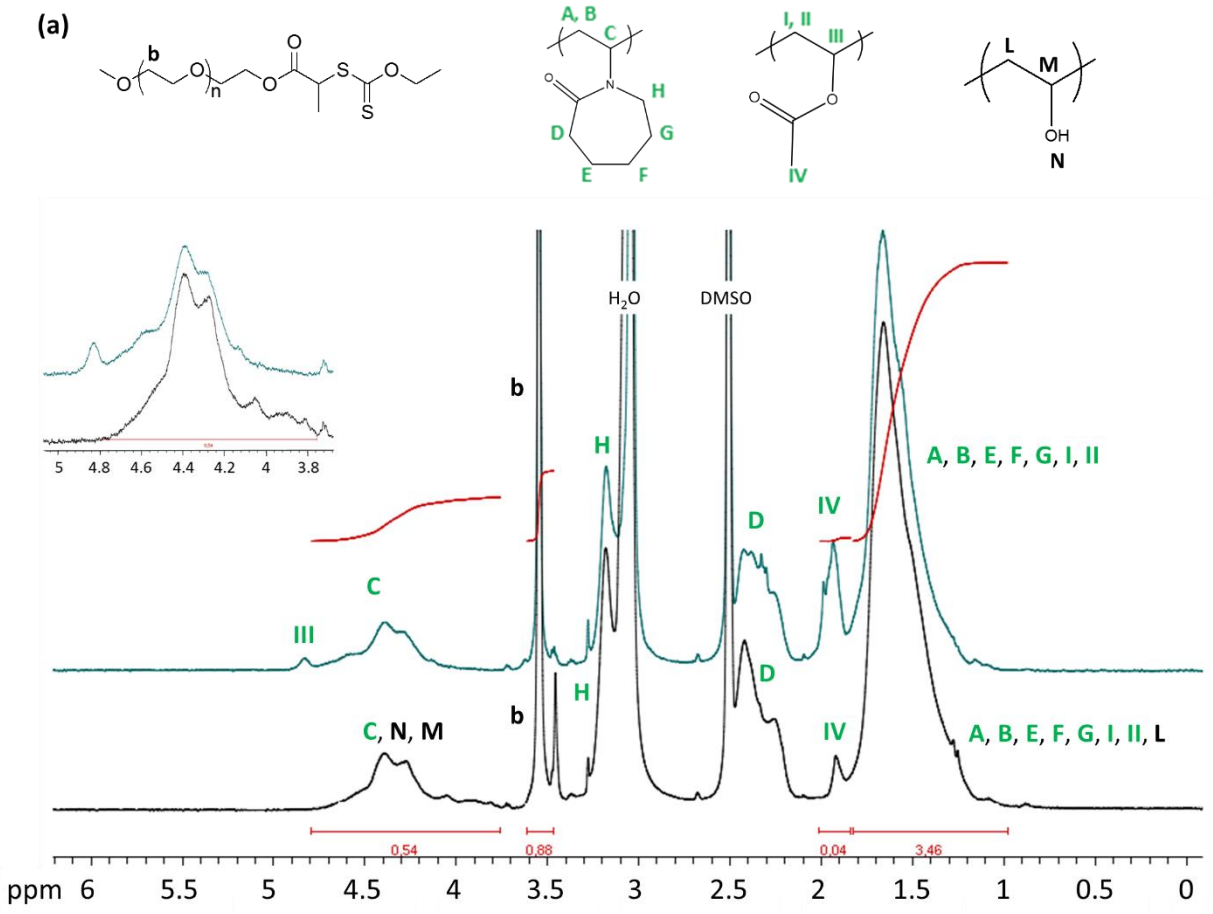

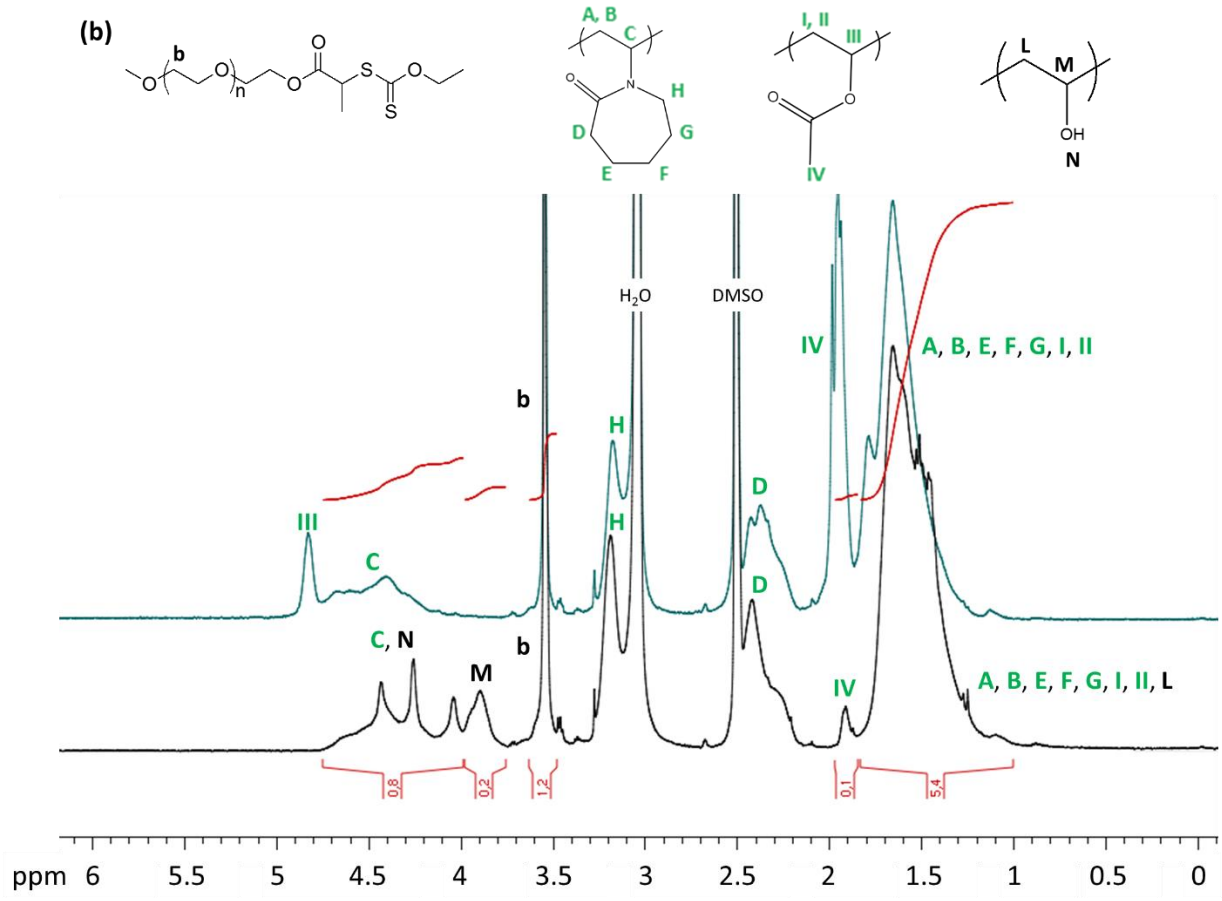

Figure 15. ^{1}H NMR spectra in DMSO-d_6 at 80°C of dialyzed (M_w cut-off: 3500 Da) and freeze-dried copolymers: **(a)** PEG_{49}-*b*-$P(VAc_{0.17}$-*co*-$VCL_{0.83})_{111}$ (expt 1 in **Table 6**) and **(b)** PEG_{49}-*b*-$P(VAc_{0.47}$-*co*-$VCL_{0.53})_{154}$ (expt 2 in **Table 6**) copolymers. Blue spectra: before hydrolysis, black spectra: after hydrolysis.

The yield of hydrolysis of the copolymers can be calculated on the basis of the integrations of characteristic NMR peaks of PVA and PVAc units (Equation 12).

$$\%\ hydrolysis = \frac{n_{PVOH}}{n_{PVOH} + n_{PVAc}} = 1 - \frac{\frac{I_{1HPVAc,after\ hydrolysis}}{I_{reference}}}{\frac{I_{1HPVAc,after\ hydrolysis}}{I_{reference}} + \frac{I_{1HPVAc,before\ hydrolysis}}{I_{reference}}} \quad \text{Equation 12}$$

$I_{1HPVAc,\ before\ hydrolysis}$ and $I_{1HPVAc,\ after\ hydrolysis}$ were obtained from the integral of *IV* protons of PVAc before and after hydrolysis and $I_{reference}$ corresponds to the integral of the signal between 1 and 1.8 ppm (**Figure 15**). The hydrolysis percentages calculated from Equation 8 are given in **Table 9**.

Table 9. Hydrolysis percentages of PEG-*b*-P(VAc-*co*-VCL) copolymers.

% hydrolysis	FTIR	^{1}H NMR	Average % hydrolysis
PEG-*b*-P(VAc$_{0.17}$-*co*-VCL$_{0.83}$)	77	87	82 ± 7
PEG-*b*-P(VAc$_{0.47}$-*co*-VCL$_{0.53}$)	85	94	90 ± 6

The hydrolysis of the PVAc units of the PEG-*b*-P(VAc-*co*-VCL) copolymers was also monitored by Fourier Transform Infra-Red (FTIR) spectroscopy via the disappearance of the characteristic ester band of the PVAc at 1730 cm^{-1} (**Figure 16**). Through a normalization with the signal of the amide bond of PVCL units of copolymers before and after hydrolysis, the yield of hydrolysis was calculated by comparing the absorbance of the ester band of PVAc (1730 cm^{-1}) before and after the hydrolysis step. The range of hydrolysis yield calculated by FTIR are slightly lower (77-85 %) in comparison with the yield calculated by NMR (87-94 %) (see **Table 9**).

(a)

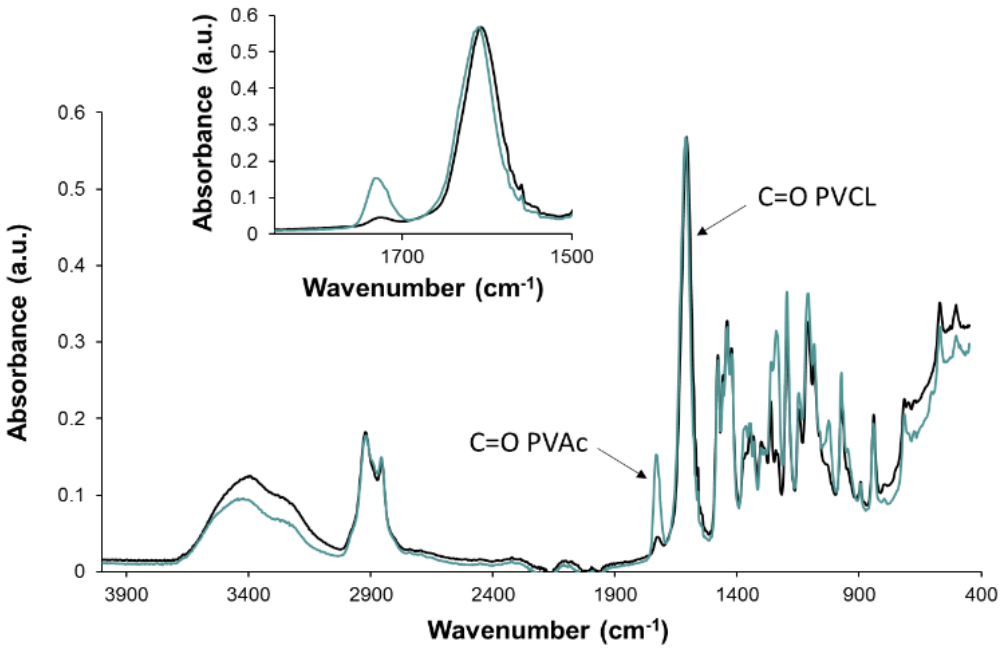

(b)

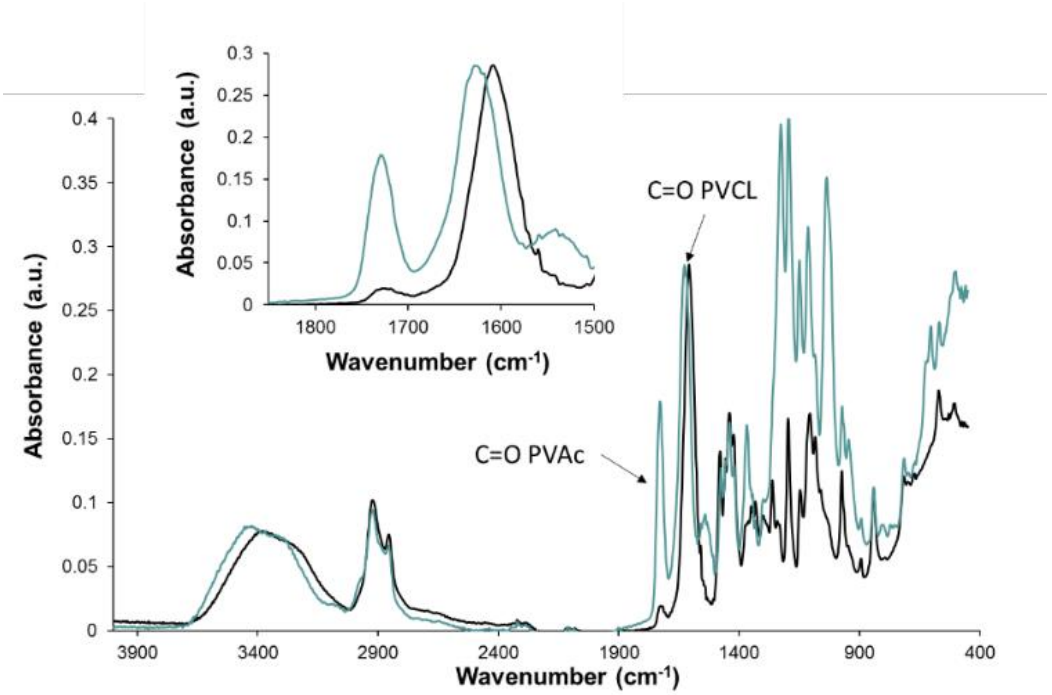

Figure 16. FTIR spectra before and after hydrolysis of **(a)** PEG_{49}-*b*-$P(VAc_{0.17}$-*co*-$VCL_{0.83})_{111}$ and **(b)** PEG_{49}-*b*-$P(VAc_{0.47}$-*co*-$VCL_{0.53})_{154}$ copolymers.

These results show that is it possible to produce biocompatible thermoresponsive P(VAc-*co*-VA-*co*-VCL) copolymers of controlled molar mass from the P(VAc-*co*-VCL) copolymers synthesized by surfactant-free emulsion polymerization process. The covalent linkage between the reactive PEG-xanthate and the P(VAc-*co*-VCL) block being an ester group, the analysis of the polymer after hydrolysis by DOSY NMR was required to provide information on the stability of the covalent bonding. A shift of the diffusion coefficient correlated to the ^{1}H NMR characteristic signals of the PEG block (I_b,, at 3.5 ppm in **Figure 17**) is observed in comparison with the diffusion coefficient of the P(VA-*co*-PVCL) block (**Figure 17**). A better alignment of PEG and P(VAc-*co*-VCL) block was observed for the PEG-*b*-P(VAc-*co*-VCL) block copolymer precursor (**Figure 9**). Therefore, DOSY-NMR analyses evidence the hydrolysis of the covalent linkage between both PEG and P(VAc-*co*-VA-*co*-VCL) blocks.

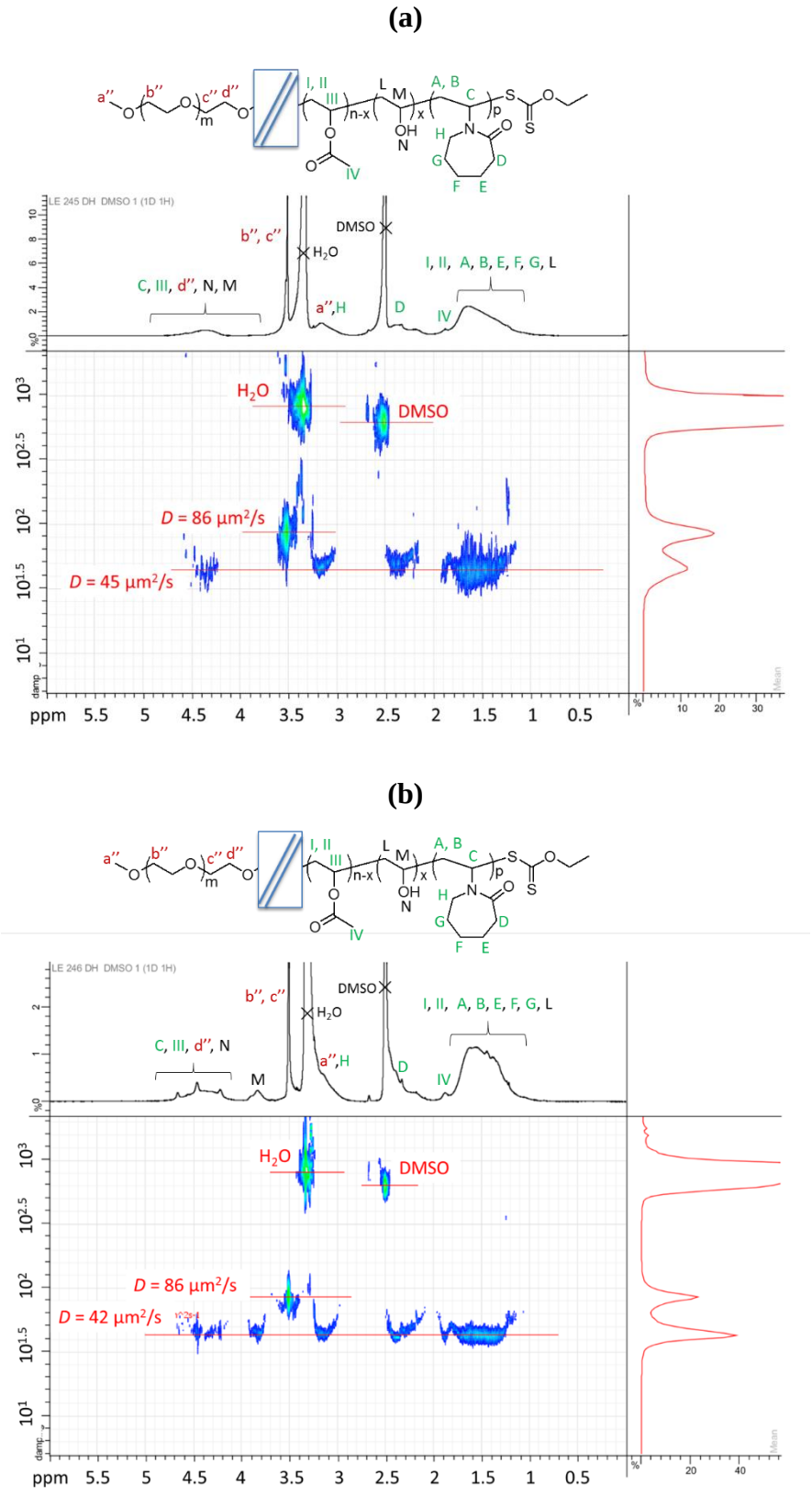

Figure 17. DOSY NMR spectra (in DMSO-d_6) of the copolymers after hydrolysis: **(a)** PEG_{49}-*b*-$P(VAc_{0.03}$-*co*-$VA_{0.14}$-*co*-$VCL_{0.83})_{111}$; **(b)** PEG_{49}-*b*-$P(VAc_{0.05}$-*co*-$VA_{0.42}$-*co*-$VCL_{0.53})_{154}$.

The thermoresponsive behavior of the P(VAc-*co*-VA-*co*-PVCL) copolymers in water was investigated by means of DLS measurements (**Figure 18**). Prior to these measurements, the copolymers were dialyzed for 4 days with 6-8 kDa cut-off membrane in order to remove the residual PEG block.

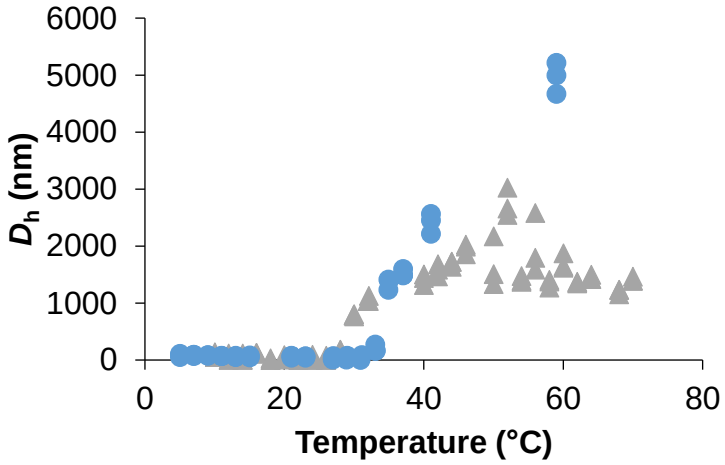

Figure 18. Evolution of the hydrodynamic diameters of the P(VAc-*co*-VA-*co*-VCL) copolymers as a function of the temperature after the second dialysis: (●) P($VAc_{0.03}$-*co*-$VA_{0.14}$-*co*-$VCL_{0.83}$) copolymer, (▲) P($VAc_{0.05}$-*co*-$VA_{0.42}$-*co*-$VCL_{0.53}$) copolymer.

The increase of the hydrodynamic diameters by increasing the temperature confirms the thermoresponsive behavior in water of both P(VAc-*co*-VA-*co*-VCL) copolymers with a phase transition temperature ranging between 26 and 30°C (**Figure 18**). As a perspective of this work, it would be interesting to investigate the opportunity to tune the LCST of these biocompatible thermoresponsive copolymers by tuning the copolymer composition. In order to ensure the stability of the covalent linkage with the PEG block, the synthesis of a PEG-xanthate through an amino-functionalized PEG should be explored. As poly(vinyl alcohol) is known to be a biodegradable polymer under suitable conditions,[33] it would be of interest to investigate if the incorporation of PVA units into PVCL copolymer particles might provide degradable linkages in order to produce more attractive degradable PVCL-based materials.[35]

IV. Conclusions

In this chapter, the RAFT/MADIX emulsion copolymerization of VAc and VCL mediated by a xanthate-terminated PEG macromolecular chain-transfer agent was investigated. In a first

step, the PEG-OH was successfully modified by a two-steps procedure to synthesize the xanthate-terminated PEG (PEG-X). Even if the presence of residual PEG-OH was evidenced by ^{13}C, ^{1}H NMR and UV-visible spectroscopy, a high degree of functionalization of the chain-end was reached (87 mol-%). The perfect overlay of the UV-visible (λ = 355 nm) and refractometer (RI) traces of the SEC chromatograms observed for the PEG-X also corroborates a good level of chain-end functionalization on the entire chain distribution.

Subsequently, the PEG-X was used as macromolecular chain transfer agent for the batch emulsion copolymerization of VAc and VCL performed at 10 wt-% of initial solids content, with two different initial VAc feed ratio. The stabilization efficiency of the PEG-X was demonstrated through the synthesis of stable dispersion of particles, free of coagulum, while the non-reactive hydrophilic PEG-OH induced an extensive precipitation of non-stabilized polymer (97 wt-% coagulum). DOSY NMR and SEC analyses both confirm the successful chain extension of the PEG-X macro chain-transfer agent enabling the direct synthesis of thermoresponsive PEG-*b*-P(VAc-*co*-VCL) block copolymers in aqueous dispersed media. The dispersity values of the final PEG-*b*-P(VAc-*co*-VCL) block statistical copolymers were higher than the dispersity of the corresponding P(VAc-*co*-VCL) statistical copolymers synthesized by RAFT/MADIX polymerization in bulk (Chapter 1, Part I) but the molar masses were still controlled in a similar range. This study is the first example of synthesis of PVCL-based amphiphilic copolymers by controlled radical emulsion polymerization.

It is important to note that the PEG-X efficiently acted as both steric stabilizer and chain-transfer agent during the RAFT/MADIX emulsion copolymerization of VAc and VCL to produce well-defined physically crosslinked thermoresponsive particles via hydrophobic interactions between the self-assembled PEG-*b*-P(VAc-*co*-VCL) block copolymers. The colloidal characterization of the final dispersions showed that a fraction of hydrophobic VAc of 47 mol-% in the second block of the copolymer was required to maintain the integrity of the particles at a temperature below the cloud point by means of hydrophobic interactions. The well-defined physically crosslinked PEG_{49}-*b*-$P(VAc_{0.47}$-*co*-$VCL_{0.53})_{154}$ particles interestingly behaved as thermoresponsive colloids able to undergo a reversible swollen-to-collapsed transition upon increasing the temperature. The presence of the hydrophobic phase of PVAc within the particles might enhance loading capacity of hydrophobic molecules. A PEG_{49}-*b*-$P(VAc_{0.17}$-*co*-$VCL_{0.83})_{111}$ block copolymer with a lower fraction of VAc in the copolymer (17 mol-%) was

also successfully synthesized by emulsion polymerization. In that case, the hydrophobic interactions were not sufficient to prevent the reversible formation of isolated polymer chains in the aqueous phase at low temperature (T < 20°C). The PEG_{49}-*b*-$P(VAc_{0.17}$-*co*-$VCL_{0.83})_{111}$ block copolymers with low VAc content self-assemble into large ill-defined aggregates by rising the temperature.

Finally, the statistical copolymers based on VAc and VCL of controlled molar mass were successfully hydrolyzed into promising thermoresponsive biocompatible statistical copolymers based on vinyl alcohol and *N*-vinylcaprolactam. In a further work, it should be interesting to investigate the influence of a change of either the P(VAc-*co*-VA-*co*-VCL) copolymer composition or its molar mass on this phase transition.

V. References

1. Zetterlund, P. B.; Kagawa, Y.; Okubo, M. *Chemical Reviews* **2008,** 108, (9), 3747-94.
2. Zetterlund, P. B.; Thickett, S. C.; Perrier, S.; Bourgeat-Lami, E.; Lansalot, M. *Chemical Reviews* **2015,** 115, (18), 9745-800.
3. Monteiro, M. J.; Cunningham, M. F. *Macromolecules* **2012,** 45, (12), 4939-4957.
4. Simms, R. W.; Davis, T. P.; Cunningham, M. F. *Macromolecular Rapid Communications* **2005,** 26, (8), 592-596.
5. Russum, J. P.; Barbre, N. D.; Jones, C. W.; Schork, F. J. *Journal of Polymer Science Part A: Polymer Chemistry* **2005,** 43, (10), 2188-2193.
6. Jiang, B.; Zhang, Q. H.; Zhan, X. L.; Chen, F. Q. *Chinese Chemical Letters* **2009,** 20, (6), 733-737.
7. Detrembleur, C.; Debuigne, A.; Bryaskova, R.; Charleux, B.; Jérôme, R. *Macromolecular Rapid Communications* **2006,** 27, (1), 37-41.
8. Zhao, F.; Mahdavian, A. R.; Teimouri, M. B.; Daniels, E. S.; Klein, A.; El-Aasser, M. S. *Colloid and Polymer Science* **2012,** 290, (13), 1247-1255.
9. Nomura, N.; Shinoda, K.; Takasu, A.; Nagata, K.; Inomata, K. *Journal of Polymer Science Part A: Polymer Chemistry* **2013,** 51, (3), 534-545.
10. Bernard, J.; Save, M.; Arathoon, B.; Charleux, B. *Journal of Polymer Science Part A: Polymer Chemistry* **2008,** 46, (8), 2845-2857.
11. Binauld, S.; Delafresnaye, L.; Charleux, B.; D'Agosto, F.; Lansalot, M. *Macromolecules* **2014,** 47, (10), 3461-3472.
12. Huang, Z.; Pan, P.; Bao, Y. *Journal of Polymer Science Part A: Polymer Chemistry* **2016,** 54, (14), 2092-2101.
13. Charleux, B.; Delaittre, G.; Rieger, J.; D'Agosto, F. *Macromolecules* **2012,** 45, (17), 6753-6765.
14. Canning, S. L.; Smith, G. N.; Armes, S. P. *Macromolecules* **2016,** 49, (6), 1985-2001.
15. Delaittre, G.; Nicolas, J.; Lefay, C.; Save, M.; Charleux, B. *Chemical communications* **2005**, (5), 614-6.

16. Delaittre, G.; Nicolas, J.; Lefay, C.; Save, M.; Charleux, B. *Soft Matter* **2006,** 2, (3), 223.
17. Warren, N. J.; Armes, S. P. *Journal of the American Chemical Society* **2014,** 136, (29), 10174-85.
18. Ramos, J.; Costoyas, Á.; Forcada, J. *Journal of Polymer Science Part A: Polymer Chemistry* **2006,** 44, (15), 4461-4478.
19. Brandrup, J.; Immergut, E. H.; Grulke, E. A., *Polymer Hanbook, 4th Edition*. 2003; p 2336.
20. Beija, M.; Marty, J. D.; Destarac, M. *Chemical communications* **2011,** 47, (10), 2826-8.
21. Otte, D. A.; Borchmann, D. E.; Lin, C.; Weck, M.; Woerpel, K. A. *Organic letters* **2014,** 16, (6), 1566-9.
22. Delaittre, G.; Save, M.; Gaborieau, M.; Castignolles, P.; Rieger, J.; Charleux, B. *Polymer Chemistry* **2012,** 3, (6), 1526.
23. Johnson, C. S. *Progress in Nuclear Magnetic Resonance Spectroscopy* **1999,** 34, 203-256.
24. BASF. *Safety Data Sheet* **2012**.
25. Barandiaran, M. J.; Cal, J. C. d. l.; Asua, J. M., Emulsion Polymerization. In *Polymer Reaction Engineering*, Blackwell Publishing Ltd: 2008; pp 233-272.
26. Liu, J.; Detrembleur, C.; De Pauw-Gillet, M.-C.; Mornet, S.; Duguet, E.; Jérôme, C. *Polymer Chemistry* **2014,** 5, (3), 799-813.
27. Imaz, A.; Forcada, J. *Macromolecular Symposia* **2009,** 281, (1), 85-88.
28. Aguirre, G.; Ramos, J.; Forcada, J. *Soft Matter* **2013,** 9, (1), 261-270.
29. Ramos, J.; Imaz, A.; Forcada, J. *Polymer Chemistry* **2012,** 3, (4), 852-856.
30. Schneider, F.; Balaceanu, A.; Feoktystov, A.; Pipich, V.; Wu, Y.; Allgaier, J.; Pyckhout-Hintzen, W.; Pich, A.; Schneider, G. J. *Langmuir : the ACS journal of surfaces and colloids* **2014,** 30, (50), 15317-26.
31. Peng, H.; Kather, M.; Rübsam, K.; Jakob, F.; Schwaneberg, U.; Pich, A. *Macromolecules* **2015,** 48, (13), 4256-4268.
32. Peng, H.; Xu, W.; Pich, A. *Polym. Chem.* **2016,** 7, (31), 5011-5022.
33. Amann, M.; Minge, O., Biodegradability of Poly(vinyl acetate) and Related Polymers, Advances in Polymer Science. In *Synthetic Biodegradable Polymers*, Rieger, B.; Künkel, A.; Coates, G. W.; Reichardt, R.; Dinjus, E.; Zevaco, T. A., Eds. Springer Berlin Heidelberg: 2012; Vol. 245, pp 137-172.
34. Sionkowska, A. *Progress in Polymer Science* **2011,** 36, (9), 1254-1276.
35. Delplace, V.; Nicolas, J. *Nature chemistry* **2015,** 7, (10), 771-84.

- PART II -

Chemically crosslinked PVCL-based thermoresponsive microgels

Introduction of Part II

Nowadays, in the field of human disease therapies and more specifically cancer therapies, pharmaceutical molecules (drugs, proteins, nucleic acids) are usually administered intravenously, which generally lead to short residence time, limited targeting and penetration of tumor tissues, toxic reactions in healthy tissues, the limitation of extensive use of hydrophobic drugs and their unavailability to reach effective doses.[1] Therefore, a major challenge consists in designing drug carriers in order to improve the safety and efficacy of therapeutic agents. Drug delivery systems are ideally able to protect the active compounds from the surrounding environment (preventing its early degradation), consequently increasing their *in-vivo* circulation time to deliver the drug concentration required for therapeutic efficacy, without damaging the health cells or tissues.[2, 3] Thus, a robust delivery platform needs to satisfy some requirements. First of all, the size of the carrier is an important parameter to consider since it plays a key role in its degradation, its cellular uptake and its blood circulation life, among other functional aspects.[4-6] For instance, the size of the vehicle should be large enough to prevent rapid leakage in blood capillaries but small enough to escape the capture of macrophages in the reticuloendothelial system, *i.e.*, sizes ranging from a few tenths to a few hundreds of nanometers. In addition, the surface of the delivery system is also an important factor since it will dictate its *in-vivo* circulation time and its interactions with the surrounding biological media. Indeed, the interaction of the carrier surface with proteins and molecules in the blood stream (in a process known as opsonization) may facilitate its removal by the phagocyte system[7] and can also induce a colloidal instability and carrier aggregation in physiological fluids.[8] However, such drawbacks can be avoided by functionalizing the vector surface with, for example, poly(ethylene glycol) (PEG) which provides a steric barrier to the adsorption of proteins.[9, 10] Biocompatibility is also an imperative criterion for a suitable delivery system.[11, 12]

Among the different nanoscale systems that have been envisaged as nanocarriers for therapeutics, polymeric nano/microgels, and especially stimuli-responsive ones, are very promising candidates due to their versatile properties such as easy production and functionalization, large surface area, porous network, high loading capacity and responsiveness to environmental factors which allows a triggered release of the therapeutics.[13-18] As unhealthy tissues and cells present different temperature than healthy ones, temperature is one of the most investigated trigger.[3] Therefore, thermoresponsive nano/microgels that undergo a volume phase

transition in water with temperature (passing from a swollen to a collapsed state) have attracted a great deal of interest within the last past years.[1, 2, 19] As a kind of thermoresponsive polymer available for the design of nano/microgels, poly(*N*-vinylcaprolactam) (PVCL) appears to be very attractive because of its biocompatibility and its lower critical solution temperature at around 32°C-38°C, near to physiological temperature.[20, 21]

In addition to stimuli-responsive carriers, polymeric cationic vehicles are also of special interest due to their ability to interact with the negatively charged cell membrane facilitating their cellular uptake.[2] Moreover, they can strongly interact with negatively charged relevant biological molecules such as DNA and siRNA (whose charge and size make them non-permeable to cell membranes) facilitating their delivery into cells.[8, 22, 23]

In this context, the objective of this part of the work is to synthesize thermoresponsive cationic PVCL-based microgels. The first chapter will describe the synthesis and characterization of the cationic macromolecular stabilizer that will functionalize the microgel outer shell. The second chapter will report the synthesis of monodisperse thermoresponsive PVCL-based microgel while the third chapter will present an evaluation of the potential application of the microgels as drug delivery nanocarriers.

References

1. Wang, Y.; Xu, H.; Ma, L. *Therapeutic delivery* **2015,** 6, (10), 1157-69.
2. Ramos, J.; Forcada, J.; Hidalgo-Alvarez, R. *Chemical reviews* **2014,** 114, (1), 367-428.
3. Mura, S.; Nicolas, J.; Couvreur, P. *Nat Mater* **2013,** 12, (11), 991-1003.
4. Shang, L.; Nienhaus, K.; Nienhaus, G. U. *Journal of nanobiotechnology* **2014,** 12, 5.
5. Wilczewska, A. Z.; Niemirowicz, K.; Markiewicz, K. H.; Car, H. *Pharmacological Reports* **2012,** 64, (5), 1020-1037.
6. Dhand, C.; Prabhakaran, M. P.; Beuerman, R. W.; Lakshminarayanan, R.; Dwivedi, N.; Ramakrishna, S. *RSC Advances* **2014,** 4, (62), 32673.
7. Belmadi, N.; Midoux, P.; Loyer, P.; Passirani, C.; Pichon, C.; Le Gall, T.; Jaffres, P. A.; Lehn, P.; Montier, T. *Biotechnology journal* **2015,** 10, (9), 1370-89.
8. Yin, H.; Kanasty, R. L.; Eltoukhy, A. A.; Vegas, A. J.; Dorkin, J. R.; Anderson, D. G. *Nature reviews. Genetics* **2014,** 15, (8), 541-55.
9. Howard, M. D.; Jay, M.; Dziubla, T. D.; Lu, X. *Journal of Biomedical Nanotechnology* **2008,** 4, (2), 133-148.
10. Suk, J. S.; Xu, Q.; Kim, N.; Hanes, J.; Ensign, L. M. *Adv Drug Deliv Rev* **2016,** 99, (Pt A), 28-51.
11. Petros, R. A.; DeSimone, J. M. *Nature reviews. Drug discovery* **2010,** 9, (8), 615-27.
12. Dobrovolskaia, M. A.; McNeil, S. E. *Nature nanotechnology* **2007,** 2, (8), 469-78.
13. Oh, J. K.; Drumright, R.; Siegwart, D. J.; Matyjaszewski, K. *Progress in Polymer Science* **2008,** 33, (4), 448-477.
14. Vinogradov, S. V. *Nanomedicine* **2010,** 5, (2), 165-8.

15. Saunders, B. R.; Laajam, N.; Daly, E.; Teow, S.; Hu, X.; Stepto, R. *Advances in colloid and interface science* **2009,** 147-148, 251-62.
16. Karimi, M.; Ghasemi, A.; Sahandi Zangabad, P.; Rahighi, R.; Moosavi Basri, S. M.; Mirshekari, H.; Amiri, M.; Shafaei Pishabad, Z.; Aslani, A.; Bozorgomid, M.; Ghosh, D.; Beyzavi, A.; Vaseghi, A.; Aref, A. R.; Haghani, L.; Bahrami, S.; Hamblin, M. R. *Chemical Society reviews* **2016,** 45, (5), 1457-501.
17. Baipaywad, P.; Udomluck, N.; Pyo, S.-G.; Park, H. H.; Park, H. *Journal of Nanoscience and Nanotechnology* **2014,** 14, (10), 7363-7373.
18. Soni, G.; Yadav, K. S. *Saudi pharmaceutical journal : SPJ : the official publication of the Saudi Pharmaceutical Society* **2016,** 24, (2), 133-9.
19. Lyon, L. A.; Meng, Z.; Singh, N.; Sorrell, C. D.; St John, A. *Chemical Society reviews* **2009,** 38, (4), 865-74.
20. Ramos, J.; Imaz, A.; Forcada, J. *Polym. Chem.* **2012,** 3, (4), 852-856.
21. Liu, J.; Debuigne, A.; Detrembleur, C.; Jerome, C. *Advanced healthcare materials* **2014,** 3, (12), 1941-68.
22. Dincer, S.; Turk, M.; Piskin, E. *Gene therapy* **2005,** 12 Suppl 1, S139-45.
23. Yue, Y.; Wu, C. *Biomater. Sci.* **2013,** 1, (2), 152-170.

PART II - CHAPTER 1. Synthesis and characterization of cationic macromolecular chain transfer agents by RAFT/MADIX polymerization

I. Introduction

Polyelectrolytes are ionically charged water-soluble polymers. Some polyelectrolytes carry permanent anionic or cationic charges while other polyelectrolytes contain ionizable functions (amines, carboxylic acid…) that can be neutralized by varying the pH of the water phase.

Cationic polymers are widely used in different fields of applications such as cosmetics, biomedical and material sciences, thanks to their ability to electrostatically interact with anionic surfaces of tissues, biomolecules, inorganic nanoparticles, cellulosic surfaces, among others. Cationic polymers are also known for their antimicrobial activity.[1, 2] Depending on the targeted application, non-permanently or permanently charged cationic polymers will be preferred. For example, the first type of cationic polymer will present a pH-sensitive behavior, a property which can be useful for the design of carriers with triggered release of the cargo. On the contrary, for applications in which stability of the polymer towards pH is required, permanent cationic polymers will be favored. Moreover, it has been shown that poly(dimethylaminoethyl acrylate) suffered self-catalyzed hydrolysis in water while its permanently quaternized derivative remained stable.[3, 4] Tamura *et al.* observed that in the case of nanogels composed of poly(dimethylaminoethyl methacrylate), the cytotoxicity was reduced when the degree of quaternization of the tertiary amine was increased.[5] It is well-known that the antimicrobial activity[6] and cytotoxicity[7, 8] of cationic polymers can be influenced by their molar mass and their charge density. Consequently, it is of special interest to carefully tailor the properties of cationic polymers (*i.e.*, to control the polymer molar masses and dispersity, the polymer composition…), by making use of controlled radical polymerization techniques. Among the different techniques of controlled radical polymerization, RAFT polymerization has been successfully applied for the design of well-defined cationic polymers, due to its versatility and tolerance to a wide variety of monomers and experimental conditions. (Meth)acrylate-, acrylamide- or styrene-based cationic polymers are examples of polymers that have been prepared by RAFT polymerization.[9-11] Chemical structures of the main cationic monomers are depicted in **Scheme 1**.

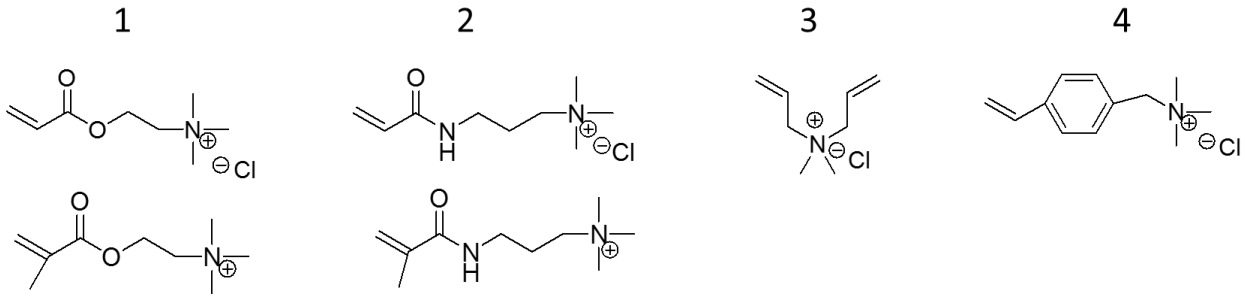

Scheme 1. Chemical structures of the main cationic monomers. 1) [2-((meth)acryloyloxy)ethyl]trimethylammonium chloride; 2) (3-(meth)acrylamidopropyl)trimethylammonium chloride; 3) diallyldimethylammonium chloride; 4) (Vinylbenzyl)trimethylammonium chloride.

In order to produce well-defined, permanently charged quaternary ammonium polymers by RAFT polymerization, two synthetic strategies can be employed. The first approach consists in a two-steps procedure: neutral amine-containing monomers are polymerized in a controlled manner and after characterization of the polymer using conventional characterization techniques in organic solvent, the amine functional groups are permanently quaternized using alkyl halides compounds for instance.[12, 13] The second strategy relies on the direct RAFT polymerization of commercially available quaternary ammonium-containing monomers. Both approaches present some advantages. While the first strategy appears convenient to overcome the problems related to the restricted solvent solubility of both quaternary ammonium monomers and polymers (which are principally soluble in water), the second strategy allows to reduce the use of hazardous solvents and chemical reagents.

Most of the studies concerning the RAFT polymerization of cationic monomers make use of dithiobenzoate[11, 14-17] or trithiocarbonate chain-transfer agents (CTA),[11, 17-20] due to the chemical nature of these monomers ((meth)acrylates, acrylamides, styrenic derivatives monomers…). Indeed, these RAFT agents are very suitable for controlling the polymerization of the abovementioned class of monomers.[21] Very few permanently-charged cationic monomers have been polymerized by RAFT/MADIX polymerization using a xanthate as control agent. The group of Destarac *et al.* reported the synthesis of either poly[(3-acrylamidopropyl)trimethylammonium chloride] (PAPTAC)[22, 23] or poly(diallyldimethylammonium chloride) (PDADMAC)[24] cationic polymers, using *O*-ethyl-*S*-(1-methoxycarbonyl)ethyl dithiocarbonate chain transfer agent. PAPTAC polymers with experimental molar masses close to the theoretical ones were obtained (reference 22: $M_{n,PAPTAC}$ = 2000 or 10000 g.mol^{-1}, no reported value of dispersity $Đ$ (NMR characterization); reference

23: $M_{n,PAPTAC}$ = 1000 g.mol^{-1}, $Đ$ = 1.5), attesting the ability of the xanthate agent to control the polymer chain growth. A moderate control of DADMAC polymerization was obtained ($Đ$ values ranging from 2.0 to 3.9 and $M_{n,exp}$ lower than $M_{n,theo}$) and was ascribed to the occurrence of chain transfer to ethanol rather than to a low transfer constant (C_{tr}) of xanthate agent for RAFT polymerization of DADMAC. The authors determined a C_{tr} value equals to 18 (C_{tr} = k_{tr}/k_p) for DADMAC RAFT polymerization. Both types of polymers (PAPTAC and PDADMAC) were successfully chain-extended to produce double hydrophilic block copolymers, which evidenced the presence of the xanthate reactive chain-end at the end of the first block synthesis.

The objective of the present work is to synthesize and characterize cationic macromolecular chain-transfer agents to be used latter as reactive macromolecular stabilizer for the emulsion polymerization of *N*-vinylcaprolactam. For that purpose, poly[2-(acryloyloxy)ethyl]trimethylammonium chloride polymers are synthesized by RAFT/MADIX polymerization, using *O*-ethyl-*S*-(1-ethoxycarbonyl)ethyldithiocarbonate as chain-transfer agent. Despite the xanthate agents are not the most suitable chain transfer agents to mediate the polymerization of acrylates, this chain-transfer agent was chosen as suitable chain-end to promote a fast transfer of the growing PVCL chains to the reactive cationic macromolecular stabilizer during the second step of VCL emulsion polymerization.[25] By varying the initial [Monomer]$_0$/[Xanthate agent]$_0$ ratio, different degrees of polymerization of the cationic polymer are targeted. The synthesized cationic polymers are characterized by different techniques (SEC, A-4F, DOSY-NMR, MALDI-TOF) to assess their macromolecular features.

II. Experimental part

1. Materials

[2-(acryloyloxy)ethyl]trimethylammonium chloride solution (AETAC, Arkema, 98 wt-% in water) was passed under inhibitors remover (Sigma Aldrich, 0.1 g in order to purify 50 mL of monomer) before use**.** 4,4'-azobis(4-cyano)pentanoic acid (ACPA, Fluka, 98 %), 1,3,5-trioxane (Sigma Aldrich, 99 %), 2-propanol (Sigma Aldrich, 99 %), cetyltrimethylammonium bromide (CTAB, Sigma Aldrich, 99 %) and sodium chloride (Sigma Aldrich, 99 %) were used as received. A mixture of deionized water and ethanol (VWR, technical grade, 98 %) was used as solvent for the synthesis of P(AETAC-X) and P(AETAC) polymers. Tetrahydrofuran (THF; VWR, technical grade, 99 %) was used as precipitation solvent. The *O*-ethyl-*S*-(1-

ethoxycarbonyl)ethyldithiocarbonate molecular transfer agent was synthesized according to the procedure described in the Part 1 - Chapter 1.

2. Synthesis of P(AETAC-X) macromolecular chain transfer agents and P(AETAC) polymer

In a typical experiment of the synthesis of P(AETAC-X) (for example, expt 2 in **Table 2**), xanthate agent (49.8 mg, 2.2×10^{-4} mol), ACPA initiator (4.5 mg, 1.4×10^{-5} mol), AETAC monomer (3.0 g, 1.6×10^{-2} mol) and 1,3,5-trioxane (142 mg, 1.6×10^{-3} mol) were introduced in a 25 mL round-bottom flask and dissolved in a mixture of 4.5 g of water and 0.5 of ethanol (90/10 wt-%). The reaction mixture was degased by nitrogen bubbling for 20 min at 0°C, under stirring. A sample was withdrawn under nitrogen at time $t = 0$. The flask was placed into an oil bath previously heated at 60°C and the reaction was allowed to continue for 6 h. Samples were withdrawn under nitrogen at different time intervals, until the reaction was stopped by cooling down into an ice-water bath and introduction of oxygen in the mixture. The polymer was then precipitated into cold THF, dissolved in water and freeze-dried. Polymers were obtained as powders.

The final monomer conversion (X) was calculated from nuclear magnetic resonance spectra according to Equation 1.

$$X = 1 - \frac{\left({}^{I\,1H_{mono.}}/_{I\,1H_{triox.}}\right)_t}{\left({}^{I\,1H_{mono.}}/_{I\,1H_{triox.}}\right)_0} \quad \text{Equation 1}$$

$I_{1H,triox}$ corresponds to the integral of one proton of 1,3,5-trioxane (5.1 ppm, 6H) used as internal standard and $I_{1H,mono}$ corresponds to the integral of the vinylic proton of AETAC monomer at 5.9-6.4 ppm. **Figure 1** presents the ^{1}H NMR attributed spectrum in DMSO-d_6 of the crude sample withdrawn at $t = 0$ for AETAC polymerization.

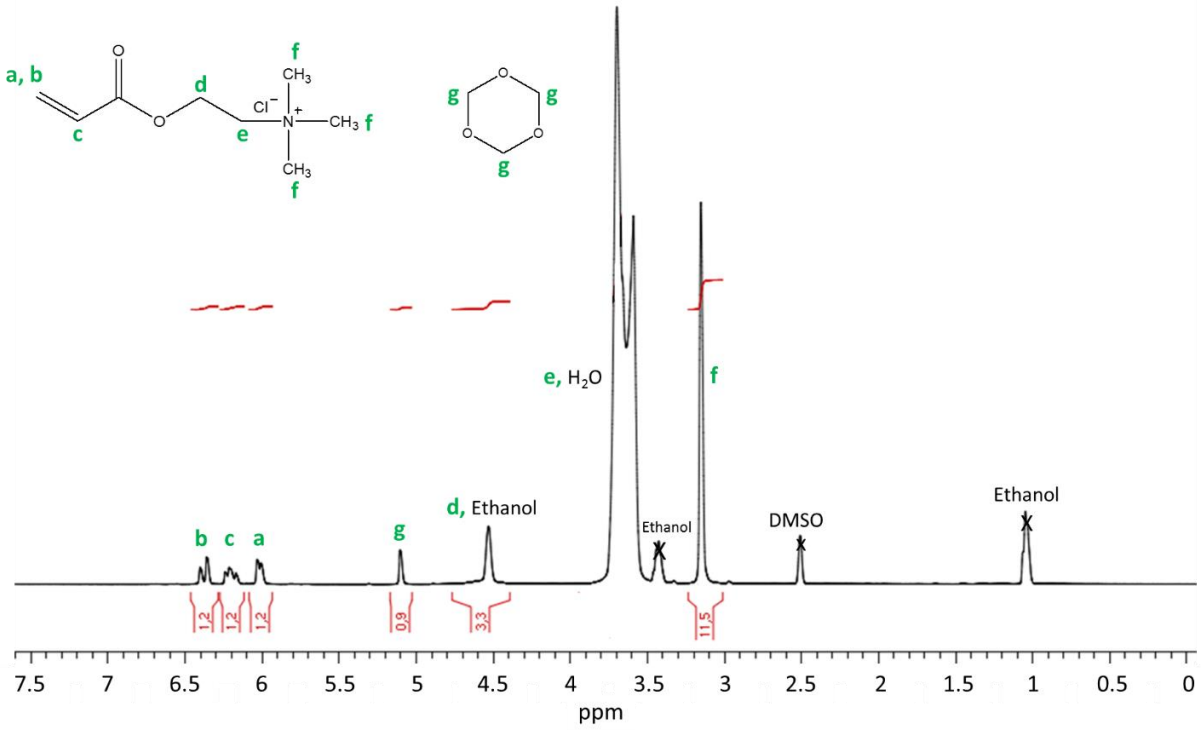

Figure 1. ^{1}H NMR spectrum in DMSO-d_6 of the crude sample withdrawn at t = 0 for AETAC polymerization.

Xanthate chain-end cleavage of P(AETAC-X)$_{76}$ polymer. The xanthate chain-end of P(AETAC-X)$_{76}$ polymer (expt 2 in **Table 2**) was cleaved according to a described procedure,[26] proceeding as follows: P(AETAC-X)$_{76}$ (1.0 g, $n_{theo.}$ = 7.1 × 10^{-5} mol) was dissolved in 160 g of double deionized (DDI) water and placed into a 250 mL jacketed reactor, fitted with a reflux condenser, stainless steel stirrer, sample device, and nitrogen inlet tube reactor. The polymer solution was stirred at 300 rpm and purged with nitrogen for 40 minutes at room temperature before heating to 70 °C. When the targeted temperature was reached, ADIBA initiator (0.474 g, 1.4 × 10^{-3} mol, 20-fold molar excess with respect to the polymer) dissolved in 10 g of DDI water was added under nitrogen flow. The solution was stirred for one hour at 70°C before cooling down to 25°C. The final solution was dialyzed against distilled water for one week to remove the excess of initiator (Spectra/Por, M_w cut-off: 12,000 - 14,000 Da). The modified polymer was recovered by freeze-drying the dialyzed solution. This polymer will be named as P(AETAC-X)$_{76,\ cleaved}$ in the following work.

3. Characterization methods

UV-Visible spectroscopy. The xanthate molecular chain-transfer agent, P(AETAC-X) and P(AETAC) polymers were characterized by UV-Visible spectroscopy in a mixture of

water:isopropanol (67:33 v:v%), with a Shimadzu UV-2450PC spectrophotometer. The polymers were systematically precipitated once into THF prior characterization to remove any unreacted molecular CTA. The molar extinction coefficient of the molecular xanthate agent ($\varepsilon_{xanthate}$) was determined in water:isopropanol (67:33 v:v%) from the slope of absorbance versus concentration at two different wavelengths (λ_1 = 306 nm and λ_2 = 355 nm, **Figure 4**).

Nuclear Magnetic Resonance (NMR) spectroscopy. Proton nuclear magnetic resonance spectroscopy (^{1}H NMR) spectra were recorded on a Bruker 400 MHz spectrometer at 25°C. DMSO-d_6 was used as solvent for the determination of monomer conversions and D_2O was used as solvent for NMR analysis of the precipitated P(AETAC-X) and P(AETAC) polymers. Polymers were characterized by Diffusion-ordered NMR spectroscopy (DOSY-NMR) either in D_2O or in 0.1 M NaCl D_2O solutions using the bipolar longitudinal eddy current delay pulse sequence (BPLED). The spoil gradients were also applied at the diffusion period and the eddy current delay. Typically, a value of 2 ms was used for the gradient duration (δ), 150 ms for the diffusion time (Δ), and the gradient strength (g) was varied from 1.67 G.cm^{-1} to 31.88 G.cm^{-1} in 32 steps. Each parameter was chosen to obtain 95 % signal attenuation for the slowest diffusion species at the last step experiment. The pulse repetition delay (including acquisition time) between each scan was larger than 2s. Data acquisition and analysis were performed using the Bruker Topspin software (version 2.1). The T1/T2 analysis module of Topspin was used to calculate the diffusion coefficients and to create 2-D spectra with NMR chemical shifts along one dimension and the calculated diffusion coefficients along the other.

Matrix assisted laser desorption ionization-time of flight mass spectrometry (MALDI-ToF MS). MALDI-TOF MS analyses were performed in collaboration with either ISM-CESAMO, Bordeaux or Polymat Institute, San Sebastian.

MALDI-TOF MS measurements were performed on a Bruker Autoflex Speed system (Bruker, Germany) instrument equipped with a 355 nm Nd:YAG laser. All spectra were acquired in the positive-ion reflectron mode (accelerating voltage 20 kV, pressure 5×10^{-6} mbar).

P(AETAC-X)$_9$ was analyzed using different matrices and cationizing agents as reported in **Table 1**. Samples were prepared by dissolving the product in methanol at a concentration of 1 mg.mL^{-1}.

Table 1. Matrices and cationizing agents used for the MALDI-TOF analysis of P(AETAC-X)$_9$ polymer at 1 mg.mL^{-1} in methanol.

Matrix	Cationizing agent
Dithranol	NaTFA
CHCA	NaI
CHCA	KTFA
DCTB	NaI
DCTB	KTFA

CHCA: α-cyano-4-hydroxycinnamic acid, NaTFA: sodium trifluoroacetate, DCTB: trans-2-[3-(4-tert-butylphenyl)-2-methyl-2-propenylidene] malononitrile.

Size exclusion chromatography (SEC). SEC analysis were carried out in collaboration with IMP, INSA/Université Claude Bernard, Lyon 1. The SEC system operates at a flow rate of 0.5 mL.min^{-1}. The SEC apparatus is equipped with a set of two columns specific to cationic polymers (TSK 6000 and TSK 2500) working in series, a Wyatt Heleos II Multi Angle Laser Light Scaterring detector (MALLS, 18 angles, λ_0 = 664 nm) and a refractive index (RI) detector Optilab T-rEX. The polymer was dissolved in 0.15 mol.L^{-1} of ammonium acetate / 0.20 mol.L^{-1} of acetic acid buffer (pH 4.5), at concentrations of either 3 or 1.5 mg.mL^{-1}.

The percentage of mass recovery is defined as the mass of analyte recovered at the end of the analysis: % mass recovery = ($m_{\text{polymer eluted}}$ / $m_{\text{polymer injected}}$) × 100.

Asymmetric flow field-flow fractionation (A-4F). Two runs of A-4F characterization were carried out, one in Polymat Institute, San Sebastian and the other at IPREM, Pau.

Polymat Institute, San Sebastian: A-4F analyses were carried out on a AF4 Wyatt Eclipse 3 system, equipped with a RI detector Optilab T-rEX from Wyatt and Wyatt Dawn Heleos II MALLS detector (λ_0 = 658 nm). Dimension of the channel: 290 × 70 × 50 mm; injection volume: 50 µL; focus flow rate: 3 mL.min^{-1}; detector flow rate: 1.0 mL.min^{-1}; cross-flow rate: 3 mL.min^{-1}. For all experiments, poly(ether sulfone) (PES) membranes with a 5 kDa molecular weight cutoff were used. Ultrapure water supplemented with 0.03 wt-% (5 × 10^{-3} mol.L^{-1}) of sodium azide NaN_3 salt was used as eluent. Polymer samples were prepared at a concentration of 6 mg.mL^{-1}.

IPREM, Pau: A-4F analyses were carried out on a AF4 Wyatt Eclipse 3 system, equipped with a RI detector Optilab T-rEX from Wyatt, a Wyatt Dawn Heleos II MALLS detector (λ_0 = 658 nm) and an UV-Visible detector (Agilent 1260 Infinity). Dimension of the channel: 290 × 70 × 50 mm; injection volume: 100 µL; constant detector flow: 1.0 mL.min^{-1}. For all experiments,

poly(ether sulfone) (PES) membranes were used with either a 1 or a 10 kDa molecular weight cutoff. Sample solutions were prepared at a concentration of 5 mg.mL^{-1}. Two types of eluents were used: 0.076 mol.L^{-1} disodium hydrogen phosphate (Na_2HPO_4) / 0.096 mol.L^{-1} sodium nitrate ($NaNO_3$) / 0.004 mol.L^{-1} sodium phosphate monobasic (NaH_2PO_4) / 0.002 mol.L^{-1}sodium azide (NaN_3) and the same eluent supplemented with 1×10^{-4} mol.L^{-1} of hexadecyltrimethylammonium bromide (CTAB) surfactant. The total ionic strength of both medium was equal to 0.18 M and the pH to 8. For a sake of clarity, the first buffer will be named as A-4F buffer throughout the following work and the second one as A-4F buffer + 0.1 mM CTAB.

The molar mass $M_{w,i}$ of each monodisperse slice of the fractogram was measured by the Debye plot from MALLS detector. The number-average molar mass (M_n) and dispersity ($Đ = M_w/M_n$) were calculated from $M_{w,i}$ on the basis of $\overline{M_n} = \frac{\sum_i N_i M_i}{\sum_i N_i}$ and $\overline{M_w} = \frac{\sum_i N_i M_i^2}{\sum_i N_i M_i}$.

The specific refractive index increment value (dn/dc) of P(AETAC-X) polymers in ultrapure water was determined at 25°C with a Brookhaven Instruments Corp. differential refractometer, operating at a wavelength of λ = 620 nm, at concentrations ranging from 2.5 to 20 g.L^{-1}. For evaluation of the data, the differential refractometer software version 5.32 was used The following value was measured: dn/dc = 0.1370 ± 0.0003 mL.g^{-1}.

The final value of dn/dc of P(AETAC-X) was 0.137 mL.g^{-1}, which is in similar range of the value determined by Plamper *et al* in water with 25 mM $NaNO_3$ and 0.2 g.L^{-1} NaN_3 for a star-shaped quaternized poly(*N*,*N*-dimethylaminoethyl methacrylate) (PDMAEMA) polymer (dn/dc = 0.109 mL.g^{-1}).[27]

Dynamic light scattering (DLS). The measurements of the hydrodynamic diameter (D_h) of P(AETAC-X)$_{14}$ polymer (expt 4 in **Table 3**) for scattering angles θ ranging from 50 to 130°, were carried out using a home-made equipment. A He-Ne 139 mW power laser was used, operating at a wavelength of 532 nm. The polymer was dissolved at 2.5 and 5 g.L^{-1} in H_2O + 0.1 M NaCl or A-4F buffer solutions. For evaluation of the data, the NanoQ program (Cordouan) was used. The hydrodynamic diameters were calculated from the diffusion coefficient using the Stokes-Einstein equation

$D_h = \frac{k_B T}{3\pi\eta D}$ where T is absolute temperature (T = 298 K), η the viscosity of the solvent ($\eta_{H2O,\ 25°C}$ = 0.891 cP), k_B the Boltzmann constant and D the diffusion coefficient.

III. Results and discussion

1. Synthesis of P(AETAC-X) macromolecular chain transfer agents and P(AETAC) polymers

The cationic polymers of [2-(acryloyloxy)ethyl]trimethylammonium chloride (AETAC) were synthesized by RAFT/MADIX polymerization, mediated by *O*-ethyl-*S*-(1-ethoxycarbonyl)ethyldithiocarbonate chain-tranfer agent. The polymerizations were carried out in a mixture of water and ethanol, at 60°C for 6 hours (**Scheme 2**).

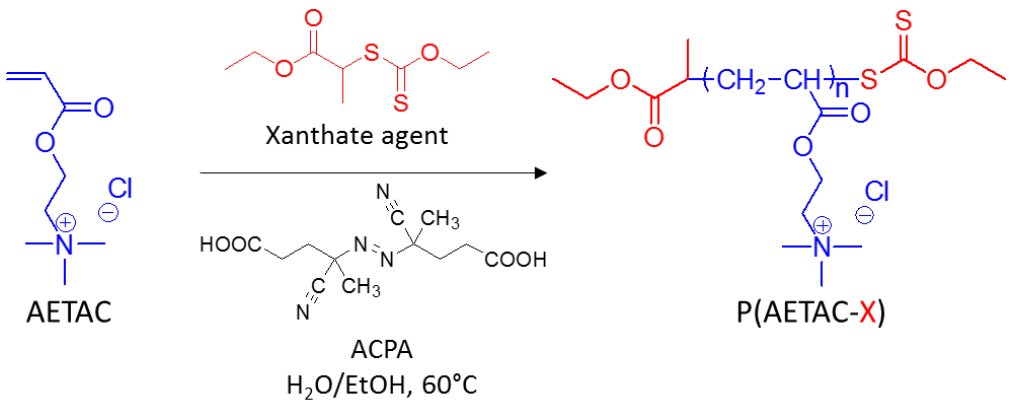

Scheme 2. Synthesis of P(AETAC-X) polymers by RAFT/MADIX polymerization mediated by *O*-ethyl-*S*-(1-ethoxycarbonyl)ethyldithiocarbonate (=xanthate chain transfer agent, CTA).

In a RAFT controlled radical polymerization process, two conditions must be fulfilled to reach an optimal control of the polymerization: 1) a rapid exchange between propagating chains and the chain transfer agent (CTA), meaning that C_{tr} must be high; 2) use of a much lower concentration of initiator than that of CTA, *i.e.* choice of an adequate $[CTA]_0/[Initiator]_0$ ratio, to provide a balance between an acceptable rate of polymerization ($R_p = k_p [P^\cdot] [M]$) and a minimum level of dead chains (radical-radical termination, $R_t = k_t [P^\cdot]^2$).[21, 28]

In this context, the effect of the ratio between the initial concentrations of the xanthate chain-tranfer agent (CTA) and the initiator (ACPA) on AETAC polymerization kinetics was first investigated. **Table 2** presents the experimental conditions for experiments carried out in a mixture of water/ethanol (90/10 wt-%) at 60°C, during 6 h, with different initial concentrations of ACPA at constant concentration of CTA.

Table 2. Experimental conditions for the RAFT/MADIX polymerization of AETAC carried out during 6 h at 60°C in a 90/10 wt-% water/ethanol mixture.

Expt	$[AETAC]_0$ *mol.L^{-1}*	$[ACPA]_0$ *mol.L^{-1}*	$[CTA]_0$ *mol.L^{-1}*	$\frac{[AETAC]_0}{[CTA]_0}$	$\frac{[CTA]_0}{[ACPA]_0}$
1	1.92	5.6×10^{-3}	2.55×10^{-2}	75	5
2	1.90	1.7×10^{-3}	2.51×10^{-2}	76	15

Figure 2 shows the evolution of AETAC conversion (X) and logarithmic conversion with time for the synthesis of P(AETAC-X)$_{76}$ with different ratios of $[CTA]_0/[ACPA]_0$.

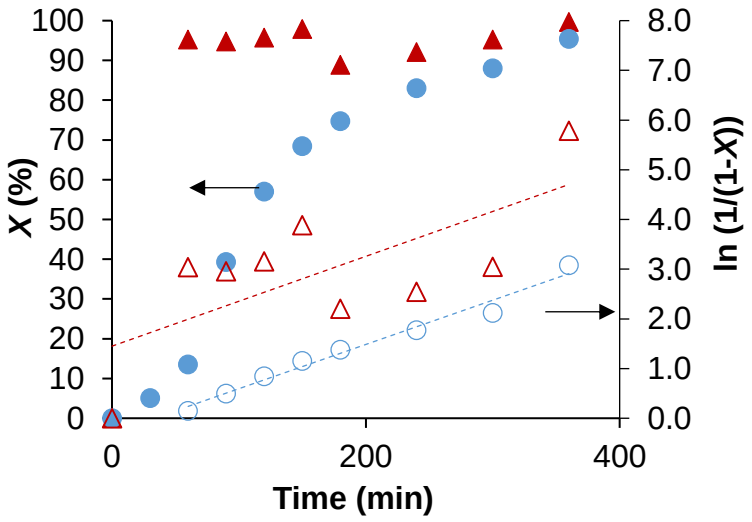

Figure 2. AETAC monomer conversion X (full symbols) and ln (1/(1-X)) (empty symbols) versus time for the synthesis of P(AETAC-X)$_{76}$ mediated by xanthate chain-transfer agent in a mixture of water/ethanol (90/10 wt-%): ▲ $[CTA]_0/[ACPA]_0$ = 5 (expt 1 in **Table 2**), ● $[CTA]_0/[ACPA]_0$ = 15 (expt 2 in **Table 2**).

As expected, when decreasing the initiator concentration from $[ACPA]_0 = 5.6 \times 10^{-3}$ mol.L^{-1} to $[ACPA]_0 = 1.7 \times 10^{-3}$ mol.L^{-1}, the polymerization rate of AETAC monomer decreases (**Figure 2**). For the experiment carried out with $[CTA]_0/[ACPA]_0$ = 5, a plateau at 95 % of AETAC conversion is reached after one hour of polymerization. For the experiment performed with $[CTA]_0/[ACPA]_0$ = 15, an inhibition period of 30 min was observed before to reach a complete conversion of monomer after 6 hours of polymerization. For the later experiment, the semilogarithmic kinetic plots of the monomer conversion versus time is linear (**Figure 2**), indicating a constant concentration of propagating radical with time.

For all the experiments presented in the following work, the ratio of $[CTA]_0/[ACPA]_0$ was set to 15. Different degrees of polymerizations were targeted by tuning the initial $[AETAC]_0/[CTA]_0$ ratio from 16 to 76 (**Table 3**).

Table 3. Experimental conditions and final monomer conversions for the synthesis of P(AETAC-X)$_n$ polymers by RAFT/MADIX polymerization and P(AETAC) polymer by free-radical polymerization, in a mixture of water/ethanol, at 60°C.

Expt	$[AETAC]_0$ *mol.L^{-1}*	Purity CTA *%*	$[CTA]_0$ *mol.L^{-1}*	$\frac{[AETAC]_0}{[CTA]_0}$	$\frac{[CTA]_0}{[ACPA]_0}$	H_2O /EtOH *wt-%*	$\frac{m_{EtOH}}{m_{CTA}}$	X^a *%*	*Polymer*[b]
1	1.9	93	2.5×10^{-2}	76	13	90/10	11	100	P(AETAC-X)$_{76}$
2	1.4	71	5.2×10^{-2}	26	13	75/25	11	96	P(AETAC-X)$_{25}$
3	1.4	84	5.2×10^{-2}	26	13	75/25	13	62	P(AETAC-X)$_{16\ (1)}$
4	1.4	84	8.5×10^{-2}	16	14	75/25	8	87	P(AETAC-X)$_{14}$
5	1.3	74	8.6×10^{-2}	16	14	56/44	11	99	P(AETAC-X)$_{16\ (2)}$
6	1.3	64	8.6×10^{-2}	16	14	56/44	11	84	P(AETAC-X)$_{13}$
7	1.3	71	8.6×10^{-2}	16	14	56/44	11	56	P(AETAC-X)$_9$
8	1.9	71	4.5×10^{-2}	42	24	75/25	11	98	P(AETAC-X)$_{41}$
9	1.8	-	-	-	-	90/10	-	99	P(AETAC)

[a] *X*: Final monomer conversion at 6 h, Equation 1; [b] The polymers are named P(AETAC-X)$_n$ with *n* the theoretical degree of polymerization, $DP_{theo.} = [AETAC]_0/[CTA]_0 \times X$.

In order to ensure the solubility of the xanthate chain-transfer agent in the reaction medium, the weight ratio of ethanol versus xanthate agent was set between 8 and 13 wt-% (**Table 3**). Note that for experiments performed with an insufficient amount of ethanol ($m_{ethanol}/m_{CTA} < 5$, not shown in **Table 3**), the presence of xanthate droplets dispersed in the aqueous phase could clearly be perceived, indicating a poor solubility of the xanthate agent. For the reaction performed with the lowest concentration of CTA (expt 1 in **Table 3**, $[CTA] = 2.5 \times 10^{-2}$ mol.L^{-1}), the xanthate agent was soluble in a mixture of 90/10 water/EtOH. This explains the varying fraction of ethanol.

For all the performed experiments, the final monomer conversion *X* is comprised between 60 and 100 %, and seems to be independent of the initial ratio of either H_2O/Ethanol or $[CTA]_0/[ACPA]_0$ (**Table 3**). As can be noticed in **Table 3**, a lack of reproducibility was observed for experiments performed in similar experimental conditions (expt 5, 6 and 7 in **Table 3**), as different final monomer conversions *X* were reached. This could be explained by the fact that different batches of xanthate agent (with diverse purities) were used for these different polymerizations. It has been shown that impurities in xanthate CTA was at the origin of inhibition period for VAc polymerization.[29]

2. Characterization of P(AETAC-X) macromolecular chain transfer agents and P(AETAC) polymer

2.i. UV-visible spectroscopy

Prior to the characterization of the polymers of **Table 3** by UV-visible spectroscopy, the molecular xanthate chain transfer agent was analyzed by UV-visible spectroscopy in a mixture of water:isopropanol (67:33 v:v%). The xanthate (dithiocarbonate) chemical group is associated with two characteristics resonance bands at wavelengths of 306 nm and 355 nm, together with an intense absorption between 200 and 280 nm (**Figure 3**).

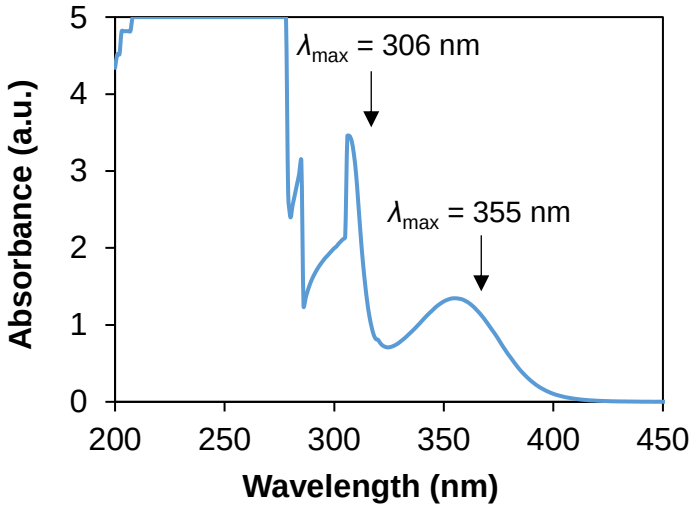

Figure 3. UV-Visible spectrum of *O*-ethyl-*S*-(1-ethoxycarbonyl)ethyldithiocarbonate at 2 mol.L^{-1} in a mixture of water:isopropanol (67:33 v:v%).

The molar extinction coefficient (ε) of the xanthate agent at either λ = 306 or λ = 355 nm was determined as the slope of the absorbance versus concentration plots (**Figure 4**), according to Beer-Lambert law, see Equation 2. The linearity of absorbance versus the concentration for both wavelengths attests that these two bands are indeed characteristics of the xanthate agent. The values of the extinction molar coefficients of the xanthate CTA in water:isopropanol (67:33 v:v%) mixture at 355 and 306 nm are respectively $\varepsilon_{xanthate,\ 355\ nm}$ = 54 L.mol^{-1}.cm^{-1} and $\varepsilon_{xanthate,\ 306\ nm}$ = 407 L.mol^{-1}.cm^{-1}.

$$A_\lambda = \varepsilon_\lambda \times l \times C$$ Equation 2

Where A_λ is the absorbance (arbitrary units) and ε_λ is the molar extinction coefficient (L.mol^{-1}.cm^{-1}) at a wavelength λ, l is the path length of the cuvette (cm) and C is the molar concentration (mol.L^{-1}).

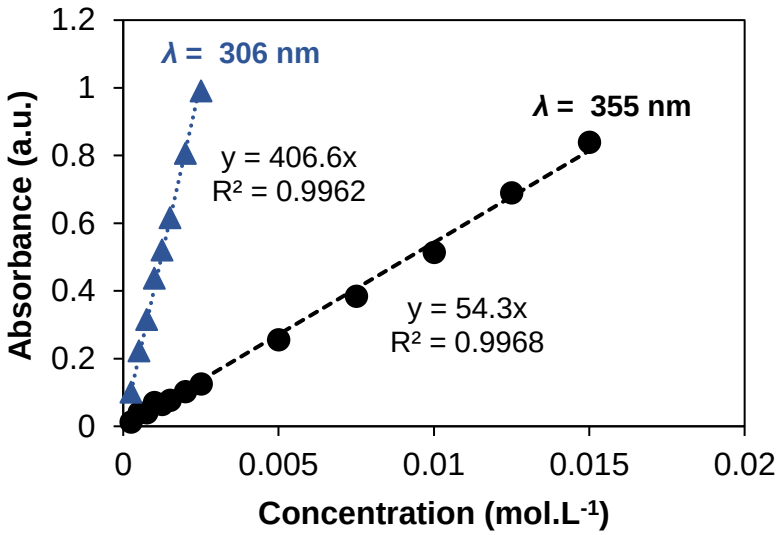

Figure 4. Absorbance of *O*-ethyl-*S*-(1-ethoxycarbonyl)ethyldithiocarbonate versus concentration for both wavelengths of 306 and 355 nm, in a mixture of water:isopropanol (67:33 v:v%).

The polymers of **Table 3** were characterized by UV-visible spectroscopy after one precipitation in THF. For a sake of clarity, selected spectra are reported in **Figure 5** to be compared with two non-functionalized PAETAC polymers: 1) the P(AETAC) synthesized by free radical polymerization in the absence of xanthate CTA (expt 9 in **Table 3**) and 2) the P(AETAC-X)$_{76,\ cleaved}$ prepared by cleavage of the xanthate chain-end of the functional P(AETAC-X)$_{76}$ polymer using a 20 fold excess of ADIBA initiator (**Scheme 3**), see experimental part. The cleaved P(AETAC-X)$_{76,\ cleaved}$ was dialyzed and freeze-dried prior to be analyzed by UV-visible spectroscopy.

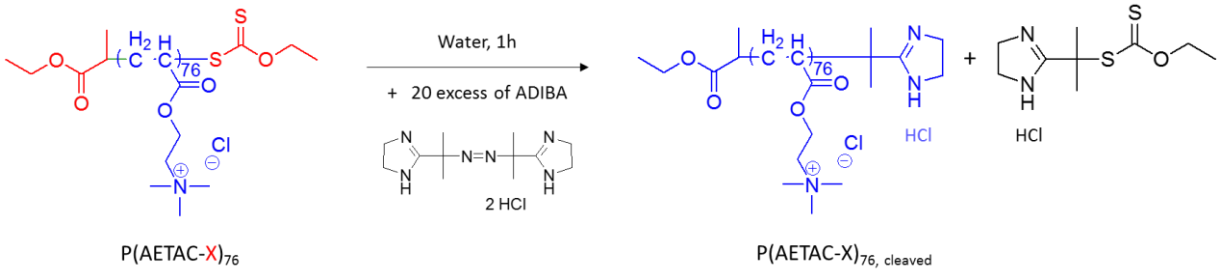

Scheme 3. Xanthate chain-end cleavage of P(AETAC-X)$_{76}$ polymer.

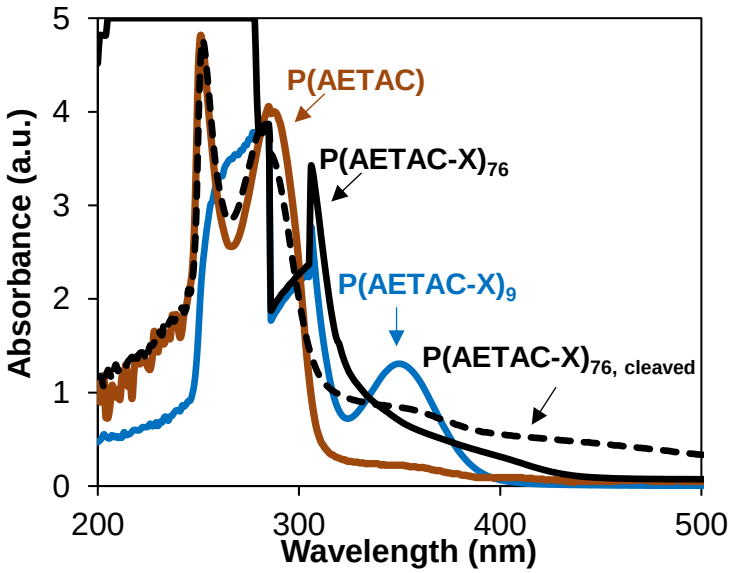

Figure 5. UV-visible spectra of P(AETAC-X)$_n$ (black and blue plain lines, respectively expt 1 (n = 76) and 7 (n = 9) in **Table 3**) , P(AETAC-X)$_{76,\ cleaved}$ (black dashed line) and P(AETAC) (brown plain line, expt 9 in **Table 3**). Polymers in a mixture of water:isopropanol (67:33 v:v%). [P(AETAC-X)$_{76}$] = 212 g.L^{-1}, [P(AETAC-X)$_9$] = 28 g.L^{-1}, [P(AETAC)] = 71 g.L^{-1} and [P(AETAC)$_{76,\ cleaved}$] = 84 g.L^{-1}.

Both P(AETAC-X) polymers synthesized by RAFT polymerization exhibit the characteristic bands of the xanthate (dithiocarbonate) chemical group at 306 and 355 nm (**Figure 5**) while these bands are absent in the UV-visible spectrum of the P(AETAC) (expt 9 **Table 3** and **Figure 5**). The intensity of the characteristic bands of the xanthate chain-end at 306 nm and 355 nm drastically decreased after cleavage of the P(AETAC-X)$_{76}$ (see P(AETAC-X)$_{76,\ cleaved,}$ **Figure 5**). Moreover, the narrow band at 250 nm was observed only for the P(AETAC) and P(AETAC-X)$_{76,\ cleaved}$ (**Figure 5**). These results confirm the presence of the xanthate chain-end in the P(AETAC-X) polymers synthesized by RAFT polymerization. Moreover, the overlay of UV-visible (λ = 355 nm) and refractometer (RI) traces of the A-4F fractograms for P(AETAC-X)$_{14}$ polymer (**Figure 6**) depicts the presence of the dithiocarbonate chain-end and so the living character.

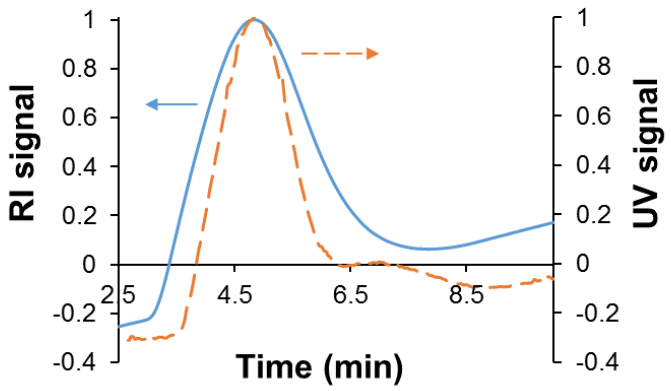

Figure 6. Overlay of the UV-visible (λ = 355 nm, dashed line) and refractometer (RI, plain line) traces of the A-4F fractograms for P(AETAC-X)$_{14}$ polymer (expt 4 in **Table 3**).

From the linearity of the logarithmic monomer conversion with time up to 100 % of conversion (**Figure 2**), a constant concentration of radicals along the polymerization suggests the low occurrence of termination reaction. The fraction of additional dead polymer chains (F) that do not carry thiocarbonylthio end group can be calculated from the number of chains created by the initiator (Equation 3). The theoretical values of F are below 5 mol-% for the series of polymerizations (see **Table 4**).

$$F = \frac{[ACPA]_0 \times (1 - e^{-k_d \times t})}{[CTA]_0}$$ Equation 3

InEquation 3, $[CTA]_0$ and $[ACPA]_0$ are the initial concentrations of respectively the xanthate agent and the initiator, k_d corresponds to the dissociation rate constant of the initiator ($k_{d,ACPA,\ water,\ 70°C} = 2.2 \times 10^{-5}\ s^{-1}$)[30] and t is the polymerization time.

By considering a complete xanthate chain-end fidelity, the number-average molar masses (M_n) of the P(AETAC-X) cationic polymers were calculated from the UV-visible spectra of polymers on the basis of Equation 4.

$$Mn_{UV} = \frac{m_{polymer}}{n_{xanthate}\,(1+F)}\ g.mol^{-1}$$ Equation 4

In this calculation, the ratio between the mass of polymer (= mass of monomer units) and the number of moles of dithiocarbonate chain end calculated from Beer-Lambert relationship ($n_{xanthate}$ = (Absorbance × V)/ $\varepsilon_{xanthate}$) is considered.

The theoretical number-average molar masses of the polymers (M_n) were calculated from Equation 5.

$$M_{n,theo.} = M_{xanthate} + \frac{[AETAC]_0 \times X \times M_{AETAC}}{([Xanthate]_0 + [ACPA]_0 \times (1-e^{-k_d \times t}))}$$ Equation 5

Where $M_{xanthate}$ and M_{AETAC} correspond to the molar masses of respectively the molecular xanthate agent ($M_{xanthate}$ = 222 g.mol^{-1}) and AETAC monomer (M_{AETAC} = 194 g.mol^{-1}), $[AETAC]_0$, $[Xanthate]_0$ and $[ACPA]_0$ are the initial concentrations of respectively AETAC monomer, xanthate agent and ACPA initiator, X is the final monomer conversion (Equation 1), k_d is the initiator dissociation constant ($k_{d,\ ACPA,\ water,\ 70°C}$ = 2.2 × 10^{-5} s^{-1})[30] and t is the polymerization time.

Table 4. Characterization of the P(AETAC-X)$_n$ cationic polymers synthesized by RAFT/MADIX polymerization.

Expt	Polymer	F [a]	$M_{n,theo}$ [b] *g.mol^{-1}*	$M_{n,UV,\ 355\ nm}$ [c] *g.mol^{-1}*	$[P(AETAC\text{-}X)_n]_{UV}$ [d] *g.L^{-1}*
1	P(AETAC-X)$_{76}$	0.025	14 450	17 530	212
2	P(AETAC-X)$_{41}$	0.026	8 060	2 770	120
3	P(AETAC-X)$_{25}$	0.048	4 980	7 740	73
4	P(AETAC-X)$_{16\ (1)}$	0.049	3 280	4 550	49
5	P(AETAC-X)$_{16\ (2)}$	0.027	3 140	7 970	47
6	P(AETAC-X)$_{14}$	0.045	2 850	9 300	43
7	P(AETAC-X)$_{13}$	0.017	2 720	11 180	50
8	P(AETAC-X)$_9$	0.027	1 870	1 170	28

[a] Theoretical fraction of dead polymer chain (see Equation 3); [b] Theoretical number-average molar mass (M_n) calculated from Equation 5 at t = 6 h; [c] Experimental M_n calculated from UV-absorbance of precipitated P(AETAC-X) at 355 nm (A_{355nm} < 1) (Equation 4 and **Figure 5**) with $\varepsilon_{xanthate,\ 355\ nm}$ = 54 L.mol^{-1}.cm^{-1} (Equation 2 and **Figure 4**); [d] Concentartion of P(AETAC-X)$_n$ for UV-Visible analysis.

As reported in **Table 4**, the values of the experimental $M_{n,UV}$ based on UV-visible spectroscopy are in the range of the theoretical M_n calculated from Equation 5, highlighting the presence of xanthate chain-end. However, the values of $M_{n,UV}$ don't follow the trend of the theoretical M_n. The randomly distributed values question the level of accuracy of UV-Visible analysis, which can be ascribed to low signal to baseline ratio of the band at 355 nm. Before UV-visible characterization, all the P(AETAC-X) polymers were precipitated once in THF which is a good solvent of the xanthate agent. However, if the molecular xanthate agent was not totally removed during the first precipitation, the experimental $M_{n,UV,355\ nm}$ should be underestimated, $n_{xanthate}$ being overestimated (Equation 4). In order to verify if one precipitation was sufficient to eliminate all the free molecular xanthate agent, the P(AETAC-X)$_{13}$ polymer (expt 7 in **Table 4**) was precipitated twice in THF. After each precipitation, the P(AETAC-X)$_{13}$ was analyzed by UV-Visible spectroscopy. The values of the experimental M_n calculated from UV-absorbance

of P(AETAC-X)$_{13}$ after the first and the second precipitations are similar (**Table 5**), which attests that most of the free xanthate agent was removed upon the first precipitation in THF.

Table 5. Results of the UV-visible characterization of P(AETAC-X)$_{13}$ polymer at 50 g.L^{-1} in a mixture of water:isopropanol (67:33 v:v%) after 1 or 2 precipitations in THF.

Number of precipitation	$M_{n,UV,\ 355\ nm}$[a] *g.mol^{-1}*
1	11 180
2	11 880

[a] Experimental M_n calculated from UV-absorbance of precipitated P(AETAC-X)$_{13}$ at 355 nm (A_{355nm} < 1) (Equation 4) with $\varepsilon_{xanthate,\ 355\ nm}$ = 54 L.mol^{-1}.cm^{-1} (Equation 2 and **Figure 4**).

2.ii. MALDI-TOF analyses

As the targeted degrees of polymerization of the synthesized P(AETAC-X) polymers are low ($10 < n < 80$), MALDI-TOF spectrometry is a suitable technique to highlight the presence of xanthate chain-end. Some cationic polymers with molar masses below 5000 g.mol^{-1} have been previously analyzed by MALDI-TOF.[31, 32] Locock *et al.*[32] have shown that this technique was not suitable for the analysis of cationic copolymers with molar masses above 5000 g.mol^{-1}, due to difficulties associated with ionizing larger species. Apart from the problem of achieving results from MALDI-TOF spectrometry for cationic polymers, the interpretation also becomes more complex due to the probable multiply charged species in the polymer chain.[33]

In the present work, all the attempts to characterize the P(AETAC-X) polymer with the lowest theoretical molar mass (P(AETAC-X)$_9$, expt 7 in **Table 3**) by MALDI-TOF were unsuccessful, which might suggest that P(AETAC-X) polymers have higher molar masses than the theoretical ones or that they are forming aggregates. **Figure 7** depicts an example of MALDI-TOF spectrum obtained for the analysis of P(AETAC-X)$_9$ polymer.

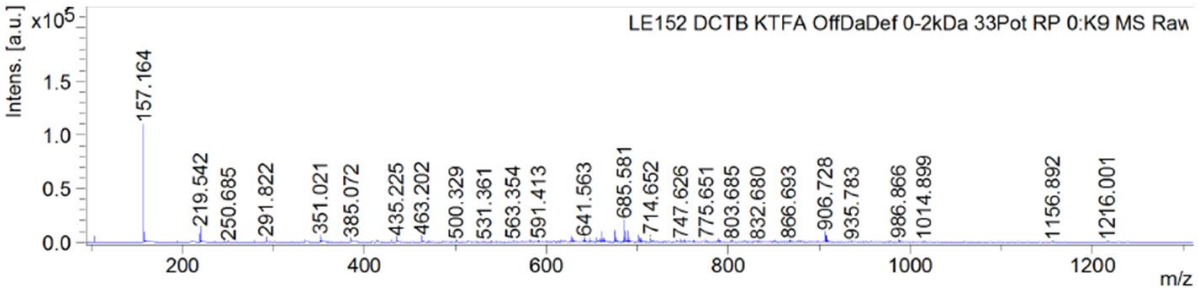

Figure 7. MALDI-TOF spectrum of P(AETAC-X)$_9$ in positive-ion reflectron mode (using DTCB as matrix and KTFA as cationizing agent).

2.i. SEC analysis in aqueous mobile phase

The P(AETAC-X)$_{76}$ polymer (expt 1 in **Table 3**, $M_{n,theo}$ = 14 450 g.mol^{-1}) was characterized by SEC at both 3 mg.mL^{-1} and 1.5 mg.mL^{-1} in 0.15 mol.L^{-1} ammonium acetate / 0.20 mol.L^{-1} acetic acid buffer (pH 4.5) using columns dedicated to the analysis of cationic polymers. The results of the SEC analyses are dependent on the polymer concentration. Indeed, for the analysis of P(AETAC-X)$_{76}$ performed at 3 mg.mL^{-1} the chromatogram displays a shoulder at higher M_n, whereas a monomodal peak was observed at a polymer concentration of 1.5 mg.mL^{-1} (**Figure 8**). Moreover, an increase of the polymer concentration provokes an increase of the $M_{n,MALLS}$ value (**Table 6**). It has been previously observed that an increase of the polyelectrolyte concentration can lead to aggregation due to electrostatic interactions between polyions.[34]

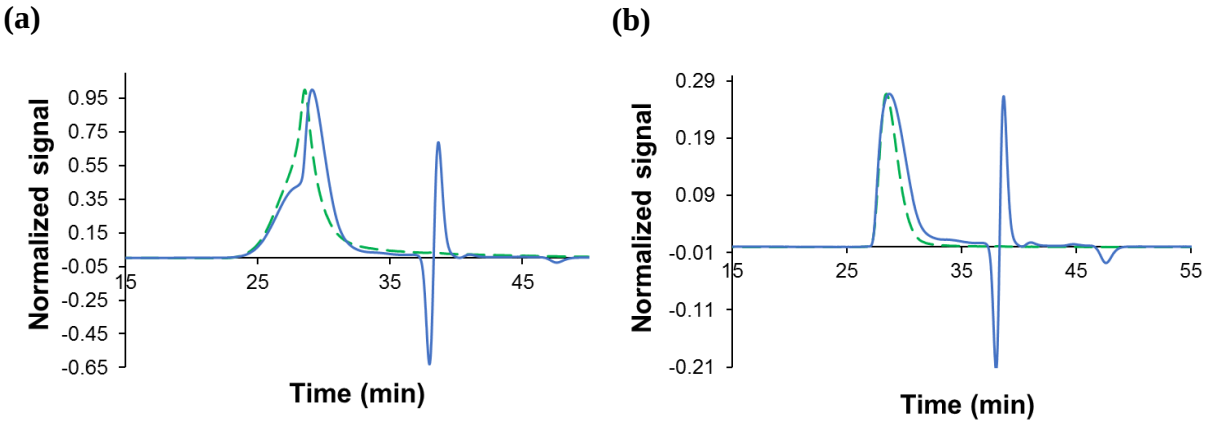

Figure 8. SEC chromatograms in 0.15 mol.L^{-1} ammonium acetate / 0.20 mol.L^{-1} acetic acid buffer (pH 4.5) of P(AETAC-X)$_{76}$ polymer. **(a)** [P(AETAC-X)$_{76}$] = 3 mg.mL^{-1} and **(b)** [P(AETAC-X)$_{76}$] = 1.5 mg.mL^{-1}. Plain line: RI signal; Dashed line: MALLS signal.

For both concentrations, the number-average molar mass of the polymer is very high in comparison with the expected M_n (**Table 6**). Molar masses ranging between 1.3 × 10^6 to 4.3 × 10^6 g.mol^{-1} with gyration radius of 50 nm (**Figure 9**) suggest significant aggregation of the polymer in the eluent. Note that the dispersity values are low ($Đ$ < 1.2, **Table 6**).

Table 6. Results of the SEC characterization of P(AETAC-X)$_{76}$ cationic polymer (expt 1 in **Table 3**, $M_{n,theo}$ = 14 450 g.mol^{-1}) synthesized by RAFT/MADIX polymerization.

[P(AETAC-X)$_{76}$] *mg.mL^{-1}*	***M*$_{n,MALLS}$**[a] *g.mol^{-1}*	***Đ*$_{MALLS}$**[a]	***Mass recovery*** *%*
3	4 314 000	1.2	130
1.5	1 278 000	1.1	66

[a] Values obtained from the SEC analysis in aqueous eluent (ammonium acetate/acetic acid) with a MALLS detector, using (d*n*/d*c*)$_{P(AETAC-X)n}$ = 0.137 mL.g^{-1}.

Moreover, the increase of the gyration radius (R_g) for increasing elution time (**Figure 9**) is the sign of an abnormal elution of the polymer. Indeed, for a normal elution, the polymer chains of lower M_n and lower gyration radius are eluting at higher elution volume (*i.e.* higher elution time). Such abnormal elution has already been observed for large branched polymers.[35] The percentages of mass recovery are reasonable in both cases, which indicates that most of the polymer elutes out of the columns.

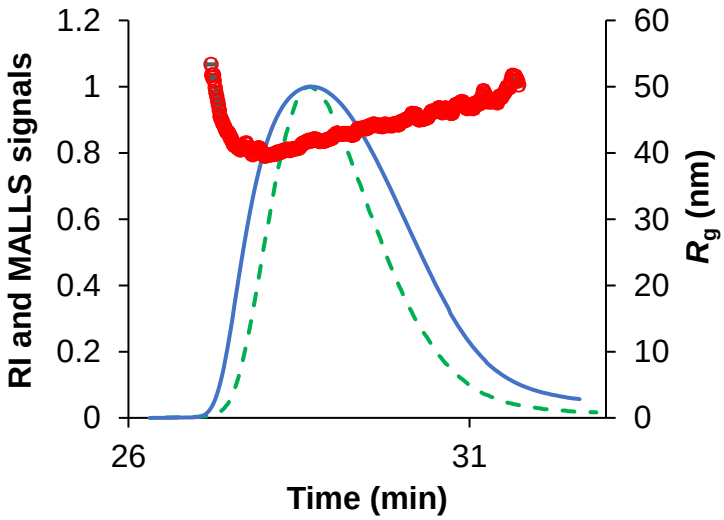

Figure 9. SEC chromatograms (Full line: RI signal; Dashed line: MALLS signal) and evolution of the gyration radius R_g (○) of $P(AETAC\text{-}X)_{76}$ polymer at 1.5 $mg.mL^{-1}$ in 0.15 $mol.L^{-1}$ ammonium acetate/0.20 $mol.L^{-1}$ acetic acid buffer (pH 4.5). Note that the error bars on R_g values are smaller than the plots.

In the literature, various eluents have been used for the SEC characterization of cationic polymers obtained by RAFT polymerization. Aqueous solution with 0.3 M Na_2SO_4 / 0.5 M acetic acid,[14-16] with 0.05 M Na_2SO_4,[20] with 0.2 M $NaNO_3$ / 50 mM TRIZMA buffer[19] and very recently with 0.5 M acetic acid / 0.3 M NaH_2PO_4,[18] are example of eluents. Water/acetonitrile solution (80/20 wt-%) with 1 M of NH_4NO_3 salts has also been employed for low M_n polymers.[23] In all these mentioned studies, polymer experimental M_n have been determined using calibration based on either poly(2-vinylpyridine)[14-16] or poly(ethylene oxide)[18-20, 23] standards. It is well-known that the use of apparent molar masses (*i.e.*, molar masses relative to standards) can induce a significant error on the molar mass determination, due to the different chemical nature and structure of the analyte compared to the standards, especially for polyelectrolytes in aqueous phase.[36]

P(AETAC-X)$_{14}$ polymer was analyzed by dynamic light scattering at two concentrations in different media, either 0.1 M NaCl solution or A-4F buffer ([Salts] = 0.18 M, pH = 8, see experimental part for the details of the salts). The results are displayed in **Figure 10**.

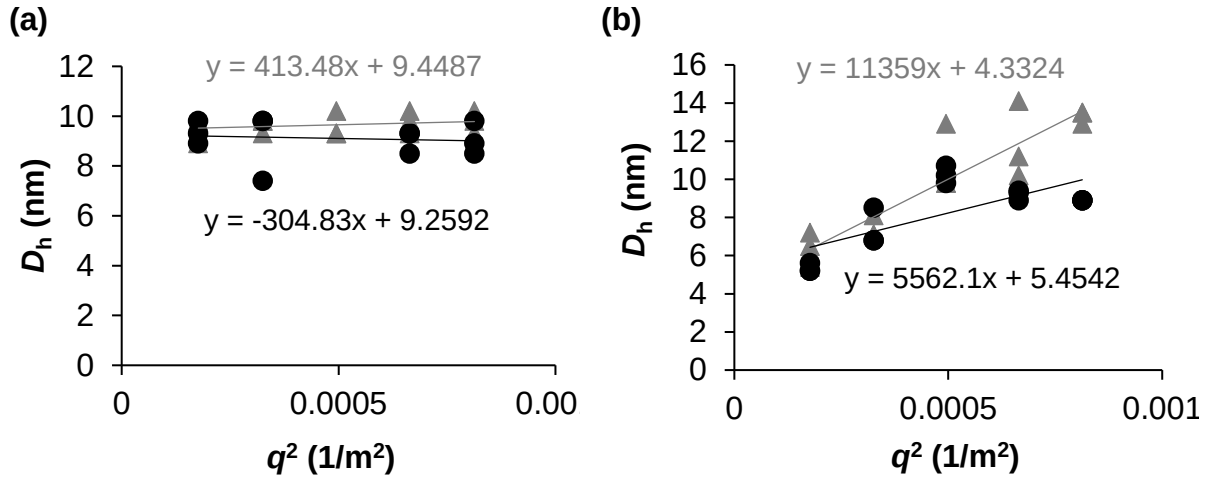

Figure 10. Angular dependence of the hydrodynamic diameter of P(AETAC-X)$_{14}$ polymer (expt 4 in **Table 3**) measured in ● 0.1 M NaCl solution and ▲ A-4F buffer: **(a)** [P(AETAC-X)$_{14}$] = 2.5 mg.mL^{-1} and **(b)** [P(AETAC-X)$_{14}$] = 5 mg.mL^{-1} .

For solutions containing 0.10 M to 0.18 M of salts, an angular dependence of the hydrodynamic radius at 5 mg.mL^{-1} was observed, while no *q*-dependence was displayed for the lowest polymer concentration of 2.5 mg.mL^{-1} (**Figure 10**). Förster *et al.*[34] revealed that a variation of the diffusion coefficient with the wave vector with a negative slope (*i.e.* positive slope for $D_h = f(q^2)$) was an evidence of intermolecular interactions. Therefore, the results of the dynamic light scattering measurements are coherent with those obtained for SEC analysis, suggesting polymer aggregation by increasing concentration.

2.ii. A-4F analyses

Asymmetrical flow field-flow fractionation (A-4F) is a technique of characterization which allows the separation of the analyte by its size. The sample is injected into a channel with a laminar flow, and a cross-flow perpendicular to the direction of the sample flow is applied. These hydrodynamic forces will allow diffusion-based separation of the sample and therefore size separation, as the diffusion coefficient of an analyte is related to its size. In comparison to size exclusion chromatography techniques, in A-4F, the separation mechanism is based on the diffusion of the analytes and not on the hydrodynamic exclusion volume with porous column, which allows to reduce in most cases unwanted interactions and adsorption effects. Also, macromolecules exhibiting low molar masses (*i.e.* high diffusion coefficients) elutes first (at

low elution volume) and macromolecules with high molar masses elutes latter (higher elution volume) due to their slower diffusion through the channel.[33, 37] The fractograms exhibit inverse $M_n = f(V_e)$ profile in comparison with SEC.

In the present work, a first series of P(AETAC-X) were analyzed by A-4F using water solution with 0.03 wt-% (5×10^{-3} mol.L^{-1}) of NaN_3 salts. It should be noted that in salt-free solutions of the protonated poly(2-vinyl pyridine), Förster *et al.* highlighted intermolecular interactions as two relaxation modes were apparent in the correlation function recorded by DLS together with a negative slope of the scattered intensity versus the wave vector.[34] However, it was also proved that a salt concentration of 0.003 M was sufficient to screen the intermolecular interactions of the polyelectrolyte as only one relaxation mode in DLS and a positive slope in SLS were observed.[34]

The results of the A-4F characterization are given in **Table 7** and the A-4F fractograms (MALLS signal) of some polymers are depicted in **Figure 11**.

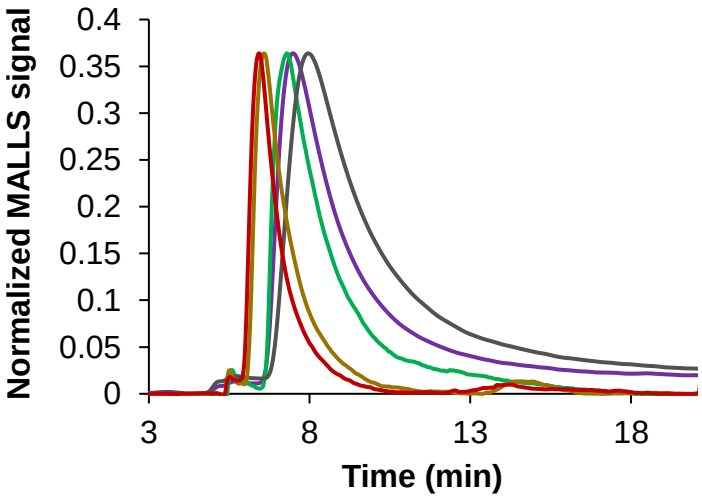

Figure 11. A-4F fractograms in ultra-pure water ([NaN_3] = 5×10^{-3} M) of P(AETAC-X) polymers: $P(AETAC\text{-}X)_{41}$ (expt 2 in **Table 7**), $P(AETAC\text{-}X)_{25}$ (expt 3 in **Table 7**), $P(AETAC\text{-}X)_{16\ (1)}$ (expt 4 in **Table 7**), $P(AETAC\text{-}X)_{14}$ (expt 5 in **Table 7**) and $P(AETAC\text{-}X)_{9}$ (expt 6 in **Table 7**).

Table 7. Results of the A-4F characterization performed in H_2O ([NaN_3] = 5 × 10^{-3} M) (see experimental part for conditions) of P(AETAC-X)$_n$ cationic polymers synthesized by RAFT/MADIX polymerization.

Expt	Polymer	$M_{n,theo}$[a] *g.mol^{-1}*	$M_{n,\ A\text{-}4F,\ MALLS}$[b] *g.mol^{-1}*	$Đ_{MALLS}$[b]	*Mass recovery* *%*
1	P(AETAC-X)$_{76}$	14 450	92 130	1.2	90
2	P(AETAC-X)$_{41}$	8 060	37 750	1.4	86
3	P(AETAC-X)$_{25}$	4 980	27 600	1.3	81
4	P(AETAC-X)$_{16\ (1)}$	3 280	19 940	1.3	43
5	P(AETAC-X)$_{14}$	2 850	17 160	1.3	50
6	P(AETAC-X)$_9$	1 870	20 150	1.3	27

[a] Theoretical M_n calculated from Equation 5 at t = 6h; [b] Values obtained from the A-4F analysis with a MALLS detector, using $(dn/dc)_{P(AETAC\text{-}X)n}$ = 0.137 mL.g^{-1}.

For all the polymers, the experimental $M_{n,MALLS}$ values are approximately 10 times greater than the theoretical ones (**Table 7**). The number-average molar masses of the P(AETAC-X)$_n$ determined from the A-4F analyses with a MALLS detector ($M_{n,MALLS}$) follows the theoretical ones, *i.e.*, $M_{n,MALLS}$ decreases by decreasing the theoretical degree of polymerization n of the P(AETAC-X)$_n$. This trend highlights the ability of the xanthate chain transfer agent to tune the experimental number-average molar mass of the P(AETAC-X) polymers. The low dispersity values (from $Đ$ = 1.2 to 1.4) of the P(AETAC-X) confirm a control of polymer growth (**Table 7**).

The percentages of mass recovery are above 80 % for polymers with theoretical degree of polymerization (n) higher than 25 but mass recovery drops below 50 % for lower theoretical degree of polymerization (n < 16, **Table 7**). As a similar membrane with cut-off of 5 kDa was used, the incomplete mass recovery of the sample of lowest M_n might be due to diffusion of low M_n chains through the membrane. This might explain the constant value of $M_{n,MALLS}$ measured for degree of polymerization n ranging between 16 and 9.

Note that the gyration radius (R_g) doesn't evolve with the elution time during the A-4F analysis of P(AETAC-X)$_{76}$ (**Figure 12**) while SEC analysis revealed abnormal elution. Podzimek *et al.* have shown that for highly branched large macromolecules, the abnormal elution observed in SEC was eliminated by using A-AF.[38] Also, the values of P(AETAC-X)$_{76}$ gyration radius determined by A-4F analysis (~ 25 nm, **Figure 12**) are lower than the one given by SEC analysis (~ 50 nm, **Figure 9**), revealing a non-permanent size.

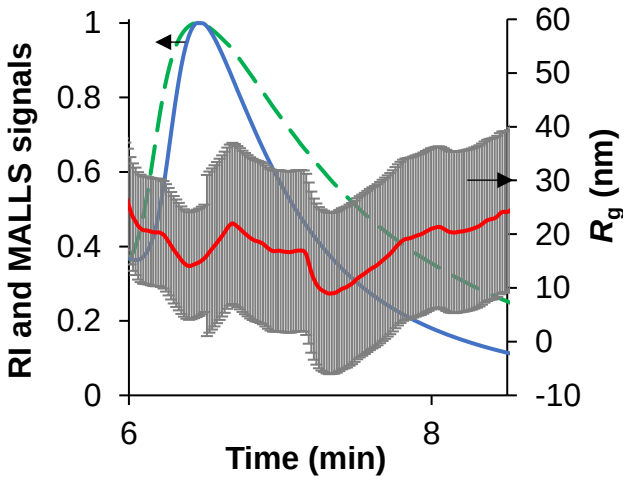

Figure 12. A-4F fractogram (Full line: RI signal; Dashed line: MALLS signal) and evolution of gyration radius (R_g) (○) of P(AETAC-X)$_{76}$ polymer (expt 1 in **Table 7**) at 6 mg.mL^{-1} in ultra-pure water with 5 × 10^{-3} mol.L^{-1} of NaN_3 salts. The error bars on R_g values are reported.

The fact that the average ratio between the experimental M_n calculated from UV-Visible spectroscopy and M_n measured by A-4F is equal to 8 (**Figure 13**, $\frac{Slope\ (M_{n,MALLS} = f(n))}{Slope\ (M_{n,UV} = f(n))} = 8$), traduces a high number of xanthate groups per analyzed polymeric object, which might traduce the formation of polyelectrolyte aggregates.

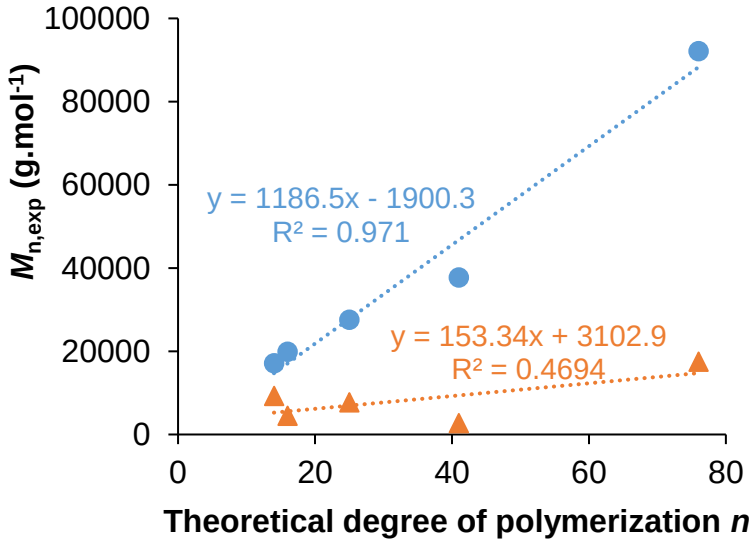

Figure 13. Evolution of $M_{n,\ UV}$ (▲) and $M_{n,\ A\text{-}4F,\ MALLS}$ (●) as a function of the theoretical degree of polymerization (n) of the P(AETAC-X)$_n$ polymers.

The P(AETAC-X)$_{76}$ polymer was analyzed by diffusion-ordered NMR spectroscopy (DOSY-NMR) at a concentration of 6 mg.mL^{-1} (**Figure 14**). DOSY-NMR allows for the identification of different components in the mixture by means of the acquisition of a two-dimensional

spectrum which correlates the diffusion coefficients of each component with their corresponding chemical shifts in ^{1}H NMR spectrum.[39]

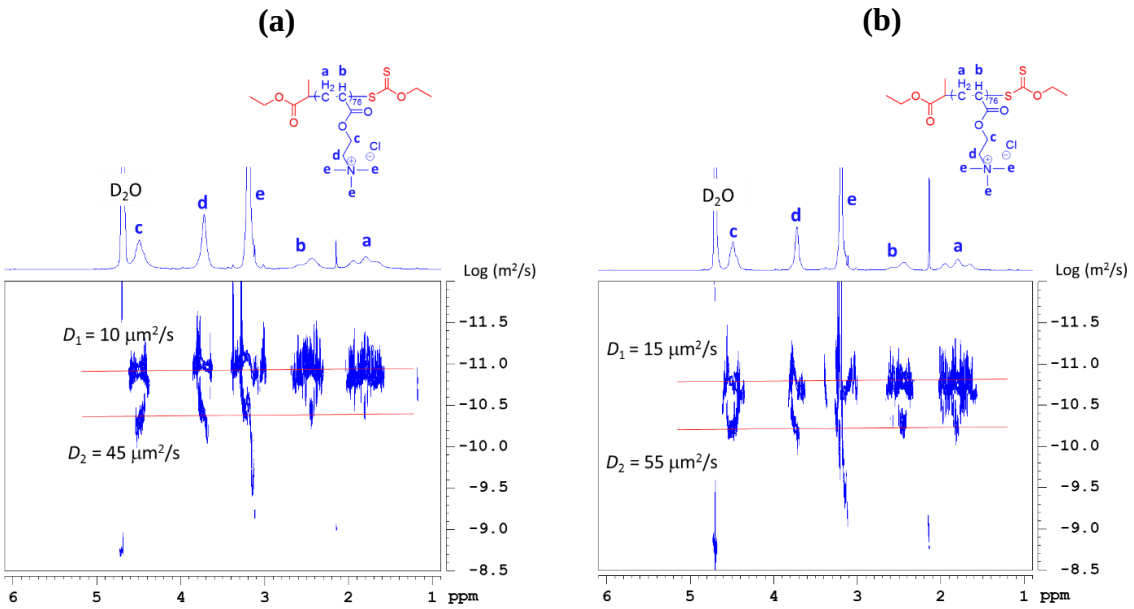

Figure 14. Effect of NaCl concentration on the DOSY NMR spectra of P(AETAC-X)$_{76}$ (expt 1 in **Table 3**): **(a)** [P(AETAC-X)$_{76}$] = 6 mg.mL^{-1} in D_2O, **(b)** [P(AETAC-X)$_{76}$] = 6 mg.mL^{-1} in [NaCl] = 0.1M in D_2O.

For P(AETAC-X)$_{76}$ dissolved at 6 mg.mL^{-1} in either pure D_2O or 0.1M NaCl D_2O, two diffusion coefficients are observed (**Figure 14**), revealing the formation of aggregates in both cases. The addition of 0.1 M NaCl salts leads to an increase of the determined diffusion coefficient values (*i.e.*, smaller diffusing species), which might be ascribed to a partial screening of the electrostatic interactions, hence reducing the apparent hydrodynamic diameter of the polyelectrolytes. However, the interchain interactions are not fully suppressed in the presence of 0.1 M NaCl salts as two diffusion coefficients are still observed (**Figure 14**).

The effect of the polymer concentration on the behavior of P(AETAC-X)$_{76}$ in salt-free solution (pure D_2O) was also studied by DOSY NMR (**Figure 15**).

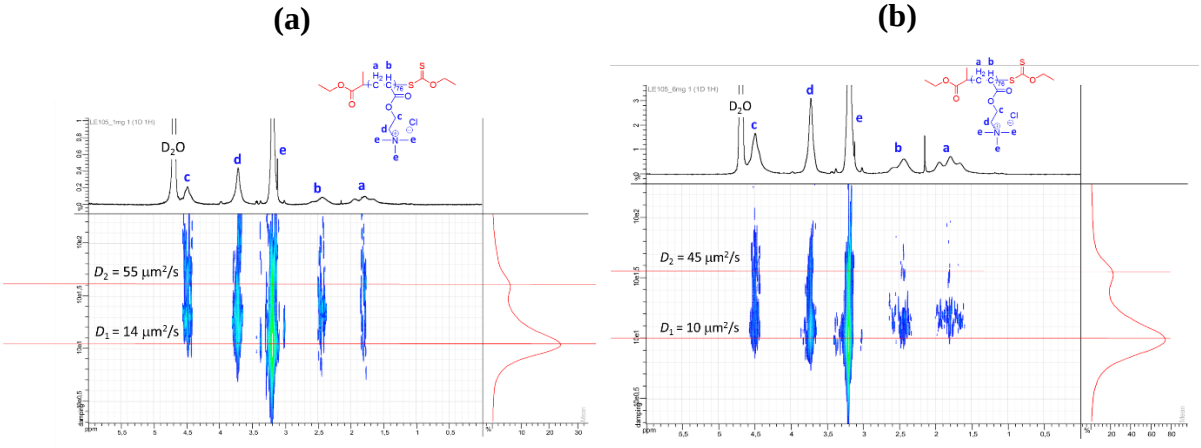

Figure 15. Effect of polymer concentration on the DOSY NMR spectra of P(AETAC-X)$_{76}$ (expt 1 in **Table 3**): **(a)** [P(AETAC-X)$_{76}$] = 1 mg.mL^{-1} in D_2O, **(b)** [P(AETAC-X)$_{76}$] = 6 mg.mL^{-1} in D_2O.

At both concentrations of 1 and 6 mg.mL^{-1} of P(AETAC-X)$_{76}$ in D_2O, two diffusion coefficients are observed on the DOSY-NMR spectra (**Figure 15**), suggesting the presence of aggregates in both cases. The diffusion coefficient D is concentration-dependent according to Equation 6.

$$D = D_0 (1 + k_D C_p) \quad \text{Equation 6}$$

Where D_0 is the translation diffusion coefficient extrapolated to zero concentration, k_D is the dynamic second virial coefficient and C_p the polymer concentration.

When plotting D as a function of C_p, a positive virial coefficient value denotes repulsive interactions between polymer chains, while a negative virial coefficient value indicates attractive interactions. In the present study, the plots of D versus the P(AETAC-X)$_{76}$ concentration (**Figure 16**) reveals attractive interactions among polymer chains for both types of populations (negative slopes in **Figure 16**).

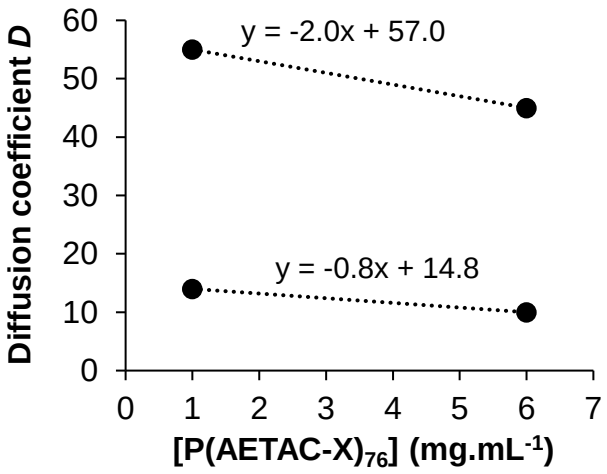

Figure 16. Evolution of the diffusion coefficients determined by DOSY-NMR as a function of P(AETAC-X)$_{76}$ concentration in D_2O.

Apart from the formation of aggregates, the difference observed between $M_{n,UV}$ and $M_{n,\ A\text{-}4F,\ MALLS}$ could also arise from the formation of branched structures bearing several xanthate chain-ends per chain. Branched poly(acrylates) can be produced by intermolecular chain transfer reactions, as depicted in **Scheme 4**. Indeed, the formation of branched poly(acrylate) with more than one functional group per chain, has already been observed by Farcet *et al.* for the polymerization of *n*-butyl acrylate by nitroxide mediated polymerization.[40] However, the authors proved by MALDI-TOF analyses that the majority of the chains contained one nitroxide per chains and fewer were composed of either 0 or 2 nitroxides.[40] In the present work, the probability to form branched structures with an average of 8 xanthates per chains is low and these branched structures should be mixed with dead polymer chains (P_n–H), hence decreasing the average-number of xanthate per chain.

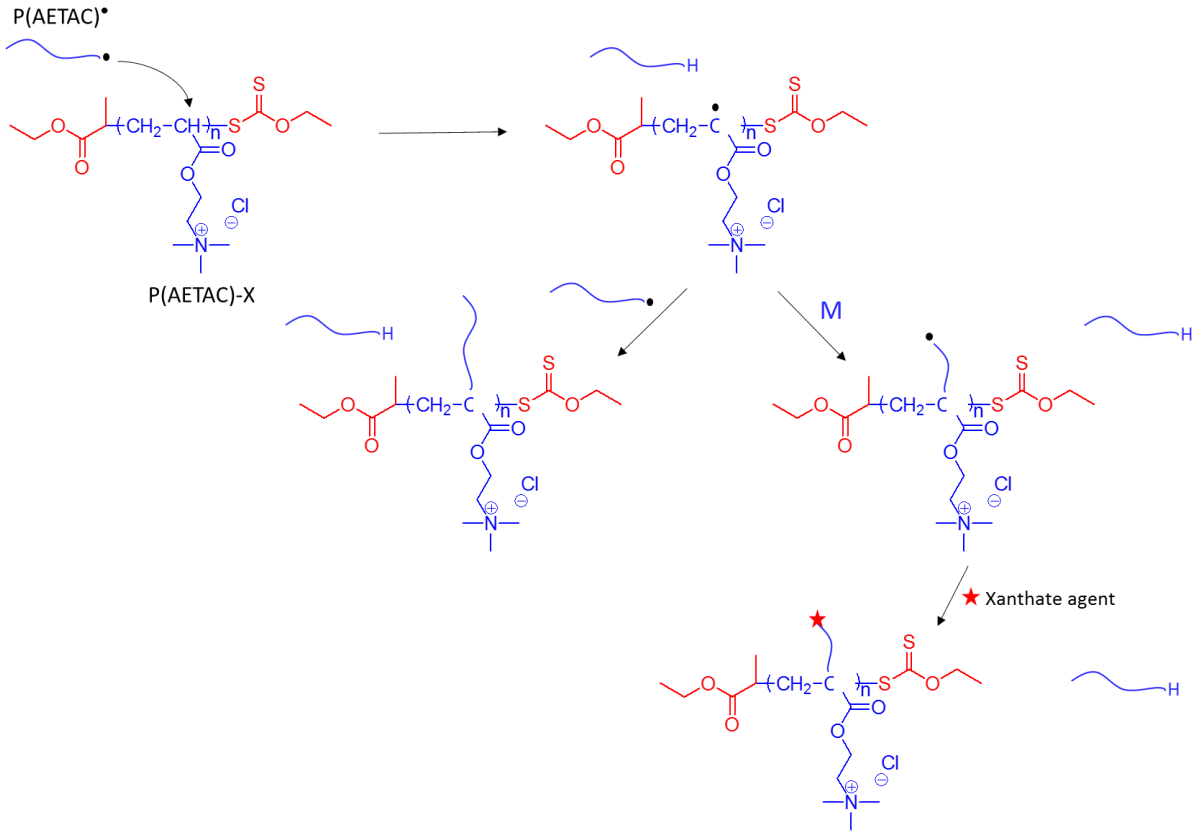

Scheme 4. Mechanism of formation of branched structures by intermolecular transfer reactions between polyacrylates.

The plot of the gyration radius against molar mass can provide information about polymer chain conformation and was often used to highlight polymer branching. Indeed, the typical value of the slope of $R_g = f(M_n)$ for linear random coils in thermodynamically good solvents is 0.6. Lower values indicate the presence of branching.[38] In the present work, the slope is equal to 0.8, excluding the formation of highly branched structures containing 8 xanthates per polymer (**Figure 17**). This value of 0.8 traduces a macromolecular conformation of P(AETAC-X)$_{76}$ which is intermediate between random coils (slope = 0.5 – 0.6) and rods (slope = 1). Stretching of polyelectrolytes in low salt concentration aqueous solution can be observed, however, the value of the conformation plot ($R_g = f(M_n)$) should be carefully considered due to the large error bar on the R_g value (**Figure 12**).

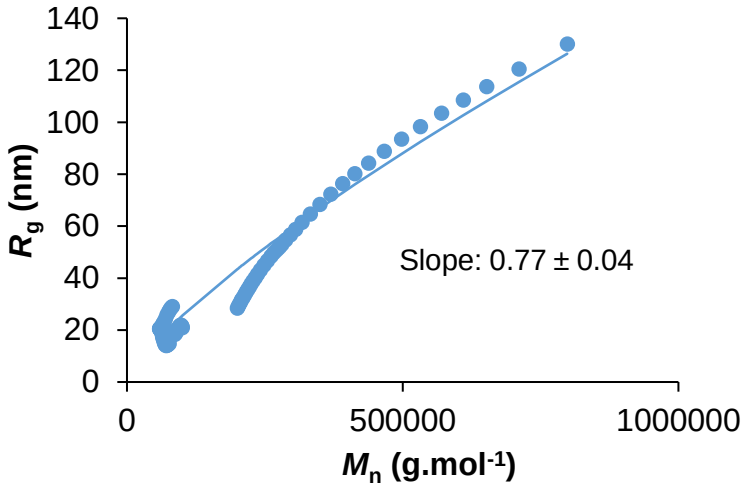

Figure 17. Plot of the gyration radius (R_g) as a function of the molar mass for the A-4F analysis of P(AETAC-X)$_{76}$ in water with 5 × 10^{-3} mol.L^{-1} of NaN_3 salts.

The SLS analyses of polyelectrolytes revealed complex picture of the properties of polyelectrolytes in solution.[34] In very dilute regimes, the polyelectrolytes are expected to be fully stretched. In salt free conditions, for high polymer concentration (C_p > 1 g.L^{-1}), flexible linear molecules were expected for high C_p while very large apparent gyration radius was observed.[34] This gyration radius was even higher than for rigid rod structure and it was unlikely corresponding to single molecules but more to aggregates.

The initial P(AETAC-X) concentration ranges from 1.5 to 6 mg.mL^{-1} for SEC and A-4F analyses but the fractionation of the chains induces a SLS analysis in dilute regime. Thus, we attempted to analyze the cationic polyelectrolytes by A-4F with higher concentration of salts to screen the electrostatic interactions among polyions. The chosen eluent was ultra-pure water with 0.076 M of Na_2HPO_4, 0.096 M of $NaNO_3$, 0.004 M of NaH_2PO_4 and 0.002 M of NaN_3 salts with a total concentration of salts of 0.18 M (pH = 8).

The first test was conducted with P(AETAC-X)$_{14}$ polymer (expt 4 in **Table 3**) with the A-4F eluent (analysis condition 1, **Table 8**).

Table 8. Analysis conditions for the runs of A-4F characterization performed in Pau.[a]

Analysis conditions	Membrane	Eluent	Spacer	Flow[b]	Analyzed polymer	Mass recovery %
1	PES 1 kDa	A-4F buffer[a]	350 µm	FOC1 DF0.5 CF1	P(ATAEC-X)$_{14}$ (expt 4 in **Table 3**)	9
2	PES 1 kDa	A-4F buffer + 0.1 mM CTAB	350 µm	FOC1 DF0.5 CF1	P(ATAEC-X)$_{14}$ (expt 4 in **Table 3**)	51
3	PES 1 kDa	A-4F buffer + 0.1 mM CTAB	490 µm	FOC1 DF0.5 CF1	All the polymers of **Table 3**	73 ± 17[c]
4	PES 10 kDa	A-4F buffer + 0.1 mM CTAB	350 µm	FOC1 DF0.5 CF1	P(ATAEC-X)$_{76}$ (expt 1 in **Table 3**)	44
5	PES 10 kDa	A-4F buffer + 0.1 mM CTAB	350 µm	FOC1 DF0.5 CF2	P(ATAEC-X)$_{76}$ (expt 1 in **Table 3**)	50
6	Regenerated cellulose 10 kDa	10 mM NaCl	490 µm	Elution	P(ATAEC-X)$_{14}$ (expt 4 in **Table 3**)	35

[a] A-4F buffer: 0.076 M Na_2HPO_4/0.096 M $NaNO_3$/0.004 M NaH_2PO_4/0.002 M NaN_3; [b] FOC: Focus flow, DF: Detector Flow and CF: Cross-flow, the number after corresponding to the flow rate in mL.min^{-1}; [c] Average value of the percentages of mass recovery obtained for the different injected samples; $(dn/dc)_{P(AETAC\text{-}X)n}$ = 0.137 mL.g^{-1}.

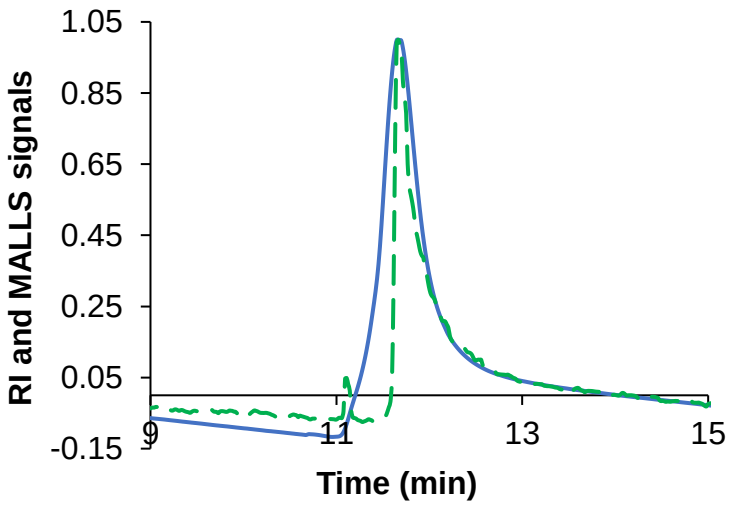

Figure 18. A-4F fractogram (Full line: RI signal; Dashed line: MALLS signal) of P(AETAC-X)$_{14}$ polymer (expt 4 in **Table 3**) at 5 mg.mL^{-1} in A-4F buffer (Analysis conditions 1 in **Table 8**).

The obtained fractogram is displayed in **Figure 18** and a $M_{n,\,MALLS}$ value of 7400 g.mol^{-1} was calculated. This value is in similar range than the experimental molar mass obtained from UV-

visible analysis ($M_{n,\,UV}$ = 9300 g.mol^{-1}) but higher than the theoretical one ($M_{n,\,theo}$ = 2850 g.mol^{-1}) and lower than the molar mass obtained from A-4F analysis performed in water with 5 × 10^{-3} M of NaN_3 salts ($M_{n,\,A\text{-}4F,\,MALLS}$ = 17160 g.mol^{-1}). However, this A-4F result should be carefully taken into account as only 9 % of the polymer was fractioned and analyzed (9 % of mass recovery). In addition, the polymer signal could be detected in three blank samples injected after the polymer analysis, revealing a possible interaction between the analyte and the membrane. Indeed, the most important limitation for the characterization of cationic samples by A-4F is adsorption onto the membrane, which acts as accumulation wall.[33, 41] The sample can interact with the membrane by means of electrostatic and/or hydrophobic interactions. Various parameters can influence these interactions: the chemical nature of the membrane, of the eluent (pH, ionic strength, nature of the salts, presence of surfactants), the hydrophilic/hydrophobic balances of the sample and the membrane, among many others. For example, membranes based on regenerated cellulose present a pKa around 3.4. Therefore, they are negatively charged at neutral pH and attractive interactions between polycation analyte and membrane are enhanced.[33] These electrostatic interactions can thus be reduced by using eluents with acidic pH or by adding surfactants and/or increasing the ionic strength to screen the charges. [33, 37, 41] Even if neutral poly(ether sulfone) membranes are used in this study, the presence of hydrophobic interactions between the sample and the membrane can explain the low percentage of mass recovery. Moreover, it has been shown that PES membrane can also interact selectively with salts, leading to a formation of a salt layer adsorbed onto the membrane surface, conferring either a cationic or anionic surface zeta potential to the membrane.[42, 43]

In this study, we attempted to add a cationic surfactant (CTAB) to the eluent to limit the interactions of the cationic P(AETAC-X) polymers with the membrane. The added concentration of the surfactant should be kept below its critical micellar concentration (CMC) to prevent the formation of micelles which can generate unwanted population of eluting species that may interfere with the detection of similar size analytes.[37] As the CMC of CTAB in water is equal to 1 mM at 25°C,[44] we chose to work with a CTAB concentration of 0.1 mM.

For the first test conducted with P(AETAC-X)$_{14}$ polymer (expt 4 in **Table 3**) with A-4F solvent supplemented with CTAB (analysis condition 2, **Table 8**), a 51 % mass recovery was reached, which confirms that the use of CTAB allows to reduce the interactions between the sample and the membrane, without suppressing it completely. For this experiment, the fractogram presented a bimodal distribution (**Figure 19**). The detection wavelength of the UV-Visible

detector was set to λ = 355 nm, which corresponds to the characteristic absorption wavelength of the xanthate agent. Since CTAB does not absorb the light at such wavelength, the presence of the UV signal in the fractogram can only be related to the presence of the polymer dithiocarbonate chain-end (**Figure 19**). As the UV signal is present on both peaks of the fractogram, these peaks can be ascribed to polymer signal. Due to the overlaps of the peaks, the determination of the molar mass integrating each peak was tough. The narrow peak observed at low elution volume was absent from the A-4F fractograms obtained either in pure water or A-4F solvent and presents high molar masses. This peak might be due to some interactions between the sample and the surfactant.

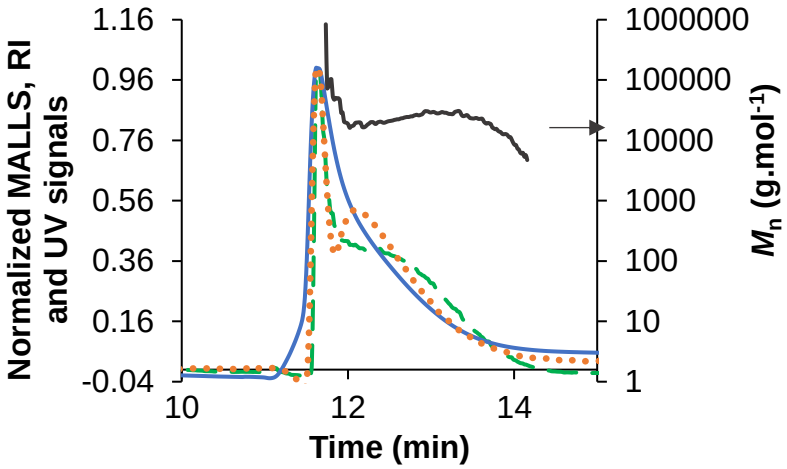

Figure 19. A-4F fractogram (Full line: RI signal; Dashed line: MALLS signal, Dotted line: UV-Visible signal at λ = 355 nm) and evolution of M_n with elution time (Full line) of P(AETAC-X)$_{14}$ polymer (expt 4 in **Table 3**) at 5 mg.mL^{-1} in A-4F buffer + 0.1 mM CTAB (Analysis conditions 2 in **Table 8**).

In A-4F technique, the thickness of the spacer can influence the fractionation and elution processes by controlling the parabolic profile velocity in the channel (an increase of the thickness provokes an increase of the sample residence time in the channel).[37] We attempted to increase the spacer thickness (analysis condition 3, **Table 8**) in order to separate the two peaks observed in **Figure 19**. This strategy was not conclusive as, for all the polymers, the two peaks were still overlapping in the fractograms (**Figure 20**), preventing an accurate determination of the number-average molar masses.

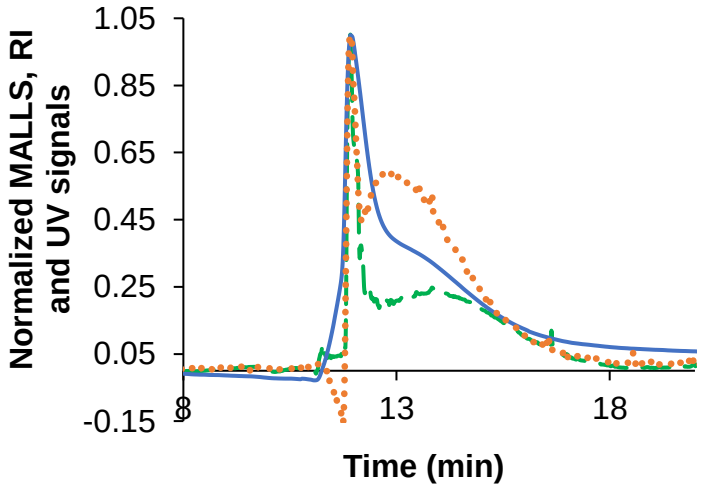

Figure 20. A-4F fractogram (Full line: RI signal; Dashed line: MALLS signal, Dotted line: UV-Visible signal at λ = 355 nm) of P(AETAC-X)$_{14}$ polymer (expt 4 in **Table 3**) at 5 mg.mL^{-1} in A-4F buffer + 0.1 mM CTAB (Analysis conditions 3 in **Table 8**).

The elution and separation processes are also dependent on the applied flow rates, and especially, the cross-flow rate. Due to pressure limitations imparted by the use of a membrane with a molecular-weight cut-off of 1 kDa, a membrane with larger cut-off (10 kDa) was used in order to assess the effect of the flow rates on the separation process (Analysis conditions 4-5 in **Table 8**). Tests were conducted with the polymer of higher theoretical degree of polymerization (P(AETAC-X)$_{76}$, expt 1 in **Table 3**). By simply changing the molecular weight cut-off of the membrane (Analysis conditions 4 in **Table 8**), same allure of the fractogram was obtained as those obtained in the same conditions but with the 1 kDa membrane (*i.e.*, two peaks). An increase of the cross-flow rate (FC2, analysis conditions 5 in **Table 8**) led to a non-fractionation of the samples, *i.e.*, all the analyte was eluted when the flows were turned off at the end of the analysis (**Figure 21**).

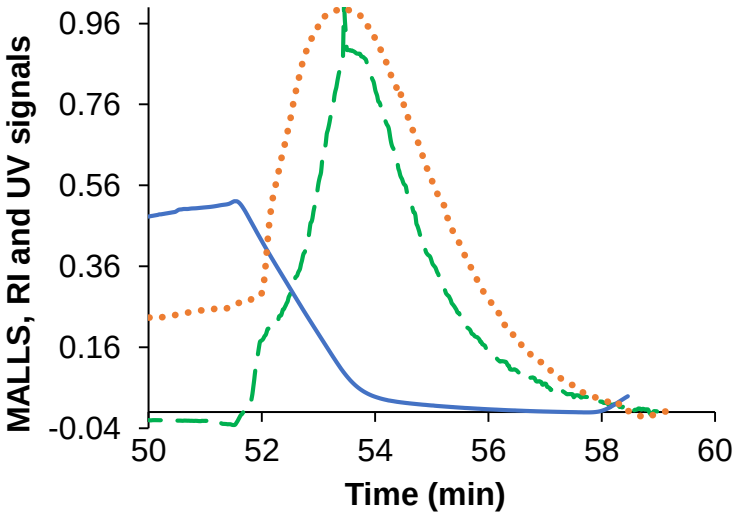

Figure 21. A-4F fractogram (Full line: RI signal; Dashed line: MALLS signal, Dotted line: UV-Visible signal at λ = 355 nm) of P(AETAC-X)$_{76}$ polymer (expt 1 in **Table 3**) at 5 mg.mL^{-1} in A-4F buffer + 0.1 mM CTAB (Analysis conditions 5 in **Table 8**).

For the analysis of cationic polymers by A-4F, strong attractive electrostatic interactions between the membrane and the analyte can be useful as it leads to the adsorption of a polymer layer onto the surface of the membrane, and thus to a passivation of the membrane. Indeed, the positive charge density confered to the membrane by the adsorbed polymer layer will increase the repulsive forces between analytes and membrane during further injections and so might prevent additional adsorption.[27, 33] Therefore, we decided to elute P(AETAC-X)$_{14}$ polymer through a negatively charged regenerated cellulose membrane (pKa = 3.4), in an attempt to promote attractive interactions between the cationic polymer and the membrane. For this study, an aqueous solution containing 10 mM of NaCl salts was used as eluent (Analysis conditions 6 in **Table 8**). However, the polymer signal could be detected in five blank samples (eluent) injected after the polymer elution, revealing an unsuccessful complete passivation of the membrane. Nevertheless, the presence of P(AETAC-X) in blank samples is sign of polymer adsorption phenomena, preventing an accurate analysis of the complete cationic P(AETAC-X) sample with the chosen eluent.

As a conclusion of this part, water with 5×10^{-3} mol.L^{-1} of NaN_3 salts appears to be the most suitable eluent for the characterization of P(AETAC-X) polymers by A-4F, allowing a good fractionation of the analyte while obtaining high percentages of mass recovery. Schubert *et al.* have shown that, for the A-4F analysis of different cationic polymers using a regenerated cellulose membrane, water containing 0.02 % NaN_3 was also the best eluent among those tested.[33] However, in the present work, the $M_{n,\,A\text{-}4F,\,MALLS}$ of the P(AETAC-X) polymers are ten times greater than the theoretical M_n and experimental M_n calculated from UV-Visible spectroscopy, questioning about the presence of polymer aggregates in aqueous eluent with low salt concentration.

The different attempts to characterize P(AETAC-X) polymers in A-4F eluent with higher salt concentration (0.18 M) revealed that the characterization of these cationic polymers by A-4F technique is not straightforward. It should require a deep optimization of the analysis conditions, in terms of eluent, membrane, set-up of the equipment, among other parameters to consider. Such optimization falls out of the scope of this thesis and should be considered as a perspective.

As polyelectrolytes exhibit complex behavior in aqueous solutions, a way to overcome this problem could be to transpose their characterization to organic solvent. On the basis of previous studies on poly(ionic liquids),[45] we attempted to favor a counter-anion exchange of P(AETAC-X)$_{13}$ polymer, using a weakly coordinating anion (bis(trifluoromethylsulfonyl) imide Tf_2N^-), in order to lead to THF soluble polymer. This experiment was performed in collaboration with Karlsruhe Institute of technology, Germany. The occurrence of counter-anion exchange should be carefully monitored by electrospray ionization mass spectrometry (ESI-MS).[45] However, the P(AETAC-X) polymer could not be analyzed by ESI-MS, probably due to the high M_n of the sample. Counter-anion exchange can also be carried out using a negatively charged surfactant as for instance, sodium dodecylbenzenesulfonate (SDBS),[46] to transpose a polycation into an organic solvent via the introduction of alkyl chains. This strategy is under current investigation at IPREM, Pau. We preliminary observed that the counter-anion exchange between P(AETAC-X)$_{13}$ and SDBS induces a precipitation of the P(AETAC-X)$_{13}$-SDBS in water. However, SLS analysis might be difficult due to the very low value of dn/dc measured in DMSO ($(dn/dc)_{P(AETAC\text{-}X)\text{-}SDBS}$ = 0.02 mL.g^{-1}).

IV. Conclusions

Poly[2-(acryloyloxy)ethyl]trimethylammonium chloride (PAETAC) cationic polymers were synthesized by RAFT/MADIX polymerization in a mixture of water:ethanol, using *O*-ethyl-*S*-(1-ethoxycarbonyl)ethyldithiocarbonate as chain-transfer agent (CTA). After setting the optimal $[CTA]_0/[Initiator]_0$ ratio, various experiments were conducted to synthesize a series of polymers with different targeted degrees of polymerization by means of varying the initial $[Monomer]_0/[CTA]_0$ ratio. As a sake of comparison, a polymer was also synthesized by free-radical polymerization, in the absence of xanthate agent. For all the experiments, monomer conversions above 60 % were reached after 6 hours of polymerization.

The synthesized polymers were characterized by UV-visible spectroscopy. Comparison of the UV-visible spectra of the polymers synthesized by RAFT/MADIX polymerization and the polymer synthesized by free-radical polymerization confirmed the presence of the dithiocarbonate functional group at the polymer chain-end for the polymers synthesized by RAFT/MADIX polymerization. The reactive extremity of the polymer with a theoretical degree of polymerization equals to 76 ($P(AETAC\text{-}X)_{76}$) was cleaved by using a 20 excess of initiator to highlight the decrease of the characteristic absorbance band of the xanthate chain-end. The number-average molar mass (M_n) of the P(AETAC-X) cationic polymers were calculated from the UV-visible spectra of polymers. The $M_{n,\,UV}$ of the polymers were in a similar range than the theoretical M_n, in accordance with a high degree of living chains with xanthate chain-end.

$P(AETAC\text{-}X)_{76}$ was characterized by size exclusion chromatography (SEC). High experimental M_n values together with gyration radius of 50 nm and abnormal elution traduced significant aggregation of the polymer in the SEC conditions. The concentration-dependence of aggregation via intermolecular interaction was highlighted by dynamic light scattering performed in aqueous solution with 0.1-0.18 M of salt concentration.

The characterization of P(AETAC-X) polymers by asymmetric flow field-flow fractionation was conducted in various analysis conditions. This study revealed the challenging characterization of the P(AETAC-X) cationic polymers by A-4F technique due to polymer-membrane interaction. Among the different conditions tested in the present work, a poly(ether sulfone) 5 kDa membrane and water with 5×10^{-3} mol.L^{-1} of NaN_3 salts as eluent appeared to be the most suitable conditions for the characterization of P(AETAC-X) polymers by A-4F, allowing for a good fractionation of the analyte while obtaining high percentages of mass recovery. The decreasing values of $M_{n,\,A\text{-}4F,\,MALLS,\,0.005\ M\ NaN3}$ with increasing initial

concentration of xanthate chain transfer agent, together with dispersity values below 1.4, both attest a certain control of the xanthate-mediated RAFT polymerization of the cationic AETAC monomer. However, the values of $M_{n,\ A\text{-}4F,\ MALLS}$ were ten times higher than the theoretical M_n and a high number of xanthate per analyzed chains was revealed by UV-visible spectrosocpy. This gap is most probably ascribed to the presence of aggregates.

The characterization of the P(AETAC-X) cationic polymers is still a challenge due to their complex behavior in aqueous solution. Therefore, an accurate determination of the molar masses of the synthesized P(AETAC-X) polymers requires further investigations. In conclusion of this chapter, xanthate end-functionalized cationic P(AETAC-X) polymers with varying M_n were successfully synthesized by RAFT/MADIX to act as reactive hydrophilic stabilizer for VCL emulsion polymerization that will be investigated in Chapter 2.

V. References

1. Ramos, J.; Forcada, J.; Hidalgo-Alvarez, R. *Chemical reviews* **2014,** 114, (1), 367-428.
2. Tabujew, I.; Peneva, K., CHAPTER 1 Functionalization of Cationic Polymers for Drug Delivery Applications. In *Cationic Polymers in Regenerative Medicine*, The Royal Society of Chemistry: 2015; pp 1-29.
3. Truong, N. P.; Jia, Z.; Burges, M.; McMillan, N. A.; Monteiro, M. J. *Biomacromolecules* **2011,** 12, (5), 1876-82.
4. Zhao, W.; Fonsny, P.; FitzGerald, P.; Warr, G. G.; Perrier, S. *Polymer Chemistry* **2013,** 4, (6), 2140.
5. Tamura, A.; Oishi, M.; Nagasaki, Y. *Journal of controlled release : official journal of the Controlled Release Society* **2010,** 146, (3), 378-87.
6. Kenawy el, R.; Worley, S. D.; Broughton, R. *Biomacromolecules* **2007,** 8, (5), 1359-84.
7. Fischer, D.; Li, Y.; Ahlemeyer, B.; Krieglstein, J.; Kissel, T. *Biomaterials* **2003,** 24, (7), 1121-1131.
8. Cai, J.; Yue, Y.; Rui, D.; Zhang, Y.; Liu, S.; Wu, C. *Macromolecules* **2011,** 44, (7), 2050-2057.
9. Xu, F. J.; Yang, W. T. *Progress in Polymer Science* **2011,** 36, (9), 1099-1131.
10. Ahmed, M.; Narain, R. *Progress in Polymer Science* **2013,** 38, (5), 767-790.
11. Lowe, A. B.; McCormick, C. L. *Progress in Polymer Science* **2007,** 32, (3), 283-351.
12. Bütün, V.; Armes, S. P.; Billingham, N. C. *Macromolecules* **2001,** 34, (5), 1148-1159.
13. Save, M.; Manguian, M.; Chassenieux, C.; Charleux, B. *Macromolecules* **2005,** 38, 280-289.
14. Mitsukami, Y.; Donovan, M. S.; Lowe, A. B.; McCormick, C. L. *Macromolecules* **2001,** 34, (7), 2248-2256.
15. Yusa, S.-i.; Konishi, Y.; Mitsukami, Y.; Yamamoto, T.; Morishima, Y. *Polymer Journal* **2005,** 37, (7), 480-488.
16. Yusa, S.-i.; Yokoyama, Y.; Morishima, Y. *Macromolecules* **2009,** 42, (1), 376-383.
17. Haladjova, E.; Mountrichas, G.; Pispas, S.; Rangelov, S. *The journal of physical chemistry. B* **2016,** 120, (9), 2586-95.

18. Williams, M.; Penfold, N. J. W.; Lovett, J. R.; Warren, N. J.; Douglas, C. W. I.; Doroshenko, N.; Verstraete, P.; Smets, J.; Armes, S. P. *Polym. Chem.* **2016,** 7, (23), 3864-3873.
19. Semsarilar, M.; Ladmiral, V.; Blanazs, A.; Armes, S. P. *Langmuir : the ACS journal of surfaces and colloids* **2013,** 29, (24), 7416-24.
20. Chai, W.; Zhang, Y.; Hou, Y. *Polym. Chem.* **2013,** 4, (4), 1006-1013.
21. Moad, G.; Rizzardo, E.; Thang, S. H. *Australian Journal of Chemistry* **2005,** 58, (6), 379.
22. Beija, M.; Palleau, E.; Sistach, S.; Zhao, X.; Ressier, L.; Mingotaud, C.; Destarac, M.; Marty, J.-D. *Journal of Materials Chemistry* **2010,** 20, (42), 9433.
23. Guinaudeau, A.; Coutelier, O.; Sandeau, A.; Mazières, S.; Nguyen Thi, H. D.; Le Drogo, V.; Wilson, D. J.; Destarac, M. *Macromolecules* **2014,** 47, (1), 41-50.
24. Destarac, M.; Guinaudeau, A.; Geagea, R.; Mazieres, S.; Van Gramberen, E.; Boutin, C.; Chadel, S.; Wilson, J. *Journal of Polymer Science Part A: Polymer Chemistry* **2010,** 48, (22), 5163-5171.
25. Moad, G.; Rizzardo, E.; Thang, S. H. *Australian Journal of Chemistry* **2012,** 65, (8), 985.
26. Perrier, S.; Takolpuckdee, P.; Mars, C. A. *Macromolecules* **2005,** 38, (6), 2033-2036.
27. Plamper, F. A.; Schmalz, A.; Penott-Chang, E.; Drechsler, M.; Jusufi, A.; Ballauff, M.; Müller, A. H. E. *Macromolecules* **2007,** 40, (16), 5689-5697.
28. Taton, D.; Destarac, M.; Zard, S. Z., Macromolecular Design by Interchange of Xanthates: Background, Design, Scope and Applications. In *Handbook of RAFT Polymerization*, Wiley-VCH Verlag GmbH & Co. KGaA: 2008; pp 373-421.
29. Favier, A.; Barner-Kowollik, C.; Davis, T. P.; Stenzel, M. H. *Macromolecular Chemistry and Physics* **2004,** 205, (7), 925-936.
30. Brandrup, J.; Immergut, E. H.; Grulke, E. A., *Polymer Hanbook, 4th Edition*. 2003; p 2336.
31. Carlsson, L.; Fall, A.; Chaduc, I.; Wågberg, L.; Charleux, B.; Malmström, E.; D'Agosto, F.; Lansalot, M.; Carlmark, A. *Polym. Chem.* **2014,** 5, (20), 6076-6086.
32. Locock, K. E.; Meagher, L.; Haeussler, M. *Analytical chemistry* **2014,** 86, (4), 2131-7.
33. Wagner, M.; Pietsch, C.; Tauhardt, L.; Schallon, A.; Schubert, U. S. *Journal of chromatography. A* **2014,** 1325, 195-203.
34. Förster, S.; Schmidt, M.; Antonietti, M. *Polymer* **1990,** 31, (5), 781-792.
35. Podzimek, S. *Macromolecular Symposia* **2013,** 330, (1), 81-91.
36. Guillaneuf, Y.; Castignolles, P. *Journal of Polymer Science Part A: Polymer Chemistry* **2008,** 46, (3), 897-911.
37. Gigault, J.; Pettibone, J. M.; Schmitt, C.; Hackley, V. A. *Analytica chimica acta* **2014,** 809, 9-24.
38. Podzimek, S.; Machotova, J.; Snuparek, J.; Vecera, M.; Prokupek, L. *Journal of Applied Polymer Science* **2014,** 131, (21), n/a-n/a.
39. Johnson, C. S. *Progress in Nuclear Magnetic Resonance Spectroscopy* **1999,** 34, 203-256.
40. Farcet, C.; Belleney, J.; Charleux, B.; Pirri, R. *Macromolecules* **2002,** 35, (13), 4912-4918.
41. Wagner, M.; Pietsch, C.; Kerth, A.; Traeger, A.; Schubert, U. S. *Journal of Polymer Science Part A: Polymer Chemistry* **2015,** 53, (7), 924-935.
42. Ernst, M.; Bismarck, A.; Springer, J.; Jekel, M. *Journal of Membrane Science* **2000,** 165, (2), 251-259.
43. Salgin, S.; Salgin, U.; Soyer, N. *International Journal of Electrochemical Science* **2013,** 8, 4073-4084.
44. Javadian, S.; Ruhi, V.; Heydari, A.; Asadzadeh Shahir, A.; Yousefi, A.; Akbari, J. *Industrial & Engineering Chemistry Research* **2013,** 52, (12), 4517-4526.

45. Steinkoenig, J.; Cecchini, M. M.; Goldmann, A. S.; Reale, S.; Angelis, F.; Barner-Kowollik, C. *Macromolecular rapid communications* **2016,** 37, (20), 1662-1666.
46. García-Valdez, O.; George, S.; Champagne-Hartley, R.; Saldívar-Guerra, E.; Champagne, P.; Cunningham, M. F. *Polymer* **2015,** 67, 139-147.

Acknowledgments

MALDI-TOF analyses were performed either at Polymat Institute, San Sebastian in collaboration with Dr. Antonio Veloso or at ISM-CESAMO, Bordeaux, in collaboration with Dr. Christelle Absalon. SEC analyses were performed in IMP, INSA/Université Claude Bernard, Lyon 1 in collaboration with Dr. Catherine Ladavière and Agnès Crepet. Dr. Amaia Agirre and Dr. Miren Aguirre are thanked for performing A-4F analyses in Polymat Institute, San Sebastian. We are grateful to Dr. Aurora Mejia, Laurent Rodriguez and Prof. Bruno Grassl for their support in A-4F analysis at IPREM-ECABIE, Pau and for fruitful discussions. Dr. Abdel Khoukh is thanked for DOSY-NMR analyses carried out at IPREM-EPCP, Pau. Dr. Anja Goldmann and Jan Steinkoenig (KIT, Karlsruhe, Germany) are acknowledged for test of electrospray ionization mass spectrometry analysis after counter-ion exchange. Dr. Elise Deniau (IPREM-Pau) is thanked for SLS analysis of P(AETAC-X)$_{13}$-SDBS and determination of refractive index increment. Prof. Petr Stepanek from the Institute of Macromolecular Chemistry, Supramolecular polymer systems Department (Prague, Czech Republic) is sincerely acknowledged for giving us the opportunity to the refractometer facility for dn/dc measurements.

PART II - CHAPTER 2. Cationic thermoresponsive Poly(*N*-vinylcaprolactam)-based microgels synthesized by surfactant free emulsion polymerization by using a reactive cationic macromolecular chain-transfer agent

I. Introduction

Stimuli responsive polymers are defined as polymers that undergo physical or chemical changes in response to small external changes in the environmental conditions. The external stimulus are the temperature, electric or magnetic field, light, pH, ionic strength, specific molecules or enzymes, among others.[1, 2] These polymers have received considerable attention within the last decade, due to their wide range of applications, especially in the biomedical field where they can be envisaged as potential drug delivery systems or biosensors.[3-5] For such applications, stimuli-responsive microgels, *i.e.*, crosslinked polymer particles able to swell in a good solvent and prevented from dissolution by cross-linking, are very promising candidates.[6-13] Special attention have been dedicated to thermoresponsive microgels that display a Volume Phase Transition Temperature (VPTT) in water, *i.e.*, microgels that undergo a transition from a swollen to a collapsed state by increasing the temperature.[13-17]

Among the different thermoresponsive polymers available for the design of microgels, poly(*N*-vinylcaprolactam) (PVCL) appears to be a promising candidate because of its biocompatibility and its lower critical solution temperature of 32°C-38°C, near to physiological temperature.[18, 19] Therefore, the synthesis of PVCL-based microgels has been attracting a growing interest within the last years.[20-37]

As mentioned in the introduction of Part II, the design of cationic thermoresponsive microgels appears to be very attractive for bio-applications. Indeed, cationic particles are able to interact with negatively charged biomolecules or surfaces of interest.[13] Cationic PVCL-based thermosensitive microgels can be prepared by: 1) the use of either positively charged initiator or surfactant during the synthesis procedure,[23, 27, 33, 38] or 2) copolymerization of the main monomer with cationic co-monomers.[39-42] Concerning the first strategy, the low amount of surfactant used (as the use of surfactant can be problematic for biomedical applications) and/or the low content of cationic charges conferred by the initiator fragments both induce sufficient stabilization only at low solids content (< 2-5 wt-%). With regard to the second strategy, the introduction of cationic moieties into PVCL-based microgels leads to a shift of the volume phase transition temperature towards higher value.[41, 43] Moreover, the amount of co-monomer and its distribution inside the network are parameters that play an important role in microgel swelling.[44] Therefore, they should be carefully considered when designing cationic thermoresponsive microgels by copolymerization with a cationic co-monomer.

In the recent years, increasing attention has been focused on the use of reactive macromolecular stabilizers (macromolecular chain transfer agent or macroalkoxyamine) to synthesize thermoresponsive microgels by polymerization in aqueous dispersed-media.[45-53] In such approach, the emulsion or precipitation polymerization is carried out in the absence of molecular surfactants while enabling the increase of solids content of the final dispersion.[48] Moreover, using a hydrophilic polymer acting as both stabilizer and macromolecular control agent is a straightforward way to synthesize core/shell particles with functional macromolecular shell. In the context of designing cationic thermoresponsive microgels, the use of cationic macromolecular stabilizer is expected to produce cationic core-shell microgels with a constant VPTT of the inner PVCL thermoresponsive network.

In the present work, we focused our attention on the synthesis of stable PVCL-based thermoresponsive microgels by batch emulsion polymerization of *N*-vinylcaprolactam by using the reactive cationic macromolecular stabilizers synthesized by RAFT/MADIX polymerization described in Chapter 1 – Part II (**Scheme 1**). The influence of different synthesis variables (*i.e*, the concentrations of monomer, stabilizer, crosslinker and initiator) on the features of the microgel particles is thoroughly investigated. The inner morphology of the microgels is assessed by high-resolution ^{1}H transverse relaxation NMR measurements. Finally, the stabilization efficiency of the reactive cationic stabilizers is compared with the one of either non-reactive polymeric stabilizers or a conventional cationic molecular surfactant (cetyltrimethylammonium bromide).

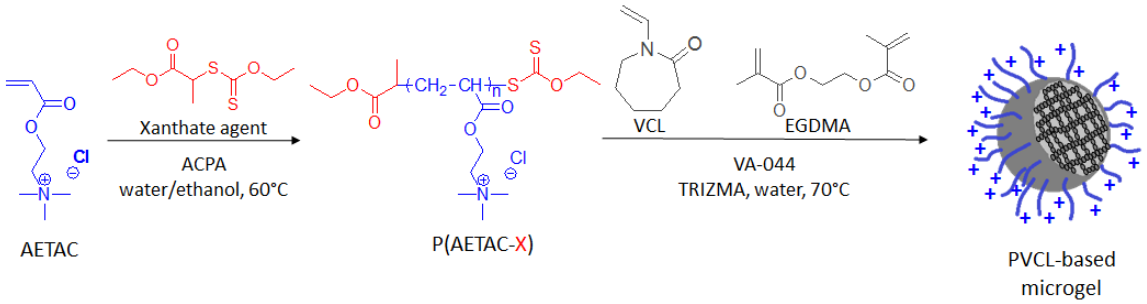

Scheme 1. RAFT/MADIX polymerization of AETAC to synthesize the reactive cationic polymers (P(AETAC-X)) used as reactive stabilizers for the synthesis of thermoresponsive PVCL-based microgel by emulsion polymerization.

II. Experimental section

1. Materials

N-Vinylcaprolactam (VCL, Sigma Aldrich, 98%), ethylene glycol dimethacrylate (EGDMA, Sigma Aldrich, 98%), potassium persulfate (KPS, Sigma Aldrich, 99%), sodium bicarbonate ($NaHCO_3$, Sigma-Aldrich, 99.7%), 2,2'-Azobis[2-(2-imidazolin-2-yl)propane] dihydrochloride (ADIBA or VA-044, Wako, 99%), cetyltrimethylammonium bromide (CTAB, Sigma Aldrich, 99%), tris(hydroxymethyl)aminomethane hydrochloride (TRIZMA, Sigma Aldrich, 99%) and 1,3,5-trioxane (Sigma Aldrich, 99%) were used as received. Different cationic buffers were used to control the pH for electrophoretic mobility measurements (all of them obtained from Sigma-Aldrich): glycine (pH 3), bis(2-hydroxyethyl)amino-tris(hydroxymethyl)methane (BIS-TRIS base, pH 6-7) and TRIZMA-HCl (pH 7-9). All the buffers were prepared at ionic strength of 1 mM. Glycine buffer was also prepared at ionic strength of 10 mM. Double deionized (DDI) water was used throughout the work.

2. Cationic reactive macromolecular stabilizers

A series of three reactive cationic P(AETAC-X)$_n$ with varying degree of polymerization (*n*) (**Table 1**) which synthesis is presented in Chapter 1 - Part II of the manuscript were used as reactive stabilizers for the subsequent synthesis of PVCL-based microgels by emulsion polymerization. Apart from this series, two non-reactive cationic polymers were prepared, either by free-radical polymerization (P(AETAC)) or by cleavage of a xanthate-functionalized polymer (P(AETAC-X)$_{76,\ cleaved}$) in order to compare their stabilization efficiency with the reactive P(AETAC-X)$_n$ polymers.

Table 1. Reactive cationic polymers and non-reactive cationic polymers used as stabilizers for the batch emulsion polymerization of VCL (see Chapter 1 of Part II).

Expt	Polymer
1	P(AETAC-X)$_9$
2	P(AETAC-X)$_{16\ (2)}$
3	P(AETAC-X)$_{76}$
4	P(AETAC)
5	P(AETAC-X)$_{76,\ cleaved}$

3. Synthesis of PVCL-based microgels

Microgels were synthesized by batch emulsion polymerization. For the synthesis of microgel particles stabilized by P(AETAC-X) (SC1-PX_{76} 4-E4 in **Table 2**), 2 g of VCL (1.4×10^{-2} mol), 0.08 g of $P(AETAC\text{-}X)_{76}$ (4 wt-% with respect to monomer), 0.06 g of TRIZMA buffer (3.7×10^{-4} mol), 0.13 g of 1,3,5-trioxane (1.4×10^{-3} mol) and 0.08 g of EGDMA (4.2×10^{-4} mol, 4 wt-% with respect to VCL) were dissolved in 190 g of DDI water and placed into a 250 mL jacketed reactor, fitted with a reflux condenser, stainless steel stirrer, sample device, and nitrogen inlet tube reactor. The reaction mixture was purged with nitrogen for 30 min at room temperature and then for other 30 min during heating from 25 °C to 70 °C, at a stirring rate of 300 rpm. The cationic initiator was added under nitrogen flow at 70°C (0.02 g of ADIBA dissolved in 10 g of DDI water, 1 wt-% with respect to VCL, 6.5×10^{-5} mol of ADIBA). The polymerization reaction was then allowed to continue with stirring for 4 h under nitrogen flow at 70°C. The reaction mixture was subsequently cooled to 25°C. The same procedure was applied for all the syntheses of PVCL-based microgels presented in this work.

The initial solids content τ is calculated as follows: $\tau = (m_{VCL}/m_{water})_0 \times 100$.

Table 2. Experimental conditions for the batch emulsion polymerization of VCL performed at 70°C, using 1 wt-% of ADIBA initiator based on VCL and 3 wt-% of TRIZMA buffer based on VCL.[a] Reaction variables: initial solids content, weight fraction of the cationic polymeric stabilizer and its degree of polymerization and weight fraction of EGDMA crosslinker.

Stabilizer	τ *wt-%*	**Stabilizer** *wt-% VCL*	**EGDMA** *wt-% VCL*	**Reaction**[b]
$P(AETAC\text{-}X)_{76}$	1	4	4	SC1-PX_{76} 4-E4
$P(AETAC\text{-}X)_{76}$	5	4	4	SC5-PX_{76} 4-E4
$P(AETAC\text{-}X)_{76}$	10	4	4	SC10-PX_{76} 4-E4
$P(AETAC\text{-}X)_{76}$	1	4	8	SC1-PX_{76} 4-E8
$P(AETAC\text{-}X)_{76}$	1	8	4	SC1-PX_{76} 8-E4
$P(AETAC\text{-}X)_{76}$	5	8	4	SC5-PX_{76} 8-E4
$P(AETAC\text{-}X)_{76}$	1	8	8	SC1-PX_{76} 8-E8
$P(AETAC\text{-}X)_{16}$	1	4	4	SC1-PX_{16} 4-E4
$P(AETAC\text{-}X)_{16}$	1	12	4	SC1-PX_{16} 12-E4
$P(AETAC\text{-}X)_{9}$	1	4	4	SC1-PX_{9} 4-E4
$P(AETAC\text{-}X)_{9}$	5	4	4	SC5-PX_{9} 4-E4

[a] Reaction conditions: rpm = 300, reaction time = 4 h; [b] Reaction name: SC for initial solids content, the number following indicates the wt-% of VCL based on water - PX_n: reactive cationic polymeric stabilizer with *n* the degree of polymerization, the number following indicates the wt-% of stabilizer based on VCL - E: EGDMA crosslinker, the number following indicates the wt-% of EGDMA based on VCL.

4. Characterizations of polymers and colloids

Proton nuclear magnetic resonance spectroscopy (^{1}H NMR) spectra of the crude samples were recorded on a Bruker 400 MHz spectrometer at 25°C, in a mixture of D_2O/H_2O. ^{1}H transverse relaxation (T_2) NMR measurements were carried out on a Bruker Avance 500 NMR spectrometer, using an already described protocol.[33, 54, 55] For these measurements, dialyzed microgel particles were centrifuged, freeze-dried and redispersed at 2 wt-% of solids content in deuterated water. For all measurements, the recycle delay time was 5 s and the dwell time was 10 µs. The decay of transverse magnetization relaxation was measured using the Hahn-echo pulse sequence: $90°_x$-*t*-$180°_x$-*t*-Hahn echo-(acquisition), where *t* is the echo time. Half of the Hahn echo decay was detected and Fourier transformed. The normalized integral intensity of various resonances was fitted by two-exponential decay functions using OriginPro8 program.

Diffusion ordered spectroscopy (DOSY) NMR measurements in D_2O of the dried supernatants recovered after one microgel centrifugation were performed using the bipolar longitudinal eddy current delay pulse sequence (BPLED). The spoil gradients were also applied at the diffusion period and the eddy current delay. Typically, a value of 2 ms was used for the gradient duration (δ), 150 ms for the diffusion time (Δ), and the gradient strength (g) was varied from 1.67 G.cm^{-1} to 31.88 G.cm^{-1} in 32 steps. Each parameter was chosen to obtain 95% signal attenuation for the slowest diffusion species at the last step experiment. The pulse repetition delay (including acquisition time) between each scan was larger than 2 s. Data acquisition and analysis were performed using the Bruker Topspin software (version 2.1). The T1/T2 analysis module of Topspin was used to calculate the diffusion coefficients and to create 2-D spectra with NMR chemical shifts along one dimension and the calculated diffusion coefficients along the other.

For the microgel synthesis, monomer conversion was calculated from nuclear magnetic resonance spectra of the crude sample dispersed in D_2O, using 1,3,5-trioxane as internal standard according to Equation 1.

$$x_{mono.} = 1 - \frac{\left(I_{^1H_{mono.}} / I_{^1H_{triox.}}\right)_t}{\left(I_{^1H_{mono.}} / I_{^1H_{triox.}}\right)_0} \quad \text{Equation 1}$$

$I_{1H,triox}$ corresponds to the integral of one proton of 1,3,5-trioxane (5.1 ppm, 6 H) used as internal standard and $I_{1H,mono}$ corresponds either to the integration of the signal of VCL monomer at 7.1 ppm or to the signal of EGDMA crosslinker at 6.2 ppm (**Figure 1**).

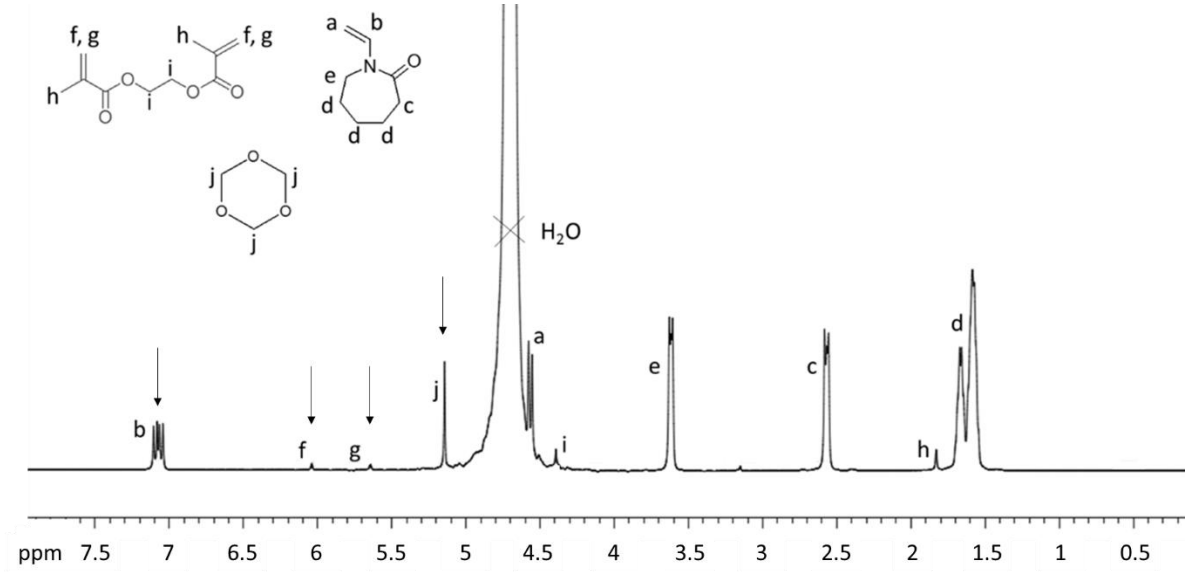

Figure 1. ^{1}H NMR spectrum in D_2O/H_2O solution of a mixture of VCL, EGDMA and 1,3,5-trioxane (5 wt-% of initial solids content, 4 wt-% of EGDMA based on VCL).

Prior to colloidal characterization, the final microgel particles were dialyzed against distilled water for one week to remove unreacted reagents and impurities (Spectra/Por, M_w cut-off: 12 000 – 14 000 Da).

The final average hydrodynamic diameters (D_h) of the microgels were measured by photon correlation spectroscopy (PCS) (or dynamic light scattering, DLS), using a Zetasizer Nano ZS instrument (Malvern Instruments). Measurements were carried out at a solids content of 0.005 wt-% from 10°C to 55°C, every to 2°C, except between 30 and 40°C where measurements were recorded each 1°C. Before each scan, the sample was maintained at the set temperature for 10 min. The hydrodynamic diameters reported in this chapter were measured before the dialysis step. Indeed, the average hydrodynamic diameters of the microgels measured before and after dialysis, as a function of the temperature are similar, as reported in **Figure 2**.

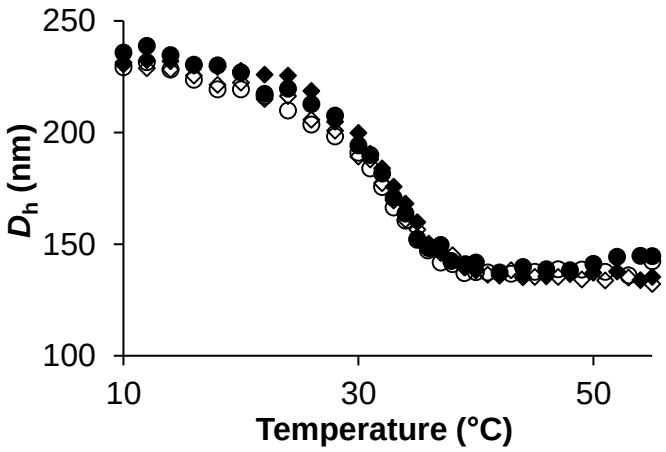

Figure 2. Effect of the dialysis on the evolution of the average hydrodynamic diameters as a function of the temperature for the experiment performed at 1wt-% of initial solids content, using 8wt-% of P(AETAC-X)$_{76}$ as stabilizer (SC1-PX$_{76}$ 8-E4 in **Table 2**): ● Non-dialyzed and ◆ Dialyzed samples; Full symbols: heating cycle, Open symbols: cooling cycle.

Regarding the determination of volume phase transition temperature (VPTT) values of the microgels, curves showing the evolution of the final hydrodynamic diameter as a function of the temperature are generally fitted using a Boltzmann function. The minimum of the fit first-order derivative is considered as the VPTT (**Figure 3**).

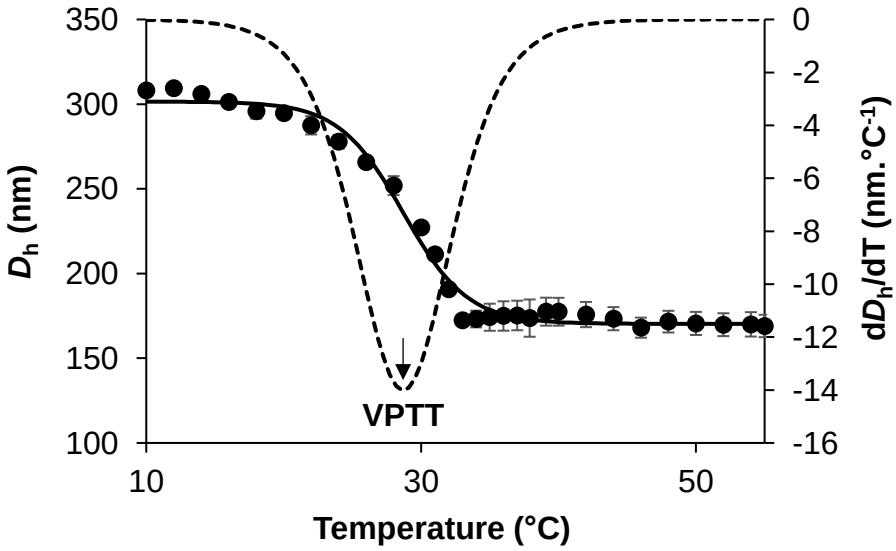

Figure 3. Hydrodynamic diameters and hydrodynamic diameter derivative versus temperature for the experiment performed at 1 wt-% of initial solids content and 4 wt-% of P(AETAC-X)$_{76}$ as stabilizer (SC1-PX$_{76}$ 4-E4 in **Table 2**): ● Experimental data, Full line: Boltzman Fit of the experimental data, Dotted line: Fit first-order derivative. The VPTT is determined as the minimum of the hydrodynamic diameter derivative, *i.e.*, as the temperature corresponding to the inflection point in the average hydrodynamic diameter as a function of temperature curves.

The swelling ratio Φ of the microgels was calculated following the expression: $\Phi = (D_{h,\ 10°C}/D_{h,\ 55°C})^3$ where $D_{h,\ 10°C}$ and $D_{h,\ 55°C}$ are respectively the average hydrodynamic diameters at 10°C (swollen state) and 55°C (collapsed state).

The average number of microgel particles per liter of latex (N_p, particles.L^{-1}_{latex}) was calculated from the microgel average hydrodynamic diameter at the temperature of the collapsed state ($D_{h,\ 55°C}$).

$$N_p = \frac{6 \times \tau}{\pi \times (D_{h,\ 55°C})^3 \times \rho_{PVCL}} \quad \text{Equation 2}$$

with τ: final solids content ($g.L^{-1}_{latex}$), ρ_{PVCL}[56] = 1.23 $g.cm^{-3}$, and $D_{h,55°C}$: microgel average hydrodynamic diameter at 55°C.

Microgel electrophoretic mobility was measured using a Zetasizer Nano ZS instrument (Malvern Instruments). Dialyzed samples were diluted at 0.05 wt-% in cationic buffer solution at different pH (3, 6, 9) and ionic strength of 1 or 10 mM. Each sample was subjected to ten measurements at 25°C, with a 60 s delay between each measurement.

Microgels were centrifuged for 3 h at 20 000 rpm, at 1 wt-% of solids content. Percentages of free-chains, *i.e.*, the contents of water-soluble polymers formed during the polymerization process were determined by gravimetry from the supernatants obtained after microgel centrifugation.

Transmission electron microscopy (TEM) was used for the direct observation of the microgel particles. Images of the centrifuged microgels were recorded on a JEOL JEM 100CXII equipment, at 100 kV. Microgel dispersions were deposited on a copper grid and dried before analyses.

III. Results and discussion

For all the experiments presented in this section, reproducibility was assessed performing each experiment twice.

1. Setting the experimental conditions for the synthesis of PVCL-based microgels

This part of the work was dedicated to the setting of the experimental conditions to determine the optimum experimental variables in terms of nature of initiator, buffer, temperature, concentration of initiator and wt-% of stabilizer based on VCL to synthesize stable PVCL-based microgels in the presence of the reactive cationic polymeric stabilizer.

1.i. Choice of the buffer and the initiator

Imaz *et al.*[57] previously showed that VCL monomer suffered hydrolysis in water due to the decrease of the pH of the reaction medium during polymerization initiated by potassium persulfate (KPS). This hydrolysis was evidenced by the presence of additional peaks corresponding to caprolactam and acetaldehyde compounds in the NMR spectrum of a sample withdrawn at the beginning of the reaction (at 7.5, 5.3, 3.3, 2.5, 1.3 ppm and 9.7, 2.3 ppm) and the disappearance of the signals corresponding to the vinylic protons of VCL. A mechanism of the hydrolysis of VCL under acidic conditions was proposed in this work, see **Scheme 2**. By adding the suitable concentration of $NaHCO_3$ buffer to the aqueous continuous phase, the hydrolysis of VCL was avoided as a constant pH of 7 was maintained all along the polymerization.[57]

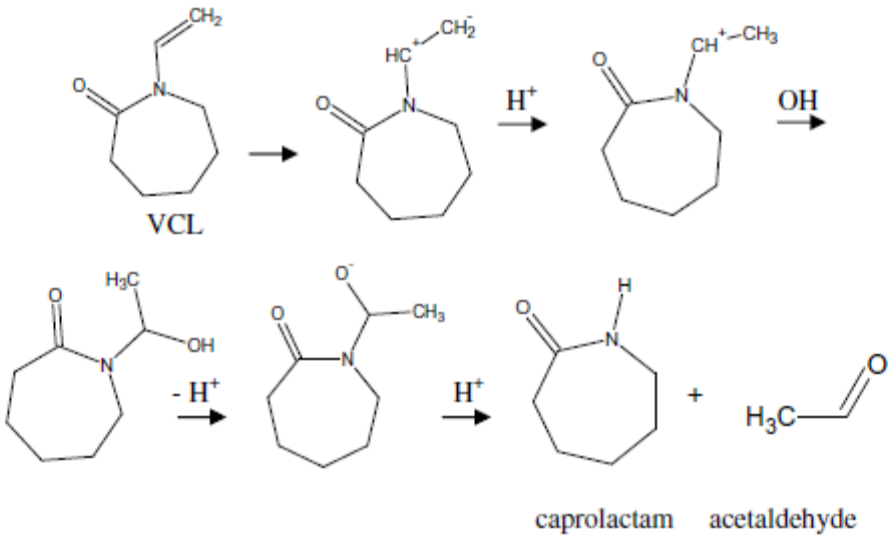

Scheme 2. Hydrolysis mechanism of VCL under acidic conditions (from reference 57).

In this context, the first step of this work consisted in setting the suitable buffer to prevent VCL hydrolysis under the chosen reaction conditions. All the reactions were performed at 1 wt-% of initial solids content, at a temperature of 70°C, using 4 wt-% of both $P(AETAC\text{-}X)_{76}$ reactive stabilizer and EGDMA crosslinker based on VCL and the ratio $[Initiator]_0/[VCL]_0$ was set to 4.4×10^{-3} (**Table 1**).

Table 3. Experimental conditions and results for the batch emulsion polymerizations of VCL carried out at 1 wt-% of initial solids content, at a temperature of 70°C, using 4 wt-% of both $P(AETAC\text{-}X)_{76}$ reactive stabilizer and EGDMA crosslinker based on VCL and a ratio $[Initiator]_0/[VCL]_0$ equals to 4.4×10^{-3}.[a] Reaction variables: type of initiator and buffer, ratio $[Buffer]_0/[Initiator]_0$.

Expt	Initiator	Buffer	$[Buffer]_0$ $mol.L^{-1}$	$\frac{[Buffer]_0}{[Initiator]_0}$	Observations
6	KPS	$NaHCO_3$	1.0×10^{-3}	3	No VCL hydrolysis - Final dispersion not stable
7	ADIBA	$NaHCO_3$	1.2×10^{-3}	4	No VCL hydrolysis - Final dispersion not stable
8	ADIBA	-	-	-	Traces of VCL hydrolysis - Final dispersion stable
9	ADIBA	TRIZMA	9.8×10^{-4}	3	Traces of VCL hydrolysis - Final dispersion stable
10	ADIBA	TRIZMA	1.8×10^{-3}	6	No VCL hydrolysis - Final dispersion stable

[a] Reaction conditions: rpm = 300, reaction time = 4 h, $[Initiator]_0 = 3.2 \times 10^{-4}$ $mol.L^{-1}$.

When using sodium bicarbonate as buffer ($NaHCO_3$, expt 6 and 7 in **Table 3**), with ADIBA or KPS as initiator, no peaks corresponding to either caprolactam or acetaldehyde could be detected on the NMR spectrum of the final dispersion and the pH was maintained constant to 7 all along the polymerization. However, the recovered polymer dispersions were not stable. Indeed, when using KPS as initiator, an inhomogeneous microgel dispersion (*i.e.* irreversible flocculation of microgel particles) could clearly be perceived (**Figure 4**) whereas when using ADIBA as initiator a reversible flocculation of the microgel particles was observed when the reaction medium was cooled down (**Figure 5**). These phenomena might be due to a screening effect of the particle surface charges. Indeed, these charges, coming from both the stabilizer and fragments of the initiator, are ensuring the stabilization of the dispersion by means of electrostatic repulsion among particles. In the present case, KPS and $NaHCO_3$ are anionic while ADIBA and P(AETAC-X) stabilizer are cationic. Therefore, the existence of electrostatic attraction among the different compounds weakens the repulsive forces among particles leading to the particle destabilization.

Figure 4. Aspect of the dispersion recovered after the emulsion polymerization of VCL using KPS as initiator, $NaHCO_3$ as buffer and $P(AETAC\text{-}X)_{76}$ as stabilizer (expt 6, **Table 3**).

Figure 5. Image of the microgel flocculation observed during the cooling for the experiment performed when using either $NaHCO_3$ as buffer and ADIBA as initiator (expt 7 in **Table 3**) or when using less than 4wt-% of reactive stabilizer at 1 wt-% of initial solids content (SC1-0-E4, $SC1\text{-}PX_{76}$ 2-E4 and $SC1\text{-}PX_{76}$ 3-E4 in **Table 6**).

Consequently, we decided to use both a cationic buffer and a cationic initiator: respectively TRIZMA hydrochloride and ADIBA. After optimization of the buffer concentration (expt 8-10 in **Table 3**), VCL hydrolysis is effectively avoided while a satisfactory dispersion stabilization is maintained. Thus, for all the syntheses of PVCL-based microgels presented in the following work, ADIBA will be used as initiator and TRIZMA will be used as buffer, with a ratio between the buffer and the initiator initial concentrations equals to 6 (*i.e.* 3 wt-% of TRIZMA buffer based on VCL).

1.ii. Choice of the initiator concentration and reaction temperature

Various experiments were carried out in order to investigate the effect of the ADIBA initiator concentration and the reaction temperature on both the VCL polymerization rate and the colloidal stability of the final microgel particles (**Table 4**).

Table 4. Experimental conditions for the batch emulsion polymerization of VCL performed at 1 wt-% of initial solids content, 4 wt-% of P(AETAC-X) stabilizer based on VCL, 4 wt-% of EGDMA based on VCL and 3 wt-% of TRIZMA buffer based on VCL.[a] Reaction variables: degree of polymerization of $P(AETAC\text{-}X)_n$ stabilizer, wt-% of initiator based on VCL and reaction temperature.

Expt	Stabilizer	[Initiator] $mol.L_{H2O}^{-1}$	Initiator *wt-% VCL*	*T* °C	Reaction[b]
11	$P(AETAC\text{-}X)_{16}$	4.9×10^{-5}	0.15	70	PX_{16} 4-A0.15-T70
12	$P(AETAC\text{-}X)_{16}$	3.2×10^{-4}	1	70	PX_{16} 4-A1-T70
13	$P(AETAC\text{-}X)_{76}$	3.2×10^{-4}	1	70	PX_{76} 4-A1-T70
14	$P(AETAC\text{-}X)_{76}$	3.2×10^{-4}	1	50	PX_{76} 4-A1-T50

[a] Reaction conditions: rpm = 300, reaction time = 4 h. $k_{d\ ADIBA,\ water,\ 70°C} = 6.7 \times 10^{-4}\ s^{-1}$ and $k_{d\ ADIBA,\ water,\ 50°C} = 4.0 \times 10^{-5}\ s^{-1}$; [b] Reaction name: PX_n : reactive cationic polymeric stabilizer with *n* the degree of polymerization, the number following indicates the wt-% of stabilizer based on VCL – A : ADIBA initiator, the number following indicates the wt-% of ADIBA based on VCL - T : Reaction temperature, the number following indicates the temperature value in °C.

The conversion of VCL monomer was monitored by proton NMR using 1,3,5-trioxane as internal standard. Polymerization kinetics were compared for VCL emulsion polymerization carried out at two concentrations in ADIBA initiator (**Figure 6**).

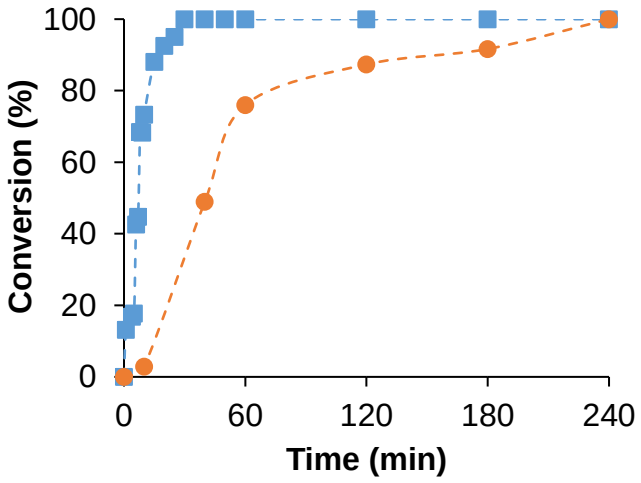

Figure 6. Conversion of VCL versus time for experiments carried out at 1 wt-% of initial solids content, using 4wt-% of $P(AETAC\text{-}X)_{16}$ as stabilizer, at T=70°C and different ADIBA concentrations: (■) [ADIBA] = 3.2×10^{-4} $mol.L_{H2O}^{-1}$ (PX_{16} 4-A1-T70 microgel, expt 12 in **Table 5**); (●) [ADIBA] = 4.9×10^{-5} $mol.L_{H2O}^{-1}$ (PX_{16} 4-A0.15-T70 microgel, expt 11 in **Table 5**).

As expected, a decrease of the initial radical flux by decreasing the initial concentration of initiator from 1 wt-% to 0.15 wt-% based on VCL, induces a decrease of the polymerization rate along with an increase of the nucleation period (**Figure 6**). When decreasing the reaction temperature from 70°C to 50°C using P(AETAC-X)$_{76}$ as stabilizer (PX$_{76}$ 4-A1-T70 and PX$_{76}$ 4-A1-T50 microgels, expt 13 and 14 in **Table 4**), the same trend was observed as 100 % of VCL conversion was reached after 30 min of polymerization at 70°C whereas only 26% of VCL conversion was obtained at 50°C ($k_{d\ ADIBA,\ water,\ 70°C} = 6.7 \times 10^{-4}\ s^{-1}$ and $k_{d\ ADIBA,\ water,\ 50°C} = 4.0 \times 10^{-5}\ s^{-1}$).[58] The polymerizations performed at such a reduced radical flux produce 50 wt-% of coagulum (PX$_{16}$ 4-A0.15-T70 and PX$_{76}$ 4-A1-T50 microgels, expt 11 and 14 in **Table 5**). The colloidal destabilization suggests that a fast nucleation and sufficiently high polymerization rate are required to synthesize stable PVCL-based microgels in the presence of the macromolecular cationic P(AETAC-X) stabilizer.

Table 5. Colloidal features of PVCL-based microgels synthesized at 1 wt-% of initial solids content, 4 wt-% of stabilizer based on VCL, 4 wt-% of EGDMA based on VCL and 3 wt-% of TRIZMA buffer based on VCL.[a] Reaction variables: degree of polymerization of P(AETAC-X)$_n$ stabilizer, wt-% of initiator based on VCL and reaction temperature.

Expt	Reaction	$D_{h,55°C}$ *nm*	N_p[b] × 10^{15} L^{-1}_{latex}	$D_{h,10°C}$ *nm*	VPTT[c] °C	Φ[d]	Observations
11	PX$_{16}$ 4-A0.15-T70	-	-	-	-	-	COAGULUM (50 wt-%)
12	PX$_{16}$ 4-A1-T70	221 ± 33	1.0 ± 0.8	397 ± 40	30.8 ± 3.1	6	STABLE
13	PX$_{76}$ 4-A1-T70	169 ± 15	3.4 ± 1.1	309 ± 4	28.2 ± 1.1	6	STABLE
14	PX$_{76}$ 4-A1-T50	-	-	-	-	-	COAGULUM (50 wt-%)

[a] Reaction conditions: rpm = 300, reaction time = 4 h. For the experiments 11 and 14 the colloidal features of the microgel final dispersions were not characterized; [b] Average number of particles measured from D_h at 55°C, Equation 2; [c] Volume Phase Transition Temperature; [d] Swelling ratio: $\Phi = (D_{h,10°C}/D_{h,55°C})^3$.

1.iii. Setting the concentration of stabilizer

A series of PVCL-based microgels was synthesized by batch emulsion polymerization carried out at 1 wt-% of solids content using different fractions of the P(AETAC-X)$_{76}$ reactive cationic stabilizer (**Table 6**).

Table 6. Experimental conditions and results for the batch emulsion polymerizations of VCL carried out at 70°C, 1 wt-% of initial solids content, 1 wt-% of ADIBA initiator based on VCL, 4 wt-% of EGDMA based on VCL and 3 wt-% of TRIZMA buffer based on VCL.[a] Reaction variables: amount of P(AETAC-X)$_{76}$ reactive stabilizer.

Reaction	Wt-% of stabilizer based on VCL	$D_{h,55°C}$ *nm*	$D_{h,10°C}$ *nm*	VPTT[c] *°C*	Φ[d]	Observations
SC1-0-E4	0	275 ± 64 [e]	385 ± 7 [e]	27.7 ± 0.1	3	NOT STABLE
SC1-PX$_{76}$ 2-E4	2	235 ± 7 [e]	392 ± 35 [e]	27.5 ± 0.2	5	NOT STABLE
SC1-PX$_{76}$ 3-E4	3	241 ± 2 [e]	380 ± 5 [e]	27.1 ± 0.4	4	NOT STABLE
SC1-PX$_{76}$ 4-E4	4	169 ± 15	309 ± 4	28.2 ± 1.1	6	STABLE

[a] Reaction conditions: rpm = 300, reaction time = 4 h.; [b] Average number of particles measured from D_h at 55°C, Equation 2; [c] Volume Phase Transition Temperature; [d] Swelling ratio: $\Phi = (D_{h,10°C}/D_{h,55°C})^3$; [e] For the non-stable microgel dispersions, hydrodynamic diameters were measured from the supernatant obtained after coagulum filtration.

The results of **Table 6** show that a minimum concentration of 4 wt-% of reactive stabilizer is required to obtain stable PVCL-based microgels as those synthesized with 0, 2, and 3 wt-% of P(AETAC-X)$_{76}$ with respect to VCL systematically flocculated upon cooling (**Figure 5**).

From the setting of the experimental conditions, it appears that the optimum experimental conditions to produce stable PVCL-based microgels stabilized by the P(AETAC-X) cationic polymers by batch emulsion polymerization of VCL carried out at 1 wt-% of initial solids content are the following ones: TRIZMA buffer with ADIBA initiator at a molar ratio of 6, a concentration of 1 wt-% of ADIBA initiator based on VCL, a temperature of 70°C and a minimum level of cationic stabilizer of 4 wt-% based on VCL. For these polymerizations, a complete monomer conversion is reached within 40 minutes (**Figure 6**) while maintaining a satisfactory stability of the final microgel dispersion.

2. Colloidal features of the thermoresponsive PVCL-based microgels

Herein, the effect of various reaction variables such as the solids content (SC as the nomenclature chosen for naming the reactions), the level of cationic macromolecular stabilizer (PX), the content of crosslinker (E) on the colloidal features of the PVCL-based microgels synthesized by batch emulsion polymerization of VCL will be investigated (see **Table 2** and polymer codes in the experimental part). The colloidal features of the microgels are gathered in **Table 7**.

Table 7. Colloidal features of PVCL-based microgels synthesized at 70°C, using 1 wt-% of ADIBA initiator based on VCL and 3 wt-% of TRIZMA buffer based on VCL.[a] Reaction variables: initial solids content, type and wt-% of stabilizer based on VCL and wt-% of EGDMA based on VCL.

Reaction	$D_{h,55°C}$ *nm*	$N_p^b \times 10^{15}$ L^{-1}_{latex}	$D_{h,10°C}$ *nm*	VPTT[c] *°C*	Φ[d]	Observations
SC1-PX_{76} 4-E4	169 ± 15	3.4 ± 1.1	309 ± 4	28.2 ± 1.1	6	STABLE
SC5-PX_{76} 4-E4	214 ± 5	8.0 ± 0.6	769 ± 41	30.7 ± 0.6	46	STABLE
SC10-PX_{76} 4-E4	215 ± 34	18.0 ± 1.0	741 ± 84	30.6 ± 2.0	41	STABLE
SC1-PX_{76} 4-E8	251 ± 41	1.1 ± 0.6	355 ± 9	28.3 ± 0.6	3	STABLE
SC1-PX_{76} 8-E4	170 ± 31	3.6 ± 2.3	238 ± 8	30.9 ± 0.2	3	STABLE
SC5-PX_{76} 8-E4	205 ± 6	9.1 ± 0.9	676 ± 14	29.7 ± 0.6	36	STABLE
SC1-PX_{76} 8-E8	129 ± 15	7.6 ± 3.1	156 ± 7	28.0 ± 2.5	2	STABLE
SC1-PX_{16} 4-E4	221 ± 33	1.0 ± 0.8	397 ± 40	30.8 ± 3.1	6	STABLE
SC1-PX_{16} 12-E4	155 ± 7	4.2 ± 0.6	154 ± 12	-	-	STABLE
SC1-PX_9 4-E4	156 ± 2	4.1 ± 0.2	330 ± 17	30.2 ± 0.6	9	STABLE
SC5-PX_9 4-E4	200 ± 2	9.7 ± 0.3	642 ± 20	30.6 ± 1.5	33	STABLE

[a] Reaction conditions: rpm = 300, reaction temperature = 70°C; reaction time = 4 h. The final conversion of VCL determined by ^{1}H NMR ranged between 96 and 100% for all experiments; [b] Average number of particles measured from D_h at 55°C, Equation 2; [c] Volume Phase Transition Temperature; [d] Swelling ratio: $\Phi = (D_{h,10°C}/D_{h,55°C})^3$.

It is noticed from results of **Table 7** that the amounts of both the reactive cationic macromolecular stabilizer and that of the crosslinker influenced the final number of particles. By increasing the concentration of P(AETAC-X)$_{76}$ stabilizer from 4 to 8 wt-%, the number of microgel particles either remained constant for emulsion polymerization carried out at 1 wt-% of solids content (SC1-PX$_{76}$ 4-E4 and SC1-PX$_{76}$ 8-E4 in **Table 7**) or slightly increased at 5 wt-% of solids content (SC5-PX$_{76}$ 4-E4 and SC5-PX$_{76}$ 8-E4 in **Table 7**). An increase of the concentration of the P(AETAC-X)$_{16}$ stabilizer from 4 to 12 wt-% induces an obvious increase of the number of particles by a factor of four (SC1-PX$_{16}$ 4-E4 and SC1-PX$_{16}$ 12-E4 in **Table 7**). Such trend confirms the involvement of the reactive P(AETAC-X) hydrophilic polymer to ensure the stability of the primary nuclei formed in the early stage of emulsion polymerization therefore acting on the final number of particles. The reactive P(AETAC-X)$_9$ with a lower theoretical degree of polymerization in comparison with the P(AETAC-X)$_{76}$ stabilizer, induces a 20 % average increase of the final number of particles at both initial solids content of 1 and 5 wt-% (SC1-PX$_{76}$ 4-E4, SC1-PX$_9$ 4-E4 and SC5-PX$_{76}$ 4-E4, SC5-PX$_9$ 4-E4 in **Table 7**). As the weight fraction of the reactive stabilizer is kept constant at 4 wt-% on the basis of VCL, the number of moles of stabilizing cationic polymer chains is indeed higher for the lower degree of polymerization.

The amount of EGDMA was varied from 4 to 8 wt-% based on VCL for two different initial concentrations of the reactive P(AETAC-X)$_{76}$ stabilizer (see **Table 7** SC1-PX$_{76}$ 4-E4, SC1-PX$_{76}$ 4-E8 and SC1-PX$_{76}$ 8-E4, SC1-PX$_{76}$ 8-E8). For polymerization carried out at a concentration of 8 wt-% of P(AETAC-X)$_{76}$ stabilizer, an increase of the EGDMA doubles the number of particles (see SC1-PX$_{76}$ 8-E4 and SC1-PX$_{76}$ 8-E8 in **Table 7**). As expected, the hydrophobicity of the EGDMA crosslinker (water solubility of EGDMA at 20°C = 5.4 mM)[59] favors the initial precipitation of the growing polymer in the aqueous phase producing more particles during the nucleation period. However, an opposite trend was observed by using 4 wt-% of P(AETAC-X)$_{76}$ based on VCL. In that case, an increase of the amount of EGDMA from 4 to 8 wt-% gives rise to a decrease of the number of particles (see SC1-PX$_{76}$ 4-E4 and SC1-PX$_{76}$ 4-E8 in **Table 7**). This lower concentration of P(AETAC-X)$_{76}$ stabilizer is probably insufficient to limit the aggregation of the nuclei due to the higher hydrophobicity imparted by EGDMA. A lower number of particle induced by the high reactivity and hydrophobicity of EGDMA has already been observed for the synthesis of oligo(ethylene glycol)-based thermoresponsive microgels.[60]

The stable PVCL-based microgels synthesized by emulsion polymerization in the presence of the reactive P(AETAC-X) stabilizers exhibit a thermoresponsive behavior with a volumetric shrinkage upon heating (**Figure 7**).

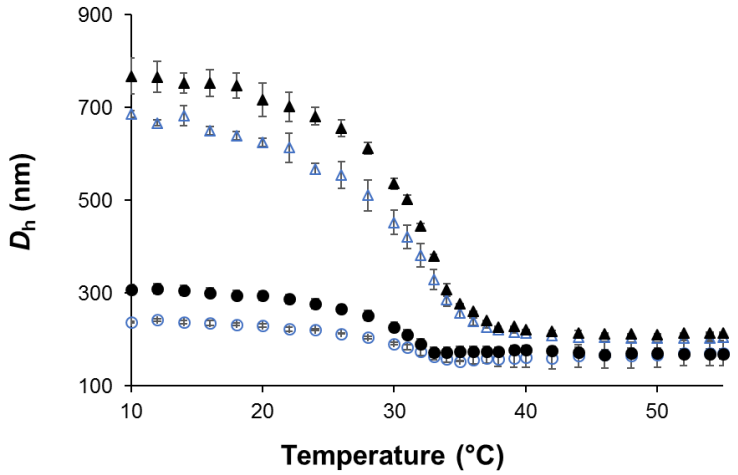

Figure 7. Final average hydrodynamic diameters as a function of the temperature for the microgels synthesized at: ● 1wt-% of initial solids content and ▲ 5 wt-% of initial solids content; Full symbols: 4 wt-% of P(AETAC-X)$_{76}$ stabilizer based on VCL (SC1-PX$_{76}$ 4-E4 and SC5-PX$_{76}$ 4-E4 in **Table 7**), Open symbols: 8 wt-% of P(AETAC-X)$_{76}$ stabilizer based on VCL (SC1-PX$_{76}$ 8-E4 and SC5-PX$_{76}$ 8-E4 in **Table 7**).

The value of the volume phase transition temperature (VPTT) ranged between 28 °C and 30°C (see **Table 7**). This value is in accordance with the range of VPTT previously reported for PVCL-based microgels.[28-30, 33] The swelling-to-collapse transition is reversible in the absence of any hysteresis (see Figure 1 of the Appendix of this chapter) which features a narrow particle size distribution. Indeed, well defined spherical, monodisperse PVCL-based microgels were observed by transmission electron microscopy (TEM) (**Figure 8**).

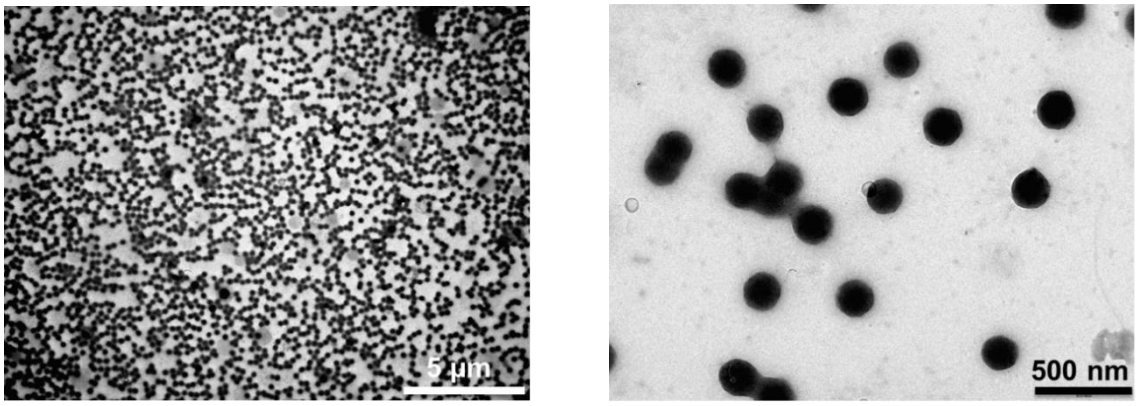

Figure 8. TEM images of the microgels synthesized at 5wt-% of initials solids content and 4 wt-% of P(AETAC-X)$_{76}$ stabilizer with respect to VCL (SC5-PX$_{76}$ 4-E4 in **Table 7**).

The volume-average diameter (D_v) was calculated from the TEM images on the basis of 200 particles using Equation 3.

$$\langle D_v \rangle = \bar{D}_v = \left(\frac{\sum n_i D_i^3}{\sum n_i} \right)^{1/3} \quad \text{Equation 3}$$

The volume-average diameter of the dried SC5-PX$_{76}$ 4-E4 microgels (D_v = 292 ± 18 nm, **Figure 8**), is in a similar range as the average hydrodynamic diameter of the microgels measured by DLS at the collapsed state ($D_{h,55°C}$ = 214 ± 5 nm, SC5-PX$_{76}$ 4-E4 in **Table 7**). Since the PVCL-based microgels are soft particles, they have tendency to spread on the surface during the drying process prior the TEM analysis and therefore the D_v calculated from TEM images are higher than $D_{h,55°C}$ measured by DLS.[61]

3. Effect of the reaction variables on the swelling behavior and inner structure of the PVCL-based microgels

3.i. Effect of the amount of crosslinker

First, the effect of the EGDMA crosslinker for the polymerization of VCL in aqueous dispersed media carried out at 1 wt-% of initial solids content was studied. The value of the VPTT remains in a similar range of 28 – 30 °C whatever the EGDMA content but a broadening of the volume phase transition by increasing the temperature was observed when the crosslinker concentration was increased from 4 to 8 wt-% based on VCL monomer (**Figure 9**). Such trend has been previously observed for PVCL-based microgels[29] and for poly(*N*-isopropylacrylamide) (PNIPAAm) microgels[62] synthesized with poly(ethylene glycol) diacrylate as a crosslinker. The volume phase transition broadening can be ascribed to an increasing heterogeneity in the polymer network,[62] which might be due to a different incorporation rate of the crosslinker following the copolymerization kinetics when increasing the initial fraction of the co-monomer. The swelling ratio of the PVCL-based microgels ($\phi = (D_{h,10°C})^3 / (D_{h,55°C})^3$) was reduced by increasing twofold the content of EGDMA. The value of ϕ decreases from 6 to 3 in the presence of 4 wt-% of P(AETAC-X)$_{76}$ stabilizer (SC1-PX$_{76}$ 4-E4 and SC1-PX$_{76}$ 4-E8 in **Table 7**) or from 3 to 2 in the presence of 8 wt-% of P(AETAC-X)$_{76}$ stabilizer (SC1-PX$_{76}$ 8-E4 and SC1-PX$_{76}$ 8-E8 in **Table 7**). This was an expected result since it is well established that the increase of the crosslinking density limits the swelling extent of the polymer network of the microgels.[29, 60]

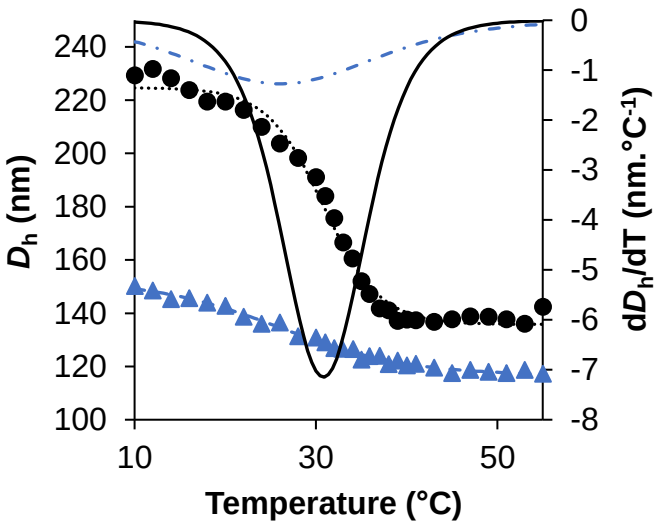

Figure 9. Final average hydrodynamic diameters as a function of the temperature for the microgels synthesized at 1 wt-% of initial solids content at 70°C, using 8 wt-% of P(AETAC-X)$_{76}$ stabilizer based on VCL and different amounts of crosslinker: ● 4 wt-% of EGDMA with respect to VCL (SC1-PX$_{76}$ 8-E4 **Table 7**), ⋯ Boltzmann fit and — fit first-order derivative for this experiment; ▲ 8 wt-% of EGDMA with respect to VCL (SC1-PX$_{76}$ 8-E8 **Table 7**), --- Boltzmann fit and -·- Fit first-order derivative for this experiment.

The PVCL-based microgels described in the next parts of this chapter will be systematically synthesized with 4 wt-% of EGDMA crosslinker based on VCL in order to investigate the influence on the microgel volume phase transition of the other reaction variables such as the solids content, the weight fraction of stabilizer or the chemical structure of stabilizer.

3.ii. Effect of the initial solids content

The initial solids content for emulsion polymerization of VCL was ranging from 1 to 10 wt-% as depicted in **Table 7** (SC1-PX$_{76}$ 4-E4, SC5-PX$_{76}$ 4-E4, SC10-PX$_{76}$ 4-E4 and SC1-PX$_{76}$ 8-E4, SC5-PX$_{76}$ 8-E4 for experiments with respectively 4 and 8 wt-% of P(AETAC-X)$_{76}$). It should first be noticed that stable PVCL-based microgels are successfully synthesized from the reactive P(AETAC-X)$_{76}$ stabilizer up to 10 wt-% of solids content in the absence of coagulum (SC1-PX$_{76}$ 4-E4, SC5-PX$_{76}$ 4-E4 and SC10-PX$_{76}$ 4-E4 in **Table 7**). It is the first time that PVCL-based thermoresponsive microgels are synthesized at such level of solids content. Most of the previous studies reported the synthesis of PVCL-based microgels at solids content below 5 wt-%.[24, 25, 28-30, 33, 60, 63] Imaz *et al.*[28] observed for instance the formation of a macroscopic gel during the emulsion polymerization of VCL carried out at 5 wt-% of solids content with 4 wt-% of sodium dodecyl sulfate as molecular surfactant, 1 wt-% of potassium persulfate as initiator

and 4 wt-% of *N,N'*-methylenebis(acrylamide) as crosslinker. The reactive P(AETAC-X) cationic polymers are effective electro-steric stabilizers to increase the solids content of the final dispersion of thermoresponsive PVCL-based microgels while maintaining colloidal stability (no coagulum formation). The specific role of the reactive chain end of these polymeric stabilizers will be investigated in more details in part 4 of this Chapter 2.

Whatever the stabilizer content and its chain length, the hydrodynamic diameter of the swollen PVCL-based microgels measured at 10°C is systematically higher for the microgels synthesized at 5 wt-% of solids content in comparison to the microgels synthesized at 1 wt-% of solids content (**Figure 7** and SC1-PX_{76} 4-E4, SC5-PX_{76} 4-E4, SC1-PX_{76} 8-E4, SC5-PX_{76} 8-E4 and SC1-PX_9 4-E4, SC5-PX_9 4-E4 in **Table 7**).

A first explanation could arise from the difference between the initial states of the VCL polymerization carried out in aqueous dispersed media. According to Aguirre *et al.* [59] and Kozanoglu *et al.*,[64] the concentrations of limited solubility in water of VCL and EGDMA are the following: $[VCL]_{limit,\ water}$ = 41 $g.L^{-1}$ and $[EGDMA]_{limit,\ water}$ = 1 $g.L^{-1}$.[64,59] Consequently, at 1 wt-% of initial solids content, both VCL monomer and EGDMA crosslinker are soluble in the continuous aqueous phase ($[VCL]_0$ = 10 $g.L^{-1}$ and $[EGDMA]_0$ = 0.4 $g.L^{-1}$) (**Figure 10**) so the polymerization follows a precipitation polymerization process. On the contrary, monomer droplets dispersed in the aqueous phase are observed for higher initial solids content (**Figure 10**) as the concentrations of both VCL and EGDMA ($[VCL]_0$ = 50 $g.L^{-1}$ and $[EGDMA]_0$ = 2 $g.L^{-1}$ for 5 wt-% of solids content) are above their concentrations of limited solubility in water.

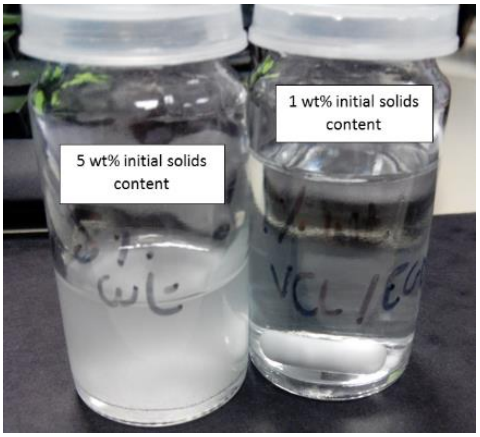

Figure 10. Aspect of the reaction mixtures at the initial state for the polymerization of VCL performed at 1 and 5 wt-% of initial solids content.

Thus, at 5 and 10 wt-% of initial solids content, the polymerization occurs via an emulsion polymerization process. The diffusion of both VCL and crosslinker across the water phase in emulsion process might induce a difference in the relative rate of polymerization of both components in comparison with precipitation polymerization starting with a homogeneous initial phase. To address this question, the individual conversions of VCL monomer and EGDMA crosslinker were monitored by proton NMR during the course of polymerization (**Figure 11**).

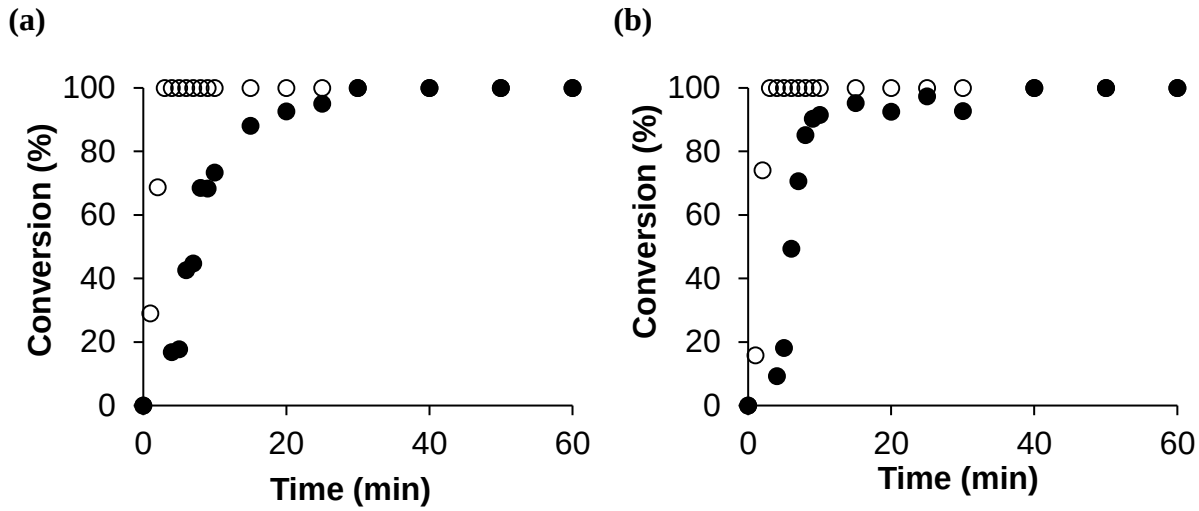

Figure 11. Conversion of VCL (full symbols) and EGDMA (open symbols) versus time for experiments carried out using 4wt-% of P(AETAC-X)$_9$ as stabilizer, at a polymerization temperature of 70°C and at: **(a)** 1 wt-% of initial solids content, [ADIBA] = 3.0×10^{-4} mol.L_{H2O}^{-1} (SC1-PX$_9$ 4-E4 **Table 7**) and **(b)** 5 wt-% of initial solids content, [ADIBA] = 1.5×10^{-3} mol.L_{H2O}^{-1} (SC5-PX$_9$ 4-E4 in **Table 7**).

As displayed in **Figure 11**, for kinetics of polymerizations carried out at both 1 wt-% and 5 wt-% of initial solids content, EGDMA crosslinker is consumed much faster than the main VCL monomer. The same trend was already observed by Imaz *et al.*[29] using poly(ethylene glycol) diacrylate (PEGDA) or *N,N'*-methylenebisacrylamide (MBA) as crosslinker for the emulsion polymerization of VCL, crosslinker reacting faster than VCL in both cases. It is rather impossible to discriminate the effect of solids content on the relative rates of polymerization of VCL and EGDMA. On the basis of the higher reactivity of the EGDMA crosslinker, a core-shell structure of the PVCL-based microgel is expected. The inner structure of the P(AETAC-X)-stabilized PVCL-based microgels was analyzed by means of proton nuclear magnetic resonance transverse relaxation (T_2 NMR) measurements (**Figure 13**).

The most intense resonance peak of PVCL that appears at 1.8 ppm on the proton high-resolution spectrum of the microgel (R_1, **Figure 12**) is used for T2 NMR measurements to investigate the heterogeneity of the inner crosslinked structure of the synthesized microgels.

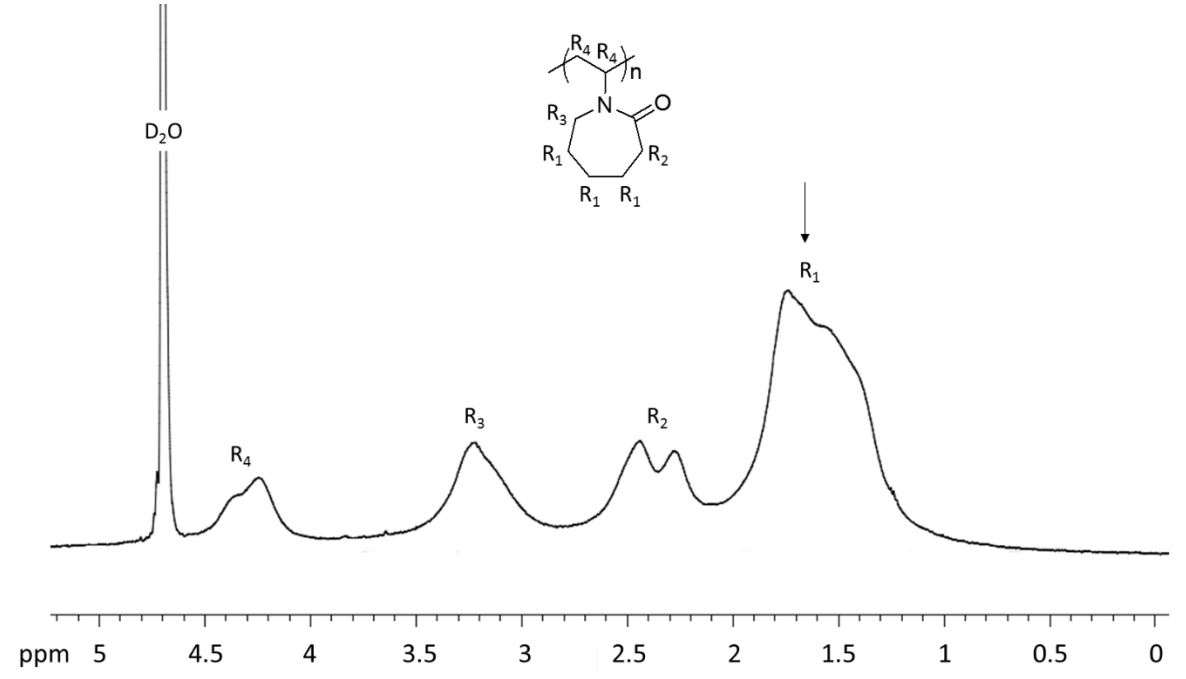

Figure 12. ^{1}H NMR high-resolution spectrum in D_2O of SC1-PX_{76} 4-E4 microgel (see **Table 7**).

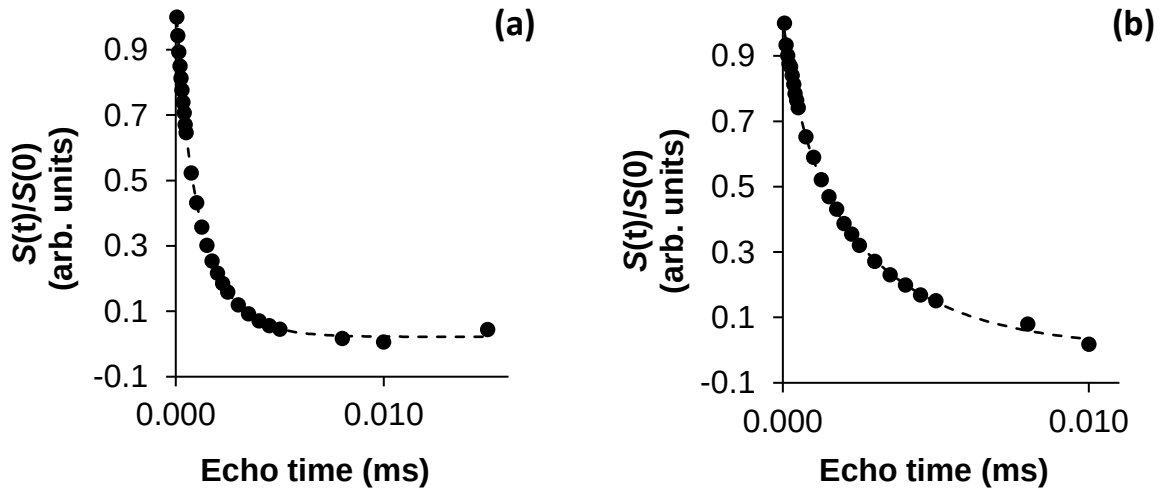

Figure 13. Proton NMR transverse relaxation decay of R_1 proton by Hahn echo for microgels synthesized using 4wt-% of $P(AETAC\text{-}X)_{76}$ stabilizer based on VCL at **(a)** 1 wt-% of initial solids content (SC1-PX_{76} 4-E4 in **Table 7**) and **(b)** 5 wt-% of initial solids content (SC5-PX_{76} 4-E4 in **Table 7**). The concentration of microgels is 2 wt-% in D_2O. The experimental plot was fitted with biexponential decay function (dotted line).

A biexponential decay for the normalized integral of R1 resonance versus echo time was considered in **Figure 13** according to the following equation:

$$\frac{S(t)}{S(0)} = C_s \exp\left\{-\frac{t}{T_{2S}}\right\} + C_L \exp\left\{-\frac{t}{T_{2L}}\right\} \quad \text{Equation 4}$$

Where, $S(t)/S(0)$ is the ratio between proton nuclear magnetic resonance transverse relaxation signal integral (S) at time t ($S(t)$) and at initial time $S(0)$). This normalized $S(t)/S(0)$ signal is plotted as a function of spin-echo time t and C_i (i = S and L) are the relative contribution of the decays characterized by short (T_{2S}) and long (T_{2L}) transverse relaxation times. The value of T_{2S} corresponds to a network with a higher value of the crosslinking density (core) as compared with T_{2L} (shell). The C_S and C_L coefficients are related to the number of protons in the methylene fragments of PVCL describing quantitatively the bimodal heterogeneity of the polymer network in microgel particles. Using the Equation 4, the values of the short (T_{2S}) and long (T_{2L}) proton transverse relaxation times, and the relative amount of methylene protons of PVCL in core (C_S) and shell (C_L) were calculated and reported in **Table 8**. Once short and long transverse relaxation times are obtained, the ratio of the crosslinking density of the microgel in core and shell (CLD^{core}/CLD^{shell}) could be determined.[33, 54, 55]

$$\frac{CLD^{core}}{CLD^{shell}} = \left(\frac{T_2^{shell}}{T_2^{core}}\right)^{1/2} \quad \text{Equation 5}$$

Table 8. Proton transverse relaxation times (T_{2S} and T_{2L}) and relative weight coefficients for the PVCL-based microgels synthesized using 4wt-% of $P(AETAC\text{-}X)_{76}$ stabilizer based on VCL, at different initial solids contents.

Reaction	T_{2S} *ms*	C_S	T_{2L} *ms*	C_L	$\frac{CLD^{core}}{CLD^{shell}}$
SC1-PX_{76} 4-E4	0.42	0.26	1.45	0.77	1.9
SC5-PX_{76} 4-E4	0.69	0.32	3.18	0.69	2.2

The results of proton nuclear magnetic resonance transverse relaxation fitted by two different transverse relaxation times (**Table 8**) confirm the core-shell morphology suggested by the polymerization kinetics reported in **Figure 11**. On the basis of the values of CLD^{core}/CLD^{shell} ratios of the PVCL-based microgels (**Table 8**) it is deduced that the core is twice more crosslinked than the shell. The content of PVCL chains located in the shell (C_L) is higher than in the core (C_S) for microgels synthesized at both solids contents (SC1-PX_{76} 4-E4 and SC5-PX_{76} 4-E4 microgels in **Table 8**). EGDMA crosslinker provides a more homogeneous microstructure in comparison with *N*,*N*'-methylenebisacrylamide (MBA) as the ratios of the

average cross-linking density between the core and shell are lower with EGDMA. Indeed values of CLD^{core}/CLD^{shell} ratios of 3.0 - 3.4 were previously reported for PVCL-based microgels crosslinked with 4 wt-% of MBA,[54,33] while CLD^{core}/CLD^{shell} ratios of 1.9 – 2.2 were observed in the present work (**Table 8**). It was shown that a dextran-based crosslinker with multiple methacrylate groups produced PVCL-based microgels with rather homogeneous network structure as the CLD^{core}/CLD^{shell} ratios ranged between 1.0 and 1.7.[33] Despite the different levels of limited water solubility of the crosslinkers (1 $g.L^{-1}$ at 20°C for EGDMA, 20 $g.L^{-1}$ at 20°C for MBA and rather hydrophilic dextran-methacrylate crosslinker), the comparison of the CLD^{core}/CLD^{shell} ratios suggest that the reactivity of methacrylic function towards vinylcaprolactam drives the formation of a more homogeneous network than with acrylamide functions.

Concerning the comparison of the microgels synthesized by polymerization in aqueous dispersed media at 1 or 5 wt-% of solids content, it can be noticed that the values of CLD^{core}/CLD^{shell} ratio are very close. Consequently, the difference between the hydrodynamic diameters of the swollen microgels synthesized at 1 and 5 wt-% of solids content ($D_{h,1\ wt\text{-}\%\ solids\ content,\ 10°C}$ = 270 - 300 nm; $D_{h,5\ wt\text{-}\%\ solids\ content,\ 10°C}$ = 700 - 770 nm) cannot be ascribed to a noticeable difference of the inner microstructure of the microgel in terms of crosslinking distribution.

The fast consumption of EGDMA during polymerization of VCL carried out in aqueous dispersed media (**Figure 11**) may produce a certain amount of free chains. The supernatant of the centrifuged microgels were recovered to investigate the content of free chains. In order to compare accurately the weight fraction of free chains versus the microgels, three centrifugations of microgels were performed for each sample at a constant solids content of 1 wt-%. This required a dilution step prior centrifugation for the microgels synthesized at higher solids content. For each set of experiments performed with a constant stabilizer content (either 4 or 8 wt-% of $P(AETAC\text{-}X)_{76}$, see **Table 7**), the fraction of free chains based on the total weight of microgel is similar for both microgels synthesized at either 1 wt-% or 5 wt-% of solids content (see SC1-PX_{76} 4-E4, SC5-PX_{76} 4-E4 and SC1-PX_{76} 8-E4, SC5-PX_{76} 8-E4 in **Table 9**). Consequently, the free chains are not at the origin of the higher swelling ability of the microgels synthesized at 5 wt-% of solids content. Moreover, the value of D_h at 10°C of the microgel

remained similar after the first centrifugation cycle ($D_{h,10\ °C,\ dialyzed}$ = 662 ± 6 nm, $D_{h,10\ °C,\ dialyzed\ and\ centrifuged}$ = 577 ± 32 nm).

Table 9. Fraction of free chains[a] for PVCL-based microgels synthesized at different initial solids contents and different wt-% of P(AETAC-X)$_{76}$ stabilizer.

Reaction	Fraction of free chains %	VCL/AETAC molar ratio[b] of the polymer mixture in the supernatant %
SC1-PX$_{76}$ 4-E4	64	97/3
SC5-PX$_{76}$ 4-E4	64	98/2
SC1-PX$_{76}$ 8-E4	27	87/14
SC5-PX$_{76}$ 8-E4	38	94/6

[a] Measured by gravimetry from the supernatant recovered by centrifugation of microgels performed at 1 wt-% of solids content for all microgels; [b] Determined by NMR analysis of the supernatant recovered after microgels centrifugation.

By increasing the solids content by a factor of 5, the final number of microgel particles increases only by a factor of 2 - 2.5 (see SC1-PX$_{76}$ 4-E4, SC5-PX$_{76}$ 4-E4, SC1-PX$_{76}$ 8-E4, SC5-PX$_{76}$ 8-E4 and SC1-PX$_{9}$ 4-E4, SC5-PX$_{9}$ 4-E4 in **Table 7**). Therefore, for a similar weight fraction of stabilizer based on VCL monomer, the amount of P(AETAC-X) stabilizer per particle ($m_{P(AETAC-X)}/N$p, **Table 10**) in the microgels synthesized at 5 wt-% of initial VCL content is higher in comparison with the microgels synthesized at 1 wt-% of initial VCL solids content (**Table 10**). At the swollen state, the hydrophilic P(AETAC-X) cationic polymer might have entered into the slightly crosslinked PVCL shell of the microgel, leading to an increase of the microgel swelling by means of an increase of the osmotic pressure due to electrostatic repulsions between cationic polymer chains. The increase of the swelling of a microgel by means of the increase of the osmotic pressure is a well-described process.[65, 66] However, for SC1-PX$_{76}$ 8-E4 microgel, (**Table 10**), the amount of P(AETAC-X) polymer per particle is similar to the one of SC5-PX$_{76}$ 4-E4 microgel (**Table 10**) whereas a gap between the swelling ratios of both microgels was observed ($\Phi_{SC1\text{-}PX76\ 8\text{-}E4}$ = 3 and $\Phi_{SC5\text{-}PX76\ 4\text{-}E4}$ = 46, **Table 10**). The assumption of the contribution of the higher amount of cationic P(AETAC-X) polymer per particle to the higher swelling ability of the microgel synthesized at 5 wt-% of solids content is not supported by the experimental results. Given that the shell of the present EGDMA-crosslinked PVCL microgels is slightly crosslinked, it largely contributes to the swelling of the thermoresponsive microgels. The average weight amount of PVCL per microgel particle

(m_{PVCL}/N_p) is also higher for microgels synthesized at 5 wt-% of initial solids content than for microgels synthesized at 1 wt% of initial solids content (**Table 10**). Such higher content of thermoresponsive PVCL polymer might enhance the volume of the swollen shell of the PVCL microgels at low temperature, explaining the discrepancy in swelling ratio.

Table 10. Average mass of PVCL and P(AETAC-X) polymer per particle for PVCL microgels synthesized by polymerization in aqueous dispersed media at 1 and 5 wt-% of initial solids content.

Reaction	$\frac{m_{P(AETAC-X)}}{N_p}$ *g.particle*$^{-1}$	$\frac{m_{PVCL}}{N_p}$ *g.particle*$^{-1}$	Φ[a]
SC1-PX$_{76}$ 4-E4	1.2×10^{-16}	2.9×10^{-15}	6
SC5-PX$_{76}$ 4-E4	2.5×10^{-16}	6.3×10^{-15}	46
SC1-PX$_{76}$ 8-E4	2.2×10^{-16}	2.8×10^{-15}	3
SC5-PX$_{76}$ 8-E4	4.4×10^{-16}	5.5×10^{-15}	36

For the calculation of $m_{P(AETAC-X)}/N_p$ and m_{PVCL}/N_p, a volume of 100 mL of latex was considered. [a] Swelling ratio: $\Phi = (D_{h,10°C}/D_{h,55°C})^3$.

3.iii. Effect of the amount of stabilizer

The impact of the initial concentration of the P(AETAC-X) reactive stabilizer on the swelling behavior of the PVCL-based microgels was investigated in this part. The initial amount of P(AETAC-X)$_{76}$ stabilizer was ranged from 4 to 8 wt-% based on VCL for both series of polymerizations in aqueous dispersed media carried out at either 1 or 5 wt-% of initial solids content (**Table 7**). The increase of the P(AETAC-X)$_{76}$ concentration slightly reduced the diameter measured at swollen state (see D_h at 10°C for SC1-PX$_{76}$ 4-E4, SC1-PX$_{76}$ 8-E4 and SC5-PX$_{76}$ 4-E4, SC5-PX$_{76}$ 8-E4 microgels in **Table 7** and **Figure 7**). A similar trend was observed by increasing the amount of the P(AETAC-X)$_{16}$ stabilizer with lower theoretical DP from 4 wt-% to 12 wt-% with a more pronounced decrease of the hydrodynamic diameter at both 10 °C and 55°C (see **Figure 14** and **Table 7**).

It has been well-established that the incorporation of ionic co-monomer into thermoresponsive microgels induces an increase of the VPTT value as the increase of the internal osmotic pressure of the gel through electrostatic repulsions and counter-ions mobility leads to additional swelling of the gel.[44, 63, 67] For instance, Pich *et al.*[25, 41] showed that the introduction of 1 to 5 mol-% of vinylimidazole cationic co-monomer into PVCL-based microgels shifted the VPTT value from 35°C to 45 °C. The interest of the present system is to enable the increase of the fraction of cationic units (from 4 to 8 wt-%, *ie*, 3 to 6 mol-% based on VCL) at the surface of the microgel

while retaining a constant VPTT close to 30°C (**Table 7**). Note that raising the content of the reactive P(AETAC-X)$_{16}$ stabilizer to 12 wt-% based on VCL induced the formation of crosslinked particles with a constant hydrodynamic diameter over the temperature range of 10 to 55°C (**Figure 14**). The absence of volume phase transition when increasing the content of the reactive P(AETAC-X) stabilizer suggests that the cationic polyelectrolyte shell is able to limit the network swelling. Indeed, some previous examples showed that the presence of a shell, consisting of either crosslinked P(NIPAAm)[68] or iron oxide nanoparticles,[69] restricted the core from swelling to its native volume. This result confirms the role of the reactive cationic macromolecular chain-transfer agent to act as stabilizer, hence anchoring a polymeric cationic outer shell onto the PVCL-based microgels.

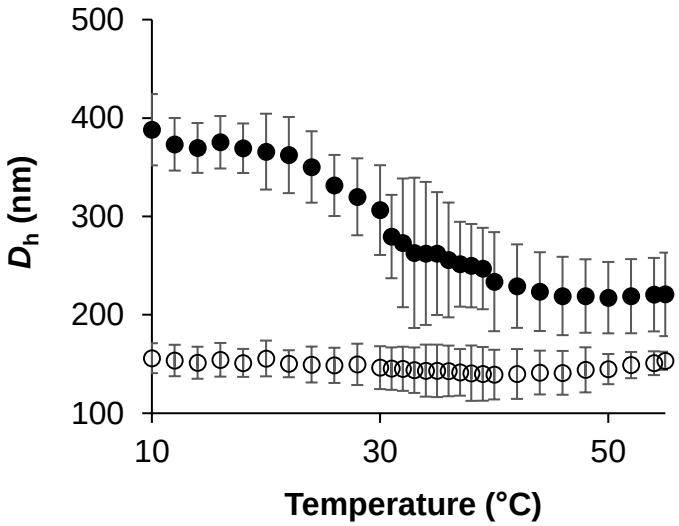

Figure 14. Final average hydrodynamic diameters as a function of the temperature for the microgels synthesized at 1 wt-% of solids content and 4 wt-% of EGDMA with respect to VCL: Full symbols: 4 wt-% (SC1-PX$_{16}$ 4-E4 in **Table 7**) and open symbols: 12 wt-% (SC1-PX$_{16}$ 12-E4 in **Table 7**) of P(AETAC-X)$_{16}$ stabilizer based on VCL.

In order to confirm the cationic character of the synthesized PVCL-based microgels, the electrophoretic mobility of the microgels synthesized using different concentrations of reactive stabilizers was measured at 25°C, in cationic buffer solution at pH 3 and 10 mM of ionic strength (**Table 11**). Microgel electrophoretic mobility measurements were also conducted in cationic buffers at different pH (3, 6 and 9) and ionic strengths equal to 1 mM. For the sake of clarity, the results are presented in the Appendix of this chapter 2.

For all the reactions, the electrophoretic mobility values are positives, which is consistent with the fact that either the cationic macromolecular stabilizer and/or the fragments coming from the cationic ADIBA initiator impart the cationic character.

Table 11. Microgel electrophoretic mobility measurements at 25°C in glycine cationic buffer solution at pH 3 and ionic strength of 10 mM, samples were analyzed at a concentration of 0.05 wt-%.

Reaction	Dialyzed sample electrophoretic mobility $m^2/Vs \times 10^{-8}$
SC1-PX_{76} 4-E4	0.42 ± 0.05
SC1-PX_{76} 8-E4	0.95 ± 0.17
SC5-PX_{76} 4-E4	0.57 ± 0.25
SC5-PX_{76} 8-E4	1.22 ± 0.04
SC10-PX_{76} 4-E4	0.88 ± 0.44
SC1-PX_{9} 4-E4	0.44 ± 0.16
SC5-PX_{9} 4-E4	0.38 ± 0.18
SC5-0-E4	0.15 ± 0.05

The values of the electrophoretic mobility of the PVCL-based microgels synthesized using reactive P(AETAC-X) as stabilizer are higher than the electrophoretic mobility of PVCL microgels synthesized in the absence of stabilizer (SC5-0-E4 in **Table 11**), attesting the presence of the cationic macromolecular stabilizer on the outer shell of the synthesized PVCL-based microgels. For experiments carried out at the same initial solids content, the microgel electrophoretic mobility increases according to the increase of the initial amount of the reactive cationic stabilizer (see SC1-PX_{76} 4-E4, SC1-PX_{76} 8-E4 and SC5-PX_{76} 4-E4, SC5-PX_{76} 8-E4 in **Table 11**). For the microgels synthesized at 1 or 5 wt-% of initial solids content and 4 wt-% of reactive stabilizer, we observed that the degree of polymerization of the reactive stabilizer (either P(AETAC-X)$_{76}$ or P(AETAC-X)$_{9}$), has no significant effect on the electrophoretic mobility (SC1-PX_{76} 4-E4, SC1-PX_{9} 4-E4 and SC5-PX_{76} 4-E4, SC5-PX_{9} 4-E4 in **Table 11**).

4. Effect of the nature of the stabilizer on the colloidal stability and features of PVCL-based microgels

The stabilization efficiency of different stabilizers was analyzed in order to investigate the role of the reactive xanthate chain-end of the cationic P(AETAC-X) macromolecular stabilizer (**Table 12**). For this purpose, polymerizations of VCL in aqueous dispersed media were carried

out at solids content ranging from 1 to 10 wt-% in the presence of the following stabilizers: i) a reactive P(AETAC-X)$_{76}$ polymer synthesized by RAFT/MADIX polymerization (**Table 1**); ii) two non-reactive P(AETAC) polymers, one P(AETAC) synthesized by free radical polymerization in the absence of control agent, and one P(AETAC-X)$_{76,\ cleaved}$ prepared by cleavage of the xanthate chain-end of P(AETAC-X)$_{76}$); iii) a conventional cationic molecular surfactant (cetyltrimethylammonium bromide, CTAB). As a matter of comparison, a series of PVCL-based microgels was also synthesized in the absence of either surfactant or stabilizer. The results are gathered in **Table 12**.

Table 12. Colloidal features of PVCL-based microgels synthesized at 70°C, using different types of stabilizers, 1 wt-% of ADIBA initiator based on VCL, 4 wt-% of EGDMA based on VCL and 3 wt-% of TRIZMA buffer based on VCL.[a] Reaction variables: initial solids content and type of stabilizer.

Stabilizer / Initials solids content τ^b (wt-%)	-	CTAB	Non- reactive P(AETAC)	Reactive P(AETAC-X)$_{76}$
1	FLOCCULATION	AGGREGATION	FLOCCULATION [d]	STABLE
	$D_{h,55°C}$ = 275 ± 64 nm	$D_{h,55°C}$ = 118 ± 14 nm	$D_{h,55°C}$ = 215 ± 61 nm	$D_{h,55°C}$ = 169 ± 15 nm
	$D_{h,10°C}$ = 385 ± 7 nm	$D_{h,10°C}$ = 91 ± 7 nm	$D_{h,10°C}$ = 288 ± 51 nm	$D_{h,10°C}$ = 309 ± 4 nm
	SC1-0-E4	SC1-CTAB 4-E4	SC1-PX$_{76,cleaved}$ 4-E4	SC1-PX$_{76}$ 4-E4
5	COAGULUM (65wt-%) [c]	COAGULUM (49 wt-%)	COAGULUM (50 wt-%) [e]	STABLE
	$D_{h,55°C}$ = 232 ± 29 nm	$D_{h,55°C}$ = 140 ± 4 nm	$D_{h,55°C}$ = 218 ± 20 nm	$D_{h,55°C}$ = 214 ± 5 nm
	$D_{h,10°C}$ = 745 ± 58 nm	$D_{h,10°C}$ = 271 ± 6 nm	$D_{h,10°C}$ = 798 ± 67 nm	$D_{h,10°C}$ = 769 ± 41 nm
	SC5-0-E4	SC5-CTAB 4-E4	SC5-P 4-E4	SC5-PX$_{76}$ 4-E4
10		COAGULUM (35 wt-%)	COAGULUM (30 wt-%) [e]	STABLE
	-	$D_{h,55°C}$ = 628 ± 485 nm	$D_{h,55°C}$ = 197 ± 28 nm	$D_{h,55°C}$ = 215 ± 34 nm
		$D_{h,10°C}$ = 524 ± 183 nm	$D_{h,10°C}$ = 718 ± 13 nm	$D_{h,10°C}$ = 741 ± 84 nm
		SC10-CTAB 4-E4	SC10-P 4-E4	SC10-PX$_{76}$ 4-E4

[a] Reaction conditions: rpm = 300; reaction temperature = 70°C; reaction time = 4 h. The final conversion of VCL determined by ^{1}H NMR ranged between 96 and 100% for all experiments; [b] See experimental part ; [c] wt-% of coagulum = 100 × $m_{coagulum}/m_{VCL,0}$; [d] Experiment performed using non-reactive P(AETAC-X)$_{76,\ cleaved}$ as stabilizer; [e] Experiment performed using non-reactive P(AETAC) synthesized by free radical polymerization as stabilizer.

Microgel synthesized in the absence of either surfactant or stabilizer, at 1 wt-% of initial solids content (SC1-0-E4 in **Table 12**), undergoes flocculation upon cooling, *i.e.*, a reversible coagulation of the particles was observed when the dispersion was cooled down but the microgels were able to redisperse in the aqueous phase. For the microgel synthesized at 1 wt-% of initial solids content with CTAB surfactant (SC1-CTAB 4-E4 in **Table 12**), the average hydrodynamic diameter measured by DLS analysis was higher at 55°C than that at 10°C, traducing the formation of particle aggregates above the VPTT. For a dispersion of PVCL-based microgels stabilized by the non-reactive $P(AETAC\text{-}X)_{76,\ cleaved}$ polymer (SC1-$PX_{76,cleaved}$ 4-E4 in **Table 12**), a microgel flocculation is observed upon cooling of the dispersion, as for the microgels synthesized in the absence of stabilizer. For experiments carried out at 1 wt-% of initial solids content, stable PVCL-based microgels were obtained only with the reactive P(AETAC-X) as stabilizer (SC1-PX_{76} 4-E4 in **Table 12**).

Increasing the initial solids content up to 5 wt-% led to the formation of 50 to 65 wt-% of coagulum (*i.e.*, macroscopic precipitated polymer) for emulsion polymerization carried out in the absence of stabilizer or surfactant (SC5-0-E4 in **Table 12**) or for emulsion polymerization stabilized either by CTAB surfactant or by the non-reactive P(AETAC) macromolecular stabilizer (respectively SC5-CTAB 4-E4 and SC5-P 4-E4 in **Table 12**). On the other hand, for the all range of initial solids content (1 to 10 wt-%), stable PVCL-based microgels free of flocculation or coagulum were synthesized in the presence of the reactive $P(AETAC\text{-}X)_{76}$ as stabilizer (SC1-PX_{76} 4-E4, SC5-PX_{76} 4-E4 and SC10-PX_{76} 4-E4 in **Table 12**). These results highlight the key role played by the reactive xanthate chain-end of the cationic P(AETAC-X) in the stabilization of microgels, offering the opportunity to synthesize for the first time stable PVCL-based microgels up to 10 wt-% of initial solids content (SC10-PX_{76} 4-E4 in **Table 12**). Note that the degree of polymerization of the reactive polymer does not significantly impact the hydrodynamic diameters of the PVCL-based thermoresponsive microgels at both 10°C and 55°C nor the microgel final stability (see SC1-PX_{76} 4-E4, SC1-PX_{9} 4-E4 and SC5-PX_{76} 4-E4, SC5-PX_{9} 4-E4 in **Table 7**).

The improvement of the colloidal stability of the PVCL-based microgels synthesized using the P(AETAC-X) reactive stabilizers emphasizes a successful transfer of PVCL growing chains to the xanthate chain-end of P(AETAC-X) during the emulsion polymerization process. Such reversible transfer reaction should promote the *in-situ* formation of P(AETAC)-*b*-PVCL amphiphilic block copolymers. In order to highlight the presence of P(AETAC)-*b*-PVCL

amphiphilic block copolymers synthesized concomitantly to the microgels, the PVCL-based microgels SC1-PX_{76} 4-E4 and SC5-PX_{76} 4-E4 (**Table 7**) were centrifuged once in order to analyze the supernatants by diffusion ordered spectroscopy (DOSY) NMR. The presence of a single diffusion coefficient in the DOSY NMR spectra of the supernatants in D_2O, correlated with characteristic proton NMR signals of both types of units (signal *d* for AETAC, signal A, B, E, F, G for PVCL in **Figure 15**) revealed the effective formation of P(AETAC)-*b*-PVCL block copolymers.

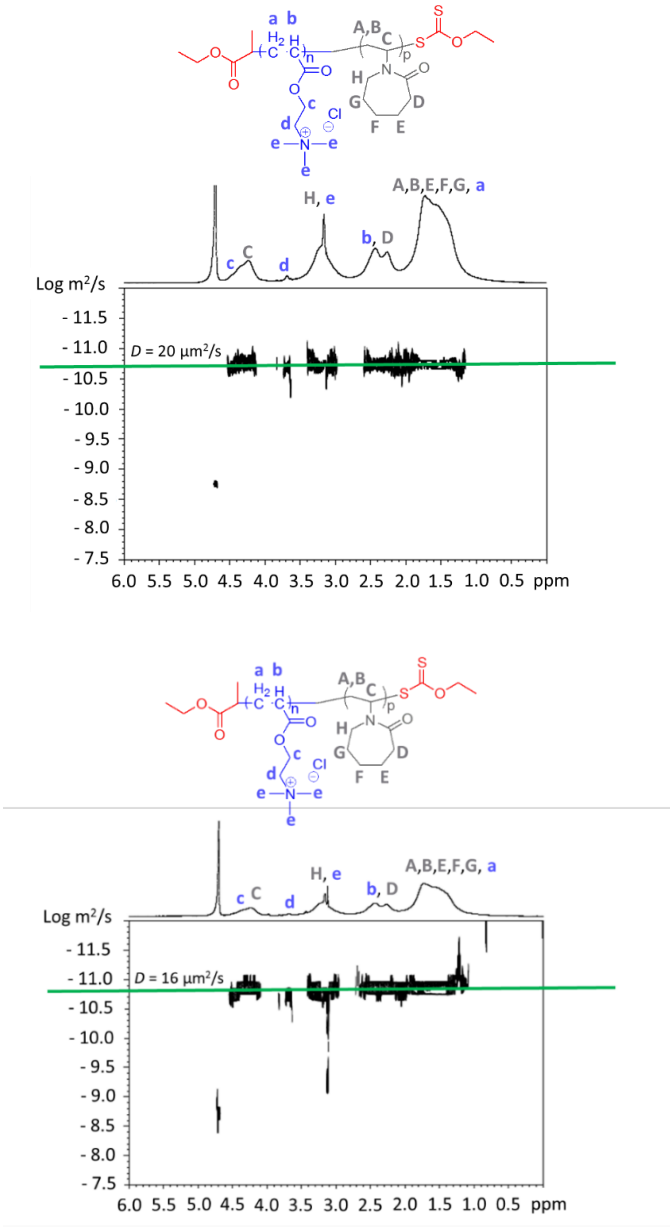

Figure 15. DOSY NMR spectra in D_2O of the supernatants recovered after centrifugation of the microgels synthesized using 4 wt-% of P(AETAC-X)$_{76}$ stabilizer based on VCL: (top spectrum) synthesis at 1 wt-% of initial solids content (SC1-PX_{76} 4-E4 in **Table 7**) and (bottom spectrum) synthesis at 5 wt-% of initial solids content (SC5-PX_{76} 4-E4 in **Table 7**).

Therefore, the *in-situ* formation of amphiphilic block copolymers gives rise to macromolecules with surface-active properties. As efficient transfer reaction between P(AETAC-X) and PVCL growing chains occurs, some P(AETAC) are prone to be covalently anchored onto the microgels (**Scheme 3**).

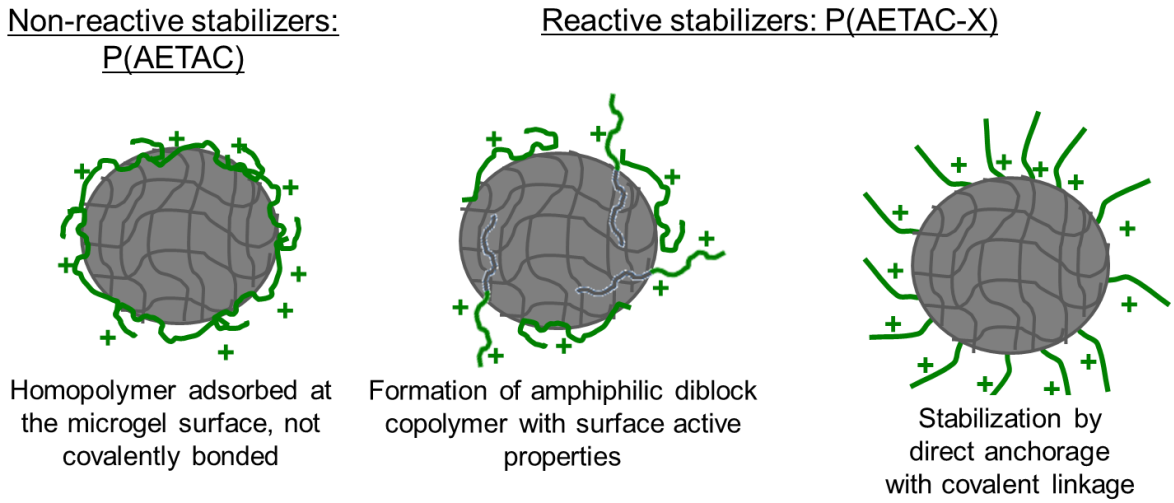

Scheme 3. Suggested stabilization modes of PVCL microgels by P(AETAC) cationic polymer.

Apart from the DOSY NMR analysis of the supernatants recovered after microgel centrifugation, a series of VCL emulsion polymerizations were carried out in the presence of P(AETAC-X) but in the absence of EGDMA crosslinker. The DOSY NMR analysis of the final polymers indicated that the diblock copolymers are probably not synthesized in the early stage of the polymerization for VCL conversion below 30%. However, due to the small weight fraction of P(AETAC-X) stabilizer with respect to that of VCL, the characteristic ^{1}H NMR signal of P(AETAC-X) polymer is likely difficult to detect for intermediate monomer conversion as the intensity of the PVCL proton signals rapidly predominates. For reasons of clarity, these results are presented in the Appendix of Chapter 2, together with a study investigating the persistence of the P(AETAC-X) shell for microgels subjected to three centrifugations.

IV. Conclusions

In this chapter, the efficiency of the reactive cationic macromolecular chain-transfer agents synthesized by RAFT/MADIX polymerization to act as stabilizers for the synthesis of cationic thermoresponsive poly(*N*-vinylcaprolactam)-based microgels by a heterogeneous polymerization process in aqueous media was thoroughly investigated. The first step of this

work consisted in optimizing the experimental conditions, *i.e.*, to set the most suitable content of buffer and initiator, the reaction temperature and the minimum amount of P(AETAC-X) reactive stabilizer to synthesize stable microgel dispersions. Once assessed these optimal experimental conditions, the effect of various synthesis variables on the final number of particles was studied. The final number of particles was influenced by the amount of P(AETAC-X) stabilizer, the EGDMA crosslinker and the chain length of the reactive P(AETAC-X) stabilizer, all these experimental variables playing a role on the nucleation period.

Stable and monodisperse PVCL-based microgels could be obtained using reactive P(AETAC-X) as macromolecular stabilizers. These microgels exhibited a thermoresponsive behavior with a volumetric shrinkage upon heating. The volume phase transition temperature (VPTT) ranged between 28 °C and 30°C for the microgels synthesized using 4 and 8 wt-% of P(AETAC-X) based on VCL. The increase of the microgel electrophoretic mobility when increasing the amount of P(AETAC-X) stabilizer highlighted the interest of using a reactive macromolecular stabilizer to design PVCL-based thermoresponsive microgels with functional cationic macromolecular shell. The swelling behavior of the microgel particles can be tuned by playing with different synthesis variables such as the initial solids content, the amounts of P(AETAC-X) stabilizer and EGDMA crosslinker. While an increase of the amount of EGDMA induced a broadening of the volume phase transition by playing a role on the inner structure of the network, the P(AETAC-X) stabilizer appeared to affect the network swelling via the polyelectrolyte outer shell. Increasing the initial solids content in the recipe produced a drastic increase of the particle diameters at the swollen state (10°C), and thus an increase of the particle swelling ratios, probably due to the higher amount of PVCL chains per particle.

According to the partial VCL and crosslinker conversions monitored by ^{1}H NMR spectroscopy, the formation of microgels with a core-shell type structure was expected since EGDMA crosslinker was consumed very fast in the early stage of polymerization. Proton high-resolution transverse relaxation NMR measurements confirmed the core-shell morphology of the microgels, with a core twice more crosslinked than the shell.

Finally, the improved stabilization efficiency of reactive P(AETAC-X) polymers was highlighted by comparing the colloidal features of the obtained microgels with those synthesized by using either non-reactive P(AETAC) polymers as stabilizers or a conventional cationic molecular surfactant (CTAB). Experiments were also conducted in the absence of

surfactant or stabilizer. For the all range of initial solids contents (τ = 1 to 10 wt-%), stable PVCL-based microgels were synthesized in the presence of the reactive xanthate functionalized P(AETAC-X)$_{76}$ stabilizer while particle flocculation or coagulation were observed during emulsion polymerization using the other stabilizers. These results highlighted the key role played by the reactive xanthate chain-end in the colloidal stabilization of microgels during the polymerization process. The involvement of this reactive chain-end in the microgel growing step was also suggested by the effect of the fraction of P(AETAC-X) on the final number of particles, on the microgel hydrodynamic diameters at swollen state, on the content of free chains and on the value of microgel electrophoretic mobility. Taking advantage of this aspect, stable PVCL-based microgels with robust colloidal features were synthesized for the first time up to a 10 wt-% of initial solids content.

V. References

1. Gil, E.; Hudson, S. *Progress in Polymer Science* **2004,** 29, (12), 1173-1222.
2. Stuart, M. A.; Huck, W. T.; Genzer, J.; Muller, M.; Ober, C.; Stamm, M.; Sukhorukov, G. B.; Szleifer, I.; Tsukruk, V. V.; Urban, M.; Winnik, F.; Zauscher, S.; Luzinov, I.; Minko, S. *Nature materials* **2010,** 9, (2), 101-13.
3. Hoffman, A. S. *Advanced drug delivery reviews* **2013,** 65, (1), 10-6.
4. de Las Heras Alarcon, C.; Pennadam, S.; Alexander, C. *Chemical Society reviews* **2005,** 34, (3), 276-85.
5. Schmaljohann, D. *Advanced drug delivery reviews* **2006,** 58, (15), 1655-70.
6. Saunders, B. R.; Laajam, N.; Daly, E.; Teow, S.; Hu, X.; Stepto, R. *Advances in colloid and interface science* **2009,** 147-148, 251-62.
7. Liu, G.; An, Z. *Polym. Chem.* **2014,** 5, (5), 1559-1565.
8. Vinogradov, S. V. *Nanomedicine* **2010,** 5, (2), 165-8.
9. Motornov, M.; Roiter, Y.; Tokarev, I.; Minko, S. *Progress in Polymer Science* **2010,** 35, (1-2), 174-211.
10. Oh, J. K.; Drumright, R.; Siegwart, D. J.; Matyjaszewski, K. *Progress in Polymer Science* **2008,** 33, (4), 448-477.
11. Kabanov, A. V.; Vinogradov, S. V. *Angewandte Chemie* **2009,** 48, (30), 5418-29.
12. Smeets, N. M. B.; Hoare, T. *Journal of Polymer Science Part A: Polymer Chemistry* **2013,** 51, (14), 3027-3043.
13. Ramos, J.; Forcada, J.; Hidalgo-Alvarez, R. *Chemical reviews* **2014,** 114, (1), 367-428.
14. Lyon, L. A.; Meng, Z.; Singh, N.; Sorrell, C. D.; St John, A. *Chemical Society reviews* **2009,** 38, (4), 865-74.
15. Kawaguchi, H. *Polymer International* **2014,** 63, (6), 925-932.
16. Raemdonck, K.; Demeester, J.; De Smedt, S. *Soft Matter* **2009,** 5, (4), 707-715.
17. Hertle, Y.; Hellweg, T. *Journal of Materials Chemistry B* **2013,** 1, (43), 5874.
18. Ramos, J.; Imaz, A.; Forcada, J. *Polym. Chem.* **2012,** 3, (4), 852-856.

19. Liu, J.; Debuigne, A.; Detrembleur, C.; Jerome, C. *Advanced healthcare materials* **2014,** 3, (12), 1941-68.
20. Laukkanen, A.; Hietala, S.; Maunu, S. L.; Tenhu, H. *Macromolecules* **2000,** 33, (23), 8703-8708.
21. Vihola, H.; Laukkanen, A.; Hirvonen, J.; Tenhu, H. *European Journal of Pharmaceutical Sciences* **2002,** 16, (1-2), 69-74.
22. Laukkanen, A.; Wiedmer, S. K.; Varjo, S.; Riekkola, M. L.; Tenhu, H. *Colloid & Polymer Science* **2002,** 280, (1), 65-70.
23. Pich, A.; Boyko, V.; Lu, Y.; Richter, S.; Adler, H. J.; Arndt, K. F. *Colloid & Polymer Science* **2003,** 281, (10), 916-920.
24. Boyko, V.; Richter, S.; Pich, A.; Arndt, K.-F. *Colloid & Polymer Science* **2003,** 282, (2), 127-132.
25. Schachschal, S.; Balaceanu, A.; Melian, C.; Demco, D. E.; Eckert, T.; Richtering, W.; Pich, A. *Macromolecules* **2010,** 43, (9), 4331-4339.
26. Pich, A.; Berger, S.; Ornatsky, O.; Baranov, V.; Winnik, M. a. *Colloid Polym. Sci.* **2008,** 287, 269-275.
27. Balaceanu, A.; Verkh, Y.; Demco, D. E.; Möller, M.; Pich, A. *Macromolecules* **2013,** 46, (12), 4882-4891.
28. Imaz, A.; Forcada, J. *Journal of Polymer Science Part A: Polymer Chemistry* **2008,** 46, (7), 2510-2524.
29. Imaz, A.; Forcada, J. *Journal of Polymer Science Part A: Polymer Chemistry* **2008,** 46, (8), 2766-2775.
30. Imaz, A.; Forcada, J. *Macromolecular Symposia* **2009,** 281, (1), 85-88.
31. Imaz, A.; Forcada, J. *European Polymer Journal* **2009,** 45, (11), 3164-3175.
32. Imaz, A.; Forcada, J. *Journal of Polymer Science Part A: Polymer Chemistry* **2011,** 49, (14), 3218-3227.
33. Aguirre, G.; Ramos, J.; Forcada, J. *Soft Matter* **2013,** 9, (1), 261-270.
34. Medeiros, S. F.; Oliveira, P. F. M.; Silva, T. M.; Lara, B. R.; Elaissari, A.; Santos, A. M. *European Polymer Journal* **2015,** 73, 191-201.
35. Sudhakar, K.; Madhusudana Rao, K.; Subha, M. C. S.; Chowdoji Rao, K.; Sadiku, E. R. *Designed Monomers and Polymers* **2015,** 18, (8), 705-713.
36. Wang, Y.; Nie, J.; Chang, B.; Sun, Y.; Yang, W. *Biomacromolecules* **2013,** 14, (9), 3034-46.
37. Wang, Y.; Zheng, J.; Tian, Y.; Yang, W. *J. Mater. Chem. B* **2015,** 3, (28), 5824-5832.
38. Berger, S.; Singh, R.; Sudha, J. D.; Adler, H.-J.; Pich, A. *Polymer* **2010,** 51, (17), 3829-3835.
39. Wu, D. Q.; Chu, C. C.; Chen, F. A. *Journal of materials science. Materials in medicine* **2008,** 19, (12), 3593-601.
40. Demirel, G. B.; von Klitzing, R. *Chemphyschem : a European journal of chemical physics and physical chemistry* **2013,** 14, (12), 2833-40.
41. Pich, A.; Tessier, A.; Boyko, V.; Lu, Y.; Adler, H.-J. P. *Macromolecules* **2006,** 39, (22), 7701-7707.
42. Bhattacharya, S.; Eckert, F.; Boyko, V.; Pich, A. *Small* **2007,** 3, (4), 650-7.
43. Hu, X.; Tong, Z.; Lyon, L. A. *Colloid Polym Sci* **2010,** 289, (3), 333-339.
44. Hoare, T.; Pelton, R. *The journal of physical chemistry. B* **2007,** 111, (41), 11895-906.
45. An, Z.; Shi, Q.; Tang, W.; Tsung, C. K.; Hawker, C. J.; Stucky, G. D. *Journal of the American Chemical Society* **2007,** 129, (46), 14493-9.

46. Rieger, J.; Grazon, C.; Charleux, B.; Alaimo, D.; Jérôme, C. *Journal of Polymer Science Part A: Polymer Chemistry* **2009,** 47, (9), 2373-2390.
47. Grazon, C.; Rieger, J.; Sanson, N.; Charleux, B. *Soft Matter* **2011,** 7, (7), 3482.
48. Delaittre, G.; Save, M.; Charleux, B. *Macromolecular rapid communications* **2007,** 28, (15), 1528-1533.
49. Liu, G.; Qiu, Q.; Shen, W.; An, Z. *Macromolecules* **2011,** 44, (13), 5237-5245.
50. Liu, G.; Qiu, Q.; An, Z. *Polym. Chem.* **2012,** 3, (2), 504-513.
51. Bhuchar, N.; Sunasee, R.; Ishihara, K.; Thundat, T.; Narain, R. *Bioconjugate chemistry* **2012,** 23, (1), 75-83.
52. Ahmed, M.; Wattanaarsakit, P.; Narain, R. *Polymer Chemistry* **2013,** 4, (13), 3829.
53. Kotsuchibashi, Y.; Narain, R. *Polymer Chemistry* **2014,** 5, (8), 3061.
54. Balaceanu, A.; Demco, D. E.; Möller, M.; Pich, A. *Macromolecules* **2011,** 44, (7), 2161-2169.
55. Pikabea, A.; Aguirre, G.; Miranda, J. I.; Ramos, J.; Forcada, J. *Journal of Polymer Science Part A: Polymer Chemistry* **2015,** 53, (17), 2017-2025.
56. Ilavský, M.; Mamytbekov, G.; Sedláková, Z.; Hanyková, L.; Dušek, K. *Polymer Bulletin* **2001,** 46, (1), 99-106.
57. Imaz, A.; Miranda, J. I.; Ramos, J.; Forcada, J. *European Polymer Journal* **2008,** 44, (12), 4002-4011.
58. Brandrup, J.; Immergut, E. H.; Grulke, E. A., *Polymer Handbook, 4th Edition*. John Wiley & Sons: 2003; p 2336.
59. Aguirre, G.; Ramos, J.; Heuts, J. P. A.; Forcada, J. *Polymer Chemistry* **2014,** 5, (15), 4569.
60. Boularas, M.; Deniau-Lejeune, E.; Alard, V.; Tranchant, J.-F.; Billon, L.; Save, M. *Polym. Chem.* **2016,** 7, (2), 350-363.
61. von Nessen, K.; Karg, M.; Hellweg, T. *Polymer* **2013,** 54, (21), 5499-5510.
62. Nolan, C. M.; Reyes, C. D.; Debord, J. D.; Garcia, A. J.; Lyon, L. A. *Biomacromolecules* **2005,** 6, (4), 2032-9.
63. Boularas, M.; Gombart, E.; Tranchant, J. F.; Billon, L.; Save, M. *Macromolecular rapid communications* **2015,** 36, (1), 79-83.
64. Kozanoğlu, S.; Özdemir, T.; Usanmaz, A. *Journal of Macromolecular Science, Part A* **2011,** 48, (6), 467-477.
65. Quesada-Pérez, M.; Maroto-Centeno, J. A.; Forcada, J.; Hidalgo-Alvarez, R. *Soft Matter* **2011,** 7, (22), 10536.
66. Schroeder, R.; Rudov, A. A.; Lyon, L. A.; Richtering, W.; Pich, A.; Potemkin, I. I. *Macromolecules* **2015,** 48, (16), 5914-5927.
67. Rzaev, Z. M. O.; Dinçer, S.; Pişkin, E. *Progress in Polymer Science* **2007,** 32, (5), 534-595.
68. Jones, C. D.; Lyon, L. A. *Macromolecules* **2003,** 36, (6), 1988-1993.
69. Rubio-Retama, J.; Zafeiropoulos, N. E.; Serafinelli, C.; Rojas-Reyna, R.; Voit, B.; Lopez Cabarcos, E.; Stamm, M. *Langmuir* **2007,** 23, (20), 10280-10285.

Acknowledgments

Dr. Josetxo Ramos from Bionanoparticles group-POLYMAT is thanked for his help and fruitful discussions. Dr. Garbiñe Aguirre, Dr. Aintzane Pikabea and Dr. Marta Vicario de la Torre are acknowledged for their help with DLS analyses on the MALVERN zetasizer available at Bionanoparticles group-POLYMAT. Dr. José Ignacio Miranda Murua from POLYMAT is thanked for 1H transverse relaxation (T2) NMR measurements. TEM analyses were performed by Patricia Beaunier (UPMC, Paris).

PART II - CHAPTER 3. Cationic thermoresponsive poly(*N*-vinylcaprolactam)-based microgels as potential drug delivery nanocarriers

I. Introduction

As mentioned in the introduction of Part II, cationic thermoresponsive PVCL-based microgels gather interesting features for application as drug delivery systems (DDS). The objective of the work reported in this Chapter 3 was to evaluate the potential use of the cationic PVCL-based microgels obtained in Part II - Chapter 2 of this manuscript for biomedical applications. For that purpose, various experiments were carried out. First of all, the stability of the cationic PVCL-based microgels during incubation at 37°C in different biological mimicking media was assessed. The *in-vitro* cytotoxicity of bare PVCL-based microgels on HeLa (cervical cancerous cells) and RAW 264.7 (macrophage healthy cells) cell lines was then evaluated at different microgel concentrations and incubation times. Subsequently, the cellular uptake of the cationic PVCL-based microgels was visualized by confocal microscopy after 3 and 24 h of incubation when corresponding. The internalization mechanism of microgels into HeLa cells were investigated by means of inhibition uptake experiments. Finally, PVCL-based microgels were subsequently loaded with a model anticancer drug (doxorubicin, DOXO) in order to test their potential use as chemotherapeutic drug delivery systems for cancer treatment. After determining the amount of drug effectively loaded into the microgels, the drug release profiles of selected microgels were assessed. Finally, the cytotoxicity of the DOXO-loaded microgels on HeLa and RAW cell lines was studied.

The experiments presented in this Chapter were performed during my stay for one month in the Colloids and Polymer Physics Group (GFCP) of the Universidade de Santiago de Compostela, under the kind collaboration of Professor Pablo Taboada and Miss Eva Villar-Alvarez.

II. Experimental part

1. Materials

1.i. Microgels used in this work

Various PVCL-based microgels were synthesized by batch emulsion polymerization of *N*-vinylcaprolactam (VCL) using ethylene glycol dimethacrylate (EGDMA) as crosslinker and a poly[2-(acryloyloxy)ethyl]trimethylammonium chloride ($P(AETAC\text{-}X)_n$) cationic reactive polymer as stabilizer (**Scheme 1**). The detailed synthesis and characterization of the cationic thermoresponsive PVCL-based microgels are presented in Chapter 2 of Part II.

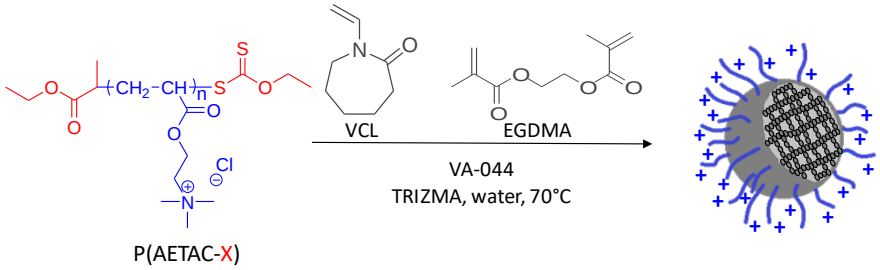

Scheme 1. Synthesis of cationic thermoresponsive PVCL-based microgel.

1.ii. Reagents and cell lines

Dulbecco's Modified Eagle's Medium (DMEM), Dulbecco's Modified Eagle's Medium/Nutrient Mixture F-12 Ham (DMEM/F-12), sodium pyruvate solution (100 mM) and non-essential amino acid solution were purchased from Life Sciences. Fetal Bovine Serum (FBS), Cell Counting Kit-8 (CCK-8), chlorpromazine hydrochloride (98 %), phosphate buffered saline (PBS, 10× concentrate, BioPerformance Certified, suitable for cell culture), triton X-100, doxorubicin hydrochloride (98-102 %, **Scheme 2**) and fluorescent dye rhodamine 6G (R6G, red, 99 %, **Scheme 2**) were obtained from Sigma Aldrich. Trypsin-EDTA (0.25 %), phenol red and penicillin-streptomycin (10,000 U/mL) were supplied by Gibco, ThermoFisher Scientific. D (+)-Sucrose (99 %, RNAse and DNAse free) was obtained from Acros Organics. Paraformaldehyde was acquired from Fisher Scientific. 4'-6-diamidino-2-phenylindole dihydrochloride, ProLong Gold antifade (DAPI, blue) was supplied by Invitrogen.

Cervical cancer HeLa cell line was obtained from Cell Biolabs and RAW 264.7 cell line from ATCC, Manassas, Virginia.

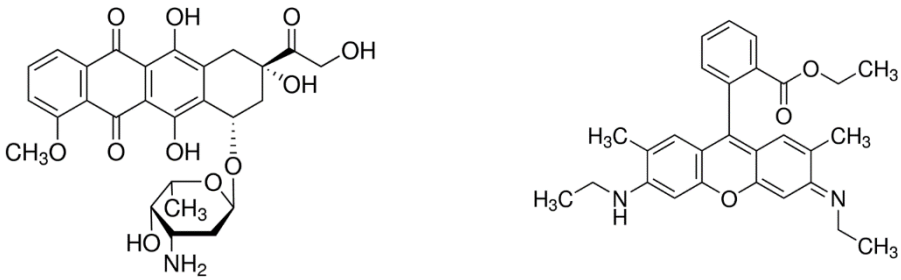

Scheme 2. Chemical structure of doxorubicin hydrochloride (left) and rhodamine 6G (right).

2. Methods

2.i. Cell culture

The cervical HeLa cancer cell line was grown in a medium composed of DMEM, 1 v/v % penicillin-streptomycin, 1 v/v % sodium pyruvate, 1 v/v % amino acid and 10 v/v % of FBS. The same medium was used for the growth of RAW cell line but DMEM/F-12 was used instead of DMEM. Both cell lines were grown in an 5 % CO_2-95 % air atmosphere at 37°C. After attaining 80-90 % confluence, cells were harvested using trypsin (0.25 %)-EDTA. Cell count was conducted using an automated cell counter (Multisizer 3 Beckman Coulter Cell Counter).

2.ii. Colloidal stability of bare PVCL-based microgels in biological mimicking media

The colloidal stability of bare PVCL-based microgels was tested at 37°C under slow stirring for 13 days, by dilution of the samples (0.05 $mg.mL^{-1}$) in different biological mimicking media: cell culture medium (DMEM) supplemented with 10 % FBS (pH 8.4), PBS (pH 7.4) and PBS supplemented with 10 % FBS (pH 7.4). Stability of the microgels was also assessed in water, following the same procedure. The changes in microgel sizes during different incubation times were recorded by dynamic light scattering, DLS, using a Zetasizer Nano ZS instrument (Malvern Instruments). Samples were allowed to equilibrate at 37°C for 2 min before analysis.

2.iii. Doxorubicin loading and release

Microgel dispersions at 2 $mg.mL^{-1}$ in water and a DOXO solution at 1 $mg.mL^{-1}$ in water were prepared and heated to 37°C using an oil-bath. Then, 500 µL of the microgel dispersion and 100 µL of the DOXO solution were mixed together at 37°C for 5 min and then the mixture was kept at 4°C for 24 h. Subsequently, microgel particles were separated from the aqueous solution containing free DOXO through centrifugation for 1 h at 15 000 rpm and 15°C. Supernatants were collected, kept away from light and analyzed by UV-Vis spectroscopy at 488 nm (Cary 50 spectrophotometer, Agilent Technologies, Germany) in order to determine the amount of encapsulated DOXO. A previously obtained calibration curve for DOXO in water was used ($Abs_{DOXO,\ 488\ nm} = 19.691 \times [DOXO] + 0.027$, with [DOXO]: DOXO concentration in $mg.mL^{-1}$). Drug loading (D.L.) and entrapment efficiency (E.E.) were calculated using the following equations.

$$D.L.\% = \frac{weight\ of\ the\ drug\ in\ nanogel\ dispersion\ (mg)}{weight\ of\ polymer + weight\ of\ the\ drug\ in\ nanogel\ dispersion\ (mg)} \times 100 \quad \text{Equation 1}$$

$$E.E.\% = \frac{weight\ of\ the\ drug\ in\ nanogel\ dispersion\ (mg)}{weight\ of\ feeding\ drug\ (mg)} \times 100 \quad \text{Equation 2}$$

The in-vitro release of DOXO from selected microgels (1 mg.mL^{-1}) was assessed by a dialysis method. DOXO-loaded SC1-PX$_{76}$ 4-E4, SC1-PX$_{76}$ 8-E8 and SC1-PX$_{9}$ 4-E4 microgel dispersions were dialyzed at 37 °C against two different serum-containing (10 % (v/v) FBS) buffer solutions: sodium acetate/acetic acid (SA) buffer solution (pH 5.5) and phosphate buffer saline (PBS) solution (pH 7.4). The DOXO release concentration in the release medium was determined spectrophotometrically at 480 nm. All experiments were performed in triplicate.

2.iv. In vitro cell cytotoxicity assays

Cytotoxicity of bare PVCL-based microgels was evaluated on cervical HeLa and RAW 264.7 cell lines utilizing the Cell Counting Kit-8 (CCK-8) cytotoxicity assay.[1, 2] Both cell lines were seeded in 96 well-plates at a density of 5000 cells per well in 100 µL of growth medium and allowed to grow for 24 h at 37°C. Then, the medium was removed and cells were exposed to 100 µL of various concentrations of cationic poly(*N*-vinylcaprolactam)-based microgels (Test 1: [Microgel] = 0.005; 0.05; 0.1; 0.25; 0.5 and 1 mg.mL^{-1} - Test 2: [Microgel] = 0.5; 1; 2; 3.5; 5 and 10 mg.mL^{-1}) dispersed in growing media for further incubation at 37°C in a 5 % CO_2 atmosphere for 24 and 48 h. After incubation, 10 % CCK-8 solution per well was added and incubated for 1 h for RAW cell line and 90 min for HeLa cell line. The absorbance of viable cells was subsequently measured at 450 nm using an UV-Vis microplate absorbance reader (Microplate Manager 5.0, Bio-Rad Laboratories, USA). The non-treated cells served as a 100 % cell viability control (blank). Survival percentage or cell viability was calculated as follow:

$$\%\ Cell\ viability = \frac{Abs_{treated\ cells} - Abs_{microgel}}{Abs_{untreated\ cells}} \times 100 \quad \text{Equation 3}$$

where $Abs_{treated\ cells}$ is the absorbance at 450 nm of cells incubated in the presence of microgels, and $Abs_{untreated\ cells}$ is the absorbance at 450 nm of control cells in the absence of microgel particles. The absorbance of microgels at 450 nm was substracted to the absorbance of treated cells for each microgel concentration.

The same procedure was followed to study the DOXO-loaded microgel cytotoxicity on RAW and HeLa cell lines after 24 h of incubation. Cells were exposed to various concentrations of DOXO-loaded microgels: [DOXO-loaded microgel] = 2; 1; 0.5; 0.25 and 0.1 mg.mL^{-1}.

2.v.Cellular uptake by fluorescence microscopy

Prior to the cellular uptake experiments, the microgels were labeled with rhodamine 6G (λ_{exc} = 530 nm) according to the following procedure. Microgel dispersions at 1 mg.mL^{-1} in water and a solution of rhodamine 6G at 10 mg.mL^{-1} also in water were prepared and heated to 37°C in an oil-bath. Then, 1 mL of the microgel dispersion and 400 µL of the rhodamine solution were mixed together at 37°C and the mixture was kept at 4°C for 24 h. Subsequently, microgel particles were separated from the aqueous solution containing free R6G through four successive centrifugations for 1 h at 15 000 rpm and 15°C. After centrifugations, the resulting pellet was re-dispersed in cell culture medium at the desired concentration. As a concentrated solution of R6G in water (10 mg.mL^{-1}) was used, several centrifugations were required to separate the R6G-loaded microgels from free R6G.

The cellular uptake of R6G-loaded microgels was followed by confocal fluorescence microscopy. HeLa cells were seeded on poly-(L-lysine) coated glass coverslips (12 × 12 mm) placed inside 6 well-plates (15 × 10^4 cells/well with 3 mL of DMEM), and allowed to grow for 24 h at standard culture conditions. The growth medium was then removed, and 500 µL of a dispersion of R6G-loaded microgels in DMEM at a concentration of 0.5 mg.mL^{-1} and 2.5 mL of DMEM were added to each well. Cells were then incubated for 3 and 24 h. For energy-dependent uptake experiments at 4°C, cells were pre-incubated at 4°C with serum-free DMEM for 1 h, followed by incubation with 500 µL of R6G-loaded microgel dispersions in serum-free DMEM (at a concentration of 0.5 mg.mL^{-1}) at the same temperature for 3 h. To inhibit a specific uptake mechanism of microgels into cells, these were pre-incubated with the following inhibitors individually for 1 h at 37°C: 400 mM hypertonic sucrose, 30 µM chlorpromazine, 30 µM cytochalasin and 30 µM nystatin. After the pre-incubation time, the inhibitor solutions were removed and the freshly prepared R6G-loaded microgel dispersed (at a concentration of 0.5 mg.mL^{-1}) in media containing inhibitor at the same concentrations were added and further incubated for 3 h at 37°C. In this study, cells incubated for 3 h at 37°C in the presence of R6G-loaded microgel and in the absence of inhibitor were used as controls.

For all the experiments described above, after the desired incubation times cell culture media were removed and the microgel-containing cells were washed three times with PBS (pH 7.4), fixed for 10 minutes with a solution of paraformaldehyde at 4 w/v % in PBS, washed with PBS, treated for 10 minutes with a solution of Triton X-100 (permeabilizer) at 0.25 (w/v) % in PBS and, finally, washed again with PBS. Coverslips were mounted on glass slides and cell nuclei

were stained with 4'-6-diamidino-2-phenylindole dihydrochloride (DAPI, blue). The samples were cured at - 20°C for 24 h before being visualized with an 63X oil-immersion objective using an inverted wide field fluorescence microscope (Leica DMI6000B, Leica Microsystems, Germany) with the blue channel for DAPI-stained cell nuclei (λ_{exc} = 355 nm), the red channel for R6G (λ_{exc} = 590 nm) and the transmitted light channel in differential interference contrast (DIC) mode.

III. Results and discussion

1. Physico-chemical features of the cationic PVCL-based microgels

The physico-chemical features of the cationic thermoresponsive PVCL-based microgels synthesized in Chapter 2 – Part II and evaluated as drug delivery systems are gathered in **Table 1**. These microgels dispersed in water will be named "bare microgels" in the following work.

Table 1. Physico-chemical features of the cationic PVCL-based microgels (name as bare microgel) in aqueous solution.

Reaction[a]	$D_{h,55°C}$[b] *nm*	$D_{h,10°C}$[b] *nm*	**VPTT**[c] *°C*	**Dialyzed sample electrophoretic mobility**[d] $m^2/Vs \times 10^{-8}$
SC1-PX_{76} 4-E4	156 ± 1	313 ± 2	29.1 ± 0.6	0.42 ± 0.05
SC1-PX_{76} 8-E4	144 ± 2	233 ± 5	31.0 ± 0.6	0.95 ± 0.17
SC5-PX_{76} 4-E4	210 ± 1	734 ± 6	30.9 ± 0.0	0.57 ± 0.25
SC10-PX_{76} 4-E4	185 ± 3	813 ± 23	32.3 ± 0.6	0.88 ± 0.44
SC1-PX_{76} 8-E8	117 ± 1	150 ± 0	27.5 ± 2.3	ND[e]
SC5-PX_{76} 8-E4	200 ± 5	673 ± 20	29.8 ± 1.0	1.22 ± 0.04
SC5-PX_{9} 4-E4	199 ± 1	630 ± 8	30.5 ± 1.3	0.38 ± 0.18
SC1-PX_{9} 4-E4	154 ± 1	345 ± 5	30.0 ± 0.7	0.44 ± 0.16
SC1-PX_{16} 4-E4	192 ± 1	365 ± 2	28.4 ± 0.3	ND[e]
SC1-PX_{16} 12-E4	161 ± 1	164 ± 4	-	ND[e]

[a] Reaction name according to the nomenclature used in Chapter 2 – Part II: SC for initial solids content, the number following indicates the wt-% of VCL based on water - PX_n : reactive cationic polymeric stabilizer with *n* the degree of polymerization, the number following indicates the wt-% of stabilizer based on VCL - E : EGDMA crosslinker, the number following indicates the wt-% of EGDMA based on VCL; [b] Hydrodynamic diameters measured in water; [c] Volume Phase Transition Temperature of the microgel; [d] Electrophoretic mobility of the final microgel, measured at 0.5 $mg.mL^{-1}$ of microgels content in cationic buffer at pH 3 and 10 mM ionic strength; [e] ND: not determined.

2. Colloidal stability of bare PVCL-based microgels in biological mimicking media

For biomedical applications, the stability of a particle in biological media is of high importance since its particle size can affect its biodistribution and cell internalization and fate.[3, 4]

In this work, the colloidal stability of the different bare microgels was tested at 37°C under slow stirring for 13 days. Microgels were dispersed (at 0.05 mg.mL^{-1}) either in water (pH 6.5) or in three different biological mimicking media: i) PBS (pH 7.4), ii) PBS supplemented with 10 % FBS (pH 7.4), iii) cell culture medium (DMEM, pH 8.4) supplemented with 10 % FBS. PBS and PBS supplemented with FBS simulate somehow physiological mimicking serum conditions of increasing complexity whereas DMEM supplemented with FBS corresponds to the cell culture medium used for the *in-vitro* studies (cytotoxicity and cell internalization). The hydrodynamic diameters of the microgels were monitored for 13 days of incubation (**Figure 1**).

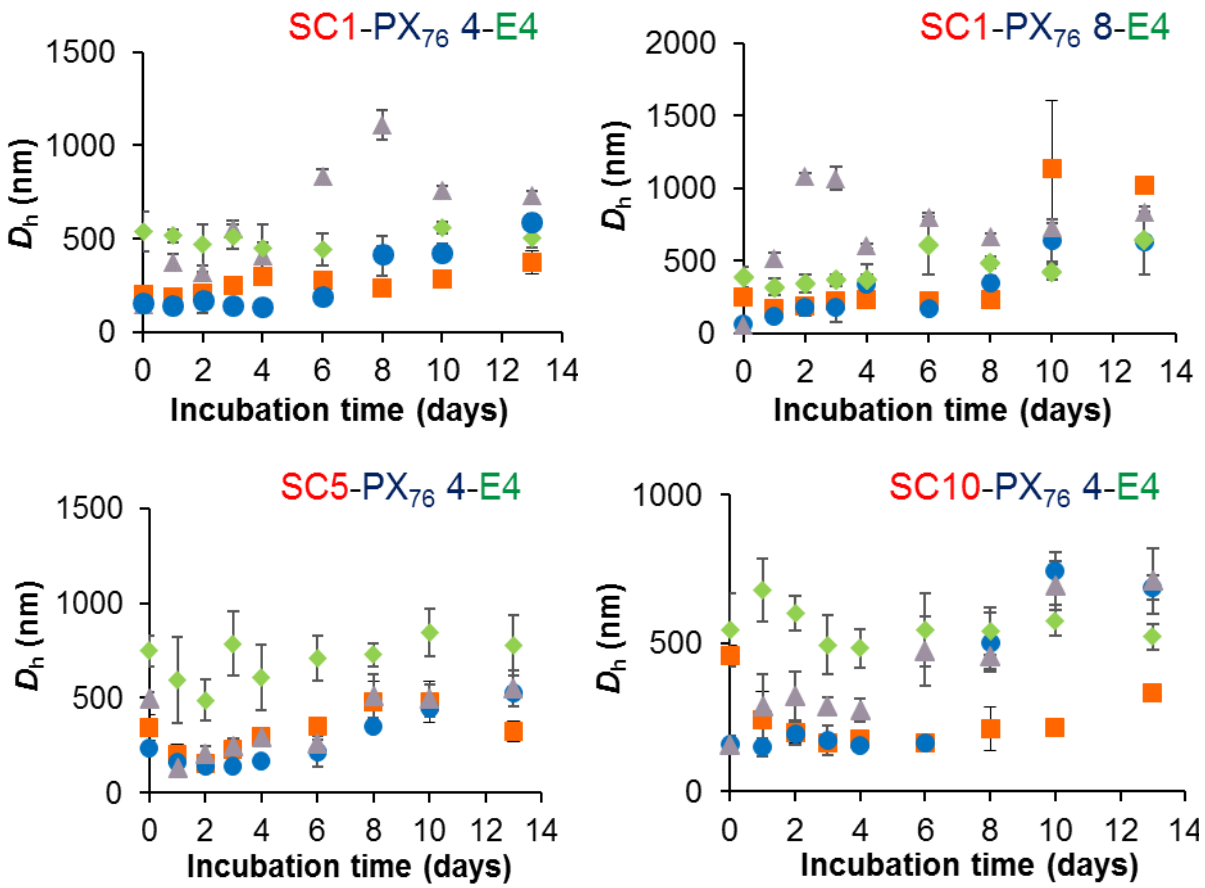

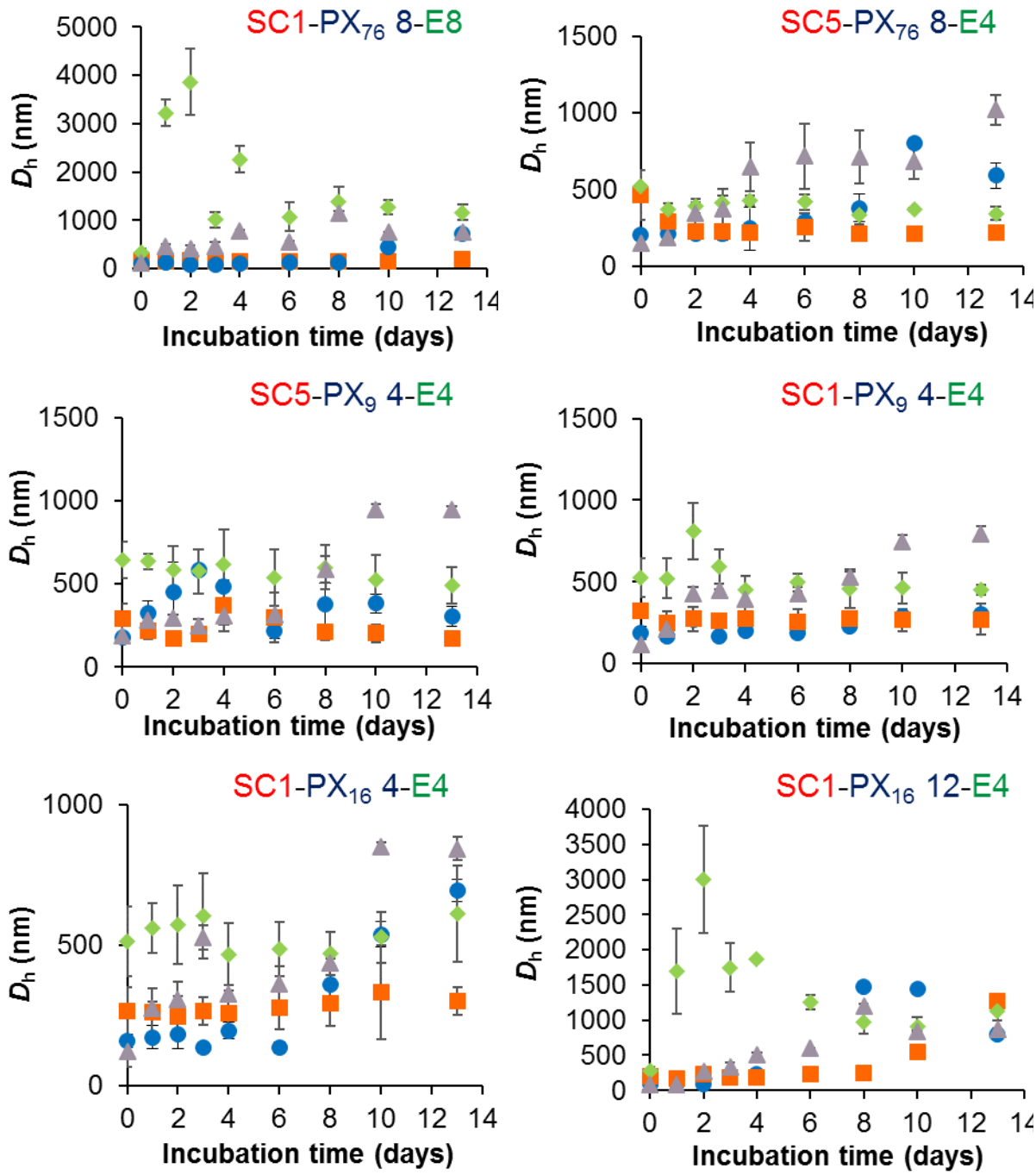

Figure 1. Temporal evolution of the hydrodynamic diameter of bare microgels at 37°C, in: (■) water, (●) cell culture medium DMEM + 10 % FBS, (◆) PBS and (▲) PBS + 10 % FBS.

In water, all microgels remained stable since their hydrodynamic diameters were almost constant during the whole incubation (13 days at 37°C). In contrast, an obvious increase of the microgel hydrodynamic diameter at the beginning of incubation was systematically observed in PBS buffer revealing a certain lack of stability. Since the ionic strength of PBS buffer is around 150 mM, the increase of the microgel hydrodynamic diameter values could be explained

by the formation of aggregates due to the ionic screening of the particle electrical charges. Indeed, the reduction of the particle surface charges might lead to the microgel destabilization by decreasing the electrostatic repulsions between particles. The salt effect on microgel stability was studied for SC5-PX$_{76}$ 4-E4 microgel in aqueous phase at different concentrations of KBr ranging from 10 mM to 100 mM. An increase of the microgel hydrodynamic diameters was observed above the microgel VPTT, suggesting the formation of aggregates (**Figure 2**). Such colloidal instability and aggregation of positively charged carriers in fluids at high salt concentration is a well-known process, being one of the main drawbacks for their use as gene delivery systems.[5, 6] It should be noted that the aggregation of the cationic PVCL-based microgels is observed at their collapsed state (T > 30°C) but a similar value of D_h was measured at low temperature (swollen state) whatever the salt concentration (**Figure 2**). The screened cationic polyelectrolyte doesn't provide a sufficient protective layer against the hydrophobic interaction of the collapsed microgels.

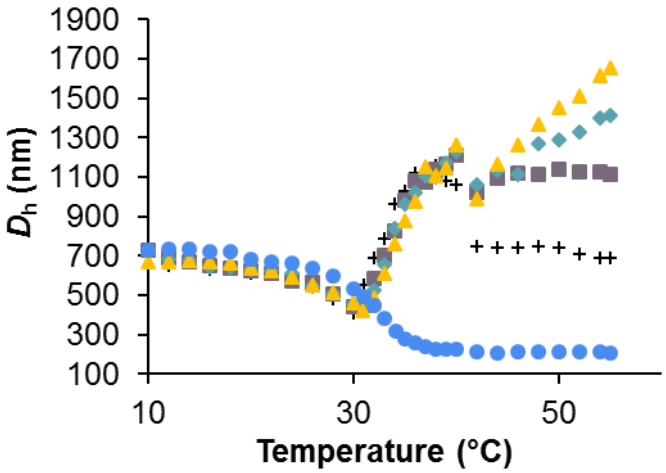

Figure 2. Final average hydrodynamic diameters as a function of the temperature for SC5-PX$_{76}$ 4-E4 microgel dispersed in water containing different concentrations of KBr: ● pure water, + 10 mM KBr in water, ■ 40 mM KBr in water, ◆ 70 mM KBr in water and ▲ 100 mM KBr in water.

In PBS supplemented with FBS, hydrodynamic diameters generally increased after a few days of incubation, depending on the microgel type. For example, SC1-PX$_{16}$ 12-E4 and SC5-PX$_9$ 4-E4 microgels were stable for 3 days whereas SC1-PX$_{76}$ 8-E4 and SC1-PX$_9$ 4-E4 ones started aggregating after the first day of incubation. Such difference is not easily correlated to the compositional features of the microgels as SC1-PX$_{16}$ 12-E4 and SC5-PX$_9$ 4-E4 were synthesized with 12 and 4 wt-% of cationic stabilizer, respectively, while SC1-PX$_{76}$ 8-E4 and SC1-PX$_9$ 4-E4 were synthesized with 8 and 4 wt-% of cationic stabilizer, respectively. In DMEM supplemented with FBS, the hydrodynamic diameters of SC1-PX$_{76}$ 8-E4, SC1-PX$_{76}$

12-E4, SC1-PX_{76} 4-E4, SC5-PX_{76} 4-E4 and SC10-PX_{76} 4-E4 microgels did not suffer any substantial changes for 6 days of incubation and started increasing after this period. Conversely, SC1-PX_9 4-E4, SC5-PX_9 4-E4, SC5-PX_{76} 8-E4, SC1-PX_{76} 8-E4 and SC1-PX_{16} 4-E4 microgels do not undergo significant size changes along the whole incubation. The relationship between the stability and the physico-chemical features of the microgels (size, cationic content, chain length of the cationic stabilizer) is difficult to be established as microgels presenting similar features (see **Table 1**) behave differently in DMEM supplemented medium.

In FBS supplemented media (either PBS or DMEM), the origin of microgel destabilization could be the formation of aggregates of microgel particles as a consequence of the absorption of proteins onto the particle surfaces. Indeed, in FBS the main constitutive plasma protein is bovine serum albumin (BSA), which is negatively charged at pH 7.4 (pI_{BSA} = 4.7).[7] Since the microgel particles used in this work are positively charged, BSA could adsorb onto microgel surfaces by electrostatic attraction, increasing their size.[8] Moreover, the reduction of the microgel surface charge by adsorption of BSA could lead to the formation of aggregates of microgel particles.[9, 10] In addition to the adsorption of BSA through electrostatic attractions, hydrophobic interactions should also be considered provided that it has been demonstrated that for poly(*N*-isopropylacrylamide)-based microgels BSA adsorption was enhanced above the microgel VPTT as a result of hydrophobic interactions between the protein and the hydrophobic collapsed microgel.[11, 12] The higher stability of the microgels in FBS supplemented media (either PBS or DMEM) than in serum free media (PBS) might arise from salt aggregating effects being initially screened by the formation of a protein corona at the microgel surfaces. This process known as opsonization enables protein adsorption and recognition of foreign elements by macrophages and the reticulo-endothelial system (RES), allowing their clearance from the body.[8] Upon incubation, this protein corona might be destabilized through exchange dynamics with smaller ions or even other less abundant proteins possessing larger affinities, leading to a reduction of the microgel surface charge and, thus, to the particle aggregation/clustering. It is also worth stressing that in the different biological mimicking media tested, the microgel colloidal stability was neither impacted by the amount of cationic reactive stabilizer nor by its chain length (number of monomer units).

Hence, these results showed that, for further uses of PVCL-based microgels in blood serum conditions, the incubation time should be carefully considered. However, in serum supplemented media, the time along which microgels remain stable is much longer than that

required for routinely *in-vitro* (maximum 72h)[10, 13-15] studies or potential *in-vivo* applications. In the present work, for experiments of microgel *in-vitro* cell cytotoxicity assays or internalization experiments microgels were used after dispersion in DMEM cell culture medium supplemented with FBS for a maximum of two days. Since in this medium the microgel hydrodynamic diameters remained constant for up to 6 days, microgel destabilization should not play a significant effect on the obtained results.

3. In vitro cell cytotoxicity assays of bare PVCL-based microgels

The cytotoxicity of the bare PVCL-based microgels at different concentrations (from 0.005 to 10 mg.mL^{-1}) was assessed on HeLa and RAW cell lines after 24 h and 48 h of incubation, using the Cell Counting Kit-8 (CCK-8) cytotoxicity assay. CCK-8 allows a sensitive colorimetric detection to assess cell cytotoxicity. The test is based on the use of a highly water-soluble tetrazolium salt, WST-8, which is reduced by dehydrogenase activity in cells to give a yellow-color formazan dye, soluble in the tissue culture media. The amount of the formazan dye, generated by the activities of dehydrogenases in cells, is directly proportional to the number of living cells. **Figure 3** exhibits the observed cell viabilities for the different microgels (expressed as cell viability percentage) as a function of the microgel concentration for HeLa and RAW cell lines after 24 h and 48 h of incubation, respectively.

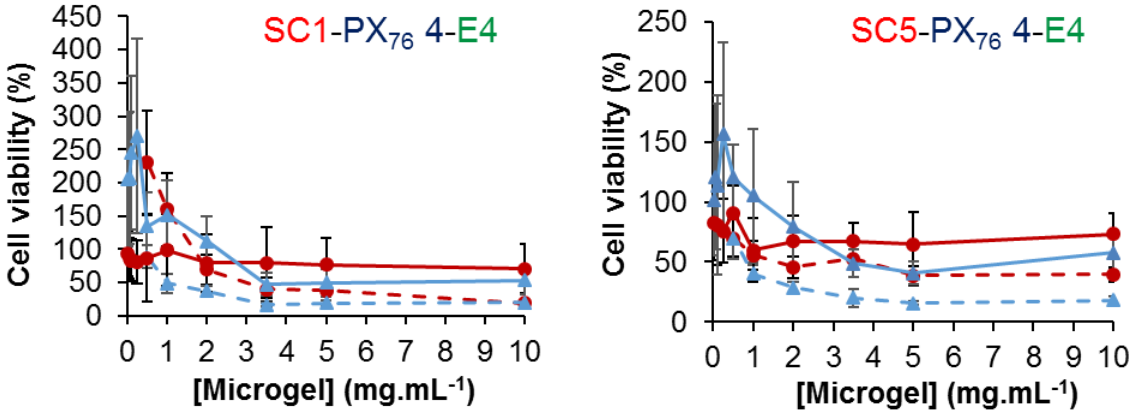

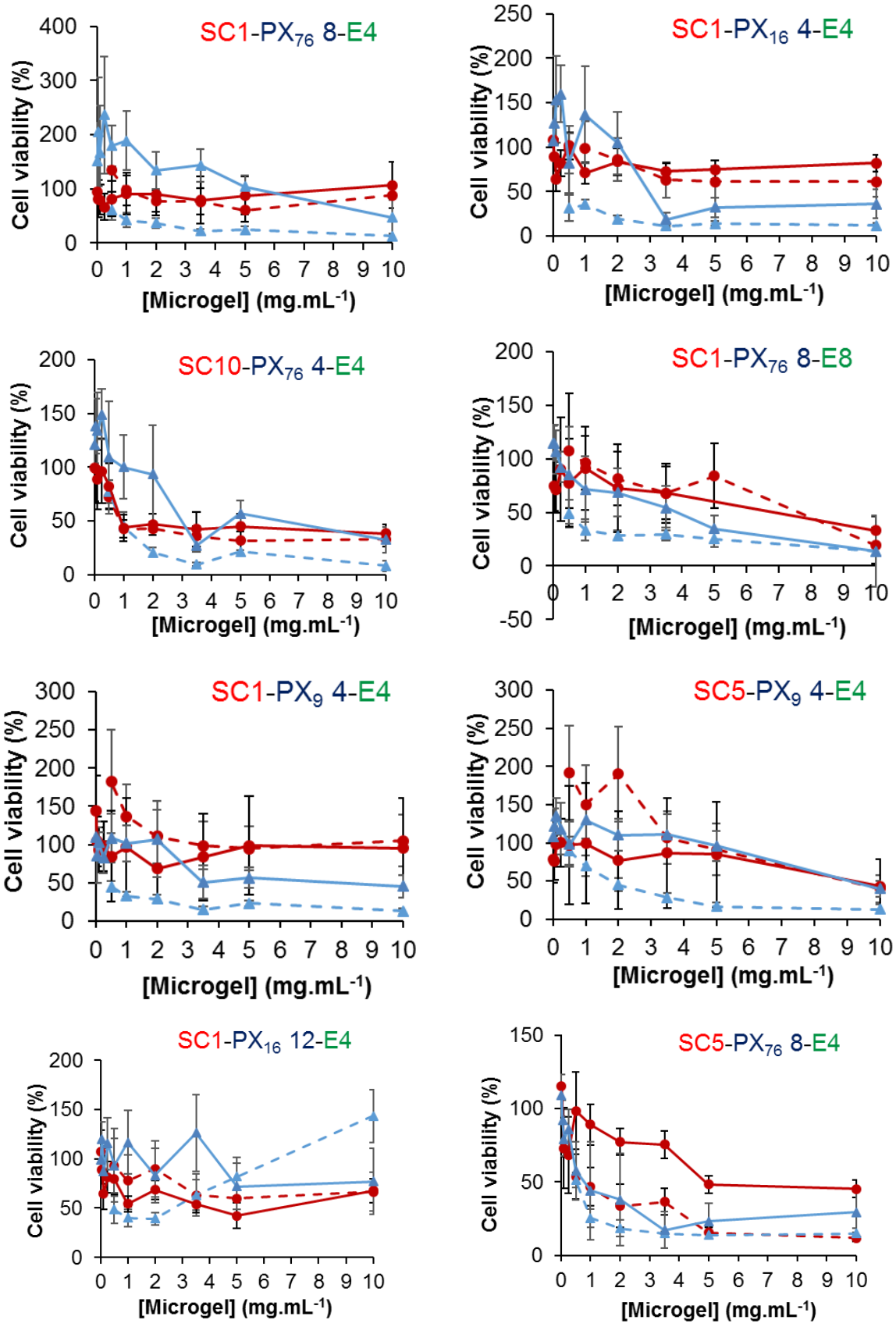

Figure 3. Cell viability of: (●) HeLa and (▲) RAW cell lines after incubation at 37°C with different concentrations of microgels. Full line: 24 h of incubation; Dotted line: 48 h of incubation.

The results here obtained show that all microgels can achieve significant cell viabilities in both types of cells with a dose-dependent behavior. A similar dose-dependent cytotoxicity was also observed for other PVCL-based nano/microgels[10] or PVCL-based copolymers.[16, 17] After 24 h of incubation, the growth inhibition observed in both HeLa and RAW cells lines is almost negligible for microgel concentrations up to 1 mg.mL^{-1}. Moreover, cell viabilities for both cell lines was above 50 % for microgel concentrations between 0.005 and 2 mg.mL^{-1} indicating that all of the microgels have a good biocompatibility.[10, 18]

Such good biocompatibility was already reported for others PVCL-based nano/microgels[10, 15, 19, 20] and polymers.[21, 22] The observed cytotoxicity of microgels at larger concentrations (above 2 mg.mL^{-1}) can be originated from an excess of microgel particles producing a cooperative damage to cells leading to their death.[23] Indeed, this overpopulation might involve membrane-cell disruption due to the high amount of nanoparticles in the medium interacting with the cells and/or large amounts of particles being internalized into cells, hence disrupting the cell cytoplasm (for example, by the formation of a high number of vacuoles),altering the cell metabolic activity and, thus, activating the programmed cell death cascade pathways. Cationic particles are usually more toxic to cells than neutral or negatively charged ones due to the stronger electrostatic interactions with the cell surface, hence, causing larger cellular membrane disruption effects (alteration of the anionic lipidic and protein domains). Also, for microgel concentrations above 2 mg.mL^{-1} the cell viability is lower for RAW cells than for HeLa ones. This result was consistent with the fact that RAW cells is a macrophage cell line which uptakes and internalizes any foreign element in the body. Thus, for nanosystems without a specific targeting, assessing the cytotoxicity on such cell line gives the ability of microgel to be uptaken by the reticulo-endothelial system.

It is well-known that the toxicity of a particle is size-dependent[24, 25] and, for cationic systems, toxicity depends on cation content.[26, 27] In this work, whatever the content of the cationic stabilizer in the microgel (4 to 12 wt-%) or their hydrodynamic diameter at 37°C (see **Table 1**), all the microgels were non-toxic for concentrations ranging from 0.005 to 2 mg.mL^{-1}.

Contrary to other systems composed of cationic polymeric chains,[28-30] the chain length of the cationic polymer used as stabilizer for the microgel synthesis has no impact on the microgel cytotoxicity. Indeed, similar percentages of cell viability were obtained after incubation of the cells with SC1-PX$_{76}$ 4-E4 and SC1-PX$_{9}$ 4-E4 microgels in contrast to previously mentioned studies in which the cytotoxicity of the systems increases as the chain length of the cationic

polymer does. This can be explained by the fact that, whatever the chain length of the P(AETAC-X) used as stabilizer for the synthesis of PVCL-based microgels, the final microgels presented similar values of the electrophoretic mobility (SC1-PX_{76} 4-E4, electrophoretic mobility = 0.42 × 10^{-8} m^2/Vs in cationic buffer at pH 3 and 10 mM ionic strength, and SC1-PX_9 4-E4, electrophoretic mobility = 0.44 × 10^{-8} m^2/Vs in cationic buffer at pH 3 and 10 mM ionic strength).

On the other hand, it should be noted that the microgel cytotoxicity in both HeLa and RAW cell lines is higher after 48 h of incubation if compared to that of 24 h. This might be due to further microgel accumulation around/within cells promoting their death. Such incubation time-dependent cytotoxicity was already observed for other PVCL-based microgels[10] and PVCL-based polymers.[21]

4. Cellular uptake by fluorescence microscopy

Prior to the microgel cellular uptake characterization using fluorescence microscopy, the microgels were labeled with a cationic dye: rhodamine 6G. The effective internalization of R6G-loaded microgels into HeLa cells after 3 and 24 h of incubation was followed by fluorescence microscopy. Six microgels were selected to carry out this study, according to their colloidal characteristics (initial size, stability during incubation) and cytotoxicity: SC1-PX_{76} 4-E4, SC1-PX_{76} 8-E4, SC5-PX_{76} 4-E4, SC1-PX_{76} 8-E8, SC1-PX_9 4-E4 and SC1-PX_{16} 4-E4 microgels, see **Table 1**. In the following section, all the displayed images correspond to: differential interference contrast (DIC) images (upper left side), DAPI-stained cell nuclei (blue, upper right side), R6G fluorescence in cells (red, lower left side) and the merged images (lower right side).

4.i. Cellular uptake of microgels

Figure 4 shows fluorescence images of the R6G-loaded microgel cellular uptake in HeLa cells after 3 h of incubation at 37°C.

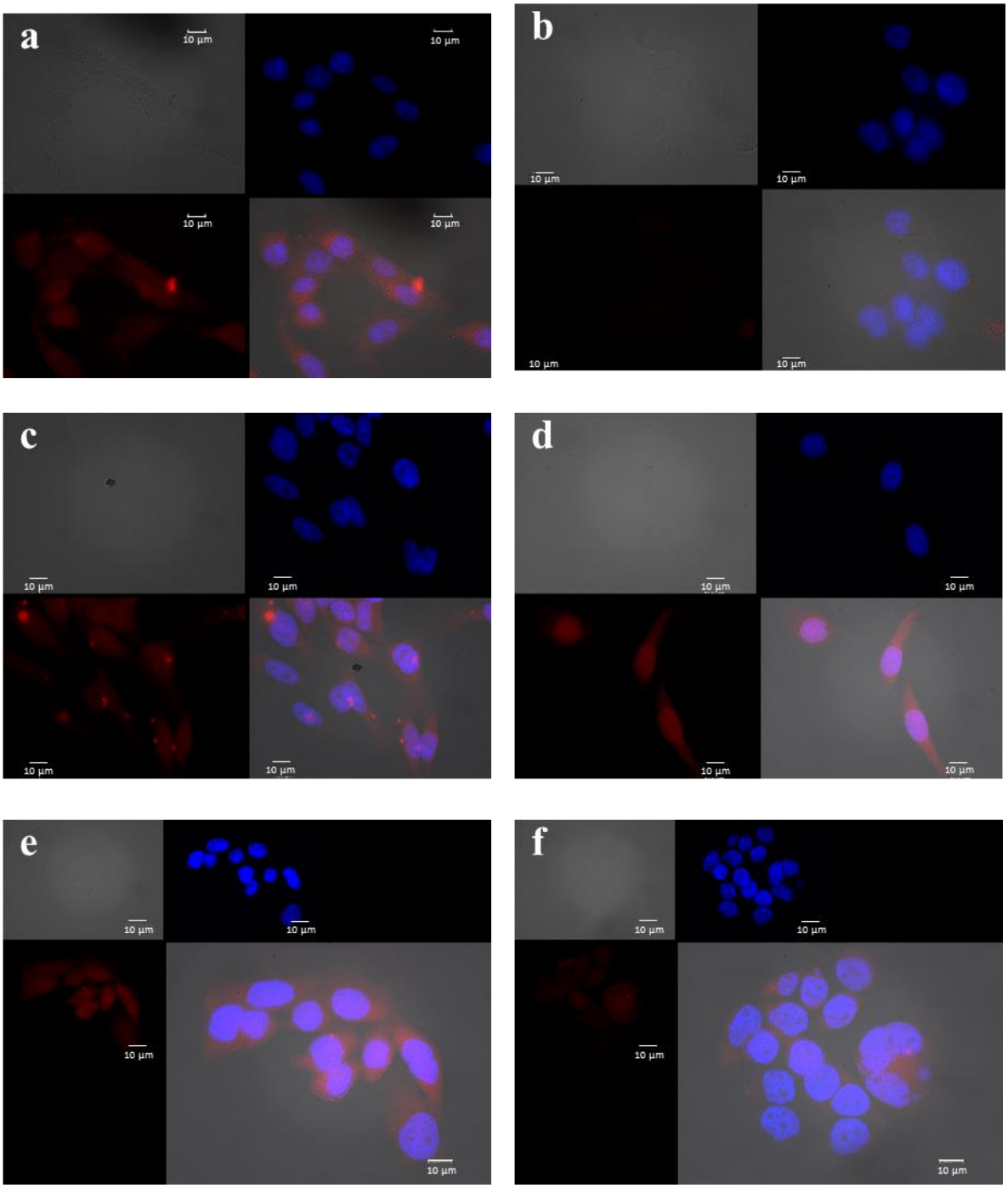

Figure 4. Fluorescence microscopy images of R6G-loaded microgels: (a) SC1-PX_{76} 4-E4, (b) SC1-PX_{76} 8-E4, (c) SC5-PX_{76} 4-E4, (d) SC1-PX_{76} 8-E8, (e) SC1-PX_{16} 4-E4, (f) SC1-PX_{9} 4-E4 microgels in HeLa cells stained with DAPI after 3 h of incubation at 37°C.

After 3 h of incubation, for most of the tested microgels, the DAPI-stained cell nuclei (blue) were surrounded by a diffuse rhodamine fluorescence (red) pattern, suggesting a successful internalization of the microgels at short time scales and the subsequent sustained dye release inside the cell cytoplasm.[31] The cationic dye was truly located at the cell cytoplasm and/or in

some intracellular compartments, specially endoplasmic reticulum and/or mitochondria, for which R6G is a specific marker; some few observed, red colored nuclei would indicate overlapping of the fluorescence signal corresponding to the red and blue channels in the 2D view, that is, microgels/dye located over the nuclei would appear as in their nucleus interior in the projection (the dye used is not permeable to the nucleus membrane). The presence of microgel clusters was also visualized via the presence of red dotted spots in the images as a result of microgel aggregation when in contact to biological medium due to their positive charges.

At longer incubation times (24 h, **Figure 5**), rather similar fluorescence patterns as at 3 h were observed, that is, the DAPI-stained cell nuclei were surrounded by rhodamine fluorescence, suggesting the successful internalization and residence of the microgels/cargo inside cells. The fluorescence intensity of the dye was relatively conserved after 24 h of incubation in agreement with a sustainable release of rhodamine 6G from microgels along time. Though for some microgels a very small decrease of fluorescence intensity is observed, pointing to a certain expulsion of the dye from the cell. However, this point would deserve further studies to rule out any possible contribution from dye quenching.

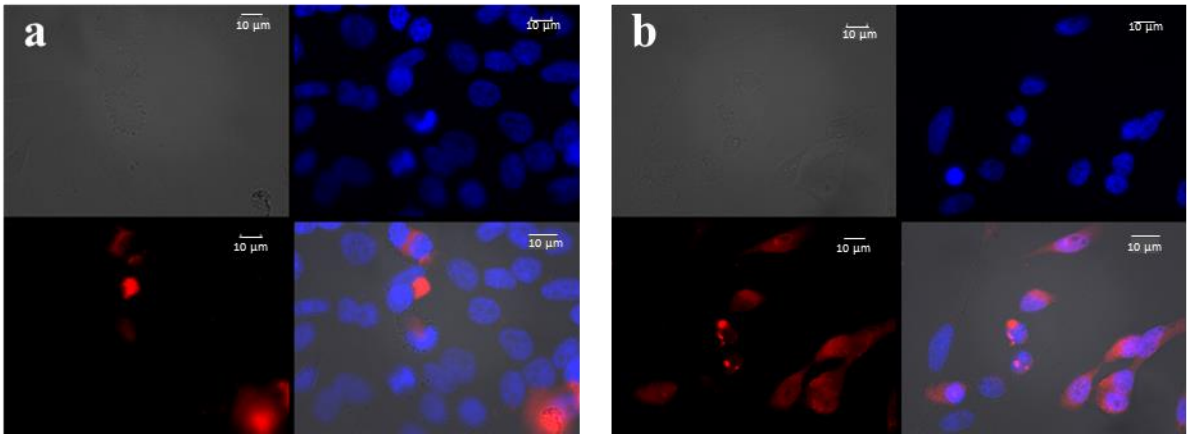

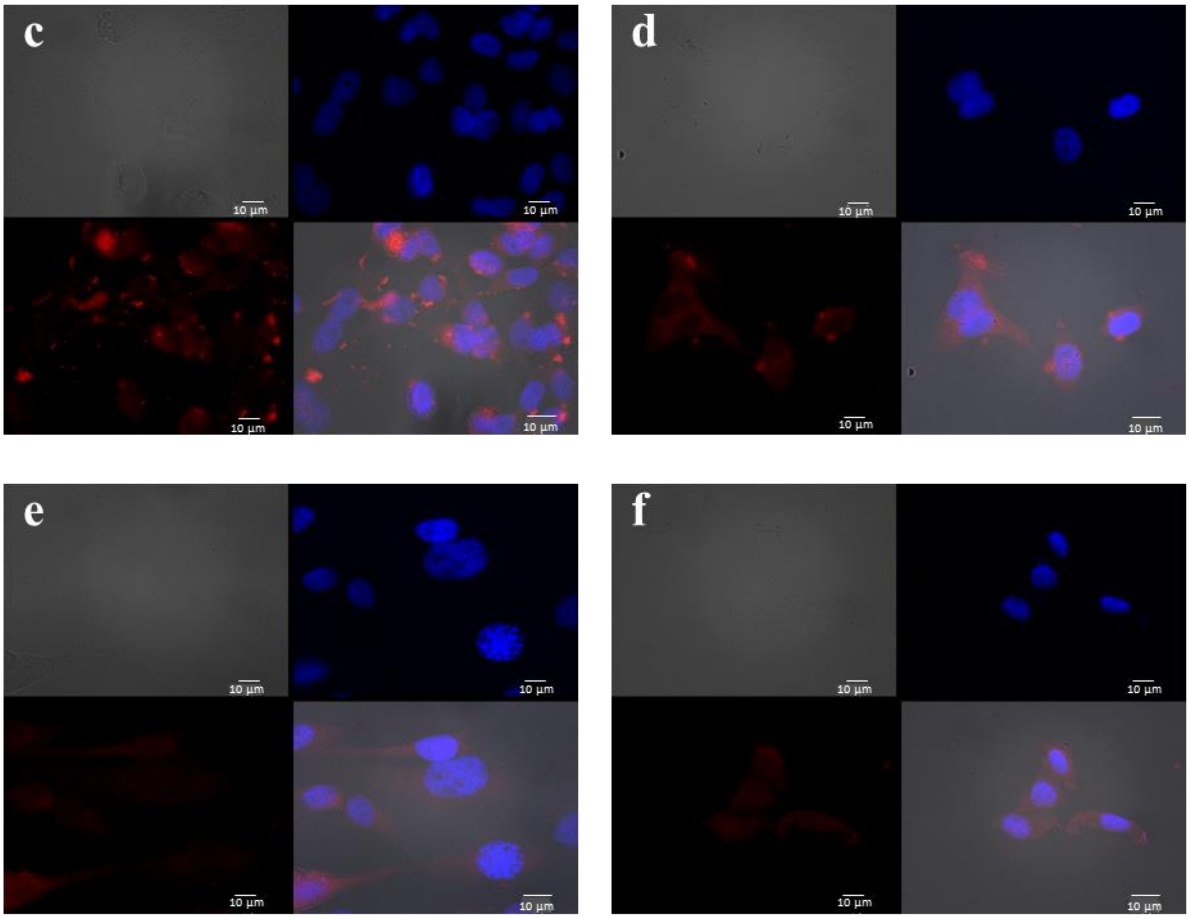

Figure 5. Fluorescence microscopy images of R6G-loaded microgels: (a) SC1-PX_{76} 4-E4, (b) SC1-PX_{76} 8-E4, (c) SC5-PX_{76} 4-E4, (d) SC1-PX_{76} 8-E8, (e) SC1-PX_{16} 4-E4, (f) SC1-PX_{9} 4-E4 microgels in HeLa cells stained with DAPI after 24 h of incubation at 37°C.

On the other hand, it should be highlighted that for high microgel cell accumulation levels, some few cells with damaged membranes could clearly be observed confirming some aforementioned statements (**Figure 6**).

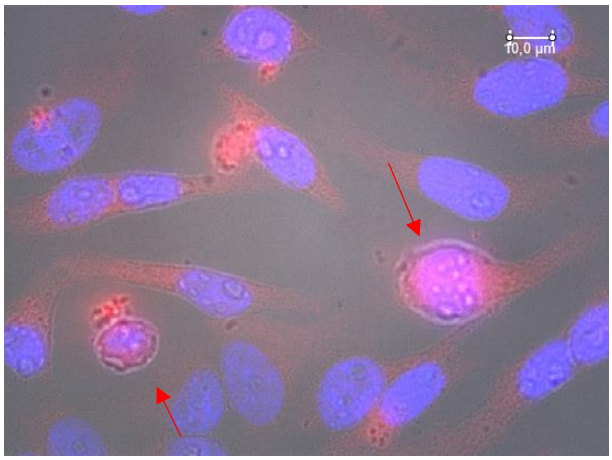

Figure 6. Fluorescence microscopy image of R6G-loaded SC1-PX76 4-E4 microgel in HeLa cells stained with DAPI after 24 h of incubation at 37°C. Arrows: Observed damaged cells.

Such loss of cell membrane integrity was already observed for cells in contact with other highly cationic nanomaterials.[28] In the present work, after incubation for 3 h at 37°C, much less cells with damaged membrane were observed, which additionally suggests that the microgel accumulation process into cells is a time-dependent process. This time-dependent cellular uptake has already been observed for other PVCL-based microgels.[10, 15, 20]

4.ii. Analysis of the cellular uptake pathway/s of microgels

In order to elucidate how microgels can be internalized into cancerous cells, inhibition experiments of different uptake pathways were performed. Endocytosis (the vesicular uptake of extracellular macromolecules) has been established as the main mechanism for the internalization of non-viral vectors into cells.[32] Endocytosis can be classified into two broad categories: phagocytosis (specialized mammalian cells) and pinocytosis (all cells). Among pinocytic pathways four main mechanisms can be distinguished: clathrin-mediated endocytosis, caveolae, macropinocytosis and clathrin/caveolae-independent endocytosis (**Figure 7**). Internalization via endocytosis can be inhibited using different cell treatments. A general procedure for hindering endocytic pathways consists in lowering the temperature as endocytosis is an energy-dependent mechanism. Furthermore, it is possible to inhibit specifically a certain endocytic pathway by adding a specific inhibitor for such route.[33]

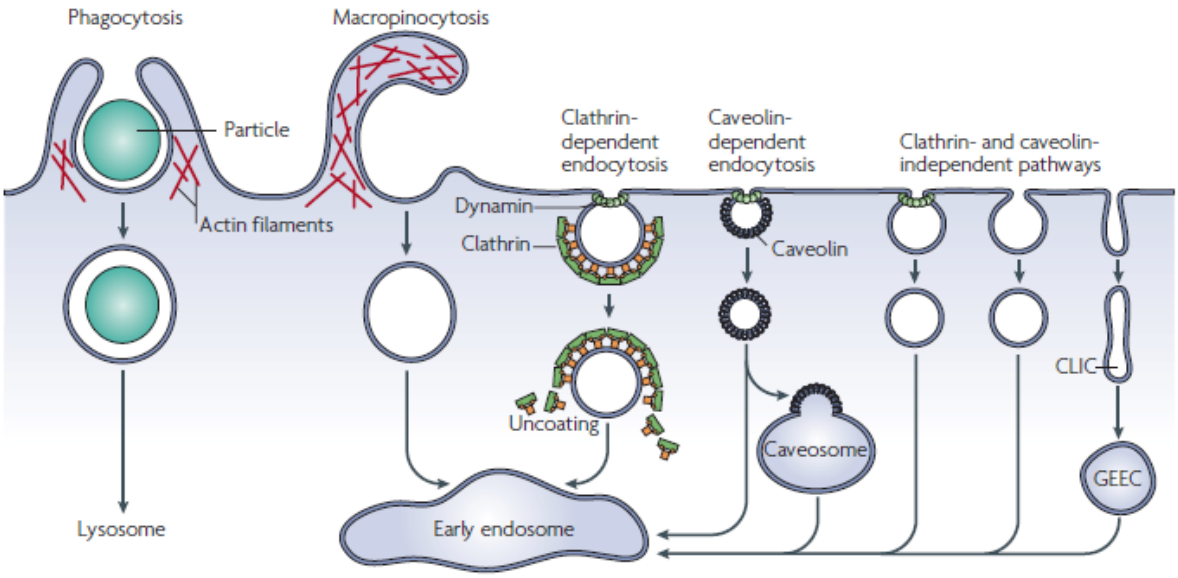

Figure 7. Pathways of entry into cells (from reference 34).

In this work the cellular uptake mechanism of several microgels was investigated using four different inhibition mechanisms. First of all, the microgel internalization was studied at 4°C in order to assess if the internalization mechanism is a chemical-mechanical energy dependent- or a simple diffusion process. Additionally, in order to know whether some specific protein/mechanism is involved in the particle incorporation within the cells, two different clathrin-mediated endocytosis specific inhibitors (hypertonic sucrose and chlorpromazine), an inhibitor of macropinicytosis/phagocytosis (cytochalasin D, an inhibitor of actin polymerization), and an inhibitor of caveolae (nystatin) were used. These inhibitors act dissociating the clathrin lattice, actin and/or caveolae, respectively, impeding the corresponding endocytic pathways.

The fluorescence images of the R6G-loaded microgel cellular uptake in HeLa cells after 3 h of incubation at 4°C are depicted in **Figure 8.**

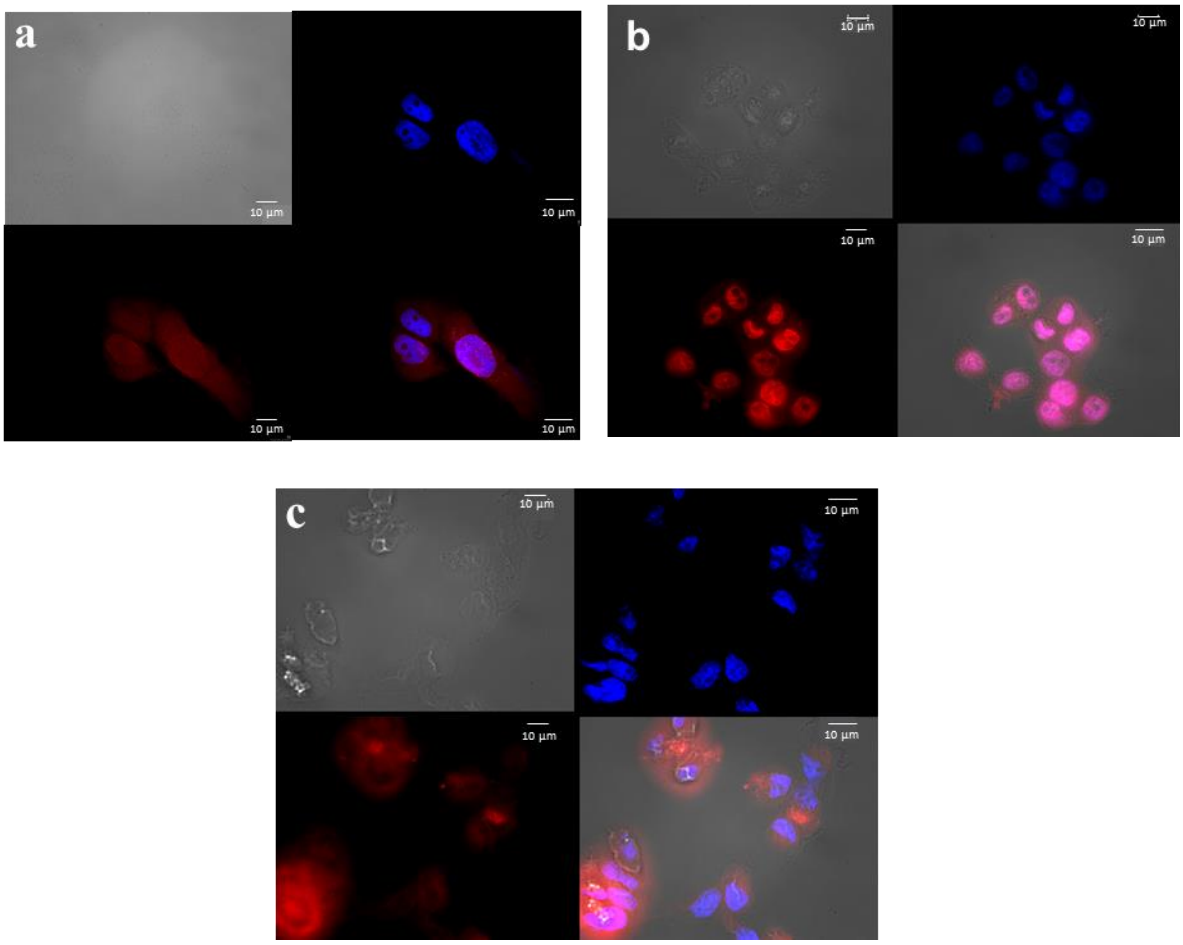

Figure 8. Fluorescence microscopy images of R6G-loaded microgels: (a) SC1-PX_{76} 4-E4, (b) SC1-PX_{76} 8-E8, (c) SC1-PX_9 4-E4 microgels in HeLa cells stained with DAPI after 3 h of incubation at 4°C.

For all the tested microgels, the internalization process took place satisfactorily at 4º C, disregarding an energy-dependent uptake pathway for the dye-loaded microgels. Indeed, the R6G release occurred into the cell cytoplasm for all the microgels. Moreover, in some cases, the microgels could be observed in the cell nuclei as observed by the reconstructed fluorescence image of SC1-PX_{76} 4-E4 microgel in HeLa cell line after 3 h of incubation at 4°C (**Figure 9**). At 4°C, R6G was also released at the cell surroundings (for SC1-PX_9 4-E4 microgel for instance, **Figure 8.c**). For these experiments, the cell density was observed to be slightly lower than for uptake experiments performed at 37°C, probably as a consequence of some cellular death and their subsequent detachment from the surface during the washing process.

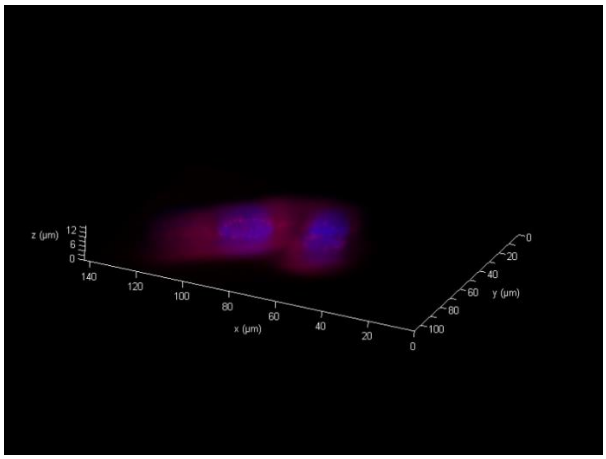

Figure 9. Reconstructed fluorescence image of R6G-loaded SC1-PX_{76} 4-E4 microgel in HeLa cells stained with DAPI after 3 h of incubation at 4°C.

Figure 10 and **Figure 11** show the fluorescence images of the R6G-loaded microgel cellular uptake in HeLa cells after 3 h of incubation at 37°C in the presence of hypertonic sucrose medium and chlorpromazine, respectively.

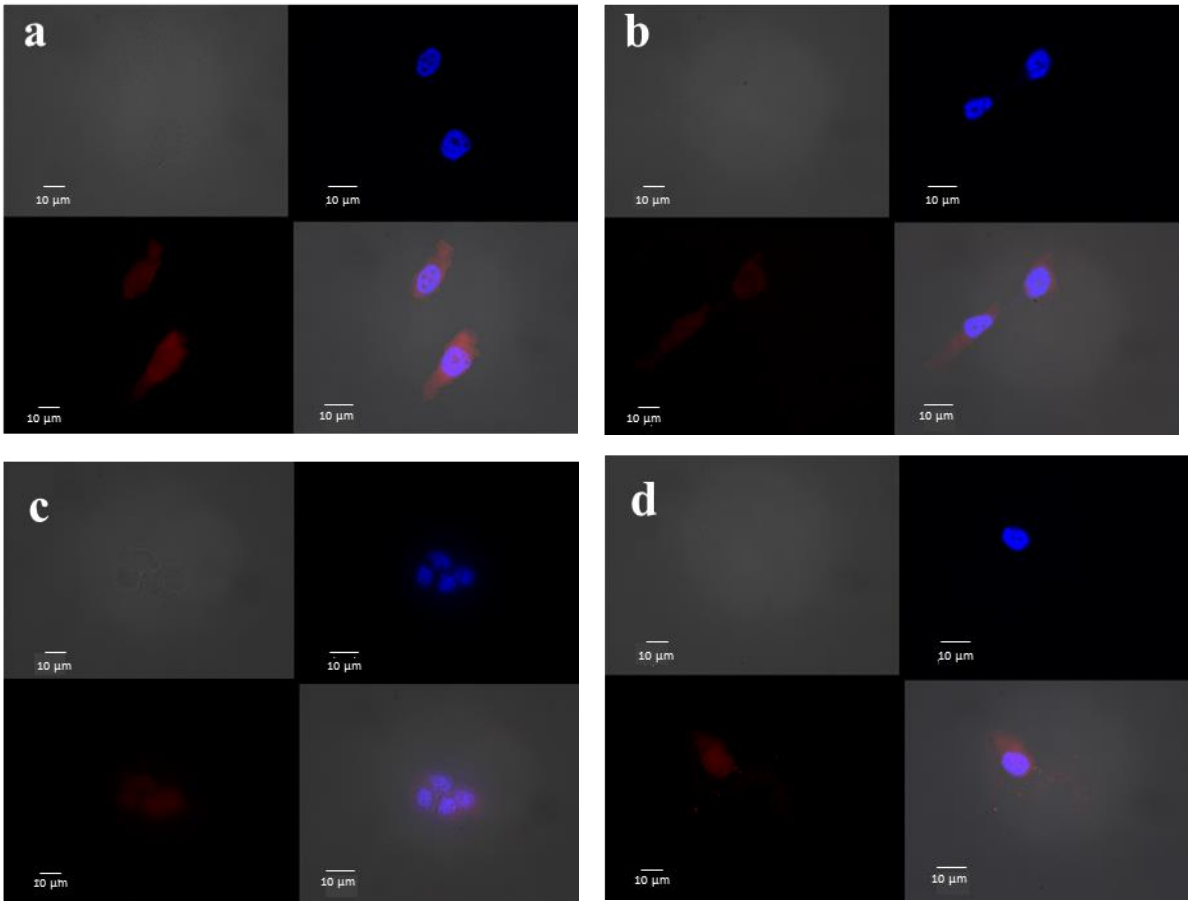

Figure 10. Fluorescence microscopy images of R6G-loaded microgels: (a) SC1-PX_{76} 4-E4, (b) SC1-PX_{76} 8-E4, (c) SC1-PX_{76} 8-E8, (d) SC1-PX_{9} 4-E4 microgels in HeLa cells stained with DAPI after 3 h of incubation at 37°C with hypertonic sucrose medium.

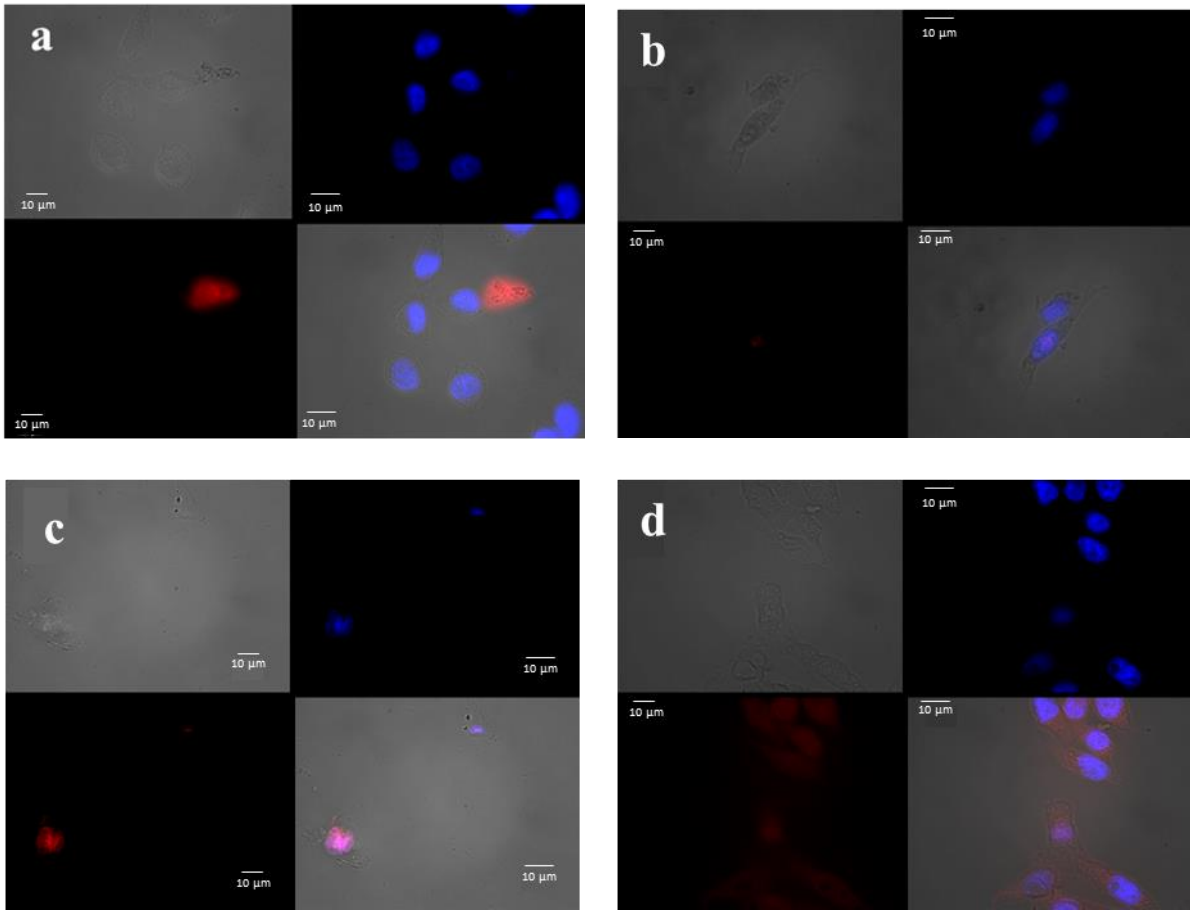

Figure 11. Fluorescence microscopy images of R6G-loaded microgels: (a) SC1-PX_{76} 4-E4, (b) SC1-PX_{76} 8-E4, (c) SC1-PX_{76} 8-E8, (d) SC1-PX_{9} 4-E4 microgels in HeLa cells stained with DAPI after 3 h of incubation at 37°C with chlorpromazine.

As mentioned above, hypertonic sucrose and chlorpromazine are clathrin-mediated endocytosis specific inhibitors. They act dissociating the clathrin lattice, impeding the clathrin-mediated endocytic uptake. From the experiments performed, it could be observed that inhibition of clathrins gave rise to a well-observed qualitative reduction in the extent of internalization of dye-loaded microgels as observed from a lower fluorescence signal observed inside cell cytoplasm, especially for microgels coded as SC1-PX_{76} 8-E4 and SC1-PX_{76} 8-E8. This points to clathrin as one of the main mechanisms responsible for microgel internalization but not the only one, since some diffuse fluorescence patterns are still observed.

Two other additional internalization routes, macropinocytosis/phagocytosis and caveolae, were additionally analyzed by fluorescence microscopy using microgel SC1-PX_{76} 8-E8 as an example. Cytochalasin D, a polymerization inhibitor of actin which is a protein largely involved in the formation of cell skeleton and mobility, and nystatin, a sterol-binding agent which

disassembles caveolae, were used, respectively. It can be observed (see **Figure 12** and **Figure 13**) that a good internalization of the microgel is observed within cells in both cases suggesting that the inhibition of these routes do not impede the incorporation of the microgel into cells.

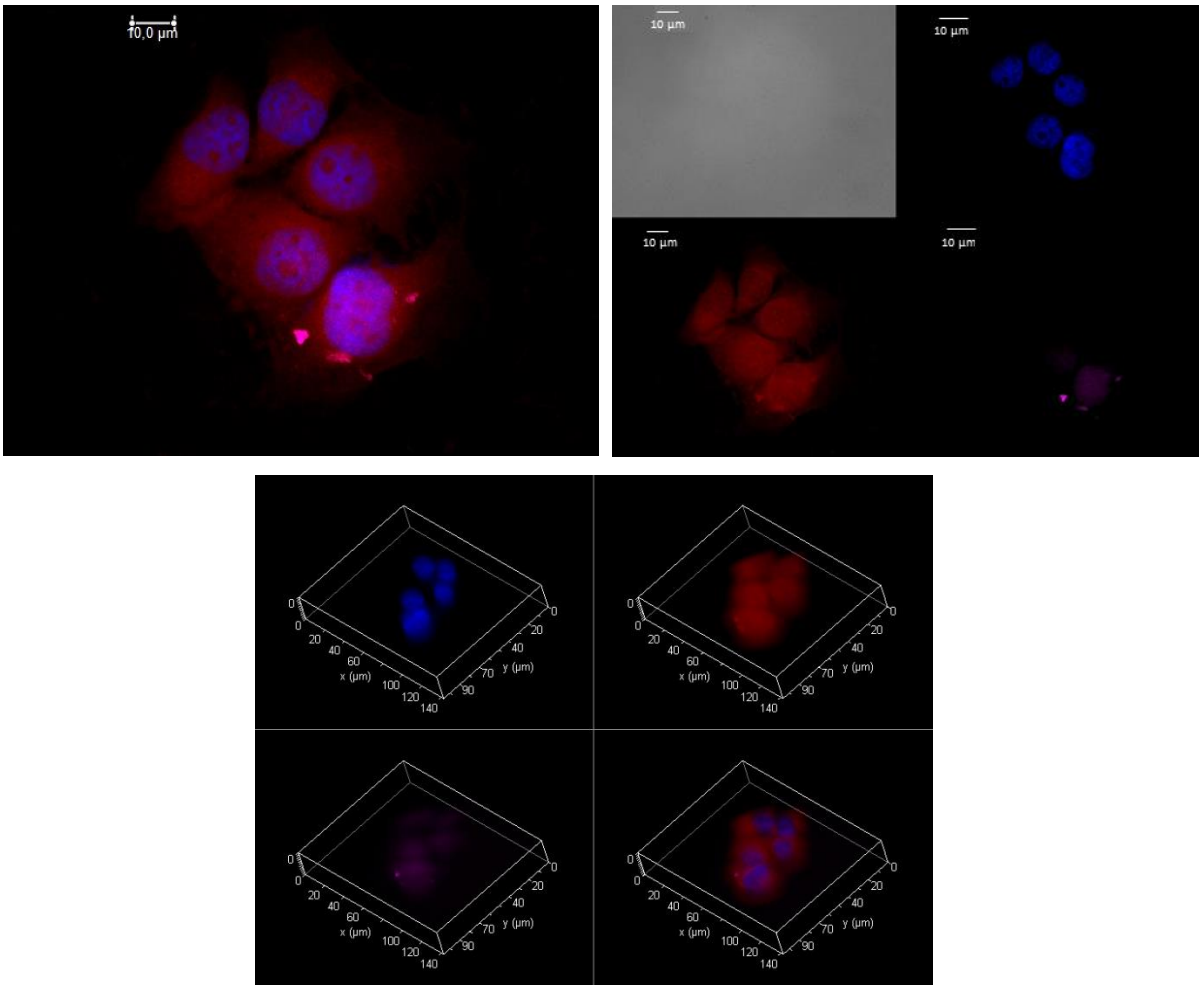

Figure 12. Fluorescence microscopy images and reconstructed fluorescence images (bottom) of R6G-loaded SC1-PX_{76} 8-E8 microgels in HeLa cells stained with DAPI after 3 h of incubation at 37°C with nystatin.

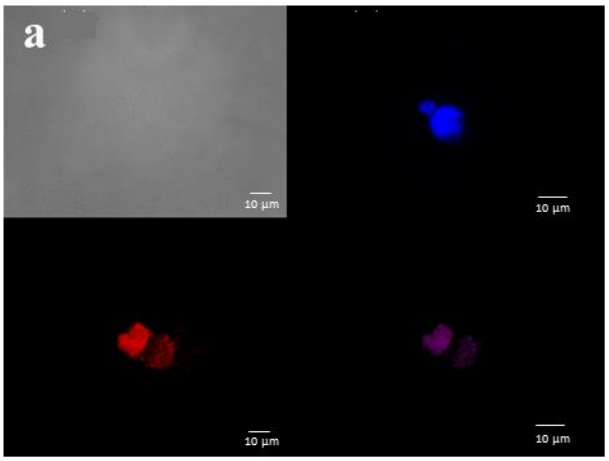

Figure 13. Fluorescence microscopy images of R6G-loaded SC1-PX_{76} 8-E8 microgels in HeLa cells stained with DAPI after 3 h of incubation at 37°C with cytochalasin D.

Finally, a quantification of the extent of internalization inhibition for microgels SC1-PX_{76} 4-E4, SC1-PX_{76} 8-E8 and SC1-PX_{9} 4-E4 loaded with the anticancer DOXO (see below) at a concentration of 20 µM using the different inhibiting compounds was performed using HeLa cells by evaluating the cell viability by the CCK-8 assay. **Figure 14** confirms the observations made by means of fluorescence microscopy, that is, a maximum cell survival is observed when the clathrin-dependent endocytic pathway is inhibited, either with sucrose or chlorpromazine. For cytochalasin D, some increase in viability is observed compared to the control thanks to a certain involvement of cytochalasin D in the clathrin-dependent-pathway.[35] Conversely, for the remaining inhibitors cell viabilities were similar as that observed for controls (that is, in the absence of any inhibitor), hence, having a similar therapeutic activity of the anticancer drug as a result of similar internalization extents.

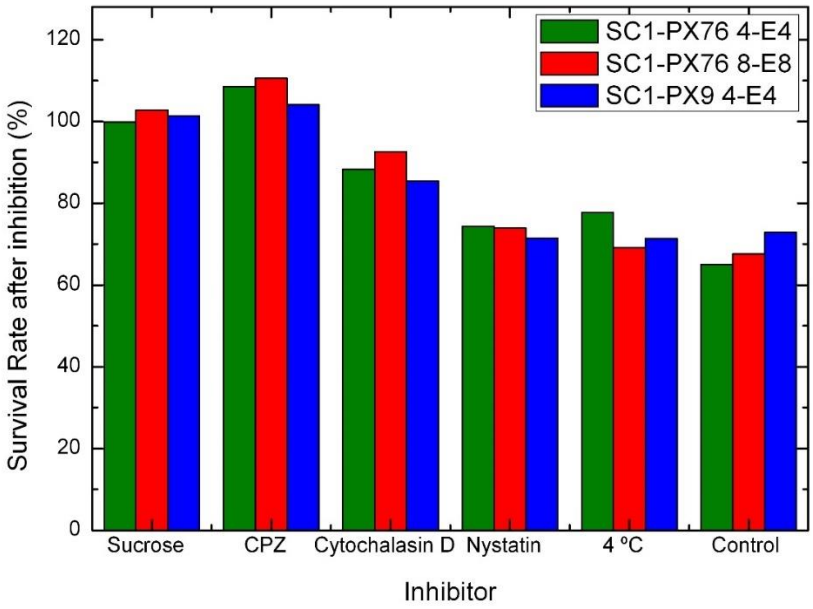

Figure 14. Cellular survival rate after inhibition of different uptake pathways.

5. In vitro cell cytotoxicity assays of DOXO-loaded microgels

The loading of doxorubicin was performed for SC1-PX_{76} 4-E4, SC1-PX_{76} 8-E4, SC5-PX_{76} 4-E4, SC1-PX_{76} 8-E8, SC1-PX_{9} 4-E4 and SC1-PX_{16} 4-E4 microgels (**Table 1**). DOXO loading was carried out by adding 100 µL of a DOXO solution at 1 $mg.mL^{-1}$ to 500 µL of microgel dispersions at 2 $mg.mL^{-1}$. The drug loading method takes advantages of the sponge like nature of the microgels, allowing solute molecules to partition into the porous particle network.[36] DOXO can be incorporated into microgels through electrostatic and/or hydrophobic interactions.[37] The drug loading (D.L.) and entrapment efficiency (E.E.) were calculated according to Equation 1 and Equation 2, respectively, and the values obtained for the different microgels are presented in **Table 2** below.

Table 2. Entrapment efficiency and drug loading for the different microgels.

Microgel	Entrapment efficiency %	Drug loading %
SC1-PX_{76} 4-E4	26 ± 15	2 ± 1
SC1-PX_{76} 8-E4	30 ± 10	3 ± 1
SC5-PX_{76} 4-E4	33 ± 13	3 ± 1
SC1-PX_{76} 8-E8	18 ± 7	2 ± 1
SC1-PX_{9} 4-E4	24 ± 14	2 ± 1
SC1-PX_{16} 4-E4	28 ± 12	3 ± 1

The values of drug loading and entrapment efficiency are relatively low compared to the values obtained for other PVCL-based nano/microgels,[10, 15, 19, 20] indicating a low amount of drug loaded into the microgels. Since the drug loading process was carried out at pH 6.5 for which DOXO is positively charged (pKa = 8.3),[38] electrostatic repulsions between the drug and the cationic PVCL-based microgels might limit the drug encapsulation. Moreover, electrostatic repulsions among DOXO molecules could also reduce the entrapment efficiency value. Also, as EGDMA crosslinker is relatively hydrophobic compared to other crosslinkers, it can hinder the penetration of DOXO molecules into the microgel network.[39] Aguirre *et al.*[10] studied the loading of DOXO into poly(2-diethylaminoethyl)methacrylate (PDEAEMA)-based microgels and PDEAEMA-based core and PVCL-based shell microgels at acidic pH for which both microgels and DOXO were positively charged. As they used a dextran-based macro-crosslinker, the main driving force to encapsulate DOXO into the microgels was the interaction by H-bonding between the -OH groups of DOXO and the -OH groups of the dextran chains. Thus, a high encapsulation efficiency of the drug could be reached (*i.e.* ranging from 80 to 90 %), even in the presence of electrostatic repulsion between the microgels and the drug. In the present work, at the DOXO concentration used (1 $mg.mL^{-1}$), the levels of entrapment efficiency and drug loading are in a similar range for all the different microgels. Therefore, the structure of the different microgels tested does not seem to influence the amount of DOXO encapsulated into the network.

The cumulative DOXO release of the microgels was also studied. DOXO-loaded SC1-PX_{76} 4-E4, SC1-PX_{76} 8-E8 and SC1-PX_{9} 4-E4 microgel dispersions were dialyzed at 37 °C against different serum-containing (10 % (v/v) FBS) buffer solutions. Sodium acetate/acetic acid (SA) buffer solution (pH 5.5) was chosen in order to simulate the extracellular environment of tumoral cancer cells, and phosphate buffer saline (PBS) solution (pH 7.4) was selected to mimic blood serum conditions. Note that at 37°C the microgels are collapsed (T > VPTT, see **Table 1**). The *in-vitro* cumulative DOXO release at 37°C under both pHs is depicted in **Figure 15**.

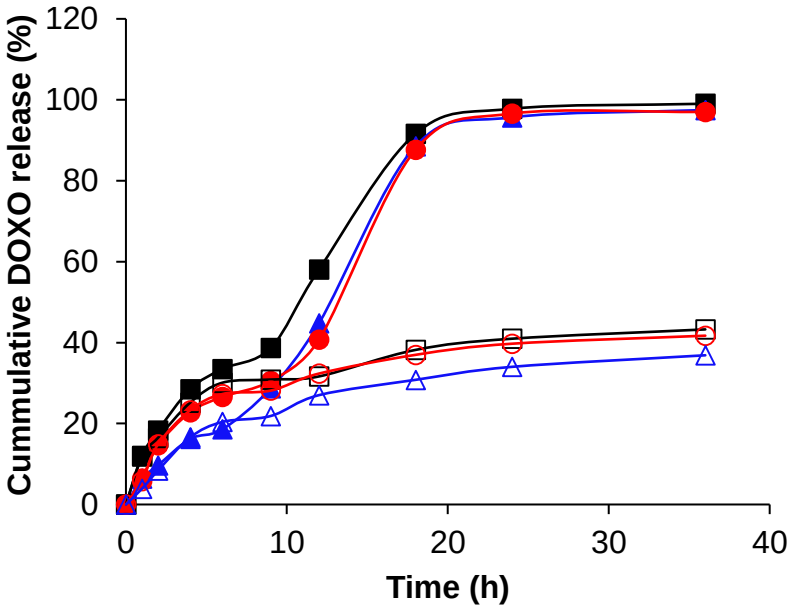

Figure 15. Cumulative DOXO release of (■) SC1-PX_{76} 4-E4, (●) SC1-PX_{76} 8-E8 and (▲) SC1-PX_{9} 4-E4 microgels at pH 5.5 (closed symbols) and 7.4 (open symbols) in the presence of 10 % (v/v) FBS, at 37°C. Error bars are not displayed for clarity but are within ±10 %.

It is well-known that the drug release rate from microgels is theoretically affected by different factors such as the drug diffusion through the microgel particles, and the extent of swelling of microgels. In the present case, at pH 7.4 the three selected SC1-PX_{76} 4-E4, SC1-PX_{76} 8-E8 and SC1-PX_{9} 4-E4 microgels displayed a clear burst release phase within the first 7 h of incubation where *ca* 29, 24 and 19 % of the drug is released, followed by a short pseudo-plateau region between *ca* 7 and 10 h. After this incubation period, the release is slightly accelerated again followed by a very sustained release phase at longer incubation times finally achieved, with cargo releases between 30-40 % (depending on the microgel) within the time framework of the present experiments (*ca* 37 h).

In contrast, under acidic conditions rather similar release patterns resembling stair-like profiles can be observed but with larger drug releases than at pH 7.4. A similar burst phase is again observed at short incubation times followed by a slowing of the release rate for a short period (more than a true pseudo-plateau region as at physiological pH). After *ca* 9-10 h of incubation an additional abrupt increase in the cumulative release is again observed up to *ca* 18 h at which *ca.* 75-80 % of the cargo is released; thereafter, a plateau region is reached along which *ca* 90 % of the drug is expelled from the microgels.

The presence of a burst phase in the release profiles of the present microgels might be related to the adsorption of drug molecules located in the outer layer of the particles, which are released at first; meanwhile, the more sustainable release phase would be controlled by the rate of DOXO release from the microgel core thanks to the hindered diffusion from the highly cross-linked inner part of the microgels. At this respect, the presence of a slight pseudo-plateau/reduction of the release rate between 7-10 h of incubation giving rise to a stair-like profile might be related to some change/gradient in the crosslinking density of microgels throughout their matrix (core-shell structure highlighted by ^{1}H transverse relaxation NMR measurements in Chapter 2-Part II), impeding a full sustained release. In addition, important differences in the release extents between acidic and basic physiological conditions can be observed. At this point, it is important to note that the cationic stabilizer used for the synthesis of the microgels is permanently charged and, thus, insensitive to pH changes. Therefore, the larger cumulative releases observed at pH 5.5 might be attributed to the fact that, at acidic pH, amine groups of DOXO molecules are protonated (*i.e.* positively charged). As the hydrophilicity of DOXO molecules is enhanced at acidic pH, the affinity of the drug with the microgel hydrophobic core might be reduced, enhancing the diffusion out of the particle.[40]

Finally, no remarkable differences in DOXO release kinetics were observed between the three selected microgels. This would hence suggest that neither the extent of polymer stabilizer nor the amount of crosslinker would have a strong impact on the release profiles, at least in the range within the tested particles. As the interactions were mainly non-covalent, it was expected that the delivery would be governed by diffusion, which is affected by the swelling capability of the microgels and their interactions with the drug (especially electrostatic repulsion at acidic conditions). Since the used microgels showed very similar swelling-de-swelling behavior, an analogous DOXO release kinetics was observed in all cases.

Cell viability of DOXO-loaded microgels was then studied at different microgel concentrations (from 0.1 to 2 mg.mL^{-1}) and, thus, different DOXO concentrations in both HeLa and RAW cell lines after 24 h of incubation (**Figure 16**). For each microgel, the concentration of DOXO was calculated from the microgel weight concentrations and the entrapment efficiency (see **Table 2**) according to Equation 4. The results are given in **Table 3.**

$$[DOXO](\mu M) = \left(\frac{[Microgel] \times E.E \times 10^{-3}}{M_{DOXO}}\right) \times 10^{6} \quad \text{Equation 4}$$

with [DOXO]: DOXO concentration, [Microgel]: microgel concentration in mg.mL^{-1}, E.E: entrapment efficiency (Equation 2) and M_{DOXO}: DOXO molar mass in g.mol^{-1} (M_{DOXO} = 579.98 g.mol^{-1})

Table 3. Concentration of DOXO in cell culture media depending on the microgel concentrations.

Microgel	SC1-PX$_{76}$ 4-E4	SC1-PX$_{76}$ 8-E4	SC5-PX$_{76}$ 4-E4	SC1-PX$_{76}$ 8-E8	SC1-PX$_{9}$ 4-E4	SC1-PX$_{16}$ 4-E4
[Microgel] $g.L^{-1}$	[DOXO] μM	[DOXO] μM	[DOXO] μM	[DOXO] μM	[DOXO] μM	[DOXO] μM
2	90	103	114	62	83	97
1	45	52	57	31	41	48
0.5	22	26	28	16	21	24
0.25	11	13	14	8	10	12
0.1	4	5	6	3	4	5

For HeLa cells, the IC$_{50}$ (*i.e*, the concentration of drug required to reduce cell growth by 50 %) of free DOXO after 24 h of incubation is equal to 5.5 µM. Therefore, for all microgels at concentrations above 0.1 mg.mL^{-1}, the DOXO concentrations loaded inside are above the minimum DOXO concentration providing cytotoxicity activities *in vitro*.

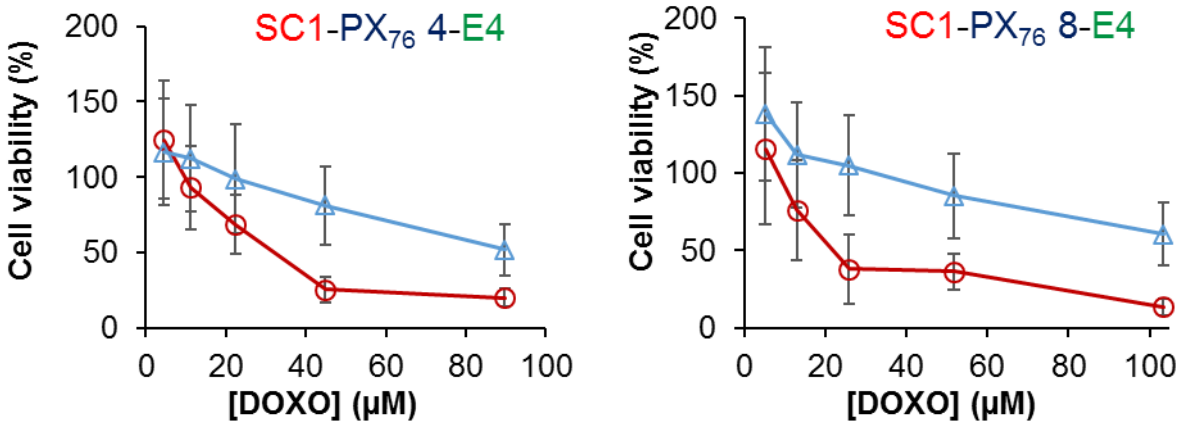

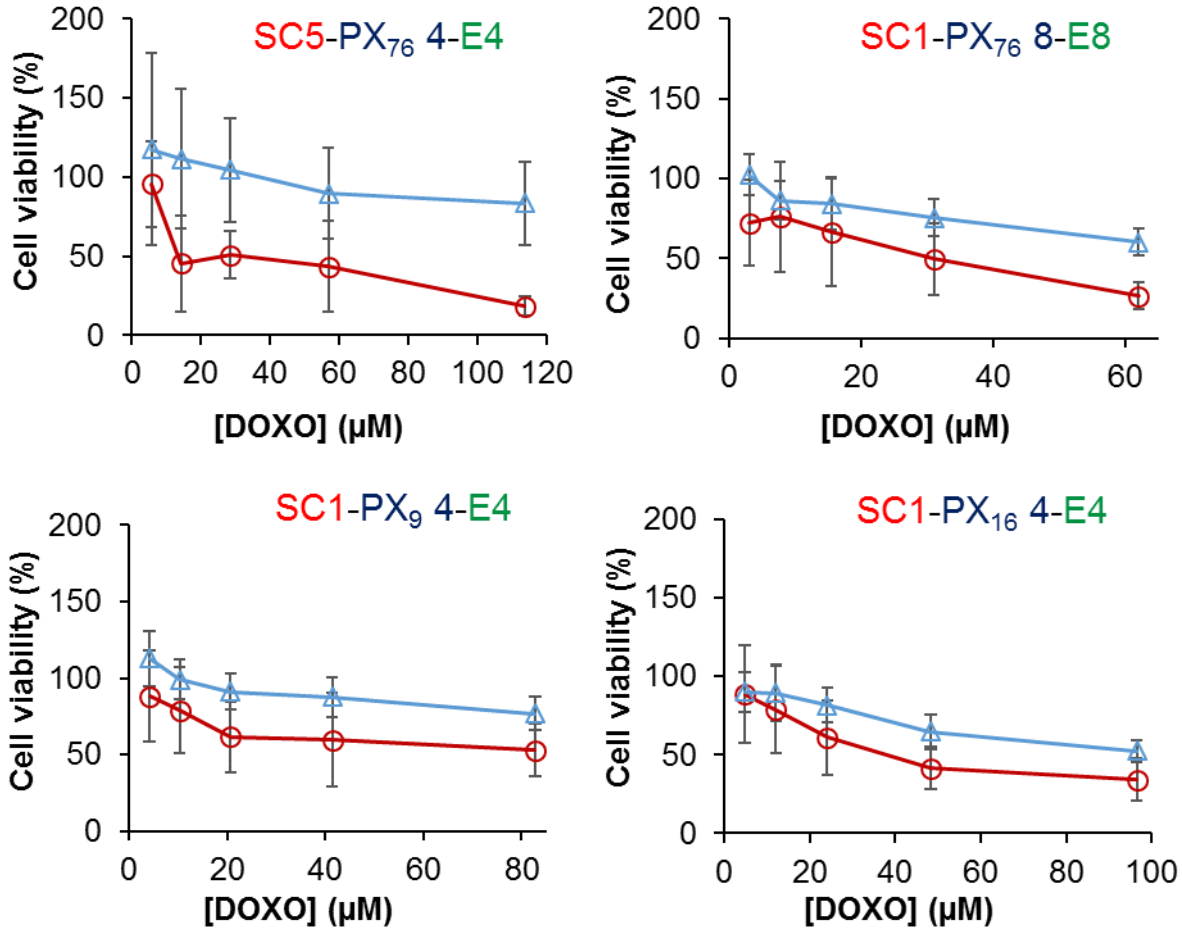

Figure 16. Cell viability of: (●) HeLa and (▲) RAW cell lines as a function of DOXO concentration after 24 h of incubation at 37°C.

As shown above, bare microgels are biocompatible and do not inhibit growth of both types of cell lines in the range of the studied microgel concentrations (0.1 to 2 mg.mL^{-1}). In contrast, DOXO-loaded microgels exhibit higher cytotoxicity due to the effect of the drug (**Figure 16**). As expected, DOXO-loaded microgel cytotoxicity is dose-dependent as cell viability decreases by increasing the concentration of DOXO-loaded microgels and, hence, by increasing the concentration of DOXO. For the highest DOXO concentration used, the decrease of cell viability in the presence of DOXO-loaded microgels was more pronounced in the case of HeLa cells than for RAW ones. This result could be explained by the fact that RAW cells grow quicker than HeLa cells leading to a higher percentage of viable cells at the same percentage of dead cells. Additionally, HeLa cells are more sensitive to DOXO-loaded microgels as a result of their higher metabolic activity, which may lead to larger particle uptakes (confirmed by the cellular uptake experiments presented in part III.4 of this Chapter), and, hence, a larger DOXO concentration inside the cells.

Figure 17 reports the cell viability of HeLa cells after incubation for 24 h with free DOXO and the different DOXO-loaded microgels in the same range of initial loaded DOXO concentrations (from 3 to 30 µM).

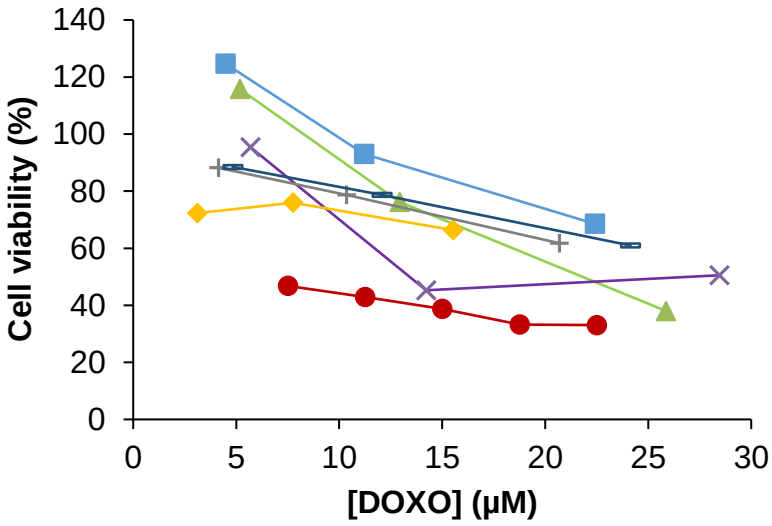

Figure 17. Cell viability of HeLa cell line as a function of DOXO concentration after incubation for 24 h at 37°C with: (●) Free DOXO, (■) DOXO-loaded SC1-PX_{76} 4-E4 microgel, (▲) DOXO-loaded SC1-PX_{76} 8-E4 microgel, (✖)DOXO-loaded SC5-PX_{76} 4-E4 microgel, (◆) DOXO-loaded SC1-PX_{76} 8-E8 microgel, (✚) DOXO-loaded SC1-PX_{9} 4-E4 microgel and (━) DOXO-loaded SC1-PX_{16} 4-E4 microgel. For clearness error bars are not plotted.

At similar loaded DOXO concentration microgels show similar cytotoxicity. This was an expected result since whatever the physico-chemical features of the bare microgels, similar cytotoxicity and DOXO release profiles were observed.

At similar initial DOXO concentrations, the viability of HeLa cells is higher when incubated in the presence of DOXO-loaded microgels than with free DOXO as a consequence of the sustained release of DOXO from the microgels. Indeed, and as observed for other PVCL-based microgels, the release of the drug from the microgels to the cells through diffusion is a time-dependent and sustained process.[10, 15, 19]

IV. Conclusions

The stability of bare PVCL-based microgels was studied after incubation for 13 days at 37°C in different biological mimicking media. An obvious increase of the microgel hydrodynamic diameter was systematically observed in PBS buffer, revealing the formation of aggregates of

microgel particles due to the screening of the particle charges in high ionic strength medium. In FBS supplemented media (either PBS or DMEM) the microgel destabilization occurred later, which can be ascribed to the adsorption of proteins, specially negatively charged BSA onto the microgel surface, leading to the reduction of their net particle charge. These results showed that, for further uses of the PVCL-based microgel in blood serum conditions, the incubation time before aggregation should be carefully considered.

Cytotoxicity assays of the bare PVCL-based microgels on HeLa and RAW cells indicated that all the microgel particles were biocompatible for concentration ranging from 0.005 to 2 $mg.mL^{-1}$. The inhibition of cell's growth was both a time and a dose-dependent process. Similar cytotoxicity profiles were observed for all the studied microgels whatever their initial colloidal and physical characteristics (size, cationic content, chain length of the cationic stabilizer).

The successful cellular uptake of the microgels was assessed using fluorescence microscopy. The microgel internalization appeared to be time-dependent as well as the release of R6G into the cell cytoplasm, with a sustained release profile of the dye from the microgels into the cells. The mechanism of internalization of microgels and the interactions between microgels and HeLa cells was investigated through blocking different endocytic uptake pathways either globally, by decreasing the incubation temperature to 4°C, or using different endocytosis specific inhibitors of each potential internalization mechanism. It could be observed that inhibition of clathrins gave rise to a reduction in the extent of internalization of R6G-loaded microgels demonstrating that this pathway was one of the main mechanisms responsible for microgel internalization. This result was confirmed by a quantification of the extent of internalization inhibition for selected DOXO-loaded microgels. Indeed, a maximum cell survival was observed when the clathrin-dependent endocytic pathway was inhibited, either with sucrose or chlorpromazine.

Doxorubicin anticancer model drug was successfully loaded into selected microgels. However, low amounts of drug were effectively encapsulated due to the existence of electrostatic repulsions between both positively charged microgels and DOXO at the pH at which the encapsulation was conducted. Therefore, the loading process should be optimized. For example, DOXO encapsulation might be increased by working at a pH for which DOXO is neutral.

The cumulative DOXO release profiles of the microgels were studied at pH 5.5 and pH 7.4. At both pH, a burst release of the drug was observed within 7 h of incubation. While a sustained release of the drug was observed after this period at pH 7.4 (30-40 % of drug released within

37 h of incubation), much higher amounts of drug were released from the microgels at pH 5.5. As the cationic PVCL-based microgels were not expected to be pH-sensitive, the observed differences could be attributed to protonation of DOXO molecules at pH 5.5, which lower the drug/microgel affinity by enhancing electrostatic repulsions between them.

The DOXO-loaded microgels exhibited higher cytotoxicity on HeLa cells than bare PVCL microgels due to the effect of the drug. At similar initial DOXO concentrations and for incubation at 37°C for 24 h, the viability of HeLa cells was higher when incubated in the presence of DOXO-loaded microgels than with free DOXO as a consequence of the sustained release of DOXO from the microgels, confirming the suitability of the cationic PVCL-based microgels as chemotherapeutic drug delivery nanocarriers.

The results presented in this Chapter highlight the potential application of the cationic PVCL-based microgels as drug delivery nanocarriers. However, further work would be still required, for example, to analyze in greater detail the mechanisms involved in exocytosis and cell death. In addition, as the degradability of synthetic polymers is still a concern for their use in biomedical applications,[41, 42] it would be interesting to design cationic PVCL-based microgels with improved degradability by means of using a degradable crosslinker or degradable polymer units. Indeed, different degradable crosslinkers have already been successfully used for the design of PVCL-based nanogels.[20, 43, 44] PEGylation of the microgel particles by means of using a reactive PEG-*b*-PAETAC as stabilizer for the emulsion polymerization of VCL could be envisaged as a mean to improve microgel stability in high ionic strength media and to decrease the adsorption of proteins into the microgel surfaces, while retaining the cationic character of the microgels. Indeed, the design of cationic PEG-containing polymers allows to maintain the cationic binding properties and simultaneously provides the protective features of the PEG moiety.[31] As a consequence, such PEGylated cationic PVCL-based microgels should enhance their *in-vivo* circulation time.

V. References

1. Chen, D.; Song, P.; Jiang, F.; Meng, X.; Sui, W.; Shu, C.; Wan, L. J. *The journal of physical chemistry. B* **2013,** 117, (5), 1261-8.
2. Jiang, Q.; Song, C.; Nangreave, J.; Liu, X.; Lin, L.; Qiu, D.; Wang, Z. G.; Zou, G.; Liang, X.; Yan, H.; Ding, B. *Journal of the American Chemical Society* **2012,** 134, (32), 13396-403.

3. Hillaireau, H.; Couvreur, P. *Cellular and molecular life sciences : CMLS* **2009,** 66, (17), 2873-96.
4. Shang, L.; Nienhaus, K.; Nienhaus, G. U. *Journal of nanobiotechnology* **2014,** 12, 5.
5. Wiethoff, C. M.; Middaugh, C. R. *Journal of pharmaceutical sciences* **2003,** 92, (2), 203-17.
6. Yin, H.; Kanasty, R. L.; Eltoukhy, A. A.; Vegas, A. J.; Dorkin, J. R.; Anderson, D. G. *Nature reviews. Genetics* **2014,** 15, (8), 541-55.
7. Van Tomme, S. R.; De Geest, B. G.; Braeckmans, K.; De Smedt, S. C.; Siepmann, F.; Siepmann, J.; van Nostrum, C. F.; Hennink, W. E. *Journal of controlled release : official journal of the Controlled Release Society* **2005,** 110, (1), 67-78.
8. Belmadi, N.; Midoux, P.; Loyer, P.; Passirani, C.; Pichon, C.; Le Gall, T.; Jaffres, P. A.; Lehn, P.; Montier, T. *Biotechnology journal* **2015,** 10, (9), 1370-89.
9. Nuhn, L.; Gietzen, S.; Mohr, K.; Fischer, K.; Toh, K.; Miyata, K.; Matsumoto, Y.; Kataoka, K.; Schmidt, M.; Zentel, R. *Biomacromolecules* **2014,** 15, (4), 1526-33.
10. Aguirre, G.; Villar-Alvarez, E.; González, A.; Ramos, J.; Taboada, P.; Forcada, J. *Journal of Polymer Science Part A: Polymer Chemistry* **2016,** 54, (12), 1694-1705.
11. Kawaguchi, H.; Fujimoto, K.; Mizuhara, Y. *Colloid & Polymer Science* **1992,** 270, (1), 53-57.
12. Trongsatitkul, T.; Budhlall, B. M. *Colloids and Surfaces B: Biointerfaces* **2013,** 103, 244-252.
13. Standardization, I. O., Tests for in-vitro cytotoxicity. 2009; Vol. ISO 10993-5:2009(E).
14. Xiong, Q.; Zhang, M.; Zhang, Z.; Shen, W.; Liu, L.; Zhang, Q. *International journal of pharmaceutics* **2014,** 474, (1-2), 232-40.
15. Wang, Y.; Nie, J.; Chang, B.; Sun, Y.; Yang, W. *Biomacromolecules* **2013,** 14, (9), 3034-46.
16. Prabaharan, M.; Grailer, J. J.; Steeber, D. A.; Gong, S. *Macromolecular bioscience* **2009,** 9, (8), 744-53.
17. Shah, S.; Pal, A.; Gude, R.; Devi, S. *European Polymer Journal* **2010,** 46, (5), 958-967.
18. Cavet, M. E.; Harrington, K. L.; VanDerMeid, K. R.; Ward, K. W.; Zhang, J. Z. *Contact lens & anterior eye : the journal of the British Contact Lens Association* **2009,** 32, (4), 171-5.
19. Lou, S.; Gao, S.; Wang, W.; Zhang, M.; Zhang, Q.; Wang, C.; Li, C.; Kong, D. *Journal of Applied Polymer Science* **2014,** 131, (23), 41146-41153.
20. Wang, Y.; Zheng, J.; Tian, Y.; Yang, W. *J. Mater. Chem. B* **2015,** 3, (28), 5824-5832.
21. Vihola, H.; Laukkanen, A.; Valtola, L.; Tenhu, H.; Hirvonen, J. *Biomaterials* **2005,** 26, (16), 3055-64.
22. Liu, F.; Kozlovskaya, V.; Medipelli, S.; Xue, B.; Ahmad, F.; Saeed, M.; Cropek, D.; Kharlampieva, E. *Chemistry of Materials* **2015,** 27, (23), 7945-7956.
23. Slowing, II; Wu, C. W.; Vivero-Escoto, J. L.; Lin, V. S. *Small* **2009,** 5, (1), 57-62.
24. Podila, R.; Brown, J. M. *Journal of biochemical and molecular toxicology* **2013,** 27, (1), 50-5.
25. Naahidi, S.; Jafari, M.; Edalat, F.; Raymond, K.; Khademhosseini, A.; Chen, P. *Journal of controlled release : official journal of the Controlled Release Society* **2013,** 166, (2), 182-94.
26. Garnett, M. C. *Critical Reviews™in Therapeutic Drug Carrier Systems* **1999,** 16, (2), 61.
27. McAllister, K.; Sazani, P.; Adam, M.; Cho, M. J.; Rubinstein, M.; Samulski, R. J.; DeSimone, J. M. *Journal of the American Chemical Society* **2002,** 124, (51), 15198-15207.
28. Zhang, H.; Xia, T.; Meng, H.; Xue, M.; George, S.; Ji, Z.; Wang, X.; Liu, R.; Wang, M.; France, B.; Rallo, R.; Damoiseaux, R.; Cohen, Y.; Bradley, K. A.; Zink, J. I.; Nel, A. E. *ACS nano* **2011,** 5, (4), 2756-69.
29. Cai, J.; Yue, Y.; Rui, D.; Zhang, Y.; Liu, S.; Wu, C. *Macromolecules* **2011,** 44, (7), 2050-2057.
30. Sahariah, P.; Benediktssdottir, B. E.; Hjalmarsdottir, M. A.; Sigurjonsson, O. E.; Sorensen, K. K.; Thygesen, M. B.; Jensen, K. J.; Masson, M. *Biomacromolecules* **2015,** 16, (5), 1449-60.
31. Hoppert, M., *Microscopic Techniques in Biotechnology*. Wiley-VCH: 2003.

32. Oliveira, C.; Ribeiro, A. J.; Veiga, F.; Silveira, I. *Journal of Biomedical Nanotechnology* **2016,** 12, (5), 841-862.
33. Khalil, I. A.; Kogure, K.; Akita, H.; Harashima, H. *Pharmacological reviews* **2006,** 58, (1), 32-45.
34. Mayor, S.; Pagano, R. E. *Nature reviews. Molecular cell biology* **2007,** 8, (8), 603-12.
35. Gratton, S. E.; Ropp, P. A.; Pohlhaus, P. D.; Luft, J. C.; Madden, V. J.; Napier, M. E.; DeSimone, J. M. *Proceedings of the National Academy of Sciences of the United States of America* **2008,** 105, (33), 11613-8.
36. Qiu, Y.; Park, K. *Advanced Drug Delivery Reviews* **2012,** 64, 49-60.
37. Shi, F.; Ding, J.; Xiao, C.; Zhuang, X.; He, C.; Chen, L.; Chen, X. *Journal of Materials Chemistry* **2012,** 22, (28), 14168.
38. Sanson, C.; Schatz, C.; Le Meins, J.-F.; Soum, A.; Thévenot, J.; Garanger, E.; Lecommandoux, S. *Journal of Controlled Release* **2010,** 147, (3), 428-435.
39. Imaz, A.; Forcada, J. *Journal of Polymer Science Part A: Polymer Chemistry* **2010,** 48, (5), 1173-1181.
40. Cambon, A.; Rey-Rico, A.; Mistry, D.; Brea, J.; Loza, M. I.; Attwood, D.; Barbosa, S.; Alvarez-Lorenzo, C.; Concheiro, A.; Taboada, P.; Mosquera, V. *International journal of pharmaceutics* **2013,** 445, (1-2), 47-57.
41. Delplace, V.; Nicolas, J. *Nature chemistry* **2015,** 7, (10), 771-84.
42. Zhang, X.; Malhotra, S.; Molina, M.; Haag, R. *Chemical Society reviews* **2015,** 44, (7), 1948-73.
43. Aguirre, G.; Ramos, J.; Forcada, J. *Soft Matter* **2013,** 9, (1), 261-270.
44. Agrawal, G.; Wang, J.; Bruster, B.; Zhu, X.; Moller, M.; Pich, A. *Soft Matter* **2013,** 9, (22), 5380-5390.

Acknowledgments

The doctoral school of Pau (ED 211) is acknowledged for financial support for the one month stay at Santiago de Compostela. Professor Pablo Taboada is thanked for hosting, giving me the opportunity to work on this project and for providing the facilities and reactants. Miss Eva Villar-Alvarez is acknowledged for her support during this work. Professor Pablo Taboada and Miss Eva Villar-Alvarez are sincerely thanked for performing the additional experiments on DOXO-loading/release and testing of additional cellular uptake pathways.

Conclusions

The objective of the present PhD work was to investigate the synthesis and characterization of thermoresponsive poly(*N*-vinylcaprolactam) (PVCL)-based particles. Two types of particles were successfully synthesized by heterogeneous polymerization process in aqueous media, using macromolecular stabilizers with a reactive xanthate chain-end.

In the first part of this work, we implemented a strategy to design thermoresponsive PEGylated PVCL-based particles by means of hydrophobic interactions between the poly(*N*-vinylcaprolactam-*co*-vinyl acetate) statistical copolymer chains of the core. A preliminary study was required to evaluate the control of the xanthate-mediated RAFT/MADIX copolymerization of VAc and VCL in bulk and to estimate reliable values of reactivity ratios for VAc and VCL radical polymerization in regards to the disparate values previously reported in the literature. This study was developed in Chapter 1 of Part I. Well-defined thermoresponsive poly(*N*-vinylcaprolactam-*co*-vinyl acetate) copolymers with controlled molar masses and low dispersity values ($Đ$ < 1.3) were successfully synthesized. Both conventional linearization methods and nonlinear least-squares methods were applied to determine values of reactivity ratios for VAc and VCL. The nonlinear least-squares (NLLS) method based on the integrated form of the copolymerization equation (Skeist equation) provided values of reactivity ratios of $r_{VAc} = 0.33 \pm 0.10$ and $r_{VCL} = 0.29 \pm 0.15$. According to this close reactivity of both monomers, P(VAc-*co*-VCL) copolymers presented nearly homogeneous distribution of VAc and VCL comonomers along the polymer chains. These P(VAc-*co*-PVCL) amphiphilic copolymers exhibited tunable phase transition temperature and self-assembly behavior depending on the fraction of hydrophobic VAc. Indeed, static light scattering measurements highlighted that P(VAc-*co*-VCL) copolymer with $F_{VAc} = 0.53$ had the capability to self-assemble in water into trimer aggregates at a temperature below the cloud point temperature, by means of hydrophobic interactions.

On the basis of the results presented in this chapter 1, the synthesis of thermoresponsive PVCL-based particles associated by hydrophobic interactions was discussed in chapter 2 of Part I of this thesis. For that purpose, a xanthate-terminated PEG (PEG-X) with high degree of chain-end functionalization (87 mol-%) was used as macromolecular chain transfer agent for the batch emulsion copolymerization of VAc and VCL performed at 10 wt-% of initial solids content, with two different initial VAc feed ratios. We highlighted that this PEG-X efficiently acted as

both stabilizer and macro chain-transfer agent during the copolymerization, enabling the direct synthesis of thermoresponsive PEG-*b*-P(VAc-*co*-VCL) block copolymers in aqueous dispersed media. The colloidal characterization of the final dispersions showed that a fraction of hydrophobic VAc of 47 mol-% in the second block of the copolymer was required to maintain the integrity of the particles formed by self-assembly of the PEG-*b*-P(VAc-*co*-VCL) block copolymers in water, at a temperature below the cloud point by means of hydrophobic interactions. The well-defined physically crosslinked PEG_{49}-*b*-$P(VAc_{0.47}$-*co*-$VCL_{0.53})_{154}$ particles interestingly behaved as thermoresponsive colloids able to undergo a reversible swollen-to-collapse transition upon increasing the temperature. On the other hand, PEG_{49}-*b*-$P(VAc_{0.17}$-*co*-$VCL_{0.83})_{111}$ block copolymer with a lower fraction of VAc in the copolymer (17 mol-%) behaved as soluble polymer chains in the aqueous phase at low temperature (T < 20 °C) and self-assembled into large ill-defined aggregates by rising the temperature. Finally, the statistical copolymers based on VAc and VCL were successfully hydrolyzed into promising thermoresponsive biocompatible statistical copolymers based on vinyl alcohol and *N*-vinylcaprolactam co-monomer units. This study was the first example of synthesis of PVCL-based amphiphilic copolymers by controlled radical emulsion polymerization.

The second part of this work was devoted to the synthesis and characterization of cationic PVCL-based thermoresponsive microgels that were evaluated as potential drug nanocarriers. Well-defined monodisperse chemically crosslinked PVCL-based microgels with a cationic stabilizing shell were successfully synthesized by heterogeneous polymerization in aqueous media, by using a reactive cationic macromolecular stabilizer.

The first chapter of Part II depicted the synthesis by RAFT/MADIX polymerization of a series of poly[2-(acryloyloxy)ethyl]trimethylammonium chloride (PAETAC-X) cationic polymers with xanthate reactive chain-end and different molar masses (M_n). Attempts to assess the macromolecular features of the synthesized cationic polymers by using different characterization techniques (SEC, A-4F, DOSY-NMR, MALDI-TOF) revealed the complex behavior of these polyelectrolytes in solution with most probably the formation of polymer aggregates due to electrostatic interactions between charged polymer chains. However, asymmetrical field flow field fractionation (A-4F) analyses in water with 5 mM NaN_3 salts attested of a certain control of the xanthate-mediated RAFT polymerization of the cationic AETAC monomer with values of $M_{n,\,A\text{-}4F,\,MALLS}$ decreasing with increasing initial concentration of xanthate chain transfer agent and dispersity values below 1.4. The UV-visible analysis of the

cationic polymers confirmed the presence of the dithiocarbonate end-functional group for the polymers synthesized by RAFT/MADIX polymerization.

As presented in the second chapter of Part II, it was proved that the xanthate extremity of the cationic P(AETAC-X) polymers played a crucial role in the colloidal stabilization of PVCL microgels during the polymerization process, allowing to synthesize for the first time stable monodisperse cationic PVCL-based microgels up to 10 wt-% of initial solids content. Indeed, for the all range of initial solids contents (τ = 1 to 10 wt-%), stable PVCL-based microgels were synthesized in the presence of the reactive P(AETAC-X) stabilizer while particle flocculation or coagulation were observed during emulsion or precipitation polymerization using either non-reactive P(AETAC) polymers as stabilizers or a conventional cationic molecular surfactant (CTAB). The stable cationic microgels exhibited a thermoresponsive behavior with a volumetric shrinkage upon heating and volume phase transition temperature values ranging between 28 °C and 30°C for the microgels synthesized using 4 and 8 wt-% of P(AETAC-X) based on VCL. The swelling behavior of the microgel particles could effectively be tuned by playing on different synthesis variables such as the initial solids content, the amounts of P(AETAC-X) stabilizer and EGDMA crosslinker.

Finally, the suitability of the cationic PVCL-based microgels for further uses as drug nanocarriers was demonstrated in the third chapter of Part II. Indeed, cytotoxicity assays of the bare PVCL-based microgels on HeLa and RAW cells indicated that all the microgel particles, whatever their initial colloidal features (size, cationic content, chain length of the cationic stabilizer), were biocompatible for microgel concentration ranging from 0.005 to 2 $mg.mL^{-1}$. The microgel cellular uptake was characterized by fluorescence microscopy. The cellular uptake pathway was investigated using three different inhibitors to conclude that the internalization of microgels into HeLa cells occurs mainly by clathrin-mediated endocytosis. Doxorubicin anticancer model drug was loaded into a series of selected microgels. The cumulative DOXO release profiles of the microgels studied at pH 7.4 showed a burst release phase for 7 h of incubation followed by a sustained release of the drug from the microgels. The DOXO-loaded microgels exhibited higher cytotoxicity on HeLa cells than bare PVCL microgels due to the effect of the drug. At similar initial DOXO concentrations and for incubation at 37°C for 24 h, the viability of HeLa cells was higher when incubated in the presence of DOXO-loaded microgels than with free DOXO as a consequence of the sustained release of DOXO from the microgels, confirming the suitability of the cationic PVCL-based microgels as chemotherapeutic drug delivery nanocarriers.

As perspectives for this work, it should be interesting to combine both approaches presented in Part I and Part II of this manuscript to synthesize PEGylated cationic PVCL-based microgels. Indeed, as previously mentioned, for further biomedical applications of the microgels, functionalization of the microgel surface with PEG should increase the stability of the microgels in biological media and hence the microgel *in-vivo* circulation time, by constituting a steric barrier to the adsorption of proteins onto the microgel surface. The PEG-xanthate macromolecular chain transfer agent could be used to mediate RAFT/MADIX polymerization of AETAC cationic monomer directly in water instead of the hydroalcoholic medium. As complete conversion of AETAC monomer was reached (see Chapter 1 Part II), the synthesis of the cationic thermoresponsive PVCL microgels might be simplified by performing in the same reactor the PEG-xanthate mediated polymerization of AETAC in water followed by emulsion polymerization of VCL in the presence of crosslinker. Moreover, the incorporation of hydrophobic VAc units in the microgel inner network by copolymerization of VCL with VAc can be envisaged to create hydrophobic nanodomains enhancing the loading of hydrophobic drugs into the microgels. Also, partial hydrolysis of the PVAc units to form biocompatible poly(vinyl alcohol) (PVA) might favor the encapsulation of hydrophilic drug by means of hydrogen bonding between the drug and PVA units. Apart from the aforementioned advantages, the PEG block might reduce the formation of aggregates between polycations to overcome the issues of cationic polymer characterization.

APPENDIX CHAPTER 2 – PART II. Cationic thermoresponsive Poly(*N*-vinylcaprolactam) microgels synthesized by surfactant free emulsion polymerization by using a reactive cationic macromolecular chain-transfer agent

1. Reversibility of the PVCL-based microgel swelling to-collapse transition

For all the stable PVCL-based microgels presented in Chapter 2 - Part II, reversibility of the swelling-de-swelling behavior was observed as the values of the final average hydrodynamic diameters as a function of the temperature and the value of the volume phase transition temperature (VPTT) were the same whatever the measurement cycle, *i.e*, heating or cooling cycle (**Figure 1**).

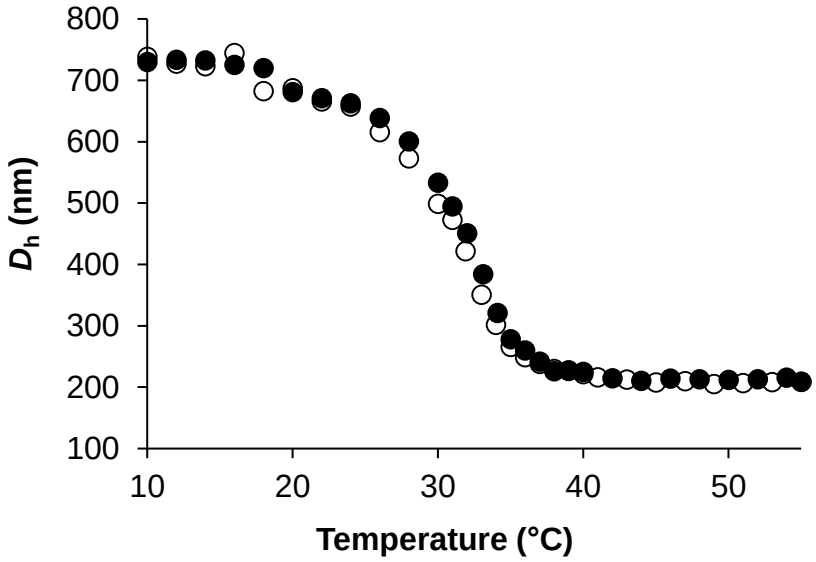

Figure 1. Final average hydrodynamic diameters as a function of the temperature for the microgel synthesized at 5 wt-% of initial solids content, 4 wt-% of P(AETAC-X)$_{76}$ as stabilizer and 4 wt-% of EGDMA (SC5-PX$_{76}$ 4-E4 in Table 7 Chapter 2 - Part II). Full symbols: heating cycle, open symbols: cooling cycle.

2. Microgel electrophoretic mobility measured at different pH and ionic strength

The microgel electrophoretic mobilities were measured at room temperature before centrifugation, in cationic buffer solutions at different pH (3, 6 and 9) and ionic strengths of 1 and 10 mM (**Table 1**).

At an ionic strength of 1 mM, the electrophoretic mobility of the microgels decreased when the pH increased. This was an unexpected result since the P(AETAC-X) cationic stabilizer is permanently charged and thus no influence of the pH should be noticed. Moreover, since the ionic strengths of the different cationic buffers were equal, differences cannot be attributed to a variation of the counterion concentration. However, the discrepancy of the microgel electrophoretic mobility might be explained by the different nature of the buffer and consequently the different nature of the ions in the solutions, resulting in different adsorption of these ions onto the microgel outer shell. The electrophoretic mobilities of the microgels

synthesized by surfactant free polymerization or using CTAB as surfactant are negative at pH 9 which is not the case using either P(AETAC-X) or P(AETAC) polymers. This might be due to the steric hindrance of the stabilizers which limit the adsorption of negatively charged ions of the buffer.

It also appeared that the microgel electrophoretic mobility was not influenced by the ionic strength of the buffer solution (in the range of concentrations studied) since the electrophoretic mobility values measured at pH 3 and 1 mM of ionic strength are similar to the one measured at pH 3 and 10 mM of ionic strength.

Table 1. Microgel electrophoretic mobility measurements in cationic buffer solutions at different pH (3, 6 and 9) and ionic strength of 1 and 10 mM.[a]

Reaction	pH	Ionic strength *mM*	Dialyzed sample electrophoretic mobility $m^2/Vs \times 10^{-8}$
SC1-PX_{76} 4-E4	3	10	0.42 ± 0.05
		1	0.38 ± 0.05
	6	1	0.50 ± 0.10
	9	1	0.03 ± 0.01
SC1-PX_{76} 8-E4	3	10	0.95 ± 0.17
		1	0.88 ± 0.31
	6	1	0.66 ± 0.14
	9	1	0.21 ± 0.06
SC5-PX_{76} 4-E4	3	10	0.57 ± 0.25
		1	0.37 ± 0.11
	6	1	0.35 ± 0.03
	9	1	0.04 ± 0.02
SC5-PX_{76} 8-E4	3	10	1.22 ± 0.04
		1	0.91 ± 0.33
	6	10	0.47 ± 0.14
		1	0.75 ± 0.05
	9	10	0.06 ± 0.04
		1	0.45 ± 0.16
SC10-PX_{76} 4-E4	3	10	0.88 ± 0.44
		1	0.61 ± 0.38
	6	1	0.59 ± 0.12
	9	1	0.11 ± 0.07
SC1-PX_{9} 4-E4	3	10	0.44 ± 0.16
		1	0.45 ± 0.08
	6	1	0.45 ± 0.05
	9	1	0.12 ± 0.03
SC5-PX_{9} 4-E4	3	10	0.38 ± 0.18
		1	0.35 ± 0.10
	6	1	0.44 ± 0.03
	9	1	0.14 ± 0.02
SC5-P 4-E4	3	10	0.95 ± 0.43
		1	0.25 ± 0.07
	6	1	0.23 ± 0.04
	9	1	0.17 ± 0.05
SC5-CTAB 4-E4	3	10	0.35 ± 0.07
		1	0.25 ± 0.14
	6	1	0.16 ± 0.02
	9	1	-0.10 ± 0.02
SC5-0-E4	3	10	0.15 ± 0.05
		1	0.16 ± 0.04
	6	1	0.04 ± 0.01
	9	1	-0.11 ± 0.01

[a] Measurements were carried out at 25°C, samples were analyzed at a concentration of 0.05 wt-% in buffer solution.

3. DOSY NMR analyses

In our attempt to emphasize the formation of P(AETAC)-*b*-PVCL block copolymers during the VCL emulsion polymerization process using P(AETAC-X) polymers as stabilizers, the emulsion polymerization of VCL was performed in the absence of crosslinker, using different amounts of reactive P(AETAC-X) polymers as stabilizer (**Table 2**). The final products were characterized by DOSY NMR spectroscopy after being dialyzed to remove unreacted monomer.

Table 2. Emulsion polymerization of VCL performed in the absence of EGDMA, at 70°C, with 1 wt-% of ADIBA initiator based on VCL and 3 wt-% of TRIZMA buffer based on VCL.

Expt	τ^a *wt-%*	**Stabilizer**	**Stabilizer** *wt-% VCL*	$DP_{\text{target PVCL block}}{}^b$	$n_{\text{macro-CTA}}/n_{\text{initiator}}{}^c$	**VCL final conversion** *%*
14	5	$P(AETAC\text{-}X)_9$ (56 % conv.)	4	195	1.16	88
15	5	$P(AETAC\text{-}X)_{16}$ (62 % conv.)	4	834	0.28	9
16	1	$P(AETAC\text{-}X)_{16}$ (100 % conv.)	4	1424	0.16	11
17	1	$P(AETAC\text{-}X)_{16}$ (100 % conv.)	8	726	0.31	25
18	1	$P(AETAC\text{-}X)_{16}$ (100 % conv.)	12	490	0.48	14

[a] τ: initial solids content; [b] $DP_{\text{target PVCL block}}$: targeted degree of polymerization for the PVCL block, $DP_{\text{target PVCL block}} = n_{VCL}/n_{\text{macro-CTA}}$, with macro-CTA: macro-chain transfer agent: P(AETAC-X) polymer; [c] $n_{\text{macro-CTA}}/n_{\text{initiator}}$: ratio of the number of moles of P(AETAC-X) macro-chain transfer agent divided by the number of moles of ADIBA initiator.

For the first experiment conducted (expt 14 in **Table 2**), the final conversion of VCL being high (88%), the signal of the cationic stabilizer was too low to be detected in the DOSY NMR spectrum. Consequently, in order to be able to distinguish the signals of P(AETAC-X) and PVCL polymers, it was required to stop the experiment at 10-30 % of VCL conversion. For such low conversions and whatever the initial amount of stabilizer based on VCL we used (expt 15-18 in **Table 2**), DOSY NMR spectra displayed two distinct diffusion coefficients for each homopolymers (**Figure 2**). Therefore, we could not highlight the presence of any block copolymers. However, the transfer constant of xanthate being low, the transfer of PVCL growing chains to the cationic reactive polymer might occur for higher conversion of VCL. In that case, we were restricted by the detection limit of the technique as we used less than 10 wt-% of cationic block versus PVCL. It was shown in Chapter 2 - Part II that the DOSY NMR spectra of the supernatants recovered after centrifugation of the PVCL-based microgels showed only one diffusion coefficient. Moreover, colloidally stable well-defined PVCL-based

microgels could be synthesized at up to 10 wt-% of solids content only by using the reactive P(AETAC-X) as stabilizers. So, the key role played by the polymer reactive chain-end in the stabilization of the PVCL-based microgels was demonstrated.

(a)

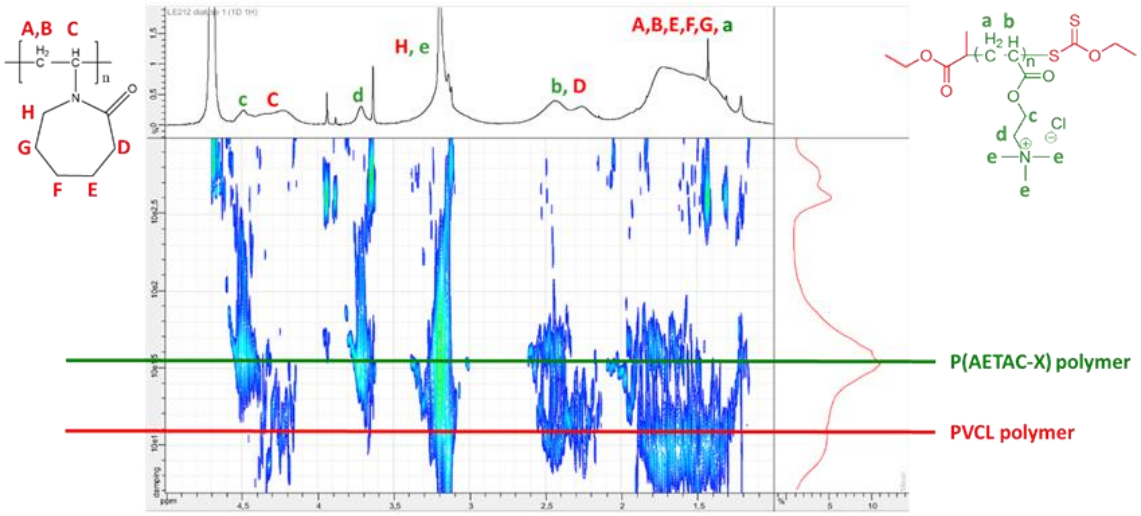

(b)

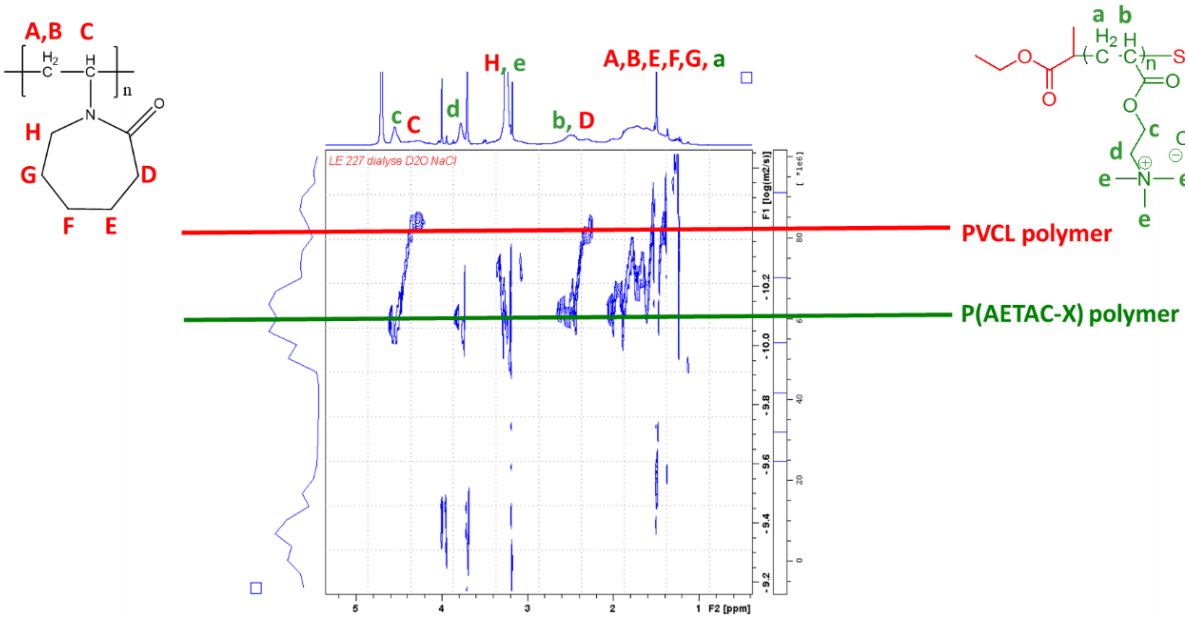

Figure 2. DOSY NMR spectra in D_2O of: **(a)** expt 15 and **(b)** expt 17 in **Table 2**.

4. Stability of the P(AETAC-X) shell anchorage through microgel centrifugation

Microgel centrifugation

The centrifugation process allows for separating the microgels from all the other compounds that are present in the medium as free molecules or polymers (not covalently bonded to the

particles). Consequently, if P(AETAC-X) polymer is not covalently bonded to the microgel particles, it should desorb from the microgel surface upon centrifugation to be transferred into the supernatant. Moreover, this desorption might induce a change of the microgel electrophoretic mobility.

The microgel dispersion were systematically centrifuged at 1 wt-% of solids content and the supernatants recovered from microgel centrifugation were analyzed by NMR spectroscopy after drying step. For all the centrifuged microgels, characteristic signals of P(AETAC-X) polymer could be detected on the NMR spectra of the supernatant (**Figure 3**).

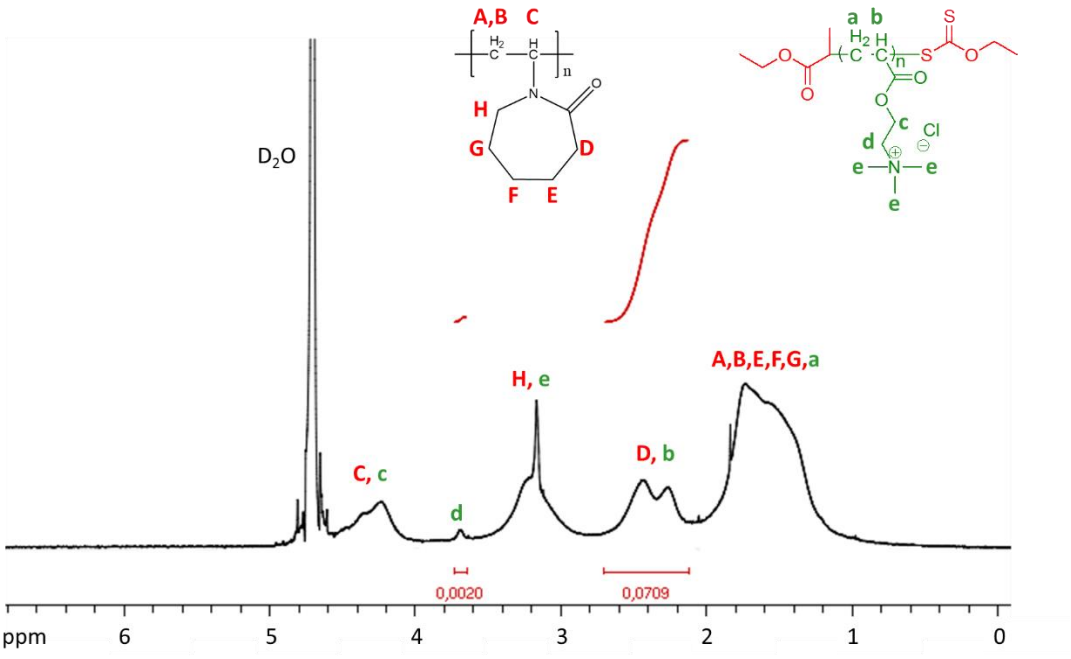

Figure 3. ^{1}H NMR spectrum in D_2O of the supernatant recovered after centrifugation of SC1-PX_{76} 4-E4 microgel (Table 7 Chapter 2 – Part II).

On the basis of the integrals of the protons of P(AETAC-X) and PVCL polymers, it is possible to determine the molar fraction of P(AETAC-X) in the supernatant and therefore to calculate the percentage of free P(AETAC-X) removed by centrifugation process.

Table 3. Analysis of supernatant of centrifuged P(AETAC)-PVCL microgels.

Reaction	$F_{P(AETAC-X)}$ [a]	$w_{P(AETAC-X)}$ [b]	% free chains [c]	$m_{P(AETAC-X)}$ supernatant for the total amount of microgel [d] g	$m_{P(AETAC-X),0}$ g	% of stabilizer removed upon centrifugation [e]
SC1-PX_{76} 4-E4	0.028	0.038	64	0.0511	0.0807	63
SC5-PX_{76} 4-E4	0.016	0.023	64	0.0757	0.2048	37
SC10-PX_{76} 4-E4	0.028	0.038	35	0.0697	0.2017	35
SC1-PX_{76} 8-E4	0.119	0.159	27	0.0927	0.1619	57
SC5-PX_{76} 8-E4	0.055	0.075	38	0.1548	0.4015	39
SC5-P 4-E4	-	-	34	-	0.2035	-
SC1-$PX_{76,cleaved}$ 4-E4	0.030	0.041	56	0.0476	0.0809	59
SC1-PX_{9} 4-E4	0.039	0.054	58	0.1632	0.2007	81
SC5-PX_{9} 4-E4	0.025	0.035	74	0.0540	0.0803	67

[a] Molar fraction of P(AETAC-X) in the supernatant, determined from the integrals of the protons of P(AETAC-X) and PVCL of ^{1}H NMR spectrum (**Figure 3**), $F_{P(AETAC-X)} = \frac{n_{AETAC}}{n_{AETAC}+n_{VCL}}$; [b] Molar fraction of P(AETAC-X) in the supernatant, $w_{P(AETAC-X)} = \frac{F_{AETAC} \times M_{AETAC}}{F_{AETAC} \times M_{AETAC} + F_{VCL} \times M_{VCL}}$ with M_{VCL} = 139 g.mol^{-1} and M_{AETAC} = 194 g.mol^{-1}; [c] Measured by gravimetry from the supernatant recovered by centrifugation of microgels performed at 1 wt-% of solids content for all microgels; [d] $m_{P(AETAC-X)super.\ total\ amount\ microgel} = w_{AETAC} \times \frac{\%\ free\ PVCL\ chains}{100} \times (m_{VCL,0} + m_{P(AETAC-X),0})$;

[e] $\%\ stabilizer\ removed = (\frac{m_{P(AETAC-X)super.\ total\ amount\ microgel}}{m_{P(AETAC-X),0}}) \times 100$.

The results of **Table 3** show that the fraction of free P(AETAC-X) removed by centrifugation ranges between 37 and 81 wt-% of the initial mass of P(AETAC-X). Thus, a part of the stabilizer is covalently bonded to the microgel particle. However, for the microgel synthesized using non-reactive P(AETAC-X)$_{76,cleaved}$ as stabilizer (SC1-$PX_{76,cleaved}$ 4-E4 in **Table 3**), the same amount of stabilizer is removed than for the microgel synthesized using reactive P(AETAC-X)$_{76}$ as stabilizer (SC1-PX_{76} 4-E4 in **Table 3**). This result can be explained by the significant experimental error on the determination of the percentage of stabilizer removed upon centrifugation.

For the microgel synthesized using non-reactive P(AETAC) polymer as stabilizer (SC5-P 4-E4 in **Table 3**), no P(AETAC) was detected in the NMR spectrum of the supernatant. This result might be due to the fact the 50 wt-% of coagulum removed at the end of the synthesis might have contained most of the non-reactive stabilizer (see Table 8 Chapter 2 - Part II).

Another strategy to determine if the stabilizer was or not covalently bonded to the microgel particles consisted in characterizing the microgel electrophoretic mobility after centrifugation.

As for the analysis of the non-centrifuged microgels, the samples were diluted at 0.05 wt-% in buffer solution at pH 3 and ionic strength of 10 mM. Each sample was subjected to ten measurements at 25°C, with a 60 s delay between each measurement. During the ten measurements, we observed a large discrepancy between the values of electrophoretic mobility of the centrifuged microgels. For all the samples, the measured electrophoretic mobility turns negative after 5 measurements which was not the case for the non-centrifuged samples. This low accuracy of the measurements could be linked with a poor stability of the centrifuged microgel dispersions.

As presented in **Figure 4**, the microgel particle sizes at the collapsed state (above the microgel VPTT) increased after the centrifugation process for almost all of the microgels and a loss of the microgel thermoresponsiveness can be observed. The SC1-PX_{76} 8-E4 remained stable with similar diameters after centrifugation.

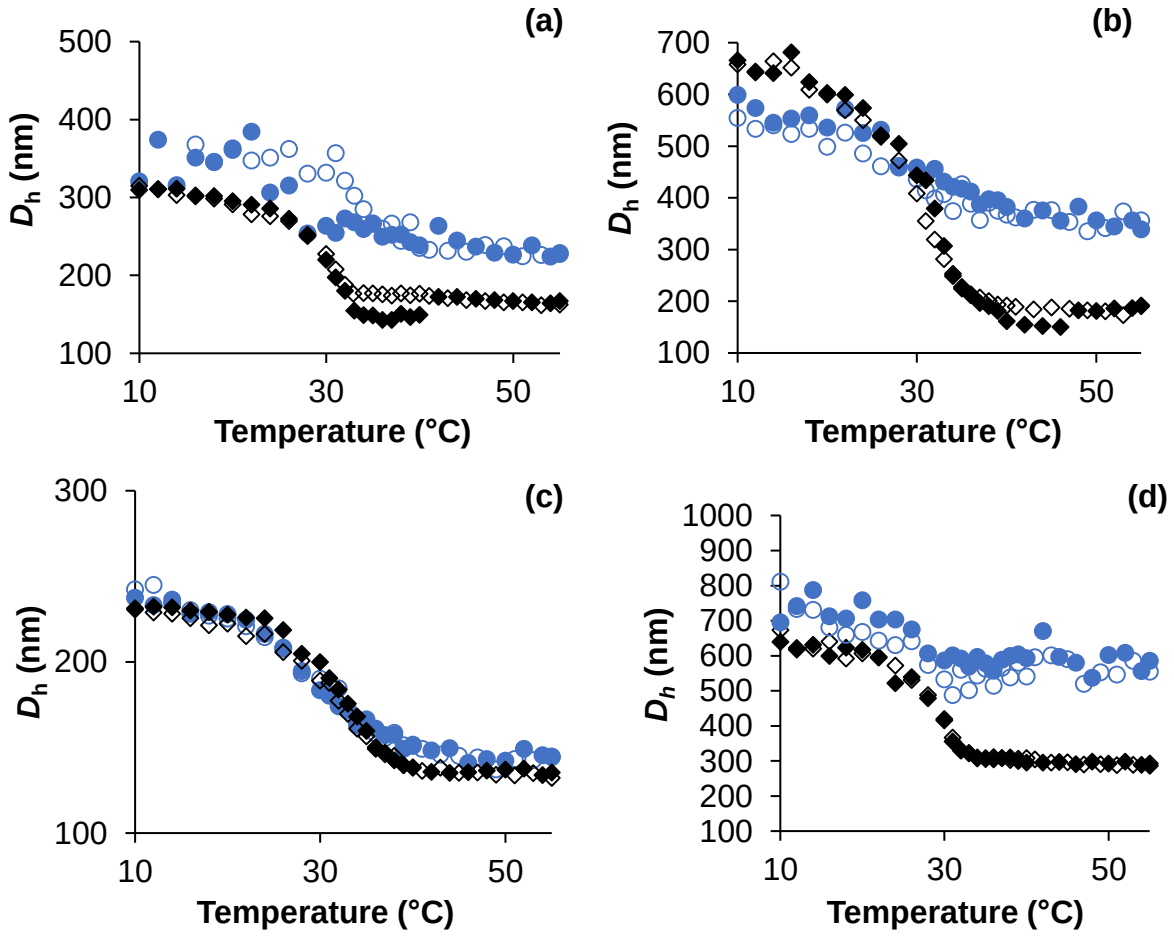

Figure 4. Final average hydrodynamic diameters as a function of the temperature for the: ● centrifuged microgels and ◆ non-centrifuged microgels, full symbols: heating cycle and open symbols: cooling cycle. **(a)** SC1-PX_{76} 4-E4 microgel (Table 7 Chapter 2 - Part II), **(b)** SC5-PX_{76} 4-E4 microgel, **(c)** SC1-PX_{76} 8-E4 microgel, **(d)** SC5-PX_{76} 8-E4 microgel.

In order to understand the consequence of the centrifugation process, various tests were conducted. The microgels were centrifuged under different conditions: 1) at either 40°C (T > VPTT) or 5°C (T < VPTT); 2) after the addition of PVCL homopolymer; 3) or after addition of P(AETAC-X)$_{76}$ polymer; in order to investigate if the microgel destabilization observed at high temperature could be due to entrance of PVCL or P(AEATC-X) chains into the microgel network through centrifugation. In all the cases, a microgel reversible aggregation could be observed when reaching the VPTT (**Figure 5**). Therefore, it appeared that the centrifugation process leads to a destabilization of the microgel particles, probably due to the fact that a fraction of P(AETAC-X) stabilizer was removed from the microgel surface upon centrifugation. Consequently, the centrifugation process should be optimized in terms of duration and speed in order to overcome these issues.

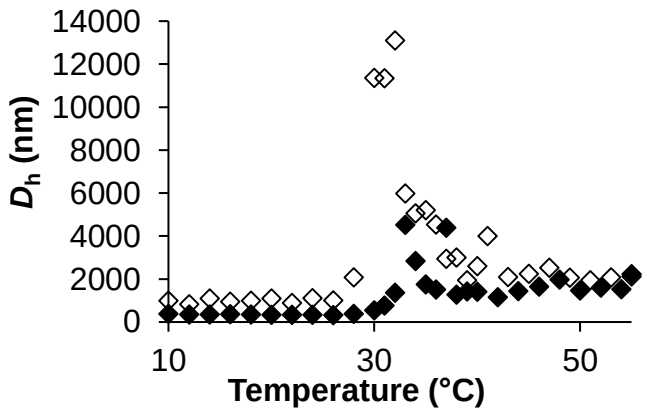

Figure 5. Final average hydrodynamic diameters as a function of the temperature after centrifugation at 40°C for SC1-PX$_{76}$ 4-E4 microgel (Table 7 Chapter 2 - Part II). Full symbols: heating cycle and open symbols: cooling cycle.

Synthesis and characterization of thermoresponsive poly(*N*-vinylcaprolactam)-based particles by emulsion polymerization by using a reactive macromolecular stabilizer

Two types of thermoresponsive poly(*N*-vinylcaprolactam) (PVCL)-based particles were synthesized by emulsion polymerization by using a reactive macromolecular stabilizer. In a first part, a xanthate functionalized poly(ethylene glycol) was used as macro-chain transfer agent and stabilizer for the reversible addition/fragmentation chain transfer (RAFT) emulsion copolymerization of VCL with the hydrophobic vinyl acetate co-monomer. This strategy allowed for the synthesis of physically crosslinked thermoresponsive particles by means of hydrophobic interactions between the poly(*N*-vinylcaprolactam-*co*-vinyl acetate) statistical copolymer chains of the core. To the best of our knowledge, this is the first example of the synthesis of PVCL-based amphiphilic copolymers by controlled radical emulsion polymerization. In a second part, chemically crosslinked cationic PVCL-based thermoresponsive particles were synthesized. For that purpose, a series of reactive cationic polymers were synthesized by RAFT/MADIX polymerization and were involved as stabilizers for the emulsion polymerization of VCL. The use of such reactive stabilizers enabled to produce stable monodisperse PVCL-based cationic thermoresponsive microgels, at initial solids content up to 10 %. Finally, the low cytotoxicity of bare PVCL microgels, the successful microgel internalization onto HeLa cancer cells by clathrin-dependent endocytosis and the sustained release of doxorubicin from the microgels highlight the potential of the cationic PVCL-based microgels to be used as chemotherapeutic drug delivery nanocarriers.

Synthèse et caractérisation de particules thermosensibles de poly(*N*-vinylcaprolactame) par polymérisation en émulsion en utilisant un stabilisant macromoléculaire réactif

Au cours de cette thèse, deux types de particules thermosensibles de poly(*N*-vinylcaprolactame) (PVCL) ont été synthétisées par polymérisation en émulsion en utilisant un stabilisant macromoléculaire porteur d'une extrémité réactive. Dans une première partie, un poly(éthylène glycol) fonctionnalisé avec un agent de contrôle de type xanthate a été utilisé en tant qu'agent de transfert macromoléculaire et stabilisant pour la copolymérisation par transfert de chaînes par addition/fragmentation réversible (RAFT) en émulsion de la *N*-vinylcaprolactame avec un co-monomère hydrophobe, l'acétate de vinyle (VAc). Cette stratégie de synthèse a permis d'aboutir à la formation de particules thermosensibles réticulées de manière physique par l'intermédiaire d'interactions hydrophobes entre les chaînes de copolymères poly(*N*-vinylcaprolactame-*co*-acétate de vinyle) constituant le cœur des particules. A notre connaissance, il s'agit du premier exemple de synthèse de copolymères amphiphiles de poly(*N*-vinylcaprolactame) par polymérisation radicalaire contrôlée en émulsion. Dans une seconde partie, des particules thermosensibles cationiques de poly(*N*-vinylcaprolactame) réticulées de manière chimique ont été synthétisées. Pour ce faire, plusieurs polymères cationiques porteurs d'une extrémité réactive de type xanthate ont été synthétisés et utilisés par la suite en tant que stabilisants réactifs pour la polymérisation en émulsion de la VCL. L'utilisation de ces polymères cationiques réactifs a permis d'obtenir des microgels cationiques de PVCL stables et monodisperses, à des taux de solides initiaux de 1 à 10 %, plus élevés que ceux généralement reportés pour la production de microgels thermosensibles (< 5 %). La faible cytotoxicité des microgels de PVCL synthétisés, leur effective internalisation par des cellules cancéreuses HeLa par un mécanisme d'endocytose clathrine-dépendante ainsi que leur capacité à relarguer de manière durable de la doxorubicine a permis de mettre en évidence le potentiel de ces microgels pour des applications en tant qu'agents de libération de principes actifs anticancéreux.

Síntesis y caracterización de partículas termosensibles de poli(*N*-vinilcaprolactama) mediante polimerización en emulsión utilizando un estabilizante macromolecular reactivo

Se han sintetizado dos tipos de partículas termosensibles basadas en la poli(*N*-vinilcaprolactama) (PVCL) mediante polimerización en emulsión utilizando un estabilizante macromolecular reactivo. En primer lugar, como agente de transferencia de cadena macromolecular y estabilizante se ha utilizado un poli(etilenglicol) modificado en su extremidad por un xantato, para copolimerizar por adición, fragmentación y transferencia reversible de cadena (RAFT) en emulsión la *N*-vinilcaprolactama con un comonómero hidrofóbico: el acetato de vinilo. Esta estrategia ha permitido sintetizar partículas sensibles a la temperatura y físicamente reticuladas gracias a las interacciones hidrofóbicas que surgen entre las cadenas estadísticas de poli(*N*-vinilcaprolactama-*co*-acetato de vinilo) y que conforman la partícula. Según nuestro conocimiento, este es el primer ejemplo de síntesis de copolímeros anfifílicos basados en la poli(*N*-vinilcaprolactama) por polimerización radical controlada en emulsión. En segundo lugar, se han sintetizado partículas termosensibles de poli(*N*-vinilcaprolactama) químicamente reticuladas. Para ello, se ha sintetizado una serie de polímeros catiónicos reactivos mediante polimerización RAFT/MADIX, siendo utilizados como estabilizantes en la polimerización en emulsión de la *N*-vinilcaprolactama. El uso de estos estabilizantes reactivos ha permitido producir microgeles catiónicos termosensibles de poli(*N*-vinilcaprolactama) estables y monodispersos, con un contenido en sólidos inicial que abarca del 1 al 10 %, que son más altos que los comúnmente utilizados al sintetizar microgeles sensibles a la temperatura (< 5 %). Y para finalizar se constata que, la baja citotoxicidad de los microgeles sintetizados, sus capacidades de internalización en células de cáncer de cuello uterino (HeLa), mediante un mecanismo de endocitosis clatrin-dependiente, así como sus facultades para liberar de manera sostenida un fármaco antitumoral (la doxorubicina), resaltan el potencial de estos microgeles catiónicos basados en la PVCL para ser utilizados como nanotransportadores para el suministro de medicamentos quimioterapéuticos.

Key words: *Thermoresponsive polymers, poly(N-vinylcaprolactam), emulsion polymerization, RAFT/MADIX polymerization, microgels, drug delivery systems*; **Mots clés**: *Polymères thermosensibles, poly(N-vinylcaprolactame), polymérisation en émulsion, polymérisation RAFT/MADIX, microgels, systèmes de libération de principes actifs*; **Palabras claves**: *Polímeros termosensibles, poli(N-vinilcaprolactama), polimerización en emulsión, polimerización RAFT/MADIX, microgeles, nanotransportadores para el suministro de principios activos*